PREDICTION OF CRACK INITIATION AND GROWTH IN SOLID PROPELLANTS

Principal Investigator: Professor E. E. Gdoutos
Xanthi, Greece

Final Report

for

European Office of
Aerospace Research and Development

April 1999

REPORT DOCUMENTATION PAGE

Form Approved OMB No. 0704-0188

1. AGENCY USE ONLY (Leave blank)	2. REPORT DATE	3. REPORT TYPE AND DATES COVERED
	April 1999	Final Report

4. TITLE AND SUBTITLE

Prediction of Crack Initiation and Growth in Solid Propellants

5. FUNDING NUMBERS

F6170898W0033

6. AUTHOR(S)

Prof E.E. Gdoutos

7. PERFORMING ORGANIZATION NAME(S) AND ADDRESS(ES)

Democritus University of Thrace
Xanthi GR-67100
Greece

8. PERFORMING ORGANIZATION REPORT NUMBER

N/A

9. SPONSORING/MONITORING AGENCY NAME(S) AND ADDRESS(ES)

EOARD
PSC 802 BOX 14
FPO 09499-0200

10. SPONSORING/MONITORING AGENCY REPORT NUMBER

SPC 98-4003

11. SUPPLEMENTARY NOTES

12a. DISTRIBUTION/AVAILABILITY STATEMENT

Approved for public release; distribution is unlimited.

12b. DISTRIBUTION CODE

A

13. ABSTRACT (Maximum 200 words)

This report results from a contract tasking Democritus University of Thrace as follows: The contractor will investigate crack initiation and growth in solid propellant grains. Solid propellants are critical to missile, launch vehicle and satellite upper stage performance. Cracks in solid propellant can cause catastrophic failures leading to loss of valuable USAF assets and even lives. Understanding these phenomena is important to their future applications.

14. SUBJECT TERMS

EOARD, Propellants, Solid Fuel, Materials

15. NUMBER OF PAGES

230

16. PRICE CODE

N/A

17. SECURITY CLASSIFICATION OF REPORT	18. SECURITY CLASSIFICATION OF THIS PAGE	19. SECURITY CLASSIFICATION OF ABSTRACT	20. LIMITATION OF ABSTRACT
UNCLASSIFIED	UNCLASSIFIED	UNCLASSIFIED	UL

PREDICTION OF CRACK INITIATION AND GROWTH IN SOLID PROPELLANTS

Principal Investigator: Professor E. E. Gdoutos
Xanthi, Greece

Final Report

for

European Office of
Aerospace Research and Development

April 1999

CONTENTS

ABSTRACT

The stress and displacement fields in an edge-cracked sheet specimen made of a solid propellant and subjected to a uniform displacement along its upper and lower faces was studied. The solid propellant was simulated as a hyperelastic material with constitutive behavior described by the Ogden strain energy potential. A nonlinear finite deformation analysis was performed based on the finite element code ABAQUS. A very detailed analysis of the stress field in the vicinity of the crack tip was undertaken. Results for stress, strain, displacement and strain energy density quantities were presented. The deformed profiles of the crack faces near the crack tip were determined. The results of stress analysis were coupled with the strain energy density theory to predict the crack growth behavior including crack initiation, stable crack growth and final termination. Crack growth resistance curves representing the variation of crack growth increment versus stress intensity factor were calculated.

1. INTRODUCTION

Solid propellants serve as both a fuel and a structural element in motor grains. Imperfections may be produced during the manufacturing and/or fabrication process of the solid propellant grain. To study the strength of a solid propellant grain these imperfections may be idealized as cracks in the material. Usually a dominant crack is formed. Determination of the residual strength or the service life of the rocket motor should be based on the study of crack growth behavior based on the principles of fracture mechanics.

During the past years, a considerable amount of work has been performed by Liu and coworkers to study crack growth behavior in solid propellants. As a result a series of publications have appeared in the literature. The solid propellant which is a particulate composite was modeled as a linear viscoelastic material characterized by the modulus of elasticity and Poisson's ratio. The analysis took place within the frame of the theory of linear elastic or linear viscoelastic fracture mechanics.

More specifically, Liu and Yee [1,2] studied the characteristics of the damage zone in a precracked composite solid propellant sheet tensile specimen subjected to a complex cyclic loading history using acoustic imaging technique. From the experimental results it was shown that the size of the damage zone and the intensity of damage in the damage zone depend highly on the cyclic loading history.

Liu [3] investigated the crack growth behavior in an eccentrically cracked sheet specimen. From the experimental data the mode I stress intensity factor and the crack growth rate were calculated. A considerable amount of stable crack growth occurs before the onset of instability. The value of stress intensity factor at the onset of unstable crack growth is approximately two times larger than that at the initiation of stable crack growth. A power low relationship was found to exist between the stress intensity factor and the crack growth rate. The crack growth rate data were calculated by four different methods, the second methods, the modified secant method, the spline fitting method and the polynomial method. It was found that the accuracy of the calculation of crack growth rate is affected by the time interval for crack length measurements.

Liu and Tang [4] investigated the effect of load history on crack growth behavior of a particulate composite made from polybutadiene rubber embedded with hard particles. Specimens were subjected to loading cycles to induce internal damage. The specimens were then stored at room temperature for six months before they were used for crack propagation tests. From the experimental results it was revealed that the pre-load had relatively small effect on the R-curve and the crack growth rate, da/dt, versus mode I stress intensity factor, K_I relationship. It was shown, however, that the resistance to crack growth in the pre-loaded specimen was lower than that in the virgin specimens. A considerable amount of stable subcritical crack growth occured before the onset of unstable crack propagation. A power law relationship was found to exist between da/dt and K_I.

Liu [5,6] investigated the effects of the cyclic loading sequence on the cumulative damage, constitutive behavior and residual strength of a solid propellant using an ultrasonic technique. The material's damage state was assessed by measuring changes in the relative acoustic attenuation coefficient for longitudinal ultrasonic waves propagating normal to the applied strain. It was established from experimental data that the cyclic stress-strain curves exhibit the phenomenon of the strain-induced stress softening, known as the "Mullin effect". The degree of stress softening depends on the cyclic loading sequence.

The local damage characteristics near the crack tip and crack growth behavior in a centrally cracked sheet specimen of a solid propellant were investigated by Liu [7,8]. From experimental results it was established that the damage characteristics have strong effects on crack growth behavior. The processes of damage initiation and evolution are the main contributing factors to the time-dependent crack growth behavior. Crack growth consists of crack tip blunting, resharpening and zig-sag crack growth. The crack opening displacement during stable crack growth appears to be a constant.

The effect of prestrain and strain rate on crack growth behavior in a highly filled polymeric material formed by embedding hard particles in a rubber was investigated by Liu [9].

From crack growth resistance and crack propagation curves obtained by experiment it was established that the crack growth behavior in predamaged specimens depends highly on the strain rate.

The crack growth behavior in an edge cracked sheet specimen made from polybutadiene filled with hard particles under different strain rates and temperatures was studied by Liu and Smith [10]. The near-tip mechanisms for crack opening and growth for different strain rates and temperature were studied by Smith et al [11]. It was found that changes in strain rate and temperature produce quantitative differencec in near-tip fields of displacement and strain, while they do not affect the near-tip mechanisms qualitatively. The effect of nonuniform strain field on the subcritical crack growth in a composite propellant was investigated by Liu [12,13].

A three-dimensional elastic finite element analysis of the interaction between a main crack and defects in a centrally cracked sharp specimen was conducted by Liu [14,15]. The defect was modelled by setting its modulus equal to 0.1 psi, while the modulus of the undamaged material was equal to 500 psi. The effect of defect characteristics on the value of the stress intensity factor, the stress distribution near the crack tip and crack growth behavior were analyzed.

A phenomenological constitutive model for modeling fracture behavior in elastic particulate composites undergoing damage was proposed by Ravichandran and Liu [16]. Based on this model the crack tip deformation and stress fields were obtained. Furthermore, a relationship between far-field applied loading and near-tip stress intensity factor based on the concept of crack tip shielding was derived. The crack opening profiles and the displacement field in the vicinity of a crack tip were calculated and compared well with experimental results.

Solid propellants are particulate composite materials containing hard particles embedded in a rubbery matrix. These materials exhibit elastic response up to large strains and can be modeled as visco-hyperelastic materials. The asymptotic behavior of the deformation and stresses near the crack tip for hyperelastic materials was studied by Knowles and Sternberg [17,18]. Results for the same problem, but for different constitutive relations than in [17,18]

provided by Gao [19]. The displacements along the flanks of an internal crack in rubber were measured by Theocaris et al. [20]. Modelling efforts for crack propagation in viscoelastic materials were done by Knauss [21] and Schapery [22].

2. OBJECTIVE

The objective of the present work is to study the characteristics of the damage zone near the crack tip and the crack growth behavior in edge and centrally cracked sheet specimens of a solid propellant. The specimens were subjected to a constant crosshead speed of 0.2 in/mm and 2.0 in/mm at room temperature.

The stress field in the cracked plates is evaluated by modeling the solid propellant as an incompressible visco-hyperelastic material. A very detailed finite element analysis in the vicinity of the crack tip takes place. A methodology based on the strain energy density criterion is developed for the determination of the critical stress at the onset of crack initiation and the history of stable crack growth up to final instability.

3. MATERIAL

Solid propellants are particulate composite materials, containing hard particles embedded in a rubbery matrix. On the microscopic scale, a highly filled solid propellant can be considered as nonhomogeneous. When the material is strained, damage in the form of microvoids in the binder or debonding at the matrix/particle interface takes place. As the applied strain in the material is progressively increased the growth of damage takes place as successive nucleation and coalescence of the microvoids or as material tears. These processes of damage initiation and evolution are time-dependent and they are mainly responsible for the time-sensitivity of the nonlinear stress-strain behavior of solid propellants. Their mechanical response is strongly influenced by the loading rate, temperature and material microstructure.

The viscoelastic response up to large strains of solid propellants will be accounted for by modeling these materials as hyperviscoelastic materials. Hyperelastic models are used to describe

the behavior of materials that exhibit elastic response up to large strains. Viscoelastic models are used for cases where dissipative losses must considered. The combination of hyperelastic and viscoelastic material models is taken for modeling the behavior of solid propellants. The material constants of the hyperelastic model are defined as a function of time for modeling the dissipative part of the material behavior. Another characteristic of solid propellants is that they have very little compressibility compared to their shear flexibility. The Poisson's ratio of these materials is almost equal to 0.5.

The load-displacement curves for the material under cyclic and monotonic load for two different load rates of 0.2 in/sec and 2.0 in/sec are shown in Figs. 1-4.

4. CONSTITUTIVE BEHAVIOR

The behavior of hyperelastic materials is described in terms of a strain energy potential $U(\varepsilon)$, which defines the strain energy stored in the material per unit of volume in the initial configuration as a function of the strain at that point in the material. The initial configuration of the long-chain molecules and hard particles distribution in solid propellants is random and, therefore, the material is initially isotropic. During stretching, the molecules are oriented and the material presents anisotropic behavior. However, the development of this anisotropy follows the direction of straining, and hence the material can be considered isotropic throughout the deformation history as a function of the strain invariants. The more frequently used forms of the strain energy potentials for modeling approximately incompressible isotropic materials are the polynomial form and the Ogden form.

The form of the polynomial strain energy potential is

$$U=\sum_{i+j=1}^{N} C_{ij}\left(\bar{I}_1-3\right)^i\left(\bar{I}_2-3\right)^j+\sum_{i=1}^{N}\frac{1}{D_i}\left(J_{el}-1\right)^{2i} \qquad (1)$$

where U is the strain energy per unit of reference volume, N is a material parameter, C_{ij} and D_i are temperature dependent material parameters, $\bar{I}_1$ and $\bar{I}_2$ are the first and second deviatoric strain invariants, defined as

$$\bar{I}_1 = \bar{\lambda}_1^2 + \bar{\lambda}_2^2 + \bar{\lambda}_3^2 \quad \text{and} \quad \bar{I}_2 = \bar{\lambda}_1^{(-2)} + \bar{\lambda}_2^{(-2)} + \bar{\lambda}_3^{(-2)}$$

with the deviatoric stretches $\bar{\lambda}_i = J^{-1/3}\lambda_i$, J is the volume ratio, λ_i are the principal stretches, and J_{el} is the elastic volume ratio without thermal expansion effects.

The form of the Ogden strain energy potential is

$$U = \sum_{i=1}^{N} \frac{2\mu_i}{\alpha_i^2}\left(\bar{\lambda}_1^{\alpha_i} + \bar{\lambda}_2^{\alpha_i} + \bar{\lambda}_3^{\alpha_i} - 3\right) + \sum_{i=1}^{N} \frac{1}{D_i}(J_{el} - 1)^{2i}, \tag{2}$$

where $\bar{\lambda}_i$ are the deviatoric principal stretches, N is a material parameter, and μ_i, α_i and D_i are temperature dependent material parameters. Because the powers α_i can be chosen by the user, the Ogden form usually provides a closer and more stable fit to the test data for a similar number of material constants in the strain energy function, especially at large strains.

If all of the D_i are zero, the material is fully incompressible. If D_1 is equal to zero, all of the D_i must be equal to zero.

For cases where the nominal strains are small or only moderately large (< 100%), the first terms in the polynomial series usually provide a sufficiently accurate model. The simplest form of the polynomial function is the form with N=1, which is the compressible form of the classical Mooney-Rivlin law:

$$U = C_{10}(\bar{I}_1 - 3) + C_{01}(\bar{I}_2 - 3) + \frac{1}{D_1}(J_{el} - 1)^2. \tag{3}$$

When $C_{01} = 0$ the strain energy function corresponds to the compressible form of the neo-Hookean law.

The initial shear modulus and bulk modulus is given by

$$\mu_0 = 2(C_{10} + C_{01}), \quad K_0 = \frac{2}{D_1}$$

The Ogden form is general in nature but particular cases are obtained for special choices of μ_i and α_i.The neo-Hookean form is obtained with N = 1, $\alpha_1 = 2$ and can be made equivalent to the polynomial form through the relation $\mu_1 = 2C_{10}$. The Mooney-Rivlin form is obtained when N=2, $\alpha_1 = 2$, $\alpha_2 = -2$ and is equivalent to the polynomial form when $\mu_1 = 2C_{10}$ and $\mu_2 = 2C_{01}$:

$$U = \frac{\mu_1}{2}(\bar{\lambda}_1^2 + \bar{\lambda}_2^2 + \bar{\lambda}_3^2 - 3) + \frac{\mu_2}{2}(\bar{\lambda}_1^{(-2)} + \bar{\lambda}_2^{(-2)} + \bar{\lambda}_3^{(-2)} - 3) + \frac{1}{D_1}(J_{el} - 1)^2 \tag{4}$$

The initial shear modulus and bulk modulus are given by

$$\mu_0 = \sum_{i=1}^{N} \mu_i, \quad K_0 = \frac{2}{D_1} \tag{5}$$

The dissipative part of the material behavior is defined by giving the Prony series representation of the constants that define the energy function in the polynomial form or in the Ogden form:

$$g_R(t) = \frac{C_{ij}^R(t)}{C_{ij}^0} \text{ (polynomial function)} = \frac{\mu_i^R(t)}{\mu_i^0} \text{ (Ogden function)} = 1 - \sum_{i=1}^{N} \bar{g}_i^P (1 - e^{-t/\tau_i}) \tag{6}$$

and

$$k_R(t) = \frac{D_i^0}{D_i^R(t)} = 1 - \sum_{i=1}^{N} \bar{k}_i^P (1 - e^{-t/\tau_i}) \tag{7}$$

No summation is intended for the expressions $C_{ij}^R(t)/C_{ij}^0$, $\mu_i^R(t)/\mu_i^0$, and $D_i^0/D_i^R(t)$. C_{ij}^0 or μ_i^0 and D_i^0 are the coefficients that determine the deviatoric and volumetric behavior and $\overline{g}_i^P$, $\overline{k}_i^P$ and τ_i are the Prony series parameters.

5. FINITE ELEMENT ANALYSIS

The finite element method was used to solve the boundary value problem of an edge cracked specimen subjected to a uniform displacement along its upper and lower faces. Two cases of rectangular sheet specimens with in-plane dimensions W=76.2 mm and h=25.4 mm and W=25.4 mm and h=76.2 mm were considered (Fig. 5). The thickness of the specimens was small enough to assume that conditions of plane stress prevail. An initial edge notch was introduced in the mid height of the specimen parallel to the specimen width. The notch root radius took the value 2.54×10^{-3} mm. The crack length took the values a = 2.54 mm, 15.24 mm and 30.48 mm for the specimen with W=76.2 mm and h=25.4 mm and the values a=2.54 mm, 5.08 mm and 10.16 mm for the specimen with W=25.4 mm and h=76.2 mm. Table I presents the dimensions of the specimens for the six cases under study. The specimens were made of a solid propellant. They were subjected to a uniform displacement u_0 along the upper and lower faces.

A very refined finite element grid was introduced in the region surrounding the notch end to accommodate the large displacements and stresses developed in that area. The finite element grid around the notch tip in its undeformed configuration is shown in Fig 6. The finite element grid in its underformed and deformed configuration for half specimen of Case I (W=76.2 mm, h=25.4 mm, a=2.54 mm) is shown in Fig. 7. The finite element grid for the missing part of Fig. 7 is shown in Fig. 8, while the finite element grid for the missing part of Fig. 8 is shown in Fig. 9.

Quadrilateral elements with four integration points were used. The number of elements for each specimen configuration was about 4200 and varied slightly from specimen to specimen.

A nonlinear large deformation analysis was performed by the ABAQUS computer code. The applied displacement u_0 was increased incrementally. Results for the strain energy density, dW/dV, the Mises stress, σ_{eff}, the displacements u_1 and u_2 along and perpendicular to the crack

axis direction, the normal stress, σ_{22}, and strain, ε_{22}, along the perpendicular to the crack axis directing are shown in Figs 10-27 for u_0=0.3388 mm. This value of applied displacement corresponds to the critical displacement for initiation of crack growth. Results analogous to those of Figs 7-27 are shown in Figs 28-48 for an applied displacement u_0=3.3295 mm.

Figs 7-48 refer to case I. Analogous results for cases II, III, IV, V and VI are shown in Figs 49-90, Figs 91-132, Figs 133-174, Figs 175-216 and Figs 217-258, respectively. For each case the first group of figures corresponds to the applied critical displacement for initiation of crack growth, while the second group of figures corresponds to an applied displacement u_0=3.3295 mm. The values of the critical displacement for initiation of crack growth are shown in Table II.

The deformed profile of crack faces near the crack tip for Case I and various values of the applied uniform displacement u_0 is shown in Fig 259.

The variation ahead of crack tip of the strain energy density, dW/dV, the Mises stress, σ_{eff}, the normal stress along the perpendicular to the crack axis direction, σ_y, the effective strain ε_{eff} and the normal strain along the perpendicular to the crack axis direction, ε_y, for various values of the applied uniform displacement u_0 is shown in Figs 260-264. The variation of the strain energy density ahead of crack tip for three values of the applied displacement for the determination of the critical displacement for initiation of crack growth is shown in Fig. 265.

The variation of strain energy density, dW/dV, Mises stress, σ_{eff}, and normal strain along the perpendicular to the crack axis direction, ε_y, versus applied displacement u_0 for nodes 10, 20 and 49 lying along the crack ligament at distances 0.005 mm, 0.018 mm and 0.254 mm from the crack tip, respectively, is shown in Figs. 266-268.

Figs 259-268 refer to Case I. Analogous results for cases II, III, IV, V and VI are shown in Figs 272-281, Figs 285-294, Figs 298-307, Figs 311-320 and Figs 324-333, respectively.

6. PREDICTION OF CRACK GROWTH

Crack growth consists of three stages: crack initiation, subcritical or slow growth and unstable crack propagation. These stages of crack growth will be addressed in a unified manner

by the strain energydensity criterion. The criterion was introduced by Sih [23,24] and it was used by Gdoutos and co-workers [25-30] for the solution of a host of problems of engineering importance.

According to the strain energy density theory crack growth takes place when the strain energy density at an element ahead of the crack tip reaches a critical value. This value is calculated from the stress-strain curve of the material in tension.

The strain energy density function dW/dV is calculated by

$$\frac{dW}{dV} = \int_0^{\varepsilon_{ij}} \sigma_{ij} d\varepsilon_{ij} \tag{8}$$

where σ_{ij} and ε_{ij} are the Cartesian stress and strain components. Equation (8) applies to all materials either linear (nondissipative) or nonlinear (dissipative).

For the case when material failure initiates from the tip of a preexisting crack in a solid attention is concentrated on the distribution of the strain energy density function along the circumference of a circle centered at the crack tip. This circle represnets the process or core region in which the continuum model fails to describe the state of stress and strain. The crack will grow in the direction of the minimum strain energy density function, $(dW/dV)_{min}$. Onset of crack extension takes place when $(dW/dV)_{min}$ becomes equal to $(dW/dV)^c_{min}$ (referred to in sequel as $(dW/dV)_c$), which is directly determined from the area underneath the stress-strain diagram of the material in tension up to the point of fracture. The condition of crack growth initiation is expressed by

$$\left(\frac{dW}{dV}\right)_{min} = \left(\frac{dW}{dV}\right)_c \tag{9}$$

where $(dW/dV)_c$ is a material parameter.

The value of the critical stress σ_i that triggers crack growth is determined from equation (9). The condition for stable crack growth is expressed by

$$\frac{dW}{dV} = \left(\frac{dW}{dV}\right)_c = \frac{S_1}{r_1} = \frac{S_2}{r_2} = \ldots = \frac{S_j}{r_j} = \ldots \frac{S_c}{r_c} \tag{10}$$

where r_m (m=1,2,...,j) are the crack growth increments. Crack growth becomes unstable when the critical increment r_c is reached. r_c is a material parameter and is calculated from $r_c = S_c/(dW/dV)_c$, where S_c is material parameter.

The crack growth resistance curves showing the variation of applied displacement, u, stress intensity factor, K_I, and strain energy density factor, S, versus crack growth length during stable crack growth were calculated. They are shown in Figs 269-271 for Case I, in Figs 282-284 for Case II, in Figs 295-297 for case III, in Figs 308-310 for Case IV, in Figs 321-323 for Case V and in Figs 334-336 for case VI. Results for the applied critical displacement for crack initiation, u_i, unstable crack growth, u_c, and stable crack growth increment for the six cases studied are shown in Table II.

Comparative results for different specimen geometries and crack lengths are shown in Figs 337-349. Thus, Fig. 337 presents the deformed profiles of crack faces near the crack tip for two specimen geometries with W=76.2 mm and h=25.4 mm and W=25.4 mm and h=76.2 mm and two values of the applied displacement u=1.2705 mm and u=3.3295 mm. Figs 338-341 present the strain energy density, dW/dV, and Mises stress, σ_{eff}, ahead of crack tip for specimen geometry with W=76.2 mm and h=25.4 mm for three different crack lengths a=2.54, 15.24 and 30.48 mm and two values of the applied displacement u=0.847 and 3.3295 mm. Analogous results for specimen geometry with W=25.4 mm and h=76.2 mm for three different crack lengths a=2.54, 5.08 and 10.16 mm and two values of the applied displacement u=0.847 and 3.3295 mm are shown in Figs 342-345. Finally, Figs 346-349 present the strain energy density and Mises stress ahead of crack tip for two specimen geometries with W=76.2 mm and h=25.4 mm and W=25.4 mm and h=76.2 mm, crack length a=2.54 mm and two values of the applied displacement u=0.847 and 3.3295 mm.

7. CONCLUSIONS

A nonlinear large deformation finite element analysis of the stress and displacement fields in a rectangular sheet specimen with an edge crack subjected to a uniform displacement perependicular to the crack along the upper and lower faces of the specimen was conducted. Two different specimen geometries with three different crack lengths each were studied. The strain energy density theory was used to predict the initiation, stable and unstable crack growth. Results showing relevant quantities of the stress and displacement fields including the deformed specimen geometry, the x-and-y displacement components, the normal stress, the Mises stress and the strain energy density were presented for all six cases of specimen geometry studied. Crack growth resistance curves showing the variation of applied displacement, stress intensity factor or strain energy density factor versus crack growth increment during stable crack growth from initiation to instability were drawn. Prediction of crack initiation was based on a value of the initial curve in the strain energy density theory equal to $r_0=1x10^{-2}$ mm. The critical increment r_c for unstable crack growth was calculated as 1.6 mm. The specimen material made of a solid propellant was modeled as a hyperelastic material. The viscoelastic response of the material was not taken into account. The main results of the present study may be summarized as follows:

i. Very large deformations are developed in the vicinity of the crack tip, even for small values of the applied displacement.

ii. The critical displacement for initiation, u_i, and unstable, u_c, crack growth is greatly influenced by specimen geometry and crack length. For the same crack length a=2.54 mm u_i and u_c are almost two and three times, respectively, higher for the long specimen (W=25.4 mm, h=76.2 mm) than for the short specimen (W=76.2 mm, h=25.4 mm).

iii. A considerable amount of stable crack growth for all specimen geometries takes place before catastrophic fracture. The extent of stable crack growth is higher for the long then for the short specimen. Furthermore, the extent of stable crack growth relative to the initial crack length is higher for the smaller cracks.

iv. The crack opening displacement (COD) near the crack tip is strongly influenced by specimen geometry. For the same applied displacement and crack length COD is much higher for the short than the long specimen.

8. REFERENCES

[1] Liu, C.T. and Yee, R., Evolution of cumulative damage in a composite solid propellant, *Proceedings of the 1986 SEM Spring Conference on Experimental Mechanics*, pp. 729-736 (1986).

[2] Liu, C. T., Crack propagation in a composite solid propellant, *Proceedings of the 1990 SEM Spring Conference on Experimental Mechanics*, pp. 614-620 (1990).

[3] Liu, C. T. and Tang, B., Load history effect on crack growth in a particulate composite material, *Proceedings of the 1995 SEM Spring Conference and Exhibit on Experimental Mechanics*, Grand Rapids, June 12-14, 1995, pp. 831-836 (1995).

[4] Liu, C. T., Effects of cyclic loading sequence on cumulative damage and constitutive behavior of a composite solid propellant, *Proceedings AIAA/ASME/ASCE/AHS 28th Structures, Structural Dynamics 1987*, pp. 847-855 (1987).

[5] Liu, C. T., Cumulative damage and the constitutive and fracture behavior in a composite solid propellant, *Proceedings of the Conference on "High Technology Composites in Modern Applications,"* edited by S. A. Paipetis and A. G. Youtsos, Corfu, Greece, 1995, pp. 129-138 (1995).

[6] Liu, C. T., Acoustic evaluation of damage characteristics in a composite solid propellant, *Journal of Spececraft and Rockets* , vol. 29, no. 5, pp. 709-712 (1992).

[7] Liu, C. T., Time dependent crack behavior in a composite solid propellant, *Proceedings of the 1995 SEM Spring Conference and Exhibit on Experimental Mechanics*, Grand Rapids, June 12-14, 1995, pp. 242-250 (1995).

[8] Liu, C. T., The effect of micro damage on time-dependent crack growth in a composite solid propellant, *Mechanics of Time Dependent Materials*, vol. 1, pp. 123-136 (1997).

[9] Liu, C. T., Effect of predamage on crack growth behavior in a particulate composite material, *Journal of Spacecraft and Rockets*, vol. 32, no. 3, pp. 533-537 (1995).

[10] Liu, C. T. and Smith, C. W., Temperature and rate effects on stable crack growth in a particulate composite material, *Proceedings of the 1994 SEM Spring Conference*, Baltimore, pp. 146-152 (1994); *Experimental Mechanics*, vol. 36, no. 3, pp. 290-295 (1996).

[11] Smith, C. W., Wang, L., Mouille, H. and Liu, C. T., Near-tip behavior of particulate composite material containing cracks at ambient and elevated temperatures, in *Fracture Mechanics: Twenty-Third Symposium*, ASTM STP 1189, edited by Ravinder Chona, American Society for Testing and Materials, Philadelphia, pp. 775-787 (1993).

[12] Liu, C. T., Crack growth behavior in a composite propellant with strain gradients - Part I, AIAA, Paper 84 - 1294 (1984).

[13] Liu, C. T., Crack growth behavior in a composite propellant with strain gradients - Part II, *AIAA*, vol. 27, no. 6, pp. 647-652 (1990).

[14] Liu, C. T, Numerical modeling of crack-defect interaction, *J. Propulsion*, vol. 7, no. 4, pp. 526-530 (1991).

[15] Liu, C. T., Three-dimensional finite element analysis of crack-defect interaction, *J. Spacecraft and Rockets*, vol. 29, no. 5, pp. 713-717 (1992).

[16] Ravichandran, G. and Liu, C. T., Crack tip shielding in elastic particulate composites undergoing damage, *Engineering Fracture Mechanics*, to appear.

[17] Knowles, J. K. and Sternberg, E., An asymptotic finite-deformation analysis of the elastostatic field near the tip of a crack, *J. Elasticity*, vol. 3, no. 2, pp. 67-107 (1973).

[18] Knowles, J. K. and Sternberg, E., Finite-deformation analysis of the elastostatic field near the tip of a crack: Reconsideration and higher-order results, *J. Elasticity,* vol. 4, no. 3, pp. 201-233 (1974).

[19] Gao, Y. C., Elastostatic crack tip behavior for a rubber-like material, *Theoretical and Applied Fracture Mechanics*, vol. 14, pp. 219-231 (1990).

[20] Theocoris, P. S., Pazis, D. and Konstantellos, B. D., Elastic displacements along the flanks of internal cracks in rubber, *Experimental Mechanics*, vol. 29, pp. 32-39 (1989).

[21] Krauss, W. G., The mechanics of polymer fracture, *Applied Mechanics Reviews*, vol. 26, pp. 1-17 (1973).

[22] Schapery, R. A., A theory of crack initiation and growth in viscoelastic media. I. Theoretical development, *International Journal of Fracture*, vol. 11, no. 1, pp. 141-159 (1975).

[23] Sih, G. C., Strain energy density factor applied to mixed mode crack problems, *International Journal of Fracture*, vol. 10, pp. 305-321 (1974).

[24] Sih, G. C., *Mechanics of Fracture Initiation and Propagation*, Kluwer Academic Publishers, 1991.

[25] Gdoutos, E. E. and Papakaliatakis, G., "The effect of load biaxiality on crack growth in non-linear materials," *Theoretical and Applied Fracture Mechanics*, vol. 5, pp. 133-140, (1986).

[26] Gdoutos, E. E. and Papakaliatakis, G., "Crack growth initiation in elastic-plastic materials," *International Journal of Fracture*, vol. 32, pp. 143-156, (1986).

[27] Gdoutos, E. E. and Papakaliatakis, G., The influence of plate geometry and material properties on crack growth, *Engineering Fracture Mechanics*, vol. 25, pp. 141-156 (1986).

[28] Gdoutos, E. E. and Papakaliatakis, G., "Crack growth in ductile materials," *Proceedings of the First National Congress on Mechanics*, Athens, Greece, June 25-27, 1986, pp. 503-525, (1987).

[29] Gdoutos, E. E. and Papakaliatakis, G., "Dependence of crack growth initiation of the form of the stress-strain diagram of the material in tension," Engineering Fracture Mechanics, vol. 34, pp. 143-151, (1989).

[30] Gdoutos, E. E. and Zacharopoulos, D. A., "A damage model for crack initiation and growth," *Theoretical and Applied Fracture Mechanics*, vol. 14, pp. 117-122, (1990).

Figure Captions

Fig. 1 Cyclic load-displacement curve for a solid propellant tension specimen. Load is in pounds and displacement is in inches. Specimen has a width of 0.501 in. and a thickness of 0.354 in. Loading rate is 0.2 in/mm.

Fig. 2 Load-displacement curve for a solid propellant tension specimen. Load is pounds and displacement is in inches. Specimen has a width of 0.50 in. and a thickness of 0.36 in. Loading rate is 0.2 in/mm.

Fig. 3 Cyclic load-displacement curve for a solid propellant tension specimen. Load is in pounds and displacement is in inches. Specimen has a width of 0.50 in. and a thickness of 0.36 in. Loading rate is 2.0 in/mm.

Fig. 4 Load-displacement curve for a a solid propellant tension specimen. Load is in pounds and displacement is in inches. Specimen has a width of 0.50 in and a thickness of 0.36 in. Loading rate is 2.0 in/mm.

Fig. 5 Geometry of edge cracked specimen subjected to uniform displacement along its upper and lower faces.

Fig. 6 Undeformed finite element grid near the crack tip. Notch root radius 2.54×10^{-3} mm.

Fig. 7 Undeformed (in red) and deformed (in black) finite element grids for half specimen. Applied displacement u_0=0.3388 mm. Case I.

Fig. 8 Undeformed (in red) and deformed (in black) finite element grids for the missing part of Figure 7. Applied displacement u_0=0.3388 mm. Case I.

Fig. 9 Undeformed (in red) and deformed (in black) finite element grids for the missing part of Figure 8. Applied displacement u_0=0.3388 mm. Case I.

Fig. 10 Strain energy density, dW/dV, contours (in the deformed specimen configuration) for Figure 7. Values in kN.mm/mm^3. Applied displacement u_0=0.3388 mm. Case I.

Fig. 11 Strain energy density, dW/dV, contours (in the deformed specimen configuration) for Figure 8. Values in kN.mm/mm^3. Applied displacement u_0=0.3388 mm. Case I.

Fig. 12 Strain energy density, dW/dV, contours (in the deformed specimen configuration) for Figure 9. Values in kN.mm/mm^3. Applied displacement u_0=0.3388 mm. Case I.

Fig. 13 Mises stress, σ_{eff}, contours (in the deformed specimen configuration) for Figure 7. Values in kN/mm^2. Applied displacement u_0=0.3388 mm. Case I.

Fig. 14 Mises stress, σ_{eff}, contours (in the deformed specimen configuration) for Figure 8. Values in kN/mm^2. Applied displacement u_0=0.3388 mm. Case I.

Fig. 15 Mises stress, σ_{eff}, contours (in the deformed specimen configuration) for Figure 9. Values in kN/mm^2. Applied displacement u_0=0.3388 mm. Case I.

Fig. 16 Displacement along the crack axis direction, u_1, contours (in the deformed specimen configuration) for Figure 7. Values in mm. Applied displacement u_0=0.3388 mm. Case I.

Fig. 17 Displacement along the crack axis direction, u_1, contours (in the deformed specimen configuration) for Figure 8. Values in mm. Applied displacement u_0=0.3388 mm. Case I.

Fig. 18 Displacement along the crack axis direction, u_1, contours (in the deformed specimen configuration) for Figure 9. Values in mm. Applied displacement u_0=0.3388 mm. Case I.

Fig. 19 Displacement along the perpendicular to the crack axis direction, u_2, contours (in the deformed specimen configuration) for Figure 7. Values in mm. Applied displacement u_0=0.3388 mm. Case I.

Fig. 20 Displacement along the perpendicular to the crack axis direction, u_2, contours (in the deformed specimen configuration) for Figure 8. Values in mm. Applied displacement u_0=0.3388 mm. Case I.

Fig. 21 Displacement along the perpendicular to the crack axis direction, u_2, contours (in the deformed specimen configuration) for Figure 9. Values in mm. Applied displacement u_0=0.3388 mm. Case I.

Fig. 22 Normal stress along the perpendicular to the crack axis direction, σ_{22}, contours (in the deformed specimen configuration) for Figure 7. Values in kN/mm^2. Applied displacement u_0=0.3388 mm. Case I.

Fig. 23 Normal stress along the perpendicular to the crack axis direction, σ_{22}, contours (in the deformed specimen configuration) for Figure 8. Values in kN/mm^2. Applied displacement u_0=0.3388 mm. Case I.

Fig. 24 Normal stress along the perpendicular to the crack axis direction, σ_{22}, contours (in the deformed specimen configuration) for Figure 9. Values in kN/mm^2 Applied displacement u_0=0.3388 mm. Case I.

Fig. 25 Normal strain along the perpendicular to the crack axis direction, ε_{22}, contours (in the deformed specimen configuration) for Figure 7. Applied displacement u_0=0.3388 mm. Case I.

Fig. 26 Normal strain along the perpendicular to the crack axis direction, ε_{22}, contours (in the deformed specimen configuration) for Figure 8. Applied displacement u_0=0.3388 mm. Case I.

Fig. 27 Normal strain along the perpendicular to the crack axis direction, ε_{22}, contours (in the deformed specimen configuration) for Figure 9. Applied displacement u_0=0.3388 mm. Case I.

Fig. 28 Undeformed (in red) and deformed (in black) finite element grids for half specimen. Applied displacement u_0=3.3295 mm. Case I.

Fig. 29 Undeformed (in red) and deformed (in black) finite element grids for the missing part of Figure 28. Applied displacement u_0=3.3295 mm. Case I.

Fig. 30 Undeformed (in red) and deformed (in black) finite element grids for the missing part of Figure 29. Applied displacement u_0=3.3295 mm. Case I.

Fig. 31 Strain energy density, dW/dV, contours (in the deformed specimen configuration) for Figure 28. Values in kN.mm/mm^3. Applied displacement u_0=3.3295 mm. Case I.

Fig. 32 Strain energy density, dW/dV, contours (in the deformed specimen configuration) for Figure 29. Values in kN.mm/mm^3. Applied displacement u_0=3.3295 mm. Case I.

Fig. 33 Strain energy density, dW/dV, contours (in the deformed specimen configuration) for Figure 30. Values in kN.mm/mm^3. Applied displacement u_0=3.3295 mm. Case I.

Fig. 34 Mises stress, σ_{eff}, contours (in the deformed specimen configuration) for Figure 28. Values in kN/mm^2. Applied displacement u_0=3.3295 mm. Case I.

Fig. 35 Mises stress, σ_{eff}, contours (in the deformed specimen configuration) for Figure 29. Values in kN/mm^2. Applied displacement u_0=3.3295 mm. Case I.

Fig. 36 Mises stress, σ_{eff}, contours (in the deformed specimen configuration) for Figure 30. Values in kN/mm^2. Applied displacement u_0=3.3295 mm. Case I.

Fig. 37 Displacement along the crack axis direction, u_1, contours (in the deformed specimen configuration) for Figure 28. Values in mm. Applied displacement u_0=3.3295 mm. Case I.

Fig. 38 Displacement along the crack axis direction, u_1, contours (in the deformed specimen configuration) for Figure 29. Values in mm. Applied displacement u_0=3.3295 mm. Case I.

Fig. 39 Displacement along the crack axis direction, u_1, contours (in the deformed specimen configuration) for Figure 30. Values in mm. Applied displacement u_0=3.3295 mm. Case I.

Fig. 40 Displacement along the perpendicular to the crack axis direction, u_2 contours (in the deformed specimen configuration) for Figure 28. Values in mm. Applied displacement u_0=3.3295 mm. Case I.

Fig. 41 Displacement along the perpendicular to the crack axis direction, u_2 contours (in the deformed specimen configuration) for Figure 29. Values in mm. Applied displacement u_0=3.3295 mm. Case I.

Fig. 42 Displacement along the perpendicular to the crack axis direction, u_2 contours (in the deformed specimen configuration) for Figure 30. Values in mm. Applied displacement u_0=3.3295 mm. Case I.

Fig. 43 Normal stress along the perpendicular to the crack axis direction, σ_{22}, contours (in the deformed specimen configuration) for Figure 28. Values in kN/mm^2. Applied displacement u_0=3.3295 mm. Case I.

Fig. 44 Normal stress along the perpendicular to the crack axis direction, σ_{22}, contours (in the deformed specimen configuration) for Figure 29. Values in kN/mm^2. Applied displacement u_0=3.3295 mm. Case I.

Fig. 45 Normal stress along the perpendicular to the crack axis direction, σ_{22}, contours (in the deformed specimen configuration) for Figure 30. Values in kN/mm^2. Applied displacement u_0=3.3295 mm. Case I.

Fig. 46 Normal strain along the perpendicular to the crack axis direction, ε_{22}, contours (in the deformed specimen configuration) for Figure 28. Applied displacement u_0=3.3295 mm. Case I.

Fig. 47 Normal strain along the perpendicular to the crack axis direction, ε_{22}, contours (in the deformed specimen configuration) for Figure 29. Applied displacement u_0=3.3295 mm. Case I.

Fig. 48 Normal strain along the perpendicular to the crack axis direction, ε_{22}, contours (in the deformed specimen configuration) for Figure 30. Applied displacement u_0=3.3295 mm. Case I.

Fig. 49 Undeformed (in red) and deformed (in black) finite element grids for half specimen. Applied displacement u_0=0.2541 mm. Case II.

Fig. 50 Undeformed (in red) and deformed (in black) finite element grids for the missing part of Figure 49. Applied displacement u_0=0.2541 mm. Case II.

Fig. 51 Undeformed (in red) and deformed (in black) finite element grids for the missing part of Figure 50. Applied displacement u_0=0.2541 mm. Case II.

Fig. 52 Strain energy density, dW/dV, contours (in the deformed specimen configuration) for Figure 49. Values in kN.mm/mm^3. Applied displacement u_0=0.2541 mm. Case II.

Fig. 53 Strain energy density, dW/dV, contours (in the deformed specimen configuration) for Figure 50. Values in kN.mm/mm^3. Applied displacement u_0=0.2541 mm. Case II.

Fig. 54 Strain energy density, dW/dV, contours (in the deformed specimen configuration) for Figure 51. Values in kN.mm/mm^3. Applied displacement u_0=0.2541 mm. Case II.

Fig. 55 Mises stress, σ_{eff}, contours (in the deformed specimen configuration) for Figure 49. Values in kN/mm^2. Applied displacement u_0=0.2541 mm. Case II.

Fig. 56 Mises stress, σ_{eff}, contours (in the deformed specimen configuration) for Figure 50. Values in kN/mm^2. Applied displacement u_0=0.2541 mm. Case II.

Fig. 57 Mises stress, σ_{eff}, contours (in the deformed specimen configuration) for Figure 51. Values in kN/mm^2. Applied displacement u_0=0.2541 mm. Case II.

Fig. 58 Displacement along the crack axis direction, u_1, contours (in the deformed specimen configuration) for Figure 49. Values in mm. Applied displacement u_0=0.2541 mm. Case II.

Fig. 59 Displacement along the crack axis direction, u_1, contours (in the deformed specimen configuration) for Figure 50. Values in mm. Applied displacement u_0=0.2541 mm. Case II.

Fig. 60 Displacement along the crack axis direction, u_1, contours (in the deformed specimen configuration) for Figure 51. Values in mm. Applied displacement u_0=0.2541 mm. Case II.

Fig. 61 Displacement along the perpendicular to the crack axis direction, u_2, contours (in the deformed specimen configuration) for Figure 49. Values in mm. Applied displacement u_0=0.2541 mm. Case II.

Fig. 62 Displacement along the perpendicular to the crack axis direction, u_2, contours (in the deformed specimen configuration) for Figure 50. Values in mm. Applied displacement u_0=0.2541 mm. Case II.

Fig. 63 Displacement along the perpendicular to the crack axis direction, u_2, contours (in the deformed specimen configuration) for Figure 51. Values in mm. Applied displacement u_0=0.2541 mm. Case II.

Fig. 64 Normal stress along the perpendicular to the crack axis direction, σ_{22}, contours (in the deformed specimen configuration) for Figure 49. Values in kN/mm^2. Applied displacement u_0=0.2541 mm. Case II.

Fig. 65 Normal stress along the perpendicular to the crack axis direction, σ_{22}, contours (in the deformed specimen configuration) for Figure 50. Values in kN/mm^2. Applied displacement u_0=0.2541 mm. Case II.

Fig. 66 Normal stress along the perpendicular to the crack axis direction, σ_{22}, contours (in the deformed specimen configuration) for Figure 51. Values in kN/mm^2 Applied displacement u_0=0.2541 mm. Case II.

Fig. 67 Normal strain along the perpendicular to the crack axis direction, ε_{22}, contours (in the deformed specimen configuration) for Figure 49. Applied displacement u_0=0.2541 mm. Case II.

Fig. 68 Normal strain along the perpendicular to the crack axis direction, ε_{22}, contours (in the deformed specimen configuration) for Figure 50. Applied displacement u_0=0.2541 mm. Case II.

Fig. 69 Normal strain along the perpendicular to the crack axis direction, ε_{22}, contours (in the deformed specimen configuration) for Figure 51. Applied displacement u_0=0.2541 mm. Case II.

Fig. 70 Undeformed (in red) and deformed (in black) finite element grids for half specimen. Applied displacement u_0=3.3295 mm. Case II.

Fig. 71 Undeformed (in red) and deformed (in black) finite element grids for the missing part of Figure 70. Applied displacement u_0=3.3295 mm. Case II.

Fig. 72 Undeformed (in red) and deformed (in black) finite element grids for the missing part of Figure 71. Applied displacement u_0=3.3295 mm. Case II.

Fig. 73 Strain energy density, dW/dV, contours (in the deformed specimen configuration) for Figure 70. Values in kN.mm/mm^3. Applied displacement u_0=3.3295 mm. Case II.

Fig. 74 Strain energy density, dW/dV, contours (in the deformed specimen configuration) for Figure 71. Values in kN.mm/mm^3. Applied displacement u_0=3.3295 mm. Case II.

Fig. 75 Strain energy density, dW/dV, contours (in the deformed specimen configuration) for Figure 72. Values in kN.mm/mm^3. Applied displacement u_0=3.3295 mm. Case II.

Fig. 76 Mises stress, σ_{eff}, contours (in the deformed specimen configuration) for Figure 70. Values in kN/mm^2. Applied displacement u_0=3.3295 mm. Case II.

Fig. 77 Mises stress, σ_{eff}, contours (in the deformed specimen configuration) for Figure 71. Values in kN/mm^2. Applied displacement u_0=3.3295 mm. Case II.

Fig. 78 Mises stress, σ_{eff}, contours (in the deformed specimen configuration) for Figure 72. Values in kN/mm^2. Applied displacement u_0=3.3295 mm. Case II.

Fig. 79 Displacement along the crack axis direction, u_1, contours (in the deformed specimen configuration) for Figure 70. Values in mm. Applied displacement u_0=3.3295 mm. Case II.

Fig. 80 Displacement along the crack axis direction, u_1, contours (in the deformed specimen configuration) for Figure 71. Values in mm. Applied displacement u_0=3.3295 mm. Case II.

Fig. 81 Displacement along the crack axis direction, u_1, contours (in the deformed specimen configuration) for Figure 72. Values in mm. Applied displacement u_0=3.3295 mm. Case II.

Fig. 82 Displacement along the perpendicular to the crack axis direction, u_2 contours (in the deformed specimen configuration) for Figure 70. Values in mm. Applied displacement u_0=3.3295 mm. Case II.

Fig. 83 Displacement along the perpendicular to the crack axis direction, u_2 contours (in the deformed specimen configuration) for Figure 71. Values in mm. Applied displacement u_0=3.3295 mm. Case II.

Fig. 84 Displacement along the perpendicular to the crack axis direction, u_2 contours (in the deformed specimen configuration) for Figure 72. Values in mm. Applied displacement u_0=3.3295 mm. Case II.

Fig. 85 Normal stress along the perpendicular to the crack axis direction, σ_{22}, contours (in the deformed specimen configuration) for Figure 70. Values in kN/mm^2. Applied displacement u_0=3.3295 mm. Case II.

Fig. 86 Normal stress along the perpendicular to the crack axis direction, σ_{22}, contours (in the deformed specimen configuration) for Figure 71. Values in kN/mm^2. Applied displacement u_0=3.3295 mm. Case II.

Fig. 87 Normal stress along the perpendicular to the crack axis direction, σ_{22}, contours (in the deformed specimen configuration) for Figure 72. Values in kN/mm^2. Applied displacement u_0=3.3295 mm. Case II.

Fig. 88 Normal strain along the perpendicular to the crack axis direction, ε_{22}, contours (in the deformed specimen configuration) for Figure 70. Applied displacement u_0=3.3295 mm. Case II.

Fig. 89 Normal strain along the perpendicular to the crack axis direction, ε_{22}, contours (in the deformed specimen configuration) for Figure 71. Applied displacement u_0=3.3295 mm. Case II.

Fig. 90 Normal strain along the perpendicular to the crack axis direction, ε_{22}, contours (in the deformed specimen configuration) for Figure 72. Applied displacement u_0=3.3295 mm. Case II.

Fig. 91 Undeformed (in red) and deformed (in black) finite element grids for half specimen. Applied displacement u_0=0.2541 mm. Case III.

Fig. 92 Undeformed (in red) and deformed (in black) finite element grids for the missing part of Figure 91. Applied displacement u_0=0.2541 mm. Case III.

Fig. 93 Undeformed (in red) and deformed (in black) finite element grids for the missing part of Figure 92. Applied displacement u_0=0.2541 mm. Case III.

Fig. 94 Strain energy density, dW/dV, contours (in the deformed specimen configuration) for Figure 91. Values in kN.mm/mm^3. Applied displacement u_0=0.2541 mm. Case III.

Fig. 95 Strain energy density, dW/dV, contours (in the deformed specimen configuration) for Figure 92. Values in kN.mm/mm^3. Applied displacement u_0=0.2541 mm. Case III.

Fig. 96 Strain energy density, dW/dV, contours (in the deformed specimen configuration) for Figure 93. Values in kN.mm/mm^3. Applied displacement u_0=0.2541 mm. Case III.

Fig. 97 Mises stress, σ_{eff}, contours (in the deformed specimen configuration) for Figure 91. Values in kN/mm^2. Applied displacement u_0=0.2541 mm. Case III.

Fig. 98 Mises stress, σ_{eff}, contours (in the deformed specimen configuration) for Figure 92. Values in kN/mm^2. Applied displacement u_0=0.2541 mm. Case III.

Fig. 99 Mises stress, σ_{eff}, contours (in the deformed specimen configuration) for Figure 93. Values in kN/mm^2. Applied displacement u_0=0.2541 mm. Case III.

Fig. 100 Displacement along the crack axis direction, u_1, contours (in the deformed specimen configuration) for Figure 91. Values in mm. Applied displacement u_0=0.2541 mm. Case III.

Fig. 101 Displacement along the crack axis direction, u_1, contours (in the deformed specimen configuration) for Figure 92. Values in mm. Applied displacement u_0=0.2541 mm. Case III.

Fig. 102 Displacement along the crack axis direction, u_1, contours (in the deformed specimen configuration) for Figure 93. Values in mm. Applied displacement u_0=0.2541 mm. Case III.

Fig. 103 Displacement along the perpendicular to the crack axis direction, u_2, contours (in the deformed specimen configuration) for Figure 91. Values in mm. Applied displacement u_0=0.2541 mm. Case III.

Fig. 104 Displacement along the perpendicular to the crack axis direction, u_2, contours (in the deformed specimen configuration) for Figure 92. Values in mm. Applied displacement u_0=0.2541 mm. Case III.

Fig. 105 Displacement along the perpendicular to the crack axis direction, u_2, contours (in the deformed specimen configuration) for Figure 93. Values in mm. Applied displacement u_0=0.2541 mm. Case III.

Fig. 106 Normal stress along the perpendicular to the crack axis direction, σ_{22}, contours (in the deformed specimen configuration) for Figure 91. Values in kN/mm^2. Applied displacement u_0=0.2541 mm. Case III.

Fig. 107 Normal stress along the perpendicular to the crack axis direction, σ_{22}, contours (in the deformed specimen configuration) for Figure 92. Values in kN/mm^2. Applied displacement u_0=0.2541 mm. Case III.

Fig. 108 Normal stress along the perpendicular to the crack axis direction, σ_{22}, contours (in the deformed specimen configuration) for Figure 93. Values in kN/mm^2 Applied displacement u_0=0.2541 mm. Case III.

Fig. 109 Normal strain along the perpendicular to the crack axis direction, ε_{22}, contours (in the deformed specimen configuration) for Figure 91. Applied displacement u_0=0.2541 mm. Case III.

Fig. 110 Normal strain along the perpendicular to the crack axis direction, ε_{22}, contours (in the deformed specimen configuration) for Figure 92. Applied displacement u_0=0.2541 mm. Case III.

Fig. 111 Normal strain along the perpendicular to the crack axis direction, ε_{22}, contours (in the deformed specimen configuration) for Figure 93. Applied displacement u_0=0.2541 mm. Case III.

Fig. 112 Undeformed (in red) and deformed (in black) finite element grids for half specimen. Applied displacement u_0=3.3295 mm. Case III.

Fig. 113 Undeformed (in red) and deformed (in black) finite element grids for the missing part of Figure 112. Applied displacement u_0=3.3295 mm. Case III.

Fig. 114 Undeformed (in red) and deformed (in black) finite element grids for the missing part of Figure 113. Applied displacement u_0=3.3295 mm. Case III.

Fig. 115 Strain energy density, dW/dV, contours (in the deformed specimen configuration) for Figure 112. Values in kN.mm/mm^3. Applied displacement u_0=3.3295 mm. Case III.

Fig. 116 Strain energy density, dW/dV, contours (in the deformed specimen configuration) for Figure 113. Values in kN.mm/mm^3. Applied displacement u_0=3.3295 mm. Case III.

Fig. 117 Strain energy density, dW/dV, contours (in the deformed specimen configuration) for Figure 114. Values in kN.mm/mm^3. Applied displacement u_0=3.3295 mm. Case III.

Fig. 118 Mises stress, σ_{eff}, contours (in the deformed specimen configuration) for Figure 112. Values in kN/mm^2. Applied displacement u_0=3.3295 mm. Case III.

Fig. 119 Mises stress, σ_{eff}, contours (in the deformed specimen configuration) for Figure 113. Values in kN/mm^2. Applied displacement u_0=3.3295 mm. Case III.

Fig. 120 Mises stress, σ_{eff}, contours (in the deformed specimen configuration) for Figure 114. Values in kN/mm^2. Applied displacement u_0=3.3295 mm. Case III.

Fig. 121 Displacement along the crack axis direction, u_1, contours (in the deformed specimen configuration) for Figure 112. Values in mm. Applied displacement u_0=3.3295 mm. Case III.

Fig. 122 Displacement along the crack axis direction, u_1, contours (in the deformed specimen configuration) for Figure 113. Values in mm. Applied displacement u_0=3.3295 mm. Case III.

Fig. 123 Displacement along the crack axis direction, u_1, contours (in the deformed specimen configuration) for Figure 114. Values in mm. Applied displacement u_0=3.3295 mm. Case III.

Fig. 124 Displacement along the perpendicular to the crack axis direction, u_2 contours (in the deformed specimen configuration) for Figure 112. Values in mm. Applied displacement u_0=3.3295 mm. Case III.

Fig. 125 Displacement along the perpendicular to the crack axis direction, u_2 contours (in the deformed specimen configuration) for Figure 113. Values in mm. Applied displacement u_0=3.3295 mm. Case III.

Fig. 126 Displacement along the perpendicular to the crack axis direction, u_2 contours (in the deformed specimen configuration) for Figure 114. Values in mm. Applied displacement u_0=3.3295 mm. Case III.

Fig. 127 Normal stress along the perpendicular to the crack axis direction, σ_{22}, contours (in the deformed specimen configuration) for Figure 112. Values in kN/mm^2. Applied displacement u_0=3.3295 mm. Case III.

Fig. 128 Normal stress along the perpendicular to the crack axis direction, σ_{22}, contours (in the deformed specimen configuration) for Figure 113. Values in kN/mm^2. Applied displacement u_0=3.3295 mm. Case III.

Fig. 129 Normal stress along the perpendicular to the crack axis direction, σ_{22}, contours (in the deformed specimen configuration) for Figure 114. Values in kN/mm^2. Applied displacement u_0=3.3295 mm. Case III.

Fig. 130 Normal strain along the perpendicular to the crack axis direction, ε_{22}, contours (in the deformed specimen configuration) for Figure 112. Applied displacement u_0=3.3295 mm. Case III.

Fig. 131 Normal strain along the perpendicular to the crack axis direction, ε_{22}, contours (in the deformed specimen configuration) for Figure 113. Applied displacement u_0=3.3295 mm. Case III.

Fig. 132 Normal strain along the perpendicular to the crack axis direction, ε_{22}, contours (in the deformed specimen configuration) for Figure 114. Applied displacement u_0=3.3295 mm. Case III.

Fig. 133 Undeformed (in red) and deformed (in black) finite element grids for half specimen. Applied displacement u_0=0.7623 mm. Case IV.

Fig. 134 Undeformed (in red) and deformed (in black) finite element grids for the missing part of Figure 133. Applied displacement u_0=0.7623 mm. Case IV.

Fig. 135 Undeformed (in red) and deformed (in black) finite element grids for the missing part of Figure 134. Applied displacement u_0=0.7623 mm. Case IV.

Fig. 136 Strain energy density, dW/dV, contours (in the deformed specimen configuration) for Figure 133. Values in kN.mm/mm^3. Applied displacement u_0=0.7623 mm. Case IV.

Fig. 137 Strain energy density, dW/dV, contours (in the deformed specimen configuration) for Figure 134. Values in kN.mm/mm^3. Applied displacement u_0=0.7623 mm. Case IV.

Fig. 138 Strain energy density, dW/dV, contours (in the deformed specimen configuration) for Figure 135. Values in kN.mm/mm^3. Applied displacement u_0=0.7623 mm. Case IV.

Fig. 139 Mises stress, σ_{eff}, contours (in the deformed specimen configuration) for Figure 133. Values in kN/mm^2. Applied displacement u_0=0.7623 mm. Case IV.

Fig. 140 Mises stress, σ_{eff}, contours (in the deformed specimen configuration) for Figure 134. Values in kN/mm^2. Applied displacement u_0=0.7623 mm. Case IV.

Fig. 141 Mises stress, σ_{eff}, contours (in the deformed specimen configuration) for Figure 135. Values in kN/mm^2. Applied displacement u_0=0.7623 mm. Case IV.

Fig. 142 Displacement along the crack axis direction, u_1, contours (in the deformed specimen configuration) for Figure 133. Values in mm. Applied displacement u_0=0.7623 mm. Case IV.

Fig. 143 Displacement along the crack axis direction, u_1, contours (in the deformed specimen configuration) for Figure 134. Values in mm. Applied displacement u_0=0.7623 mm. Case IV.

Fig. 144 Displacement along the crack axis direction, u_1, contours (in the deformed specimen configuration) for Figure 135. Values in mm. Applied displacement u_0=0.7623 mm. Case IV.

Fig. 145 Displacement along the perpendicular to the crack axis direction, u_2, contours (in the deformed specimen configuration) for Figure 133. Values in mm. Applied displacement u_0=0.7623 mm. Case IV.

Fig. 146 Displacement along the perpendicular to the crack axis direction, u_2, contours (in the deformed specimen configuration) for Figure 134. Values in mm. Applied displacement u_0=0.7623 mm. Case IV.

Fig. 147 Displacement along the perpendicular to the crack axis direction, u_2, contours (in the deformed specimen configuration) for Figure 135. Values in mm. Applied displacement u_0=0.7623 mm. Case IV.

Fig. 148 Normal stress along the perpendicular to the crack axis direction, σ_{22}, contours (in the deformed specimen configuration) for Figure 133. Values in kN/mm^2. Applied displacement u_0=0.7623 mm. Case IV.

Fig. 149 Normal stress along the perpendicular to the crack axis direction, σ_{22}, contours (in the deformed specimen configuration) for Figure 134. Values in kN/mm^2. Applied displacement u_0=0.7623 mm. Case IV.

Fig. 150 Normal stress along the perpendicular to the crack axis direction, σ_{22}, contours (in the deformed specimen configuration) for Figure 135. Values in kN/mm^2 Applied displacement u_0=0.7623 mm. Case IV.

Fig. 151 Normal strain along the perpendicular to the crack axis direction, ε_{22}, contours (in the deformed specimen configuration) for Figure 133. Applied displacement u_0=0.7623 mm. Case IV.

Fig. 152 Normal strain along the perpendicular to the crack axis direction, ε_{22}, contours (in the deformed specimen configuration) for Figure 134. Applied displacement u_0=0.7623 mm. Case IV.

Fig. 153 Normal strain along the perpendicular to the crack axis direction, ε_{22}, contours (in the deformed specimen configuration) for Figure 135. Applied displacement u_0=0.7623 mm. Case IV.

Fig. 154 Undeformed (in red) and deformed (in black) finite element grids for half specimen. Applied displacement u_0=3.3295 mm. Case IV.

Fig. 155 Undeformed (in red) and deformed (in black) finite element grids for the missing part of Figure 154. Applied displacement u_0=3.3295 mm. Case IV.

Fig. 156 Undeformed (in red) and deformed (in black) finite element grids for the missing part of Figure 155. Applied displacement u_0=3.3295 mm. Case IV.

Fig. 157 Strain energy density, dW/dV, contours (in the deformed specimen configuration) for Figure 154. Values in kN.mm/mm^3. Applied displacement u_0=3.3295 mm. Case IV.

Fig. 158 Strain energy density, dW/dV, contours (in the deformed specimen configuration) for Figure 155. Values in kN.mm/mm^3. Applied displacement u_0=3.3295 mm. Case IV.

Fig. 159 Strain energy density, dW/dV, contours (in the deformed specimen configuration) for Figure 156. Values in kN.mm/mm^3. Applied displacement u_0=3.3295 mm. Case IV.

Fig. 160 Mises stress, σ_{eff}, contours (in the deformed specimen configuration) for Figure 154. Values in kN/mm^2. Applied displacement u_0=3.3295 mm. Case IV.

Fig. 161 Mises stress, σ_{eff}, contours (in the deformed specimen configuration) for Figure 155. Values in kN/mm^2. Applied displacement u_0=3.3295 mm. Case IV.

Fig. 162 Mises stress, σ_{eff}, contours (in the deformed specimen configuration) for Figure 156. Values in kN/mm^2. Applied displacement u_0=3.3295 mm. Case IV.

Fig. 163 Displacement along the crack axis direction, u_1, contours (in the deformed specimen configuration) for Figure 154. Values in mm. Applied displacement u_0=3.3295 mm. Case IV.

Fig. 164 Displacement along the crack axis direction, u_1, contours (in the deformed specimen configuration) for Figure 155. Values in mm. Applied displacement u_0=3.3295 mm. Case IV.

Fig. 165 Displacement along the crack axis direction, u_1, contours (in the deformed specimen configuration) for Figure 156. Values in mm. Applied displacement u_0=3.3295 mm. Case IV.

Fig. 166 Displacement along the perpendicular to the crack axis direction, u_2 contours (in the deformed specimen configuration) for Figure 154. Values in mm. Applied displacement u_0=3.3295 mm. Case IV.

Fig. 167 Displacement along the perpendicular to the crack axis direction, u_2 contours (in the deformed specimen configuration) for Figure 155. Values in mm. Applied displacement u_0=3.3295 mm. Case IV.

Fig. 168 Displacement along the perpendicular to the crack axis direction, u_2 contours (in the deformed specimen configuration) for Figure 156. Values in mm. Applied displacement u_0=3.3295 mm. Case IV.

Fig. 169 Normal stress along the perpendicular to the crack axis direction, σ_{22}, contours (in the deformed specimen configuration) for Figure 154. Values in kN/mm^2. Applied displacement u_0=3.3295 mm. Case IV.

Fig. 170 Normal stress along the perpendicular to the crack axis direction, σ_{22}, contours (in the deformed specimen configuration) for Figure 155. Values in kN/mm^2. Applied displacement u_0=3.3295 mm. Case IV.

Fig. 171 Normal stress along the perpendicular to the crack axis direction, σ_{22}, contours (in the deformed specimen configuration) for Figure 156. Values in kN/mm^2. Applied displacement u_0=3.3295 mm. Case IV.

Fig. 172 Normal strain along the perpendicular to the crack axis direction, ε_{22}, contours (in the deformed specimen configuration) for Figure 154. Applied displacement u_0=3.3295 mm. Case IV.

Fig. 173 Normal strain along the perpendicular to the crack axis direction, ε_{22}, contours (in the deformed specimen configuration) for Figure 155. Applied displacement u_0=3.3295 mm. Case IV.

Fig. 174 Normal strain along the perpendicular to the crack axis direction, ε_{22}, contours (in the deformed specimen configuration) for Figure 156. Applied displacement u_0=3.3295 mm. Case IV.

Fig. 175 Undeformed (in red) and deformed (in black) finite element grids for half specimen. Applied displacement u_0=0.5082 mm. Case V.

Fig. 176 Undeformed (in red) and deformed (in black) finite element grids for the missing part of Figure 175. Applied displacement u_0=0.5082 mm. Case V.

Fig. 177 Undeformed (in red) and deformed (in black) finite element grids for the missing part of Figure 176. Applied displacement u_0=0.5082 mm. Case V.

Fig. 178 Strain energy density, dW/dV, contours (in the deformed specimen configuration) for Figure 175. Values in kN.mm/mm^3. Applied displacement u_0=0.5082 mm. Case V.

Fig. 179 Strain energy density, dW/dV, contours (in the deformed specimen configuration) for Figure 176. Values in kN.mm/mm^3. Applied displacement u_0=0.5082 mm. Case V.

Fig. 180 Strain energy density, dW/dV, contours (in the deformed specimen configuration) for Figure 177. Values in kN.mm/mm^3. Applied displacement u_0=0.5082 mm. Case V.

Fig. 181 Mises stress, σ_{eff}, contours (in the deformed specimen configuration) for Figure 175. Values in kN/mm^2. Applied displacement u_0=0.5082 mm. Case V.

Fig. 182 Mises stress, σ_{eff}, contours (in the deformed specimen configuration) for Figure 176. Values in kN/mm^2. Applied displacement u_0=0.5082 mm. Case V.

Fig. 183 Mises stress, σ_{eff}, contours (in the deformed specimen configuration) for Figure 177. Values in kN/mm^2. Applied displacement u_0=0.5082 mm. Case V.

Fig. 184 Displacement along the crack axis direction, u_1, contours (in the deformed specimen configuration) for Figure 175. Values in mm. Applied displacement u_0=0.5082 mm. Case V.

Fig. 185 Displacement along the crack axis direction, u_1, contours (in the deformed specimen configuration) for Figure 176. Values in mm. Applied displacement u_0=0.5082 mm. Case V.

Fig. 186 Displacement along the crack axis direction, u_1, contours (in the deformed specimen configuration) for Figure 177. Values in mm. Applied displacement u_0=0.5082 mm. Case V.

Fig. 187 Displacement along the perpendicular to the crack axis direction, u_2, contours (in the deformed specimen configuration) for Figure 175. Values in mm. Applied displacement u_0=0.5082 mm. Case V.

Fig. 188 Displacement along the perpendicular to the crack axis direction, u_2, contours (in the deformed specimen configuration) for Figure 176. Values in mm. Applied displacement u_0=0.5082 mm. Case V.

Fig. 189 Displacement along the perpendicular to the crack axis direction, u_2, contours (in the deformed specimen configuration) for Figure 177. Values in mm. Applied displacement u_0=0.5082 mm. Case V.

Fig. 190 Normal stress along the perpendicular to the crack axis direction, σ_{22}, contours (in the deformed specimen configuration) for Figure 175. Values in kN/mm^2. Applied displacement u_0=0.5082 mm. Case V.

Fig. 191 Normal stress along the perpendicular to the crack axis direction, σ_{22}, contours (in the deformed specimen configuration) for Figure 176. Values in kN/mm^2. Applied displacement u_0=0.5082 mm. Case V.

Fig. 192 Normal stress along the perpendicular to the crack axis direction, σ_{22}, contours (in the deformed specimen configuration) for Figure 177. Values in kN/mm^2 Applied displacement u_0=0.5082 mm. Case V.

Fig. 193 Normal strain along the perpendicular to the crack axis direction, ε_{22}, contours (in the deformed specimen configuration) for Figure 175. Applied displacement u_0=0.5082 mm. Case V.

Fig. 194 Normal strain along the perpendicular to the crack axis direction, ε_{22}, contours (in the deformed specimen configuration) for Figure 176. Applied displacement u_0=0.5082 mm. Case V.

Fig. 195 Normal strain along the perpendicular to the crack axis direction, ε_{22}, contours (in the deformed specimen configuration) for Figure 177. Applied displacement u_0=0.5082 mm. Case V.

Fig. 196 Undeformed (in red) and deformed (in black) finite element grids for half specimen. Applied displacement u_0=3.3295 mm. Case V.

Fig. 197 Undeformed (in red) and deformed (in black) finite element grids for the missing part of Figure 196. Applied displacement u_0=3.3295 mm. Case V.

Fig. 198 Undeformed (in red) and deformed (in black) finite element grids for the missing part of Figure 197. Applied displacement u_0=3.3295 mm. Case V.

Fig. 199 Strain energy density, dW/dV, contours (in the deformed specimen configuration) for Figure 196. Values in kN.mm/mm^3. Applied displacement u_0=3.3295 mm. Case V.

Fig. 200 Strain energy density, dW/dV, contours (in the deformed specimen configuration) for Figure 197. Values in kN.mm/mm^3. Applied displacement u_0=3.3295 mm. Case V.

Fig. 201 Strain energy density, dW/dV, contours (in the deformed specimen configuration) for Figure 198. Values in kN.mm/mm^3. Applied displacement u_0=3.3295 mm. Case V.

Fig. 202 Mises stress, σ_{eff}, contours (in the deformed specimen configuration) for Figure 196. Values in kN/mm^2. Applied displacement u_0=3.3295 mm. Case V.

Fig. 203 Mises stress, σ_{eff}, contours (in the deformed specimen configuration) for Figure 197. Values in kN/mm^2. Applied displacement u_0=3.3295 mm. Case V.

Fig. 204 Mises stress, σ_{eff}, contours (in the deformed specimen configuration) for Figure 198. Values in kN/mm^2. Applied displacement u_0=3.3295 mm. Case V.

Fig. 205 Displacement along the crack axis direction, u_1, contours (in the deformed specimen configuration) for Figure 196. Values in mm. Applied displacement u_0=3.3295 mm. Case V.

Fig. 206 Displacement along the crack axis direction, u_1, contours (in the deformed specimen configuration) for Figure 197. Values in mm. Applied displacement u_0=3.3295 mm. Case V.

Fig. 207 Displacement along the crack axis direction, u_1, contours (in the deformed specimen configuration) for Figure 198. Values in mm. Applied displacement u_0=3.3295 mm. Case V.

Fig. 208 Displacement along the perpendicular to the crack axis direction, u_2 contours (in the deformed specimen configuration) for Figure 196. Values in mm. Applied displacement u_0=3.3295 mm. Case V.

Fig. 209 Displacement along the perpendicular to the crack axis direction, u_2 contours (in the deformed specimen configuration) for Figure 197. Values in mm. Applied displacement u_0=3.3295 mm. Case V.

Fig. 210 Displacement along the perpendicular to the crack axis direction, u_2 contours (in the deformed specimen configuration) for Figure 198. Values in mm. Applied displacement u_0=3.3295 mm. Case V.

Fig. 211 Normal stress along the perpendicular to the crack axis direction, σ_{22}, contours (in the deformed specimen configuration) for Figure 196. Values in kN/mm^2. Applied displacement u_0=3.3295 mm. Case V.

Fig. 212 Normal stress along the perpendicular to the crack axis direction, σ_{22}, contours (in the deformed specimen configuration) for Figure 197. Values in kN/mm^2. Applied displacement u_0=3.3295 mm. Case V.

Fig. 213 Normal stress along the perpendicular to the crack axis direction, σ_{22}, contours (in the deformed specimen configuration) for Figure 198. Values in kN/mm^2. Applied displacement u_0=3.3295 mm. Case V.

Fig. 214 Normal strain along the perpendicular to the crack axis direction, ε_{22}, contours (in the deformed specimen configuration) for Figure 196. Applied displacement u_0=3.3295 mm. Case V.

Fig. 215 Normal strain along the perpendicular to the crack axis direction, ε_{22}, contours (in the deformed specimen configuration) for Figure 197. Applied displacement u_0=3.3295 mm. Case V.

Fig. 216 Normal strain along the perpendicular to the crack axis direction, ε_{22}, contours (in the deformed specimen configuration) for Figure 198. Applied displacement u_0=3.3295 mm. Case V.

Fig. 217 Undeformed (in red) and deformed (in black) finite element grids for half specimen. Applied displacement u_0=0.4235 mm. Case VI.

Fig. 218 Undeformed (in red) and deformed (in black) finite element grids for the missing part of Figure 217. Applied displacement u_0=0.4235 mm. Case VI.

Fig. 219 Undeformed (in red) and deformed (in black) finite element grids for the missing part of Figure 218. Applied displacement u_0=0.4235 mm. Case VI.

Fig. 220 Strain energy density, dW/dV, contours (in the deformed specimen configuration) for Figure 217. Values in kN.mm/mm^3. Applied displacement u_0=0.4235 mm. Case VI.

Fig. 221 Strain energy density, dW/dV, contours (in the deformed specimen configuration) for Figure 218. Values in kN.mm/mm^3. Applied displacement u_0=0.4235 mm. Case VI.

Fig. 222 Strain energy density, dW/dV, contours (in the deformed specimen configuration) for Figure 219. Values in kN.mm/mm^3. Applied displacement u_0=0.4235 mm. Case VI.

Fig. 223 Mises stress, σ_{eff}, contours (in the deformed specimen configuration) for Figure 217. Values in kN/mm^2. Applied displacement u_0=0.4235 mm. Case VI.

Fig. 224 Mises stress, σ_{eff}, contours (in the deformed specimen configuration) for Figure 218. Values in kN/mm^2. Applied displacement u_0=0.4235 mm. Case VI.

Fig. 225 Mises stress, σ_{eff}, contours (in the deformed specimen configuration) for Figure 219. Values in kN/mm^2. Applied displacement u_0=0.4235 mm. Case VI.

Fig. 226 Displacement along the crack axis direction, u_1, contours (in the deformed specimen configuration) for Figure 217. Values in mm. Applied displacement u_0=0.4235 mm. Case VI.

Fig. 227 Displacement along the crack axis direction, u_1, contours (in the deformed specimen configuration) for Figure 218. Values in mm. Applied displacement u_0=0.4235 mm. Case VI.

Fig. 228 Displacement along the crack axis direction, u_1, contours (in the deformed specimen configuration) for Figure 219. Values in mm. Applied displacement u_0=0.4235 mm. Case VI.

Fig. 229 Displacement along the perpendicular to the crack axis direction, u_2, contours (in the deformed specimen configuration) for Figure 217. Values in mm. Applied displacement u_0=0.4235 mm. Case VI.

Fig. 230 Displacement along the perpendicular to the crack axis direction, u_2, contours (in the deformed specimen configuration) for Figure 218. Values in mm. Applied displacement u_0=0.4235 mm. Case VI.

Fig. 231 Displacement along the perpendicular to the crack axis direction, u_2, contours (in the deformed specimen configuration) for Figure 219. Values in mm. Applied displacement u_0=0.4235 mm. Case VI.

Fig. 232 Normal stress along the perpendicular to the crack axis direction, σ_{22}, contours (in the deformed specimen configuration) for Figure 217. Values in kN/mm^2. Applied displacement u_0=0.4235 mm. Case VI.

Fig. 233 Normal stress along the perpendicular to the crack axis direction, σ_{22}, contours (in the deformed specimen configuration) for Figure 218. Values in kN/mm^2. Applied displacement u_0=0.4235 mm. Case VI.

Fig. 234 Normal stress along the perpendicular to the crack axis direction, σ_{22}, contours (in the deformed specimen configuration) for Figure 219. Values in kN/mm^2 Applied displacement u_0=0.4235 mm. Case VI.

Fig. 235 Normal strain along the perpendicular to the crack axis direction, ε_{22}, contours (in the deformed specimen configuration) for Figure 217. Applied displacement u_0=0.4235 mm. Case VI.

Fig. 236 Normal strain along the perpendicular to the crack axis direction, ε_{22}, contours (in the deformed specimen configuration) for Figure 218. Applied displacement u_0=0.4235 mm. Case VI.

Fig. 237 Normal strain along the perpendicular to the crack axis direction, ε_{22}, contours (in the deformed specimen configuration) for Figure 219. Applied displacement u_0=0.4235 mm. Case VI.

Fig. 238 Undeformed (in red) and deformed (in black) finite element grids for half specimen. Applied displacement u_0=3.3295 mm. Case VI.

Fig. 239 Undeformed (in red) and deformed (in black) finite element grids for the missing part of Figure 238. Applied displacement u_0=3.3295 mm. Case VI.

Fig. 240 Undeformed (in red) and deformed (in black) finite element grids for the missing part of Figure 239. Applied displacement u_0=3.3295 mm. Case VI.

Fig. 241 Strain energy density, dW/dV, contours (in the deformed specimen configuration) for Figure 238. Values in kN.mm/mm^3. Applied displacement u_0=3.3295 mm. Case VI.

Fig. 242 Strain energy density, dW/dV, contours (in the deformed specimen configuration) for Figure 239. Values in kN.mm/mm^3. Applied displacement u_0=3.3295 mm. Case VI.

Fig. 243 Strain energy density, dW/dV, contours (in the deformed specimen configuration) for Figure 240. Values in kN.mm/mm^3. Applied displacement u_0=3.3295 mm. Case VI.

Fig. 244 Mises stress, σ_{eff}, contours (in the deformed specimen configuration) for Figure 238. Values in kN/mm^2. Applied displacement u_0=3.3295 mm. Case VI.

Fig. 245 Mises stress, σ_{eff}, contours (in the deformed specimen configuration) for Figure 239. Values in kN/mm^2. Applied displacement u_0=3.3295 mm. Case VI.

Fig. 246 Mises stress, σ_{eff}, contours (in the deformed specimen configuration) for Figure 240. Values in kN/mm^2. Applied displacement u_0=3.3295 mm. Case VI.

Fig. 247 Displacement along the crack axis direction, u_1, contours (in the deformed specimen configuration) for Figure 238. Values in mm. Applied displacement u_0=3.3295 mm. Case VI.

Fig. 248 Displacement along the crack axis direction, u_1, contours (in the deformed specimen configuration) for Figure 239. Values in mm. Applied displacement u_0=3.3295 mm. Case VI.

Fig. 249 Displacement along the crack axis direction, u_1, contours (in the deformed specimen configuration) for Figure 240. Values in mm. Applied displacement u_0=3.3295 mm. Case VI.

Fig. 250 Displacement along the perpendicular to the crack axis direction, u_2 contours (in the deformed specimen configuration) for Figure 238. Values in mm. Applied displacement u_0=3.3295 mm. Case VI.

Fig. 251 Displacement along the perpendicular to the crack axis direction, u_2 contours (in the deformed specimen configuration) for Figure 239. Values in mm. Applied displacement u_0=3.3295 mm. Case VI.

Fig. 252 Displacement along the perpendicular to the crack axis direction, u_2 contours (in the deformed specimen configuration) for Figure 240. Values in mm. Applied displacement u_0=3.3295 mm. Case VI.

Fig. 253 Normal stress along the perpendicular to the crack axis direction, σ_{22}, contours (in the deformed specimen configuration) for Figure 238. Values in kN/mm^2. Applied displacement u_0=3.3295 mm. Case VI.

Fig. 254 Normal stress along the perpendicular to the crack axis direction, σ_{22}, contours (in the deformed specimen configuration) for Figure 239. Values in kN/mm^2. Applied displacement u_0=3.3295 mm. Case VI.

Fig. 255 Normal stress along the perpendicular to the crack axis direction, σ_{22}, contours (in the deformed specimen configuration) for Figure 240. Values in kN/mm^2. Applied displacement u_0=3.3295 mm. Case VI.

Fig. 256 Normal strain along the perpendicular to the crack axis direction, ε_{22}, contours (in the deformed specimen configuration) for Figure 238. Applied displacement u_0=3.3295 mm. Case VI.

Fig. 257 Normal strain along the perpendicular to the crack axis direction, ε_{22}, contours (in the deformed specimen configuration) for Figure 239. Applied displacement u_0=3.3295 mm. Case VI.

Fig. 258 Normal strain along the perpendicular to the crack axis direction, ε_{22}, contours (in the deformed specimen configuration) for Figure 240. Applied displacement u_0=3.3295 mm. Case VI.

Fig. 259 Deformed profile of crack faces near the crack tip for various values of uniform displacement. Case I.

Fig. 260 Strain energy density, dW/dV, ahead of crack tip for various values of uniform displacement. Values in kN.mm/mm^3. Case I.

Fig. 261 Mises stress, σ_{eff}, ahead of crack tip for various values of uniform displacement. Values in kN/mm^2. Case I.

Fig. 262 Normal stress along the perpendicular to the crack axis direction, σ_y, ahead of crack tip for various values of uniform displacement. Values in kN/mm^2. Case I.

Fig. 263 Effective strain, ε_{eff}, ahead of crack tip for various values of uniform displacement. Case I.

Fig. 264 Normal strain along the perpendicular to the crack axis direction, ε_y, ahead of crack tip for various values of uniform displacement. Case I.

Fig. 265 Strain energy density ahead of crack tip for three values of the applied displacement. The critical value of strain energy density is 15×10^{-5} kNmm/mm^3. Case I.

Fig. 266 Strain energy density, dW/dV, versus applied displacement (1 sec=0.0847 mm) at nodes 10 (red line, at a distance 0.005 mm from the crack tip), 20 (green line, at a distance 0.018 mm from the crack tip) and 49 (blue line, at a distance 0.254 mm from the crack tip). Nodes 10, 20 and 49 lie along the crack ligament. Values in $kN.mm/mm^3$. Case I.

Fig. 267 Mises stress, σ_{eff}, versus applied displacement (1 sec=0.0847 mm) at nodes 10 (red line, at a distance 0.005 mm from the crack tip), 20 (green line, at a distance 0.018 mm from the crack tip) and 49 (blue line, at a distance 0.254 mm from the crack tip). Nodes 10, 20 and 49 lie along the crack ligament. Values in kN/mm^2. Case I.

Fig. 268 Normal strain along the perpendicular to the crack axis direction, ε_y, versus applied displacement (1 sec=0.0847 mm) at nodes 10 (red line, at a distance 0.005 mm from the crack tip), 20 (green line, at a distance 0.018 mm from the crack tip) and 49 (blue line, at a distance 0.254 mm from the crack tip). Nodes 10, 20 and 49 lie along the crack ligament. Case I.

Fig. 269 Applied displacement versus crack growth length during stable crack growth. Case I.

Fig. 270 Stress intensity factor versus crack growth length during stable crack growth. Case I.

Fig. 271 Strain energy density factor versus crack growth length during stable crack growth. Case I.

Fig. 272 Deformed profile of crack faces near the crack tip for various values of uniform displacement. Case II.

Fig. 273 Strain energy density, dW/dV, ahead of crack tip for various values of uniform displacement. Values in $kN.mm/mm^3$. Case II.

Fig. 274 Mises stress, σ_{eff}, ahead of crack tip for various values of uniform displacement. Values in kN/mm^2. Case II.

Fig. 275 Normal stress along the perpendicular to the crack axis direction, σ_y, ahead of crack tip for various values of uniform displacement. Values in kN/mm^2. Case II.

Fig. 276 Effective strain, ε_{eff}, ahead of crack tip for various values of uniform displacement. Case II.

Fig. 277 Normal strain along the perpendicular to the crack axis direction, ε_y, ahead of crack tip for various values of uniform displacement. Case II.

Fig. 278 Strain energy density ahead of crack tip for three values of the applied displacement. The critical value of strain energy density is $15x10^{-5}$ $kNmm/mm^3$. Case II.

Fig. 279 Strain energy density, dW/dV, versus applied displacement (1 sec=0.0847 mm) at nodes 10 (red line, at a distance 0.005 mm from the crack tip), 20 (green line, at a distance 0.018 mm from the crack tip) and 49 (blue line, at a distance 0.254 mm from the crack tip). Nodes 10, 20 and 49 lie along the crack ligament. Values in $kN.mm/mm^3$. Case II.

Fig. 280 Mises stress, σ_{eff}, versus applied displacement (1 sec=0.0847 mm) at nodes 10 (red line, at a distance 0.005 mm from the crack tip), 20 (green line, at a distance 0.018 mm from the crack tip) and 49 (blue line, at a distance 0.254 mm from the crack tip). Nodes 10, 20 and 49 lie along the crack ligament. Values in kN/mm^2. Case II.

Fig. 281 Normal strain along the perpendicular to the crack axis direction, ε_y, versus applied displacement (1 sec=0.0847 mm) at nodes 10 (red line, at a distance 0.005 mm from the crack tip), 20 (green line, at a distance 0.018 mm from the crack tip) and 49 (blue line, at a distance 0.254 mm from the crack tip). Nodes 10, 20 and 49 lie along the crack ligament. Case II.

Fig. 282 Applied displacement versus crack growth length during stable crack growth. Case II.

Fig. 283 Stress intensity factor versus crack growth length during stable crack growth. Case II.

Fig. 284 Strain energy density factor versus crack growth length during stable crack growth. Case II.

Fig. 285 Deformed profile of crack faces near the crack tip for various values of uniform displacement. Case III.

Fig. 286 Strain energy density, dW/dV, ahead of crack tip for various values of uniform displacement. Values in $kN.mm/mm^3$. Case III.

Fig. 287 Mises stress, σ_{eff}, ahead of crack tip for various values of uniform displacement. Values in kN/mm^2. Case III.

Fig. 288 Normal stress along the perpendicular to the crack axis direction, σ_y, ahead of crack tip for various values of uniform displacement. Values in kN/mm^2. Case III.

Fig. 289 Effective strain, ε_{eff}, ahead of crack tip for various values of uniform displacement. Case III.

Fig. 290 Normal strain along the perpendicular to the crack axis direction, ε_y, ahead of crack tip for various values of uniform displacement. Case III.

Fig. 291 Strain energy density ahead of crack tip for three values of the applied displacement. The critical value of strain energy density is $15x10^{-5}$ $kNmm/mm^3$. Case III.

Fig. 292 Strain energy density, dW/dV, versus applied displacement (1 sec=0.0847 mm) at nodes 10 (red line, at a distance 0.005 mm from the crack tip), 20 (green line, at a distance 0.018 mm from the crack tip) and 49 (blue line, at a distance 0.254 mm from the crack tip). Nodes 10, 20 and 49 lie along the crack ligament. Values in $kN.mm/mm^3$. Case III.

Fig. 293 Mises stress, σ_{eff}, versus applied displacement (1 sec=0.0847 mm) at nodes 10 (red line, at a distance 0.005 mm from the crack tip), 20 (green line, at a distance 0.018 mm from the crack tip) and 49 (blue line, at a distance 0.254 mm from the crack tip). Nodes 10, 20 and 49 lie along the crack ligament. Values in kN/mm^2. Case III.

Fig. 294 Normal strain along the perpendicular to the crack axis direction, ε_y, versus applied displacement (1 sec=0.0847 mm) at nodes 10 (red line, at a distance 0.005 mm from the crack tip), 20 (green line, at a distance 0.018 mm from the crack tip) and 49 (blue line, at a distance 0.254 mm from the crack tip). Nodes 10, 20 and 49 lie along the crack ligament. Case III.

Fig. 295 Applied displacement versus crack growth length during stable crack growth. Case III.

Fig. 296 Stress intensity factor versus crack growth length during stable crack growth. Case III.

Fig. 297 Strain energy density factor versus crack growth length during stable crack growth. Case III.

Fig. 298 Deformed profile of crack faces near the crack tip for various values of uniform displacement. Case IV.

Fig. 299 Strain energy density, dW/dV, ahead of crack tip for various values of uniform displacement. Values in $kN.mm/mm^3$. Case IV.

Fig. 300 Mises stress, σ_{eff}, ahead of crack tip for various values of uniform displacement. Values in kN/mm^2. Case IV.

Fig. 301 Normal stress along the perpendicular to the crack axis direction, σ_y, ahead of crack tip for various values of uniform displacement. Values in kN/mm^2. Case IV.

Fig. 302 Effective strain, ε_{eff}, ahead of crack tip for various values of uniform displacement. Case IV.

Fig. 303 Normal strain along the perpendicular to the crack axis direction, ε_y, ahead of crack tip for various values of uniform displacement. Case IV.

Fig. 304 Strain energy density ahad of from crack tip for three values of the applied displacement. The critical value of strain energy density is $15x10^{-5}$ kNmm/mm^3 . Case IV.

Fig. 305 Strain energy density, dW/dV, versus applied displacement (1 sec=0.0847 mm) at nodes 10 (red line, at a distance 0.005 mm from the crack tip), 20 (green line, at a distance 0.018 mm from the crack tip) and 49 (blue line, at a distance 0.254 mm from the crack tip). Nodes 10, 20 and 49 lie along the crack ligament. Values in kN.mm/mm^3. Case IV.

Fig. 306 Mises stress, σ_{eff}, versus applied displacement (1 sec=0.0847 mm) at nodes 10 (red line, at a distance 0.005 mm from the crack tip), 20 (green line, at a distance 0.018 mm from the crack tip) and 49 (blue line, at a distance 0.254 mm from the crack tip). Nodes 10, 20 and 49 lie along the crack ligament. Values in kN/mm^2. Case IV.

Fig. 307 Normal strain along the perpendicular to the crack axis direction, ε_y, versus applied displacement (1 sec=0.0847 mm) at nodes 10 (red line, at a distance 0.005 mm from the crack tip), 20 (green line, at a distance 0.018 mm from the crack tip) and 49 (blue line, at a distance 0.254 mm from the crack tip). Nodes 10, 20 and 49 lie along the crack ligament. Case IV.

Fig. 308 Applied displacement versus crack growth length during stable crack growth. Case IV.

Fig. 309 Stress intensity factor versus crack growth length during stable crack growth. Case IV.

Fig. 310 Strain energy density factor versus crack growth length during stable crack growth. Case IV.

Fig. 311 Deformed profile of crack faces near the crack tip for various values of uniform displacement. Case V.

Fig. 312 Strain energy density, dW/dV, ahead of crack tip for various values of uniform displacement. Values in kN.mm/mm^3. Case V.

Fig. 313 Mises stress, σ_{eff}, ahead of crack tip for various values of uniform displacement. Values in kN/mm^2. Case V.

Fig. 314 Normal stress along the perpendicular to the crack axis direction, σ_y, ahead of crack tip for various values of uniform displacement. Values in kN/mm^2. Case V.

Fig. 315 Effective strain, ε_{eff}, ahead of crack tip for various values of uniform displacement. Case V.

Fig. 316 Normal strain along the perpendicular to the crack axis direction, ε_y, ahead of crack tip for various values of uniform displacement. Case V.

Fig. 317 Strain energy density ahead of crack tip for three values of the applied displacement. The critical value of strain energy density is $15x10^{-5}$ kNmm/mm^3 . Case V.

Fig. 318 Strain energy density, dW/dV, versus applied displacement (1 sec=0.0847 mm) at nodes 10 (red line, at a distance 0.005 mm from the crack tip), 20 (green line, at a distance 0.018 mm from the crack tip) and 49 (blue line, at a distance 0.254 mm from the crack tip). Nodes 10, 20 and 49 lie along the crack ligament. Values in kN.mm/mm^3. Case V.

Fig. 319 Mises stress, σ_{eff}, versus applied displacement (1 sec=0.0847 mm) at nodes 10 (red line, at a distance 0.005 mm from the crack tip), 20 (green line, at a distance 0.018 mm from the crack tip) and 49 (blue line, at a distance 0.254 mm from the crack tip). Nodes 10, 20 and 49 lie along the crack ligament. Values in kN/mm^2. Case V.

Fig. 320 Normal strain along the perpendicular to the crack axis direction, ε_y, versus applied displacement (1 sec=0.0847 mm) at nodes 10 (red line, at a distance 0.005 mm from the crack tip), 20 (green line, at a distance 0.018 mm from the crack tip) and 49 (blue line, at a distance 0.254 mm from the crack tip). Nodes 10, 20 and 49 lie along the crack ligament. Case V.

Fig. 321 Applied displacement versus crack growth length during stable crack growth. Case V.

Fig. 322 Stress intensity factor versus crack growth length during stable crack growth. Case V.

Fig. 323 Strain energy density factor versus crack growth length during stable crack growth. Case V.

Fig. 324 Deformed profile of crack faces near the crack tip for various values of uniform displacement. Case VI.

Fig. 325 Strain energy density, dW/dV, ahead of crack tip for various values of uniform displacement. Values in kN.mm/mm^3. Case VI.

Fig. 326 Mises stress, σ_{eff}, ahead of crack tip for various values of uniform displacement. Values in kN/mm^2. Case VI.

Fig. 327 Normal stres s along the perpendicular to the crack axis direction, σ_y, ahead of crack tip for various values of uniform displacement. Values in kN/mm^2. Case VI.

Fig. 328 Effective strain, ε_{eff} , ahead of crack tip for various values of uniform displacement. Case VI.

Fig. 329 Normal strain along the perpendicular to the crack axis direction, ε_y, ahead of crack tip for various values of uniform displacement. Case VI.

Fig. 330 Strain energy density ahead of crack tip for three values of the applied displacement. The critical value of strain energy density is 15×10^{-5} kNmm/mm^3 . Case VI.

Fig. 331 Strain energy density, dW/dV, versus applied displacement (1 sec=0.0847 mm) at nodes 10 (red line, at a distance 0.005 mm from the crack tip), 20 (green line, at a distance 0.018 mm from the crack tip) and 49 (blue line, at a distance 0.254 mm from the crack tip). Nodes 10, 20 and 49 lie along the crack ligament. Values in kN.mm/mm^3. Case VI.

Fig. 332 Mises stress, σ_{eff}, versus applied displacement (1 sec=0.0847 mm) at nodes 10 (red line, at a distance 0.005 mm from the crack tip), 20 (green line, at a distance 0.018 mm from the crack tip) and 49 (blue line, at a distance 0.254 mm from the crack tip). Nodes 10, 20 and 49 lie along the crack ligament. Values in kN/mm^2. Case VI.

Fig. 333 Normal strain along the perpendicular to the crack axis direction, ε_y, versus applied displacement (1 sec=0.0847 mm) at nodes 10 (red line, at a distance 0.005 mm from the crack tip), 20 (green line, at a distance 0.018 mm from the crack tip) and 49 (blue line, at a distance 0.254 mm from the crack tip). Nodes 10, 20 and 49 lie along the crack ligament. Case VI.

Fig. 334 Applied displacement versus crack growth length during stable crack growth. Case VI.

Fig. 335 Stress intensity factor versus crack growth length during stable crack growth. Case VI.

Fig. 336 Strain energy density factor versus crack growth length during stable crack growth. Case VI.

Fig. 337 Deformed profiles of crack faces near the crack tip for two specimen geometries with W=76.2 mm and h=25.4 mm (dotted lines) and W=25.4 mm and h=76.2 mm (continuous lines). Crack length a=2.54 mm. Applied displacement u=1.2705 mm and u=3.3295 mm.

Fig. 338 Strain energy density, dW/dV, ahead of crack tip for specimen geometry with W=76.2 mm and h=25.4 mm and three different crack lengths a=2.54 mm (red line), a=15.24 mm (green line) and a=30.48 mm (blue line). Applied displacement u=0.847 mm.

Fig. 339 Mises stress, σ_{eff}, ahead of crack tip for specimen geometry with W=76.2 mm and h=25.4 mm and three different crack lengths a=2.54 mm (red line), a=15.24 mm (green line) and a=30.48 mm (blue line). Applied displacement u=0.847 mm.

Fig. 340 Strain energy density, dW/dV, ahead of crack tip for specimen geometry with W=76.2 mm and h=25.4 mm and three different crack lengths a=2.54 mm (red line), a=15.24 mm (green line) and a=30.48 mm (blue line). Applied displacement u=3.3295 mm.

Fig. 341 Mises stress, σ_{eff}, ahead of crack tip for specimen geometry with W=76.2 mm and h=25.4 mm and three different crack lengths a=2.54 mm (red line), a=15.24 mm (green line) and a=30.48 mm (blue line). Applied displacement u=3.3295 mm.

Fig. 342 Strain energy density, dW/dV, ahead of crack tip for specimen geometry with W=25.4 mm and h=76.2 mm and three different crack lengths a=2.54 mm (red line), a=5.08 mm (green line) and a=10.16 mm (blue line). Applied displacement u=0.847 mm.

Fig. 343 Mises stress, σ_{eff}, ahead of crack tip for specimen geometry with W=25.4 mm and h=76.2 mm and three different crack lengths a=2.54 mm (red line), a=5.08 mm (green line) and a=10.16 mm (blue line). Applied displacement u=0.847 mm.

Fig. 344 Strain energy density, dW/dV, ahead of crack tip for specimen geometry with W=25.4 mm and h=76.2 mm and three different crack lengths a=2.54 mm (red line), a=5.08 mm (green line) and a=10.16 mm (blue line). Applied displacement u=3.3295 mm.

Fig. 345 Mises stress, σ_{eff}, ahead of crack tip for specimen geometry with W=25.4 mm and h=76.2 mm and three different crack lengths a=2.54 mm (red line), a=5.08 mm (green line) and a=10.16 mm (blue line). Applied displacement u=3.3295 mm.

Fig. 346 Strain energy density, dW/dV, ahead of crack tip for specimens geometries with W=76.2 mm and h=25.4 mm (red line) and W=25.4 mm and h=76.2 mm (green line). a=2.54 mm. Applied displacement u=0.847 mm.

Fig. 347 Mises stress, σ_{eff}, ahead of crack tip for specimens geometries with W=76.2 mm and h=25.4 mm (red line) and W=25.4 mm and h=76.2 mm (green line). a=2.54 mm. Applied displacement u=0.847 mm.

Fig. 348 Strain energy density, dW/dV, ahead of crack tip for specimens geometries with W=76.2 mm and h=25.4 mm (red line) and W=25.4 mm and h=76.2 mm (green line). a=2.54 mm. Applied displacement u=3.3295 mm.

Fig. 349 Mises stress, σ_{eff}, ahead of crack tip for specimens geometries with W=76.2 mm and h=25.4 mm (red line) and W=25.4 mm and h=76.2 mm (green line). a=2.54 mm. Applied displacement u=3.3295 mm.

Table I

Geometry of Edge Cracked Specimen

Case	W(mm)	h(mm)	a(mm)
I	76.2	25.4	2.54
II	76.2	25.4	15.24
III	76.2	25.4	30.48
IV	25.4	76.2	2.54
V	25.4	76.2	5.08
VI	25.4	76.2	10.16

Table II

Critical values of the applied displacement for crack initiation, u_i, and unstable growth, u_c and crack growth incrtement (a_c-a) from initiation to instablility.

Case	u_i (mm)	u_c (mm)	a_c-a (mm)
I	0.3388	3.1339	16.3621
II	0.2541	2.6120	14.6200
III	0.2541	2.4610	13.6900
IV	0.7623	8.9633	49.202
V	0.5082	6.6913	37.6684
VI	0.4235	4.9973	29.5561

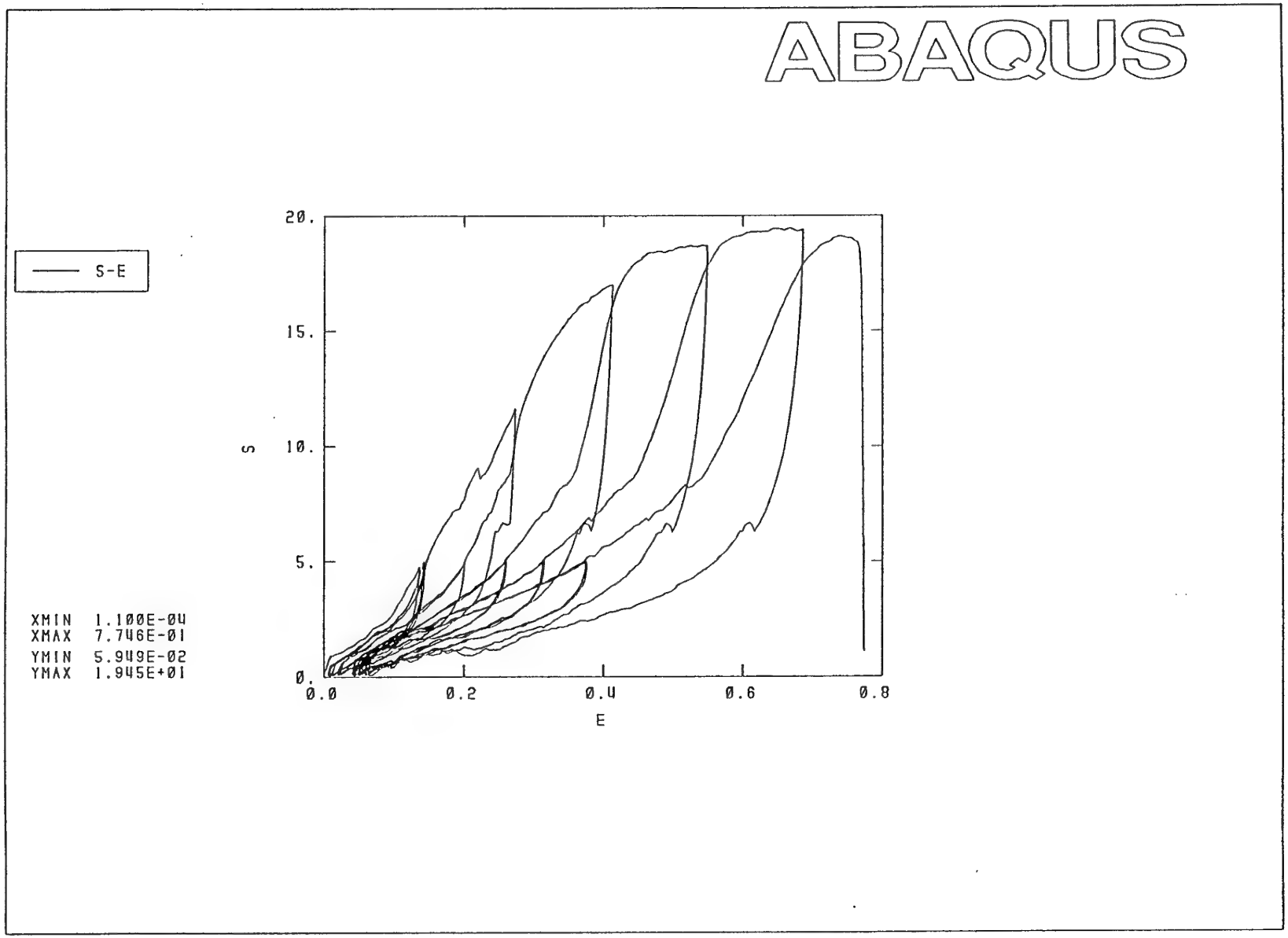

Fig. 1 Cyclic load-displacement curve for a solid propellant tension specimen. Load is in pounds and displacement is in inches. Specimen has a width of 0.501 in. and a thickness of 0.354 in. Loading rate is 0.2 in/mm.

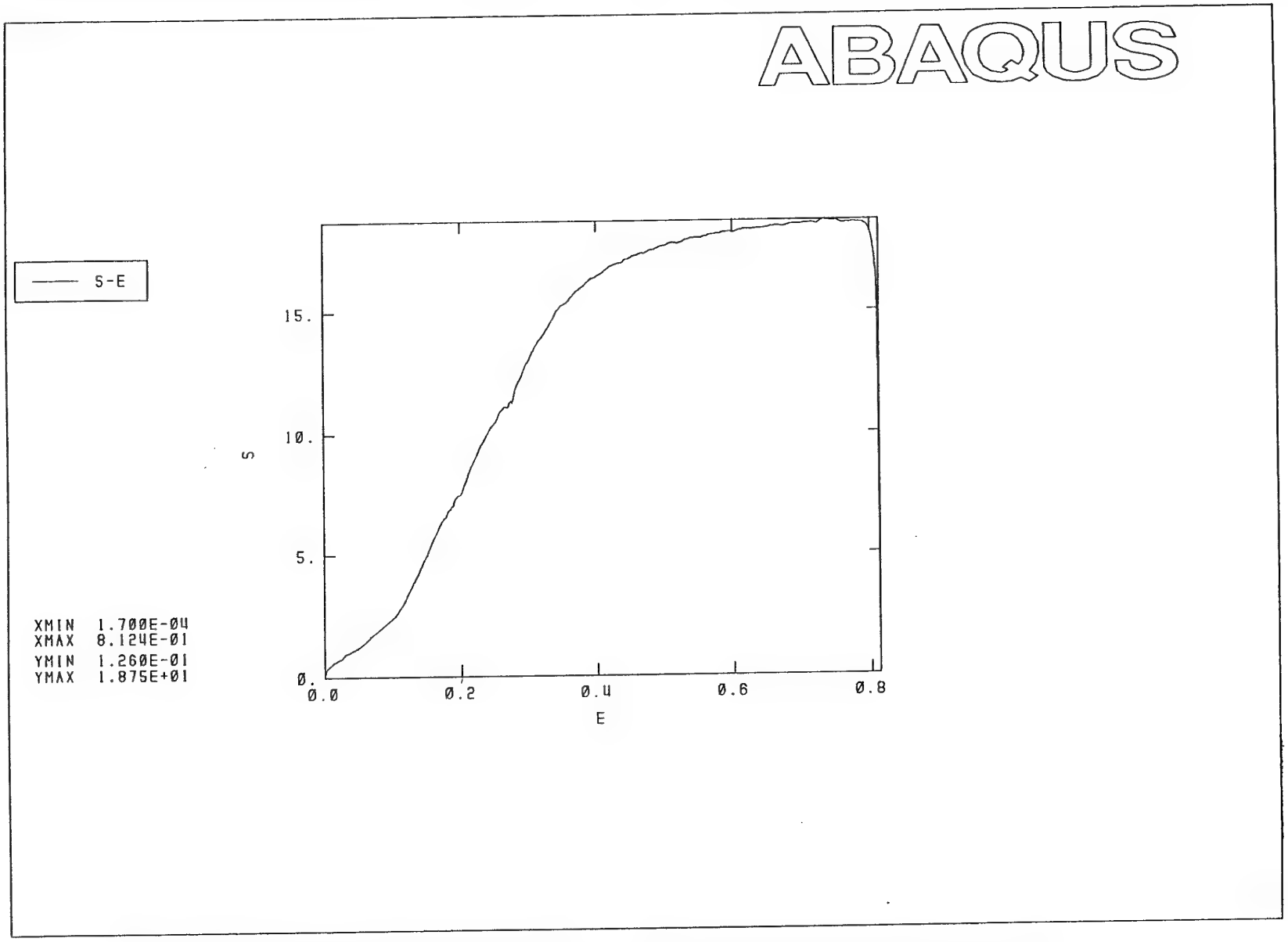

Fig. 2 Load-displacement curve for a solid propellant tension specimen. Load is pounds and displacement is in inches. Specimen has a width of 0.50 in. and a thickness of 0.36 in. Loading rate is 0.2 in/mm.

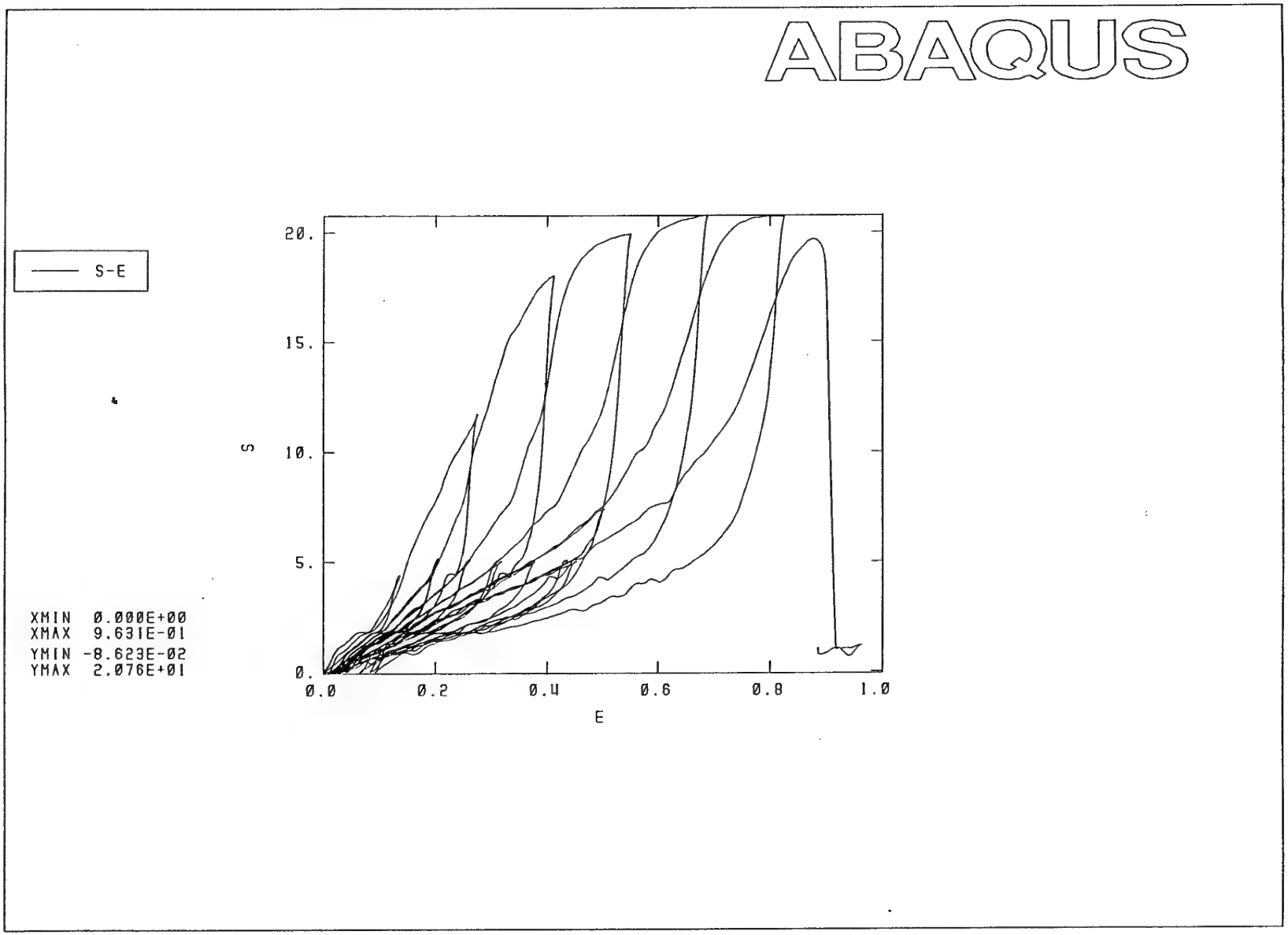

Fig. 3 Cyclic load-displacement curve for a solid propellant tension specimen. Load is in pounds and displacement is in inches. Specimen has a width of 0.50 in. and a thickness of 0.36 in. Loading rate is 2.0 in/mm.

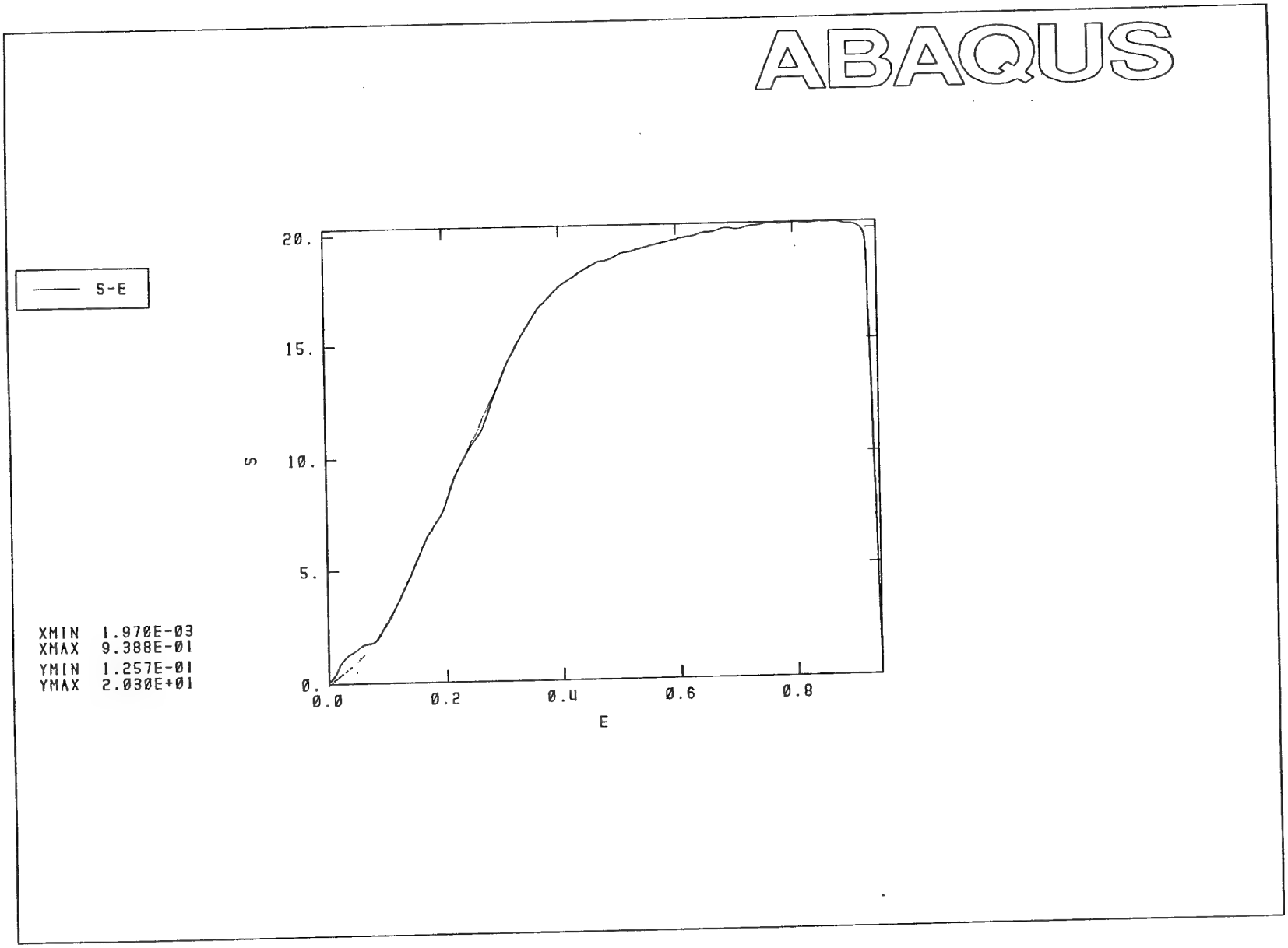

Fig. 4 Load-displacement curve for a a solid propellant tension specimen. Load is in pounds and displacement is in inches. Specimen has a width of 0.50 in and a thickness of 0.36 in. Loading rate is 2.0 in/mm.

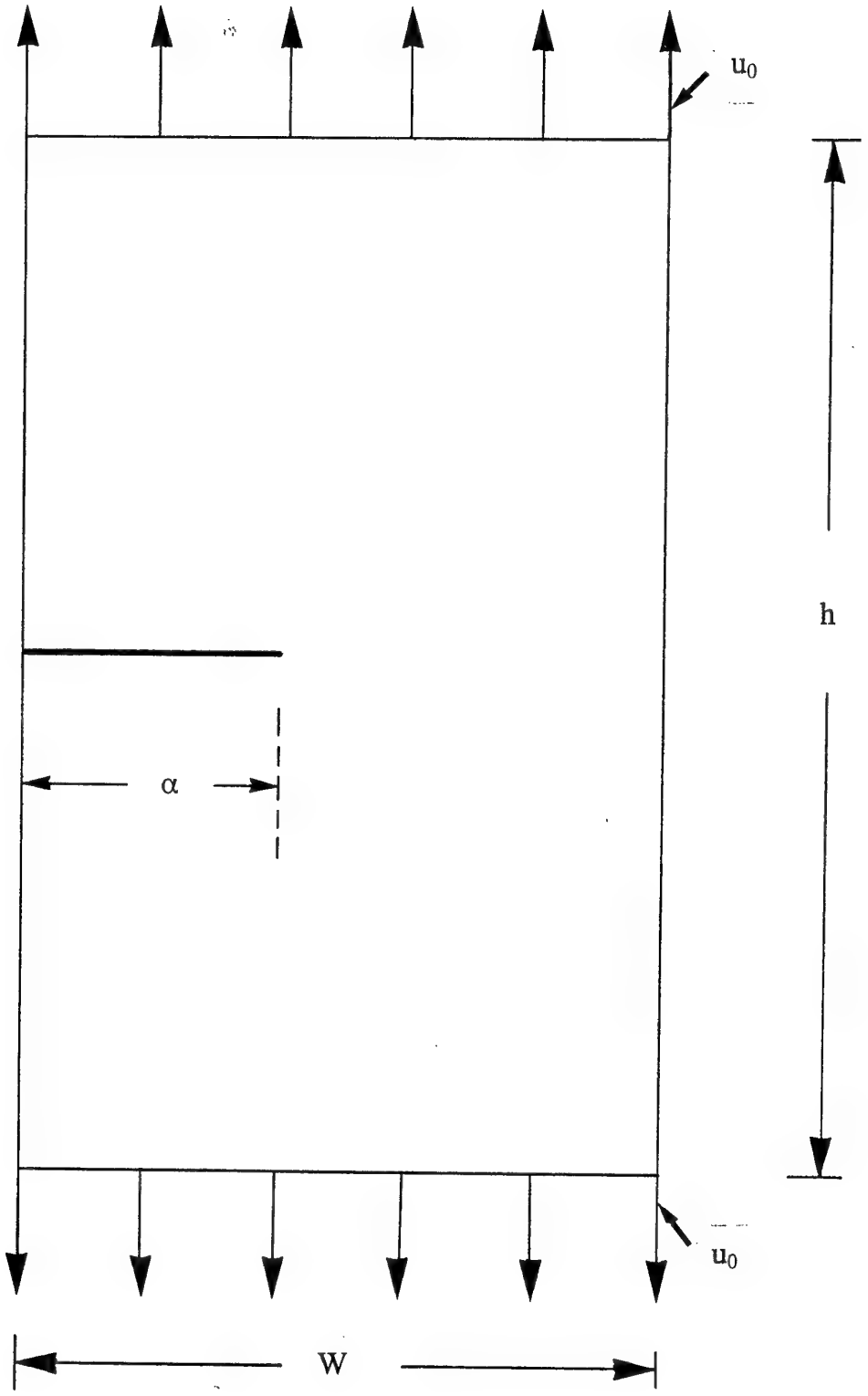

Fig. 5 Geometry of edge cracked specimen subjected to uniform displacement along its upper and lower faces.

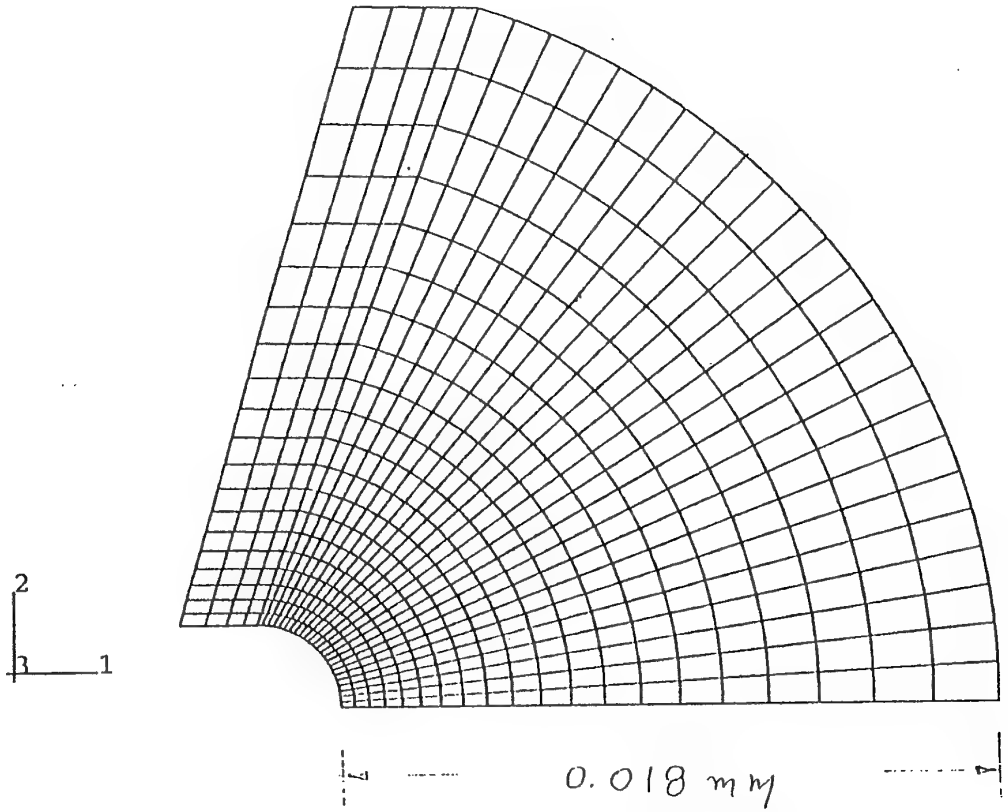

Fig. 6 Undeformed finite element grid near the crack tip. Notch root radius 2.54×10^{-3} mm.

Case I

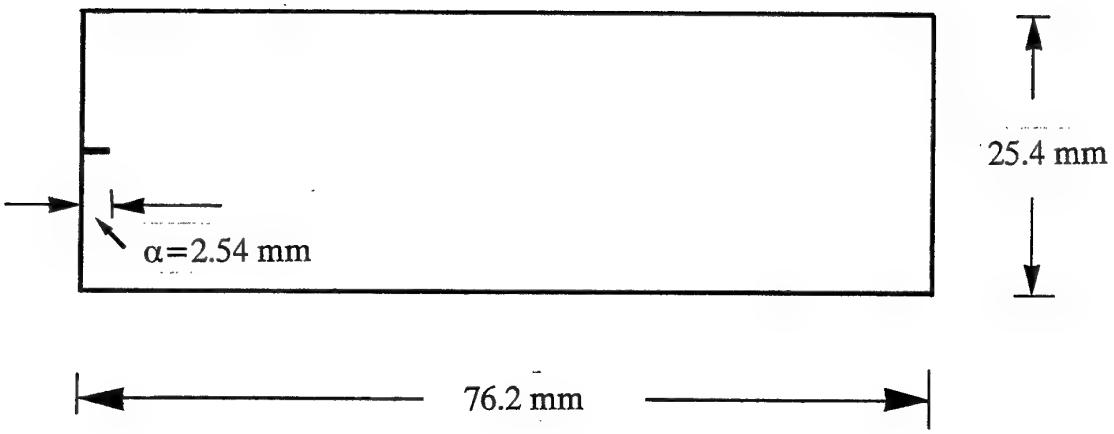

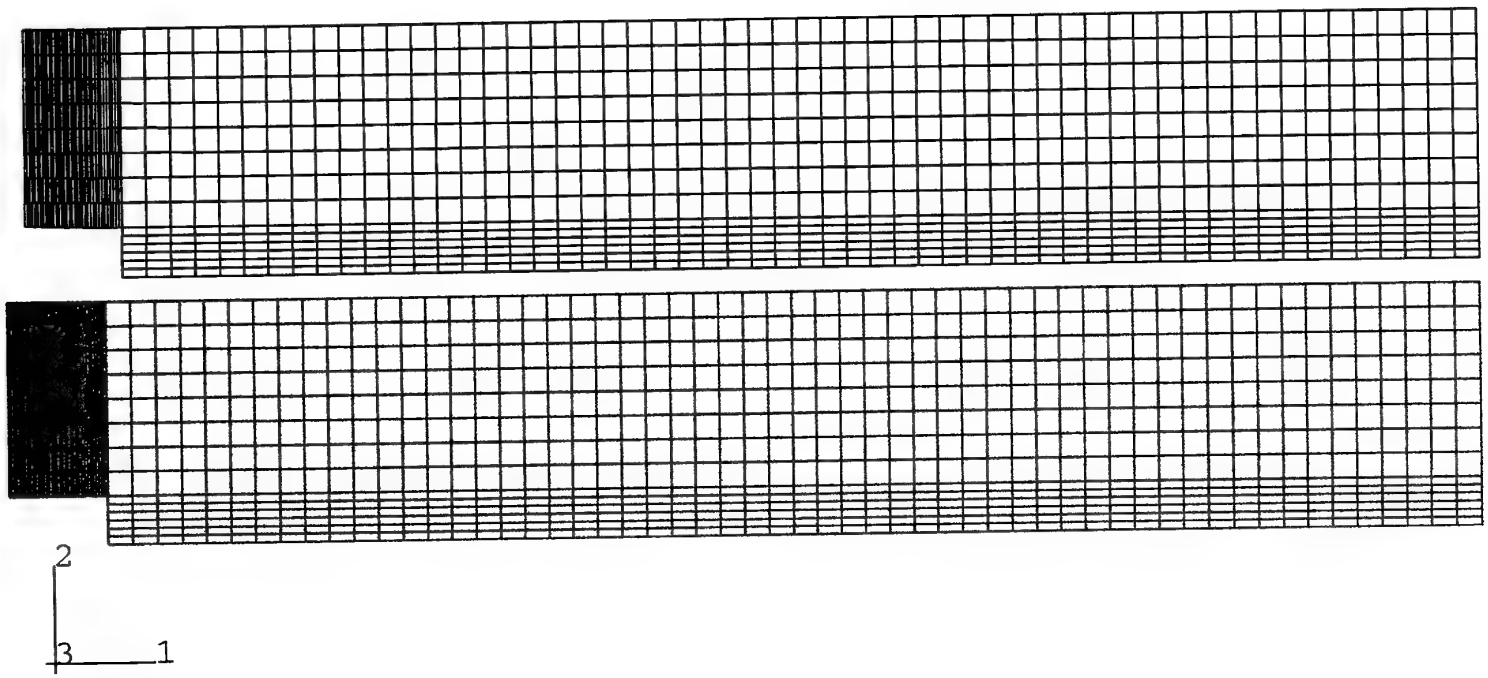

Fig. 7 Undeformed (in red) and deformed (in black) finite element grids for half specimen. Applied displacement u_0=0.3388 mm. Case I.

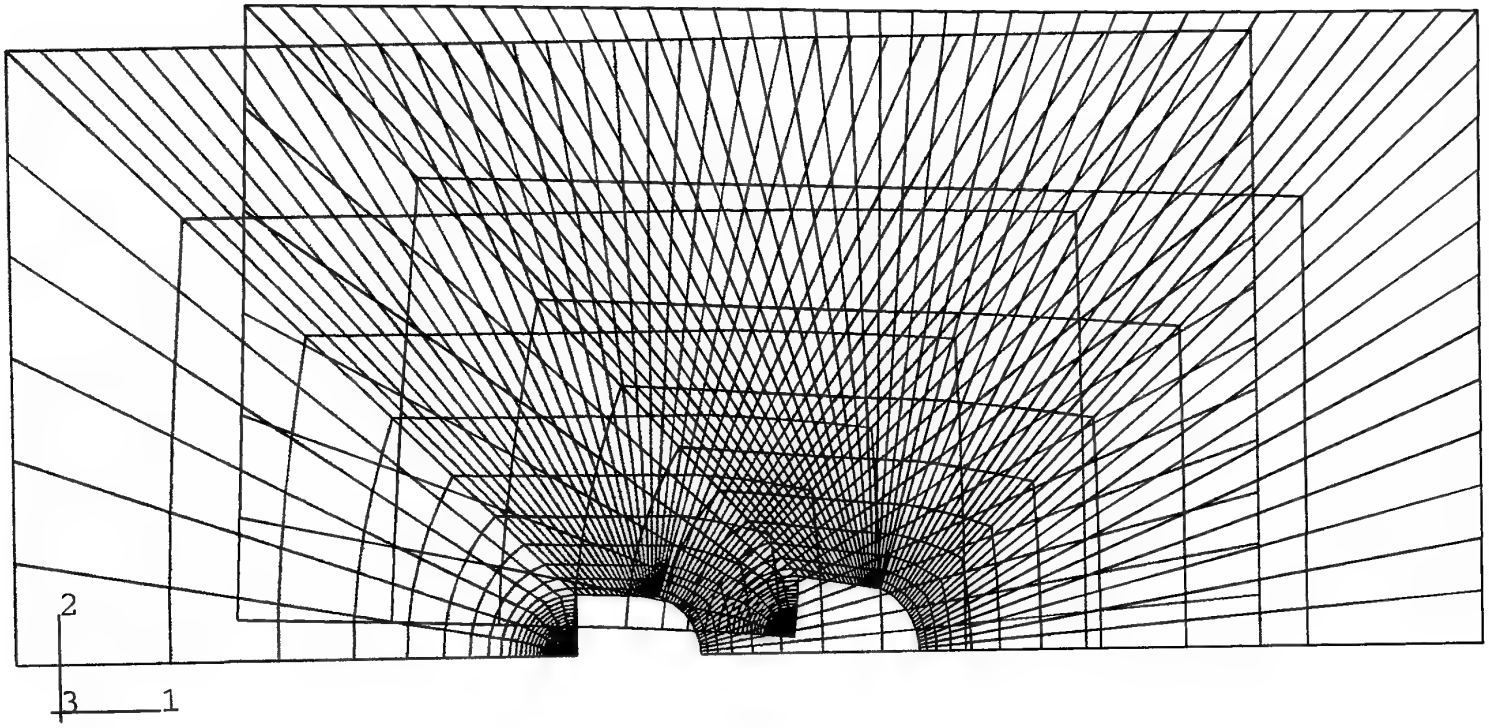

Fig. 8 Undeformed (in red) and deformed (in black) finite element grids for the missing part of Figure 7. Applied displacement u_0=0.3388 mm. Case I.

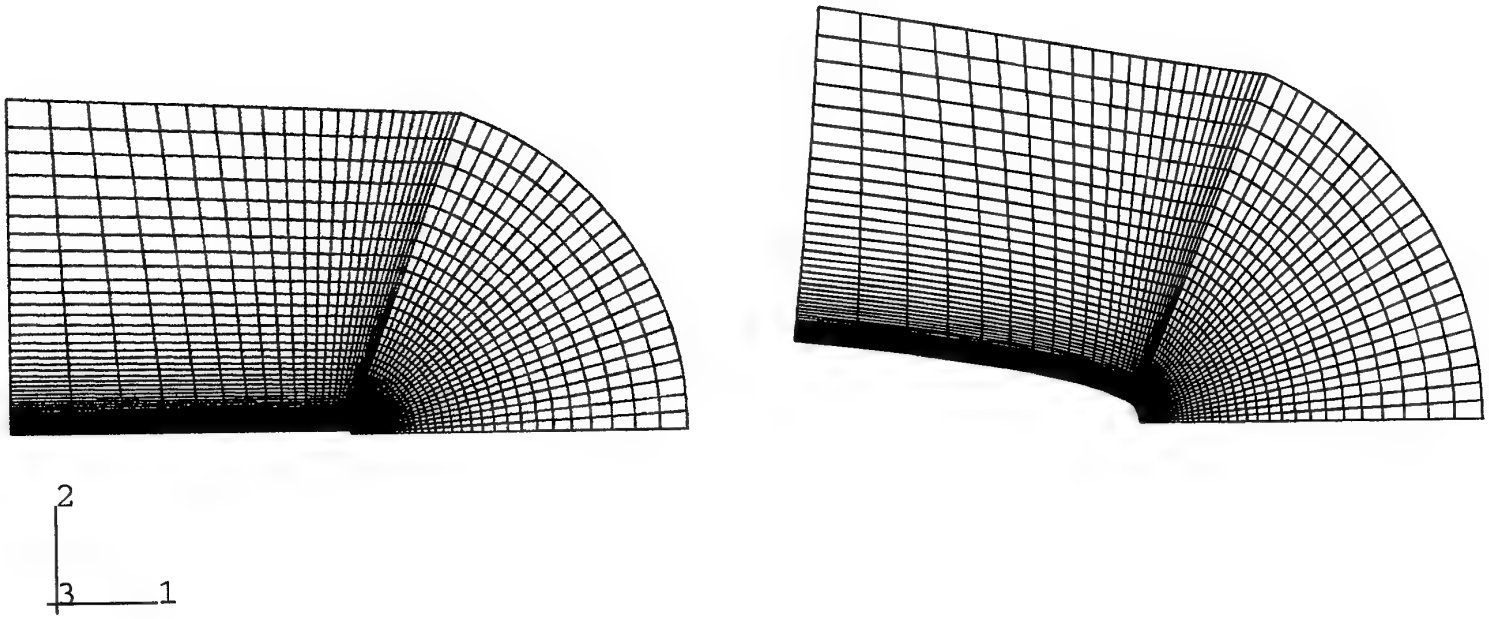

Fig. 9 Undeformed (in red) and deformed (in black) finite element grids for the missing part of Figure 8. Applied displacement u_0=0.3388 mm. Case I.

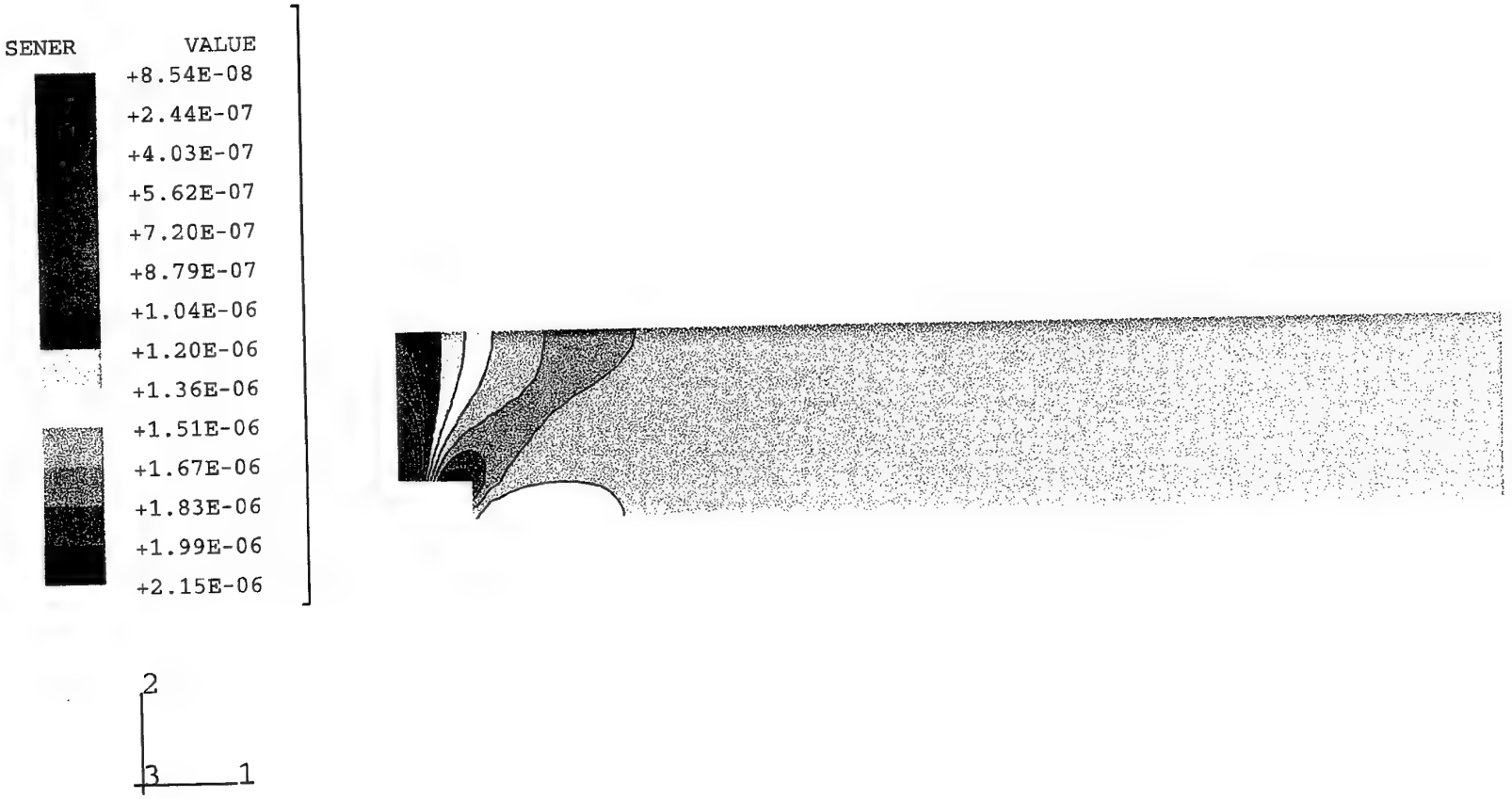

Fig. 10 Strain energy density, dW/dV, contours (in the deformed specimen configuration) for Figure 7. Values in kN.mm/mm^3. Applied displacement u_0=0.3388 mm. Case I.

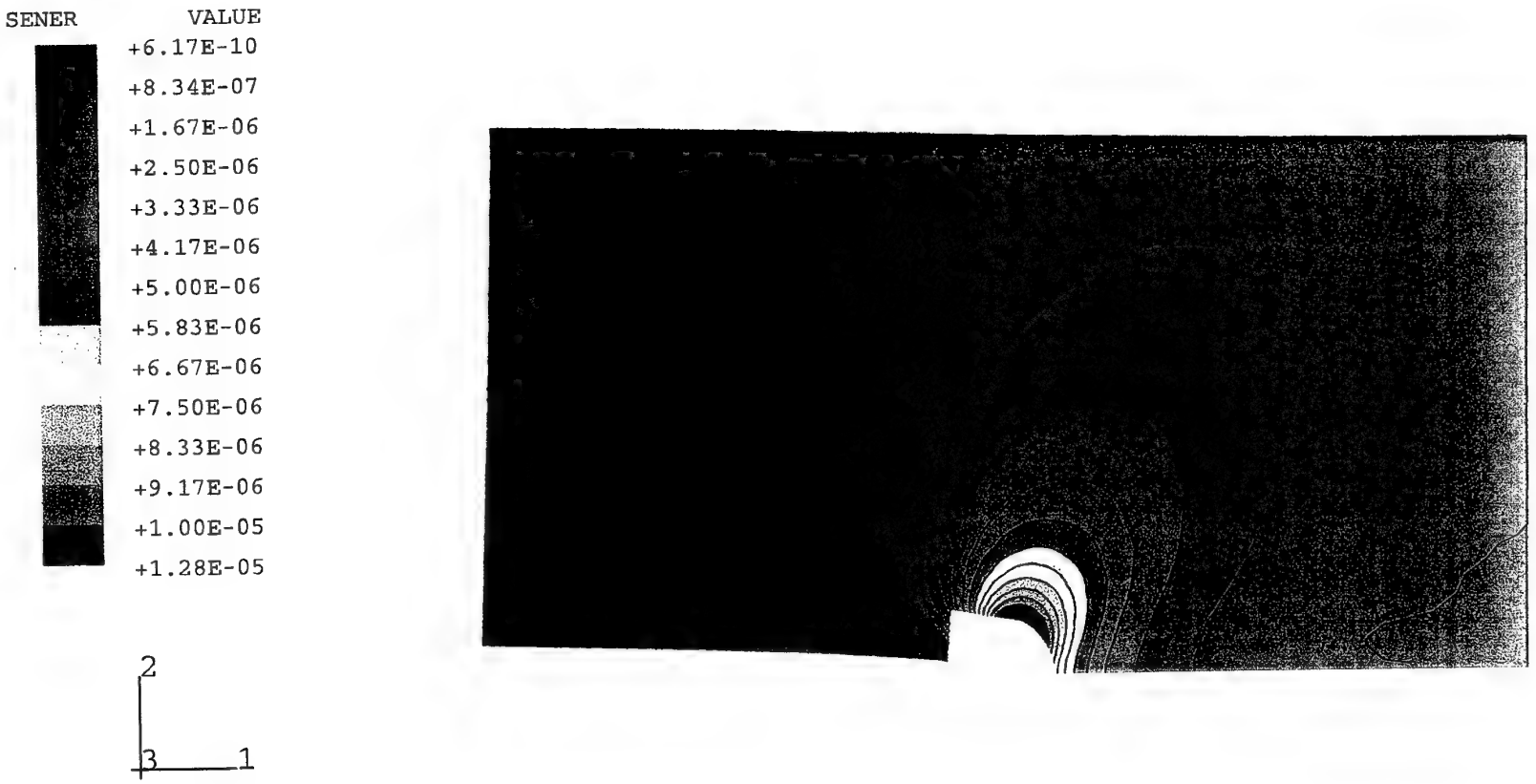

Fig. 11 Strain energy density, dW/dV, contours (in the deformed specimen configuration) for Figure 8. Values in kN.mm/mm^3. Applied displacement u_0=0.3388 mm. Case I.

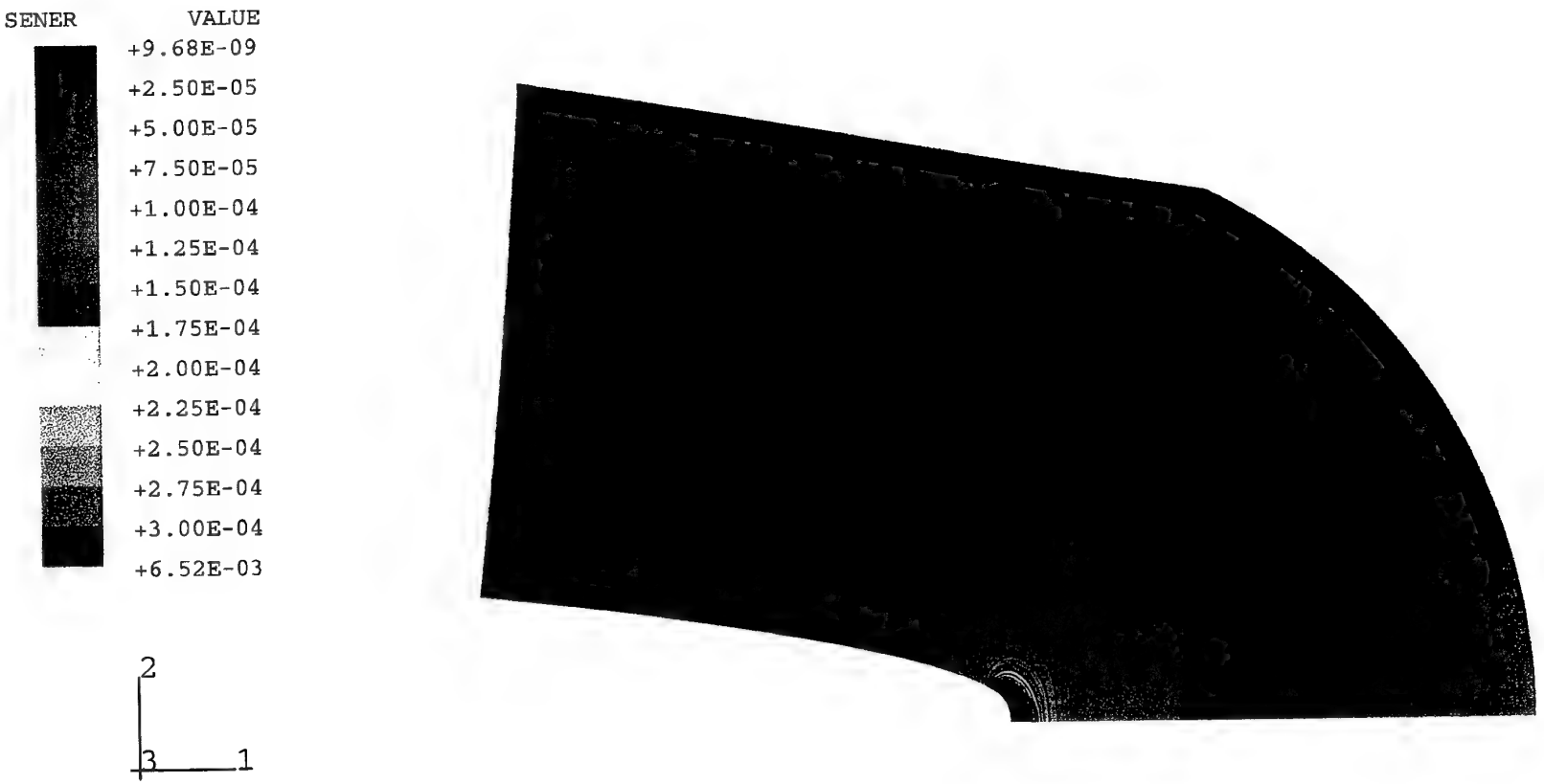

Fig. 12 Strain energy density, dW/dV, contours (in the deformed specimen configuration) for Figure 9. Values in kN.mm/mm^3. Applied displacement u_0=0.3388 mm. Case I.

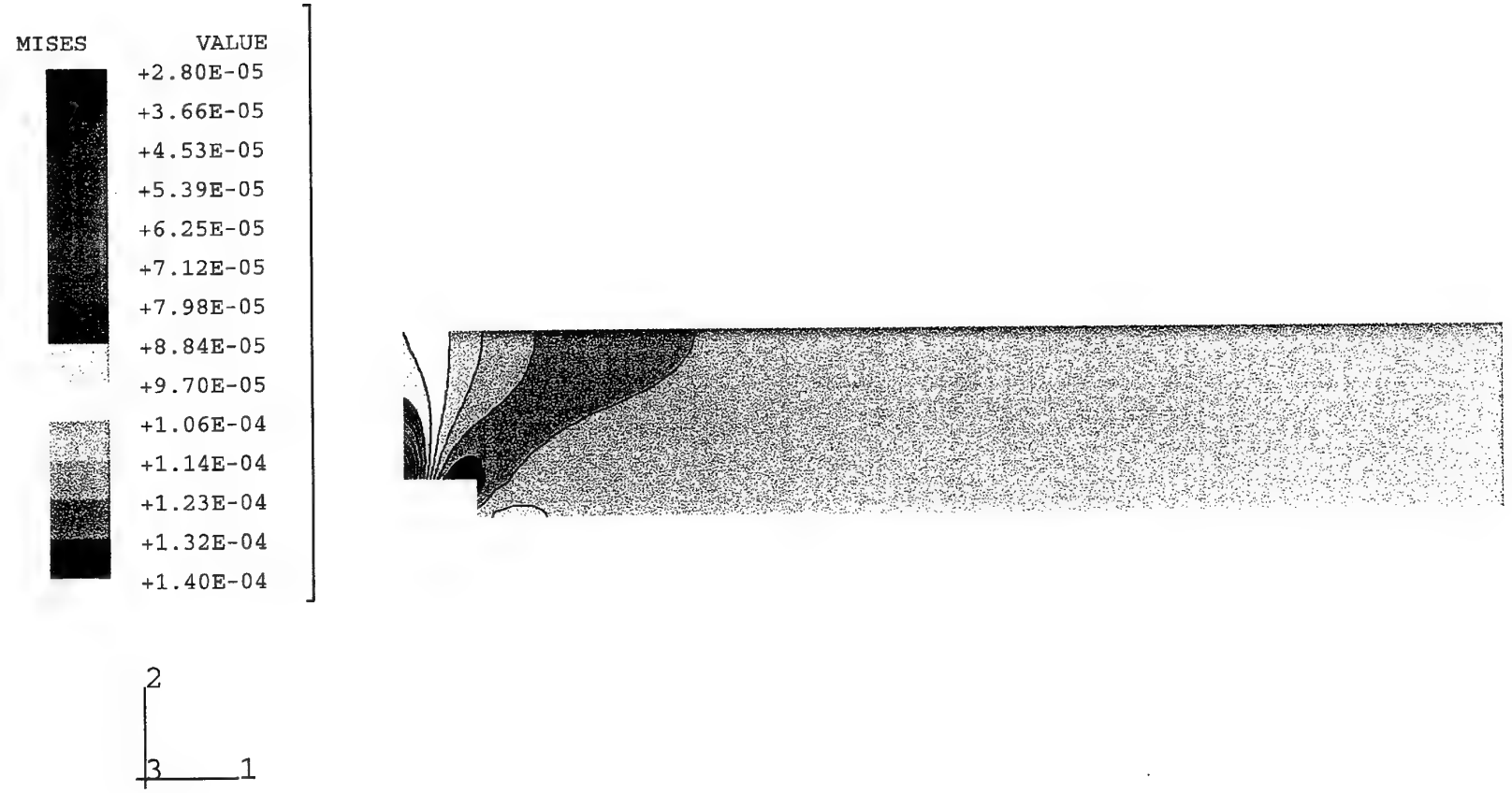

Fig. 13 Mises stress, σ_{eff}, contours (in the deformed specimen configuration) for Figure 7. Values in kN/mm^2. Applied displacement u_0=0.3388 mm. Case I.

Fig. 14 Mises stress, σ_{eff}, contours (in the deformed specimen configuration) for Figure 8. Values in kN/mm^2. Applied displacement u_0=0.3388 mm. Case I.

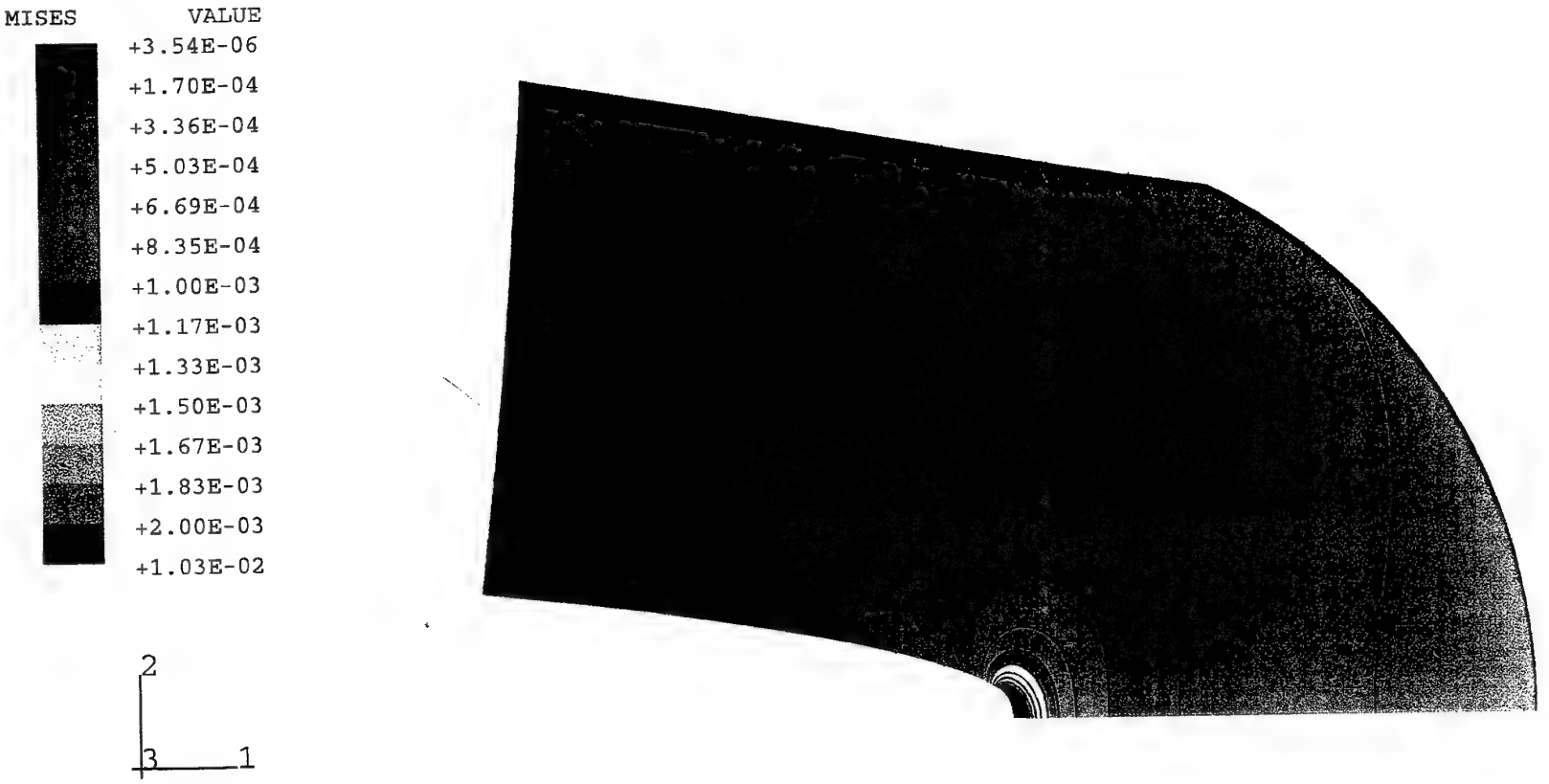

Fig. 15 Mises stress, σ_{eff}, contours (in the deformed specimen configuration) for Figure 9. Values in kN/mm^2. Applied displacement u_0=0.3388 mm. Case I.

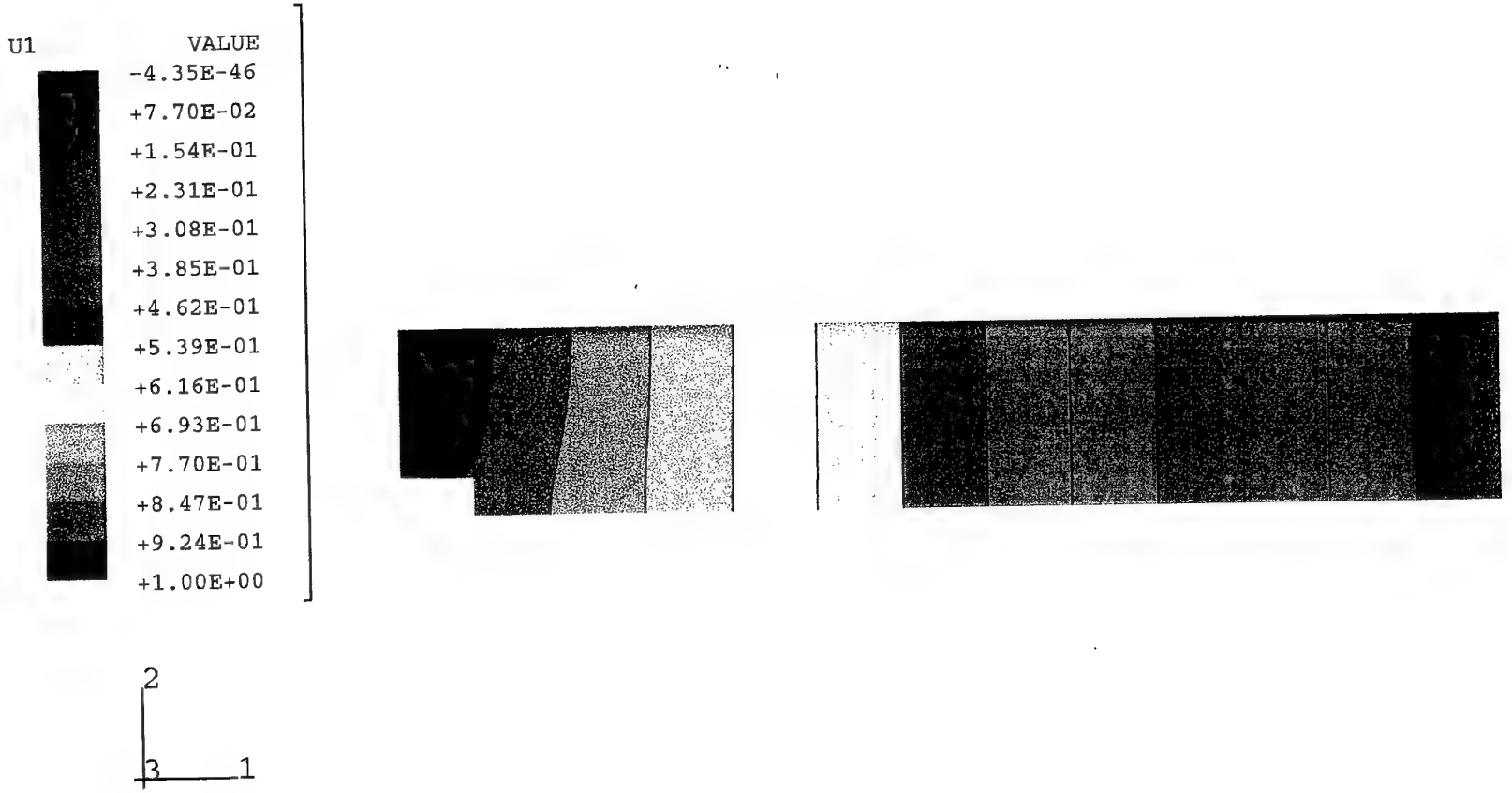

Fig. 16 Displacement along the crack axis direction, u_1, contours (in the deformed specimen configuration) for Figure 7. Values in mm. Applied displacement u_0=0.3388 mm. Case I.

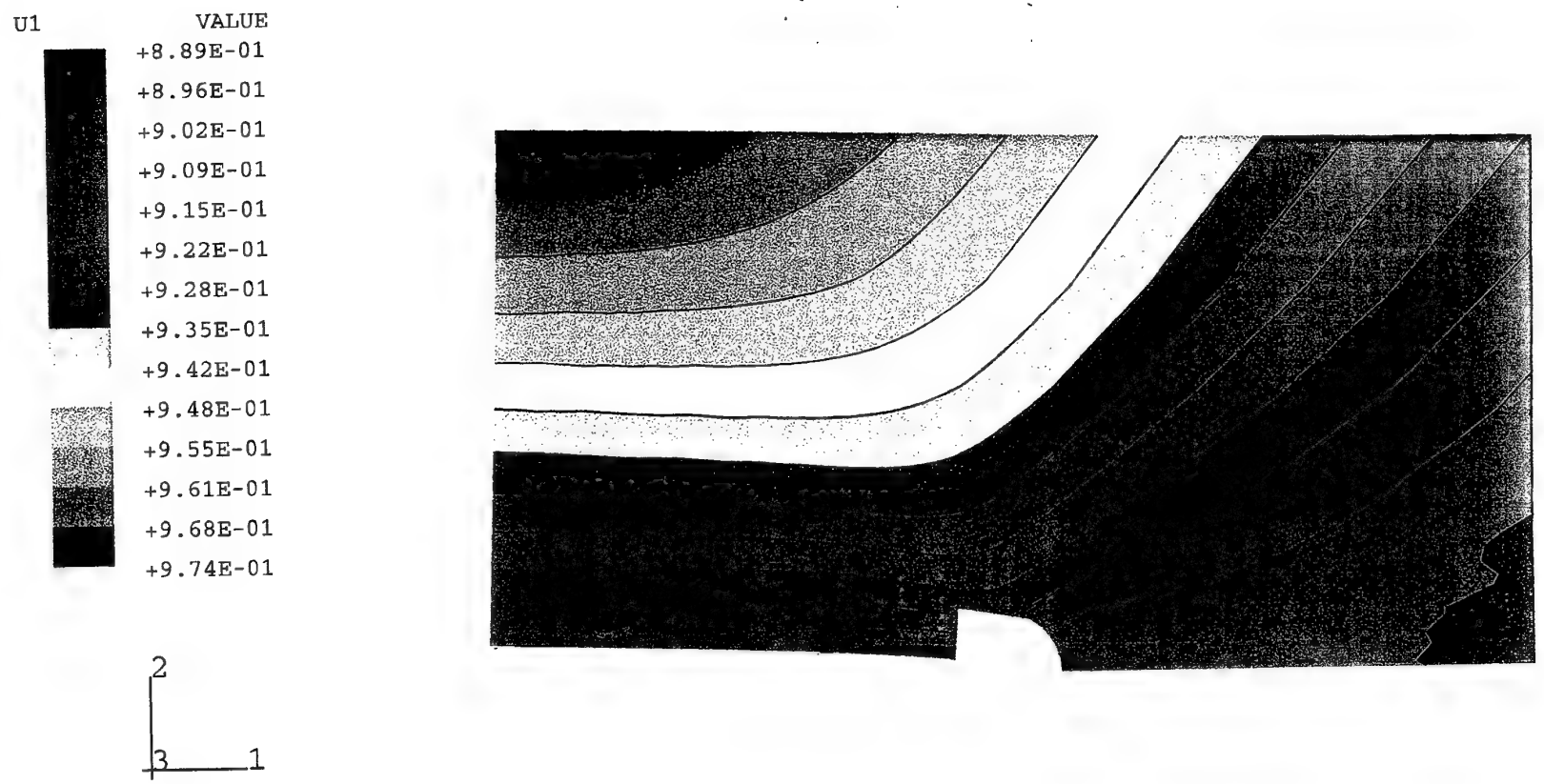

Fig. 17 Displacement along the crack axis direction, u_1, contours (in the deformed specimen configuration) for Figure 8. Values in mm. Applied displacement u_0=0.3388 mm. Case I.

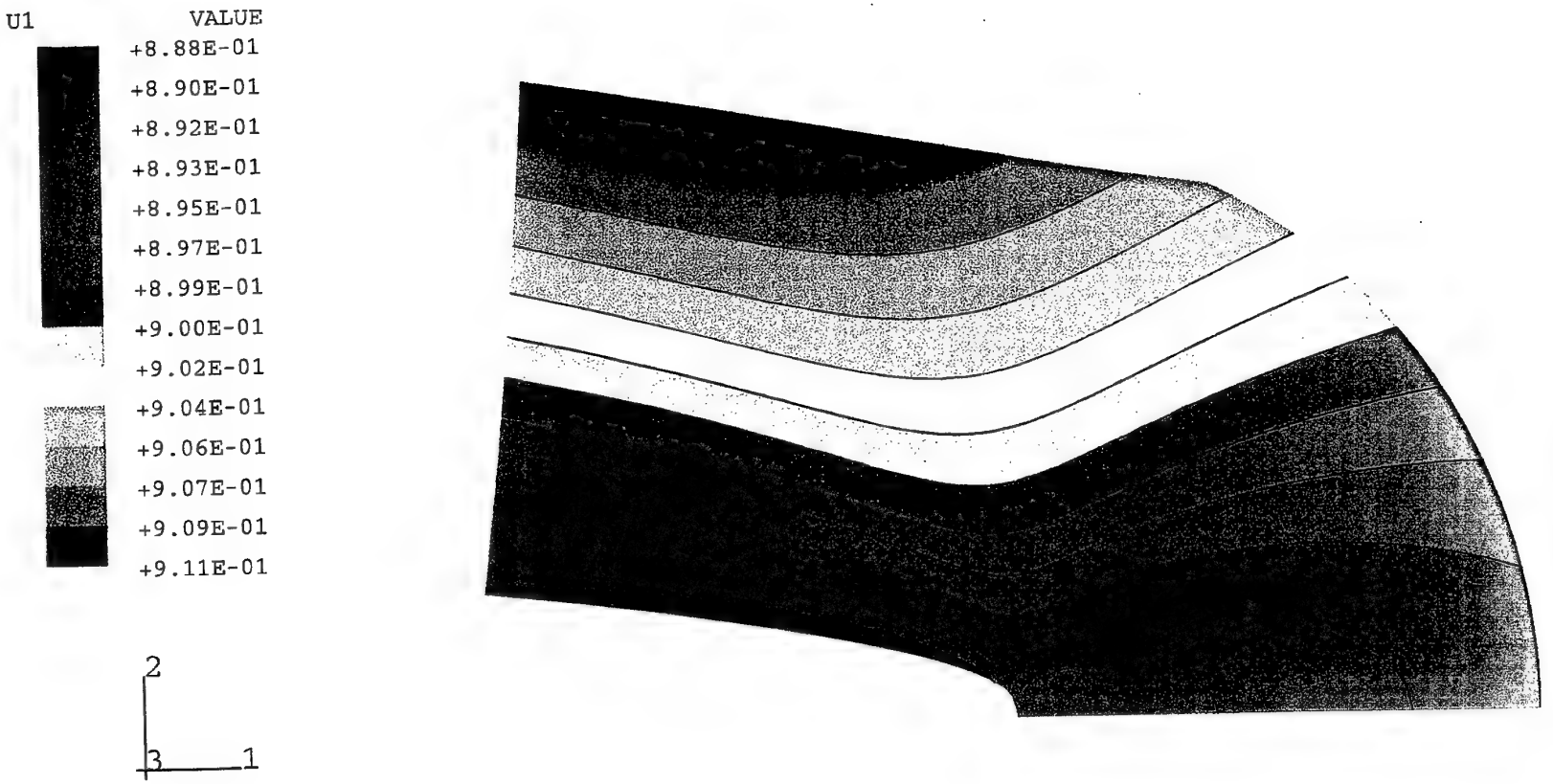

Fig. 18 Displacement along the crack axis direction, u_1, contours (in the deformed specimen configuration) for Figure 9. Values in mm. Applied displacement u_0=0.3388 mm. Case I.

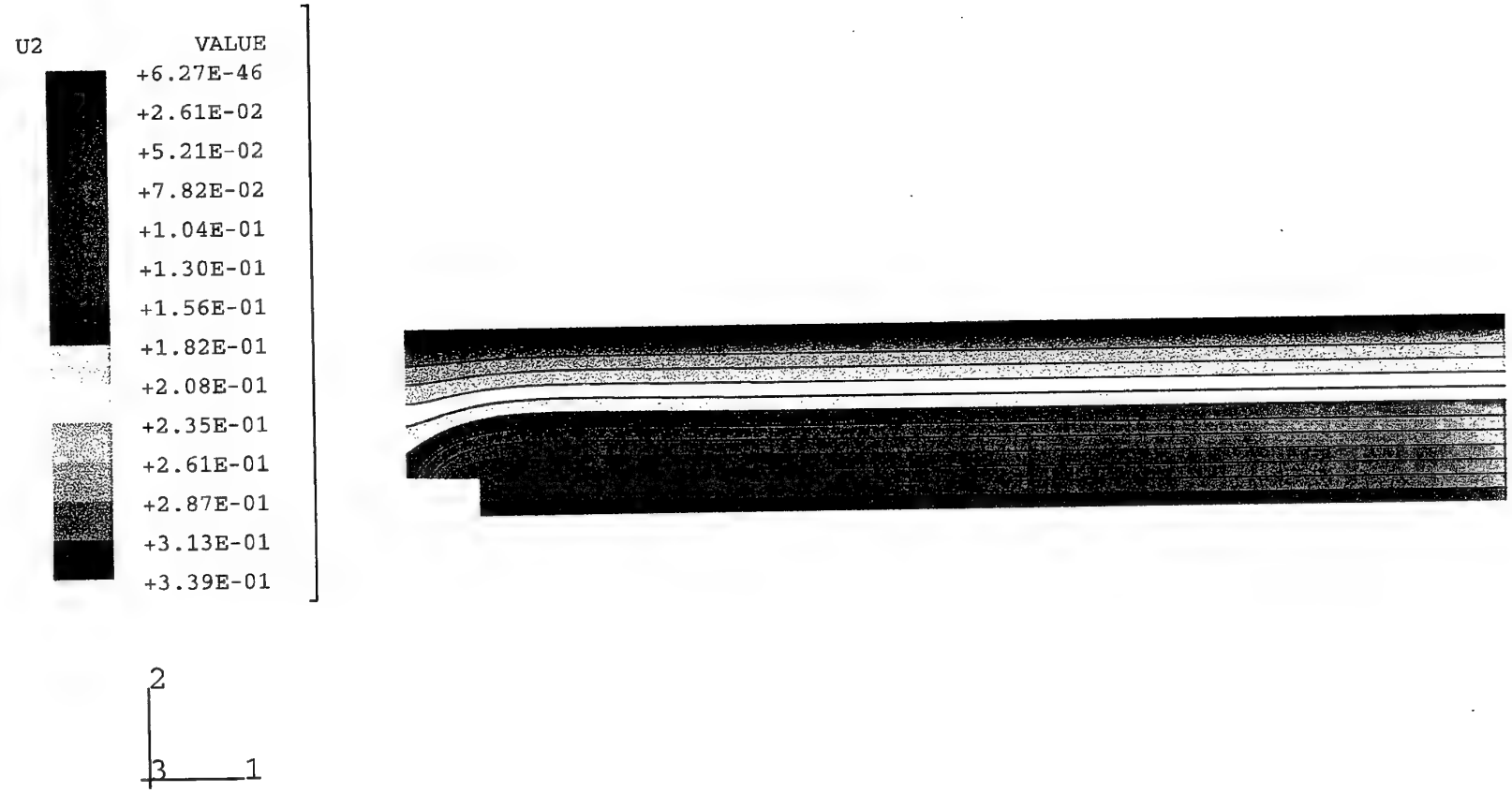

Fig. 19 Displacement along the perpendicular to the crack axis direction, u_2, contours (in the deformed specimen configuration) for Figure 7. Values in mm. Applied displacement u_0=0.3388 mm. Case I.

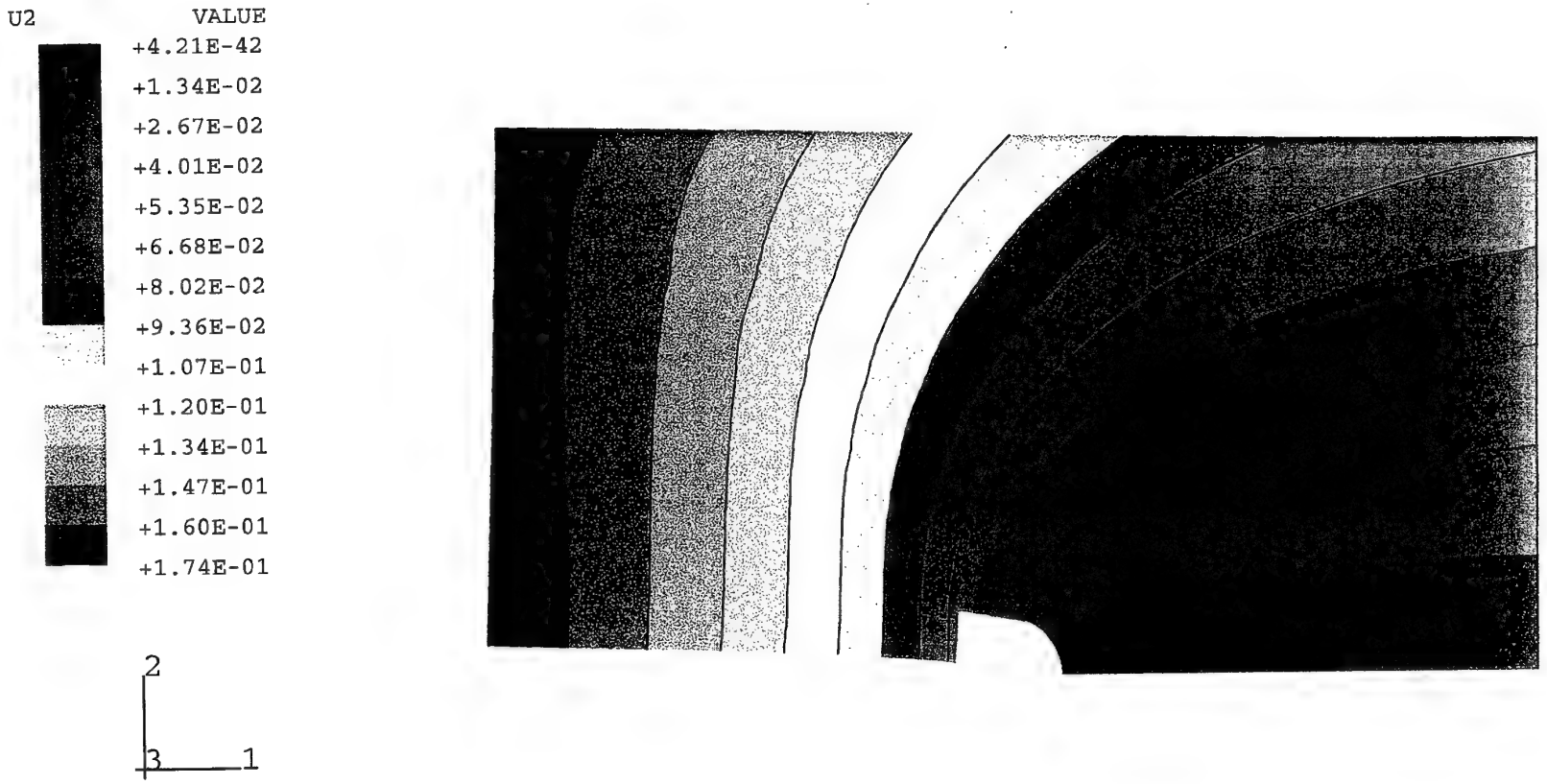

Fig. 20 Displacement along the perpendicular to the crack axis direction, u_2, contours (in the deformed specimen configuration) for Figure 8. Values in mm. Applied displacement u_0=0.3388 mm. Case I.

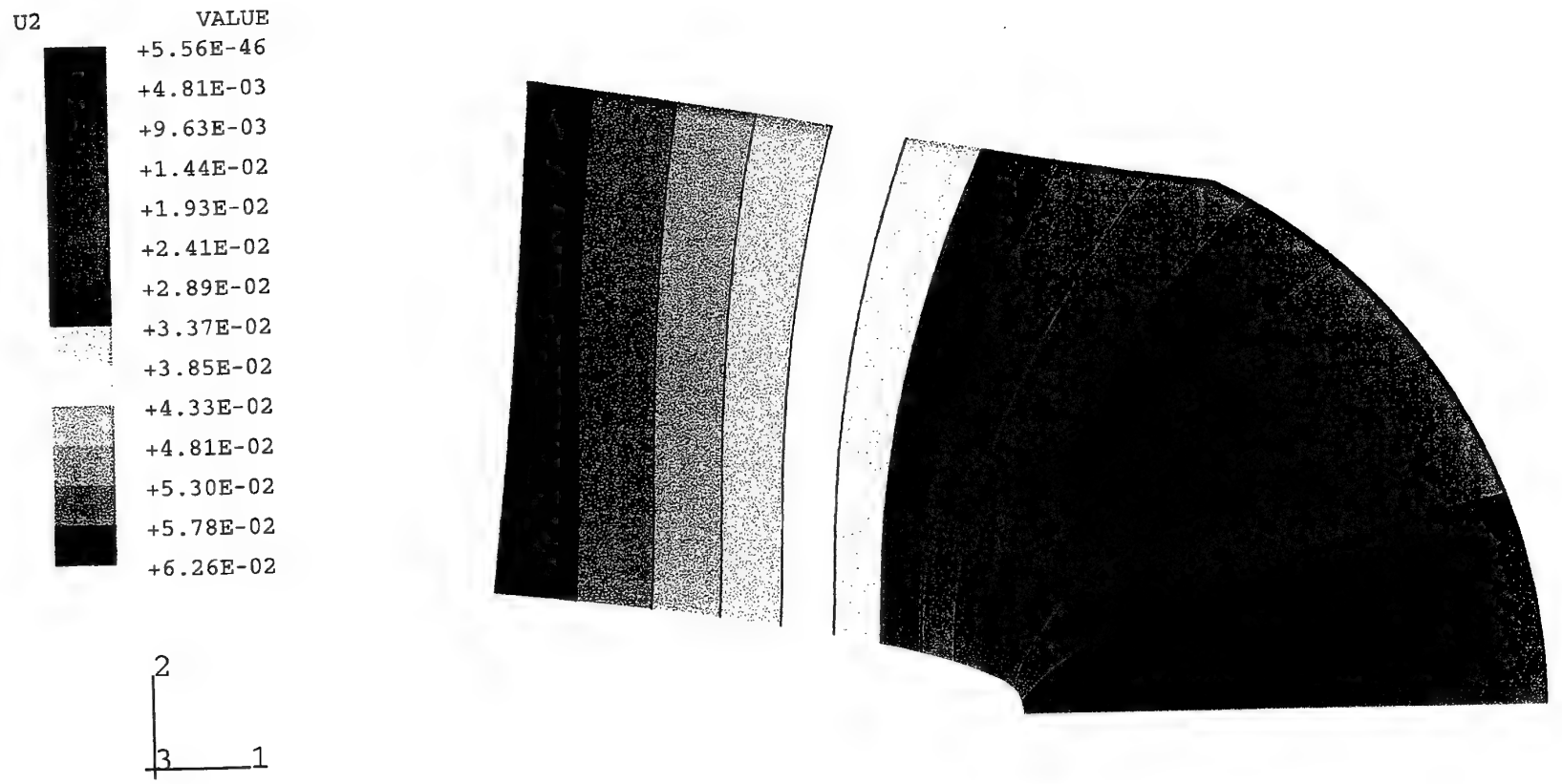

Fig. 21 Displacement along the perpendicular to the crack axis direction, u_2, contours (in the deformed specimen configuration) for Figure 9. Values in mm. Applied displacement u_0=0.3388 mm. Case I.

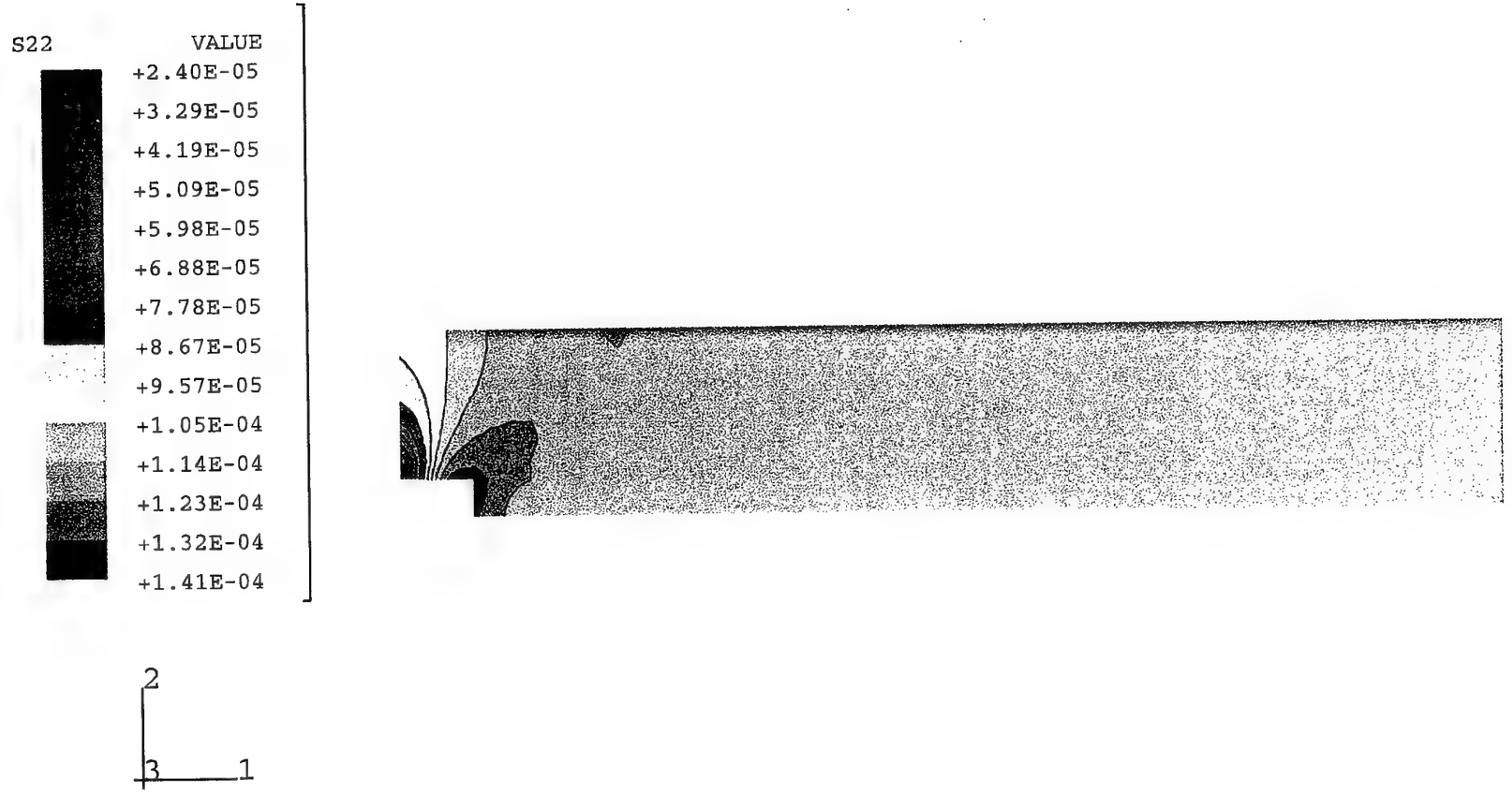

Fig. 22 Normal stress along the perpendicular to the crack axis direction, σ_{22}, contours (in the deformed specimen configuration) for Figure 7. Values in kN/mm^2. Applied displacement u_0=0.3388 mm. Case I.

Fig. 23 Normal stress along the perpendicular to the crack axis direction, σ_{22}, contours (in the deformed specimen configuration) for Figure 8. Values in kN/mm^2. Applied displacement u_0=0.3388 mm. Case I.

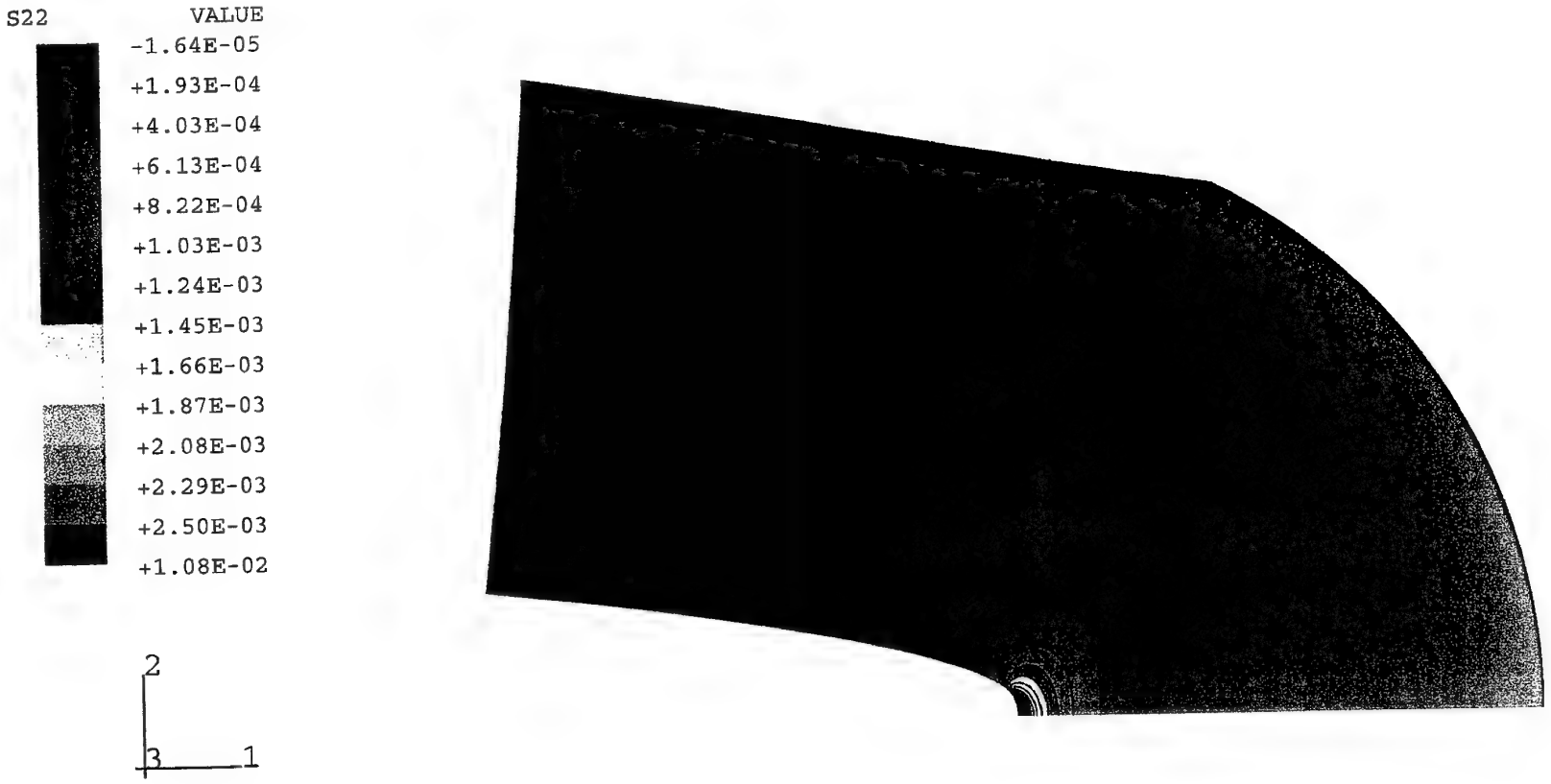

Fig. 24 Normal stress along the perpendicular to the crack axis direction, σ_{22}, contours (in the deformed specimen configuration) for Figure 9. Values in kN/mm^2 Applied displacement u_0=0.3388 mm. Case I.

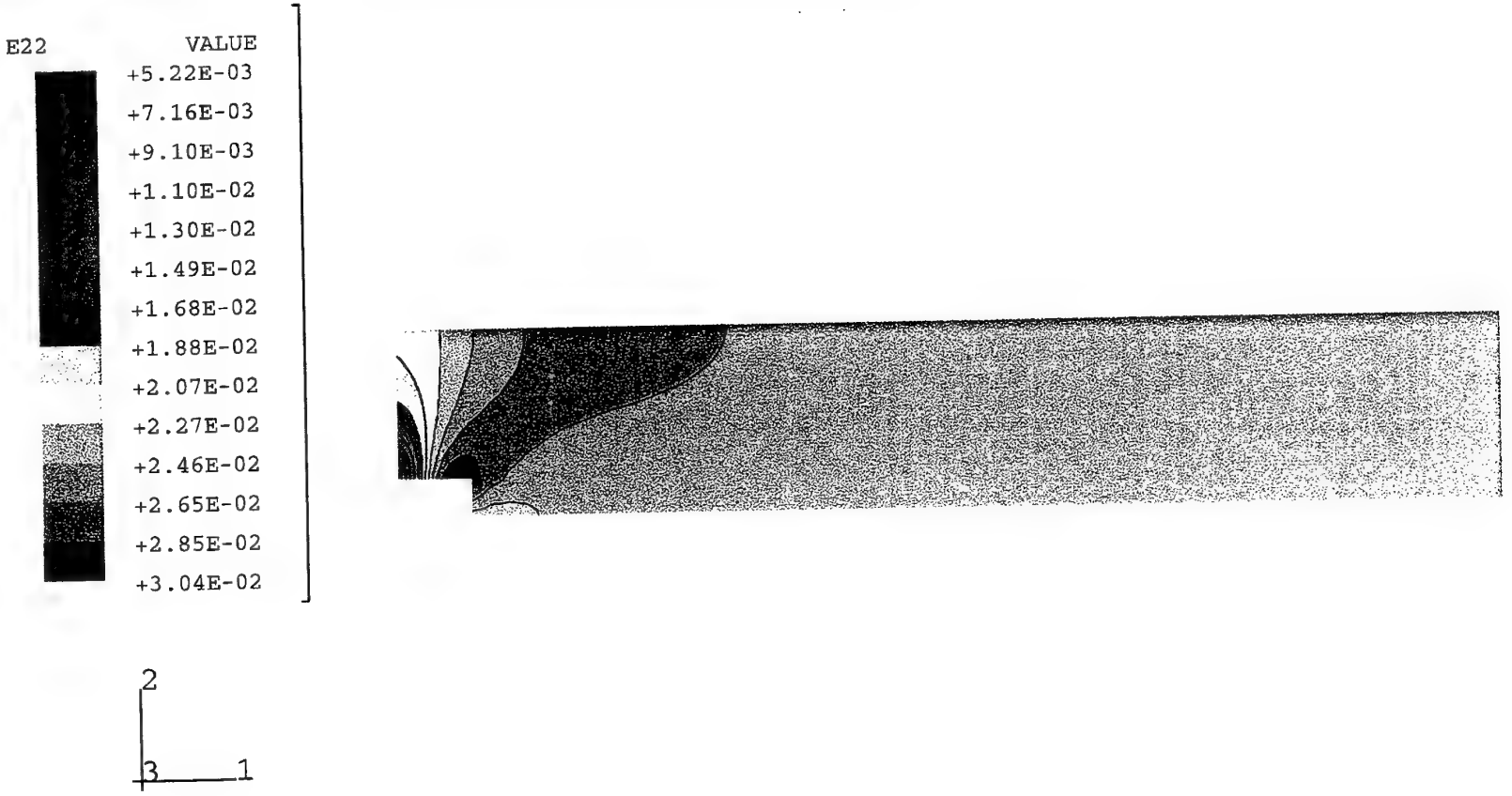

Fig. 25 Normal strain along the perpendicular to the crack axis direction, ε_{22}, contours (in the deformed specimen configuration) for Figure 7. Applied displacement u_0=0.3388 mm. Case I.

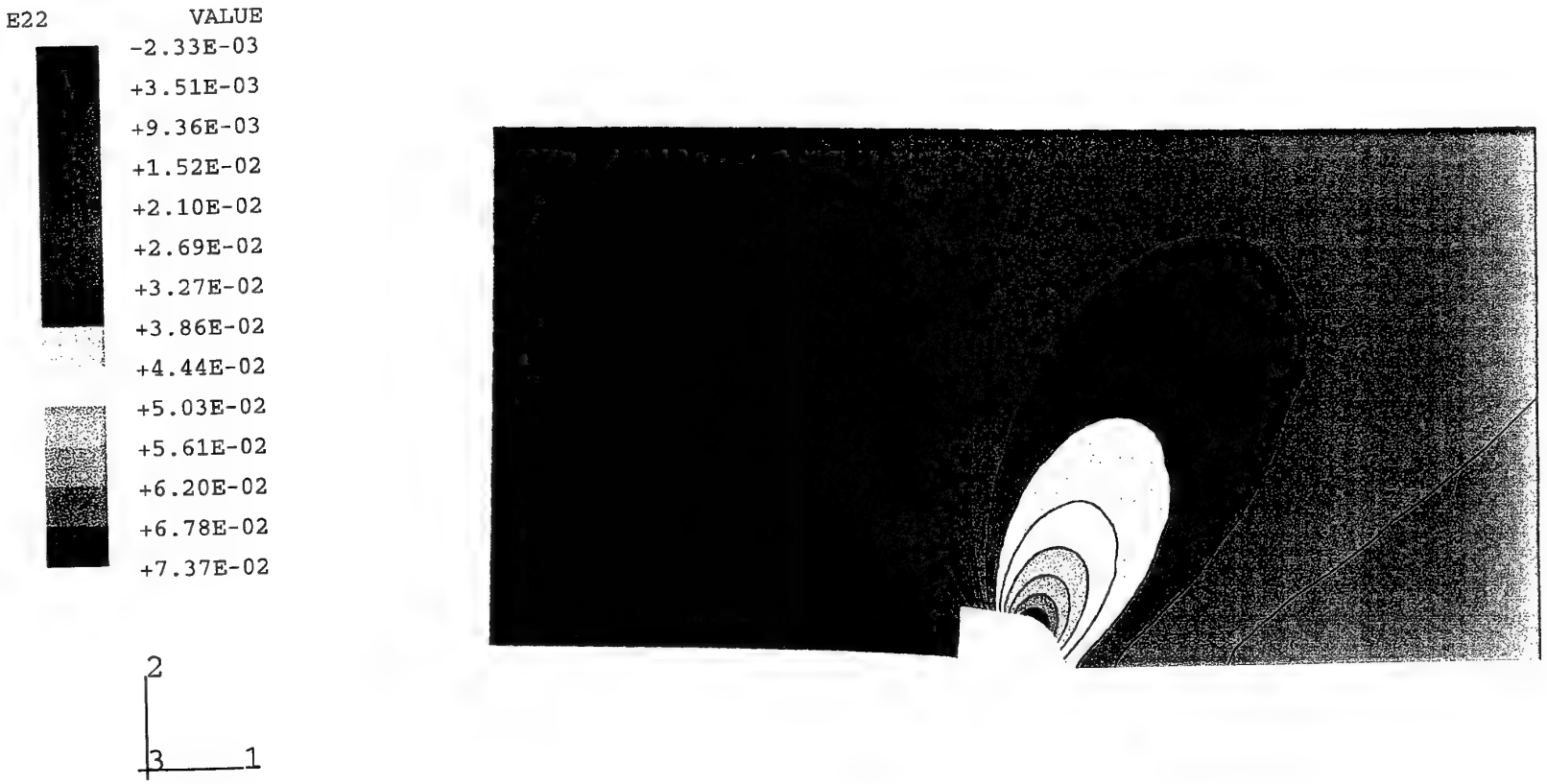

Fig. 26 Normal strain along the perpendicular to the crack axis direction, ε_{22}, contours (in the deformed specimen configuration) for Figure 8. Applied displacement u_0=0.3388 mm. Case I.

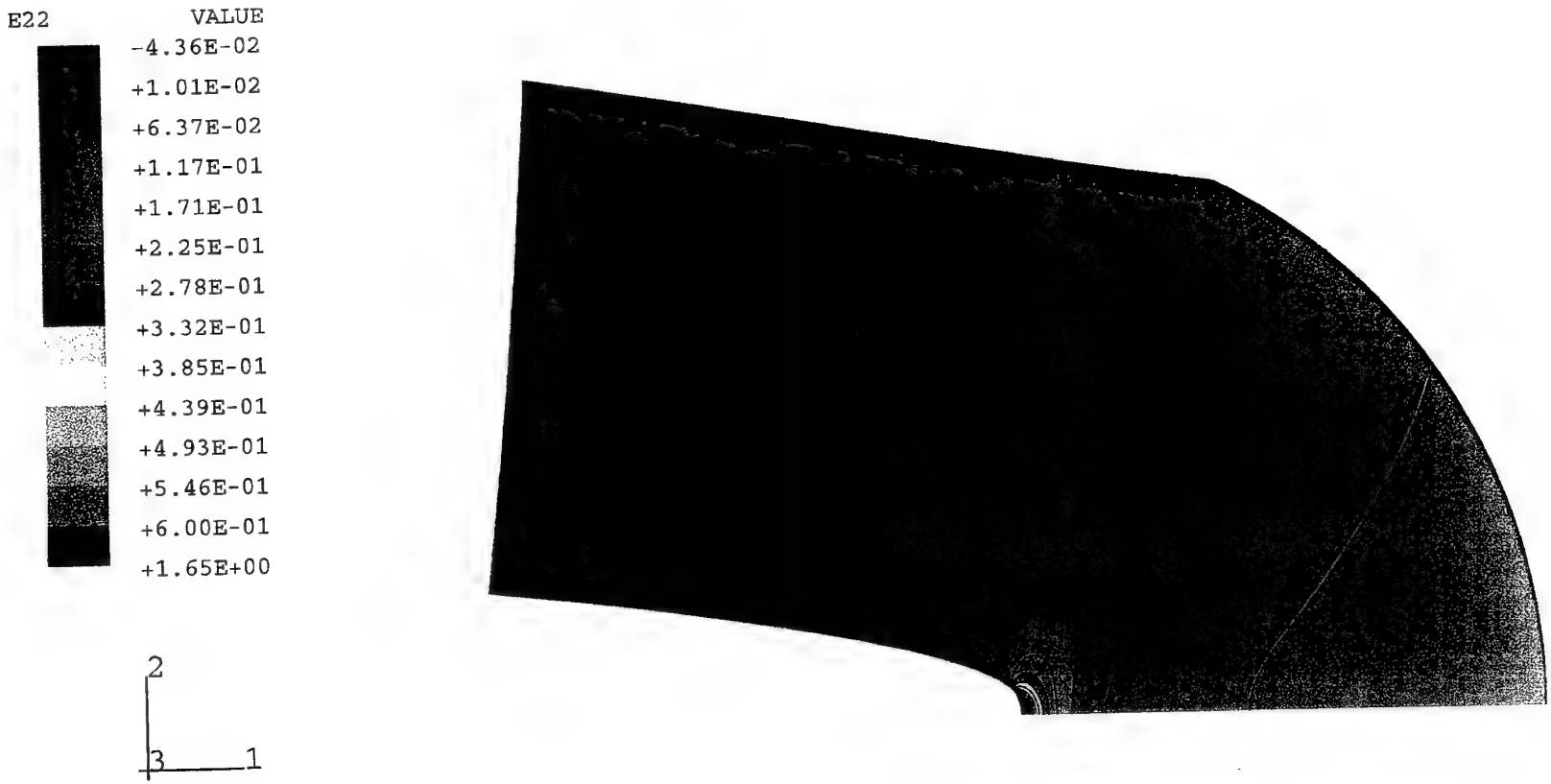

Fig. 27 Normal strain along the perpendicular to the crack axis direction, ε_{22}, contours (in the deformed specimen configuration) for Figure 9. Applied displacement u_0=0.3388 mm. Case I.

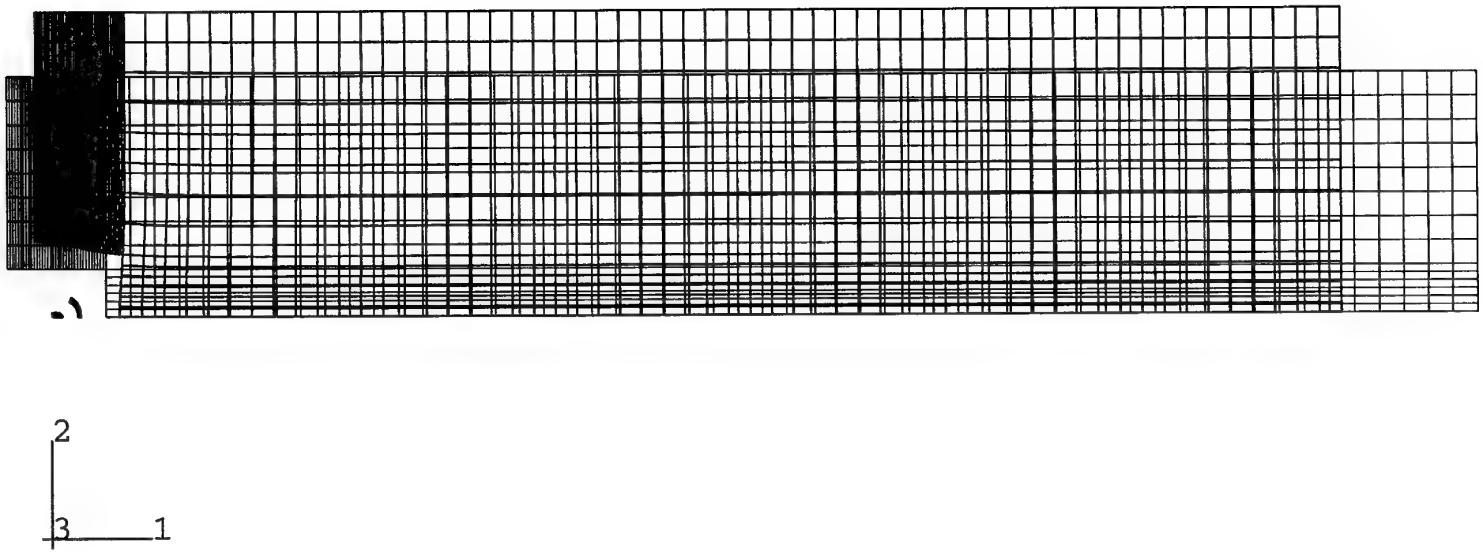

Fig. 28 Undeformed (in red) and deformed (in black) finite element grids for half specimen. Applied displacement u_0=3.3295 mm. Case I.

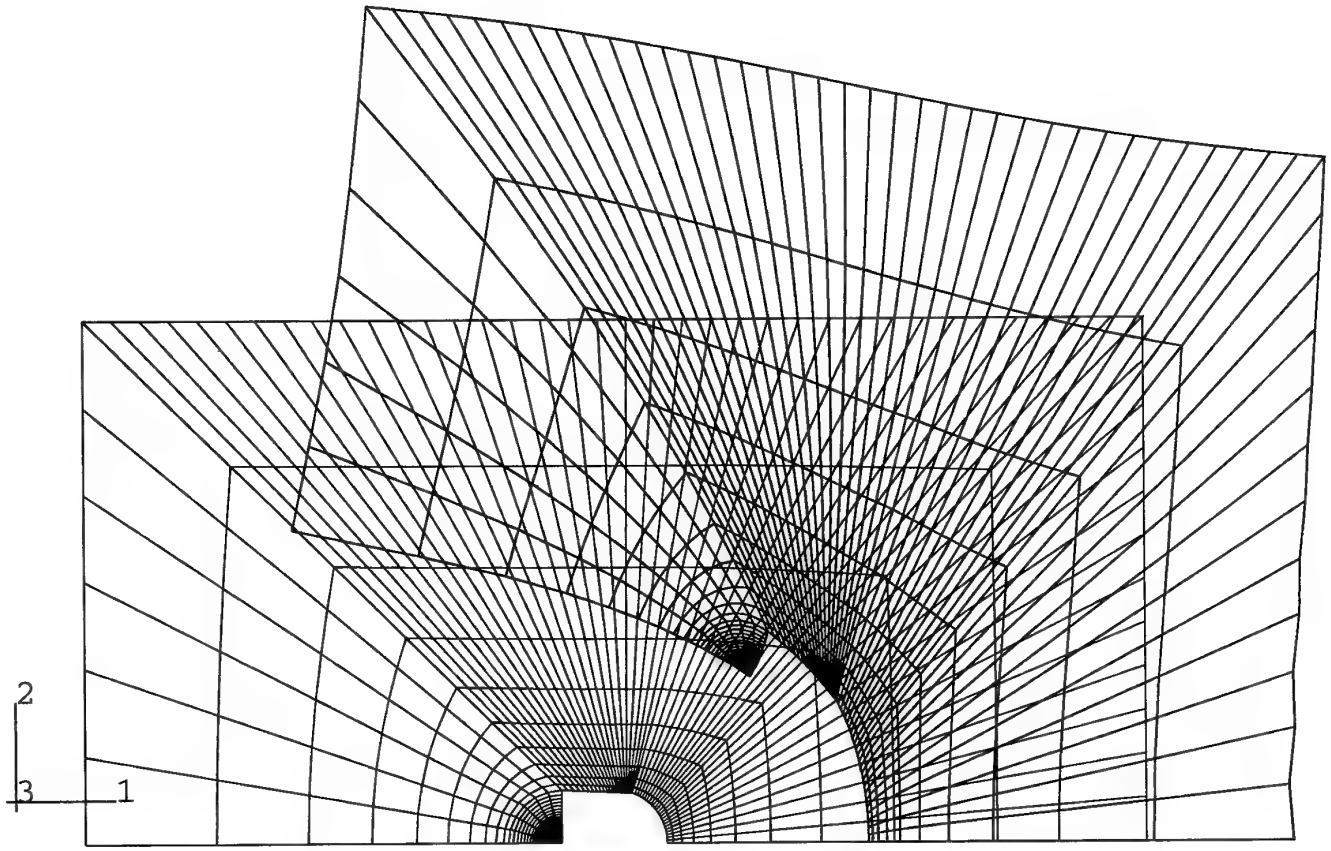

Fig. 29 Undeformed (in red) and deformed (in black) finite element grids for the missing part of Figure 28. Applied displacement u_0=3.3295 mm. Case I.

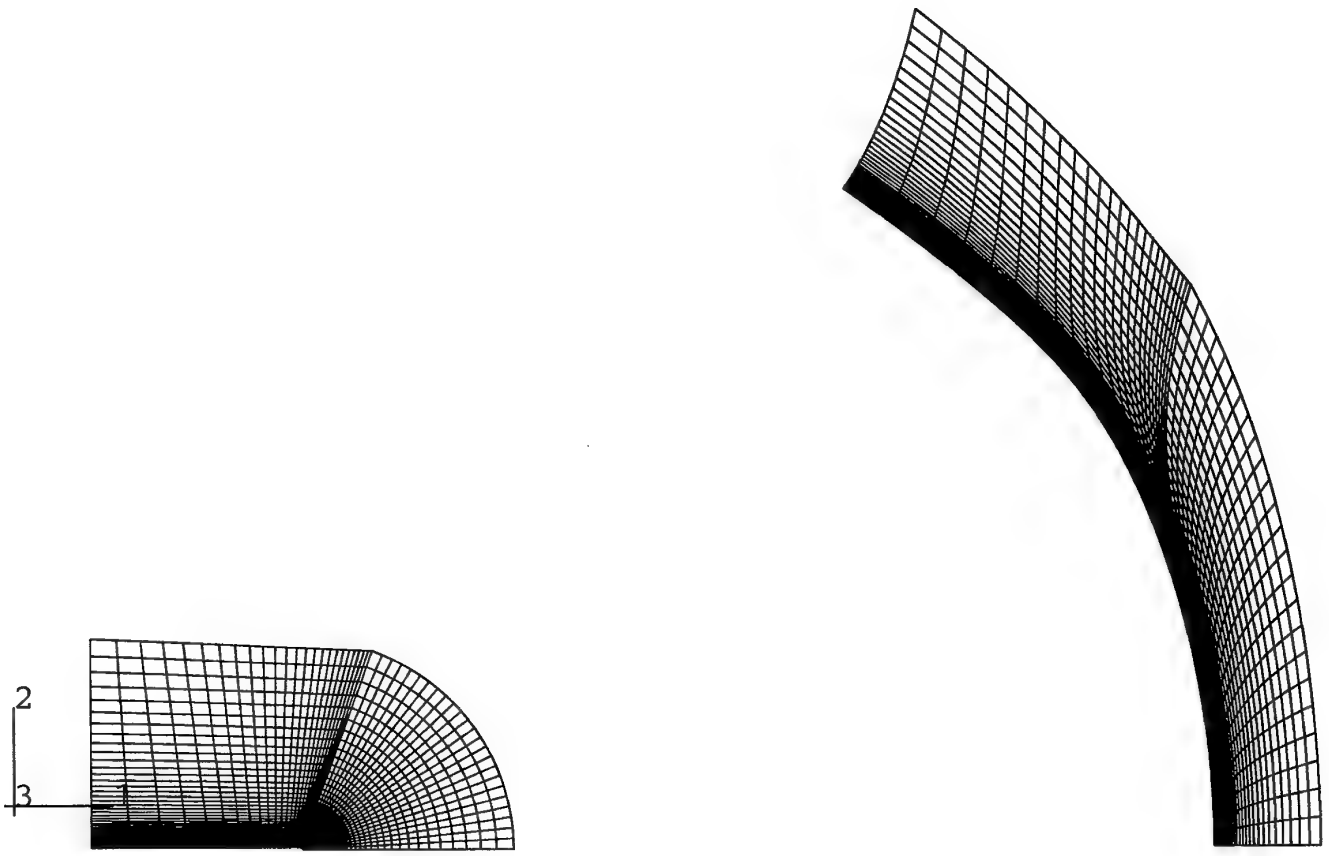

Fig. 30 Undeformed (in red) and deformed (in black) finite element grids for the missing part of Figure 29. Applied displacement u_0=3.3295 mm. Case I.

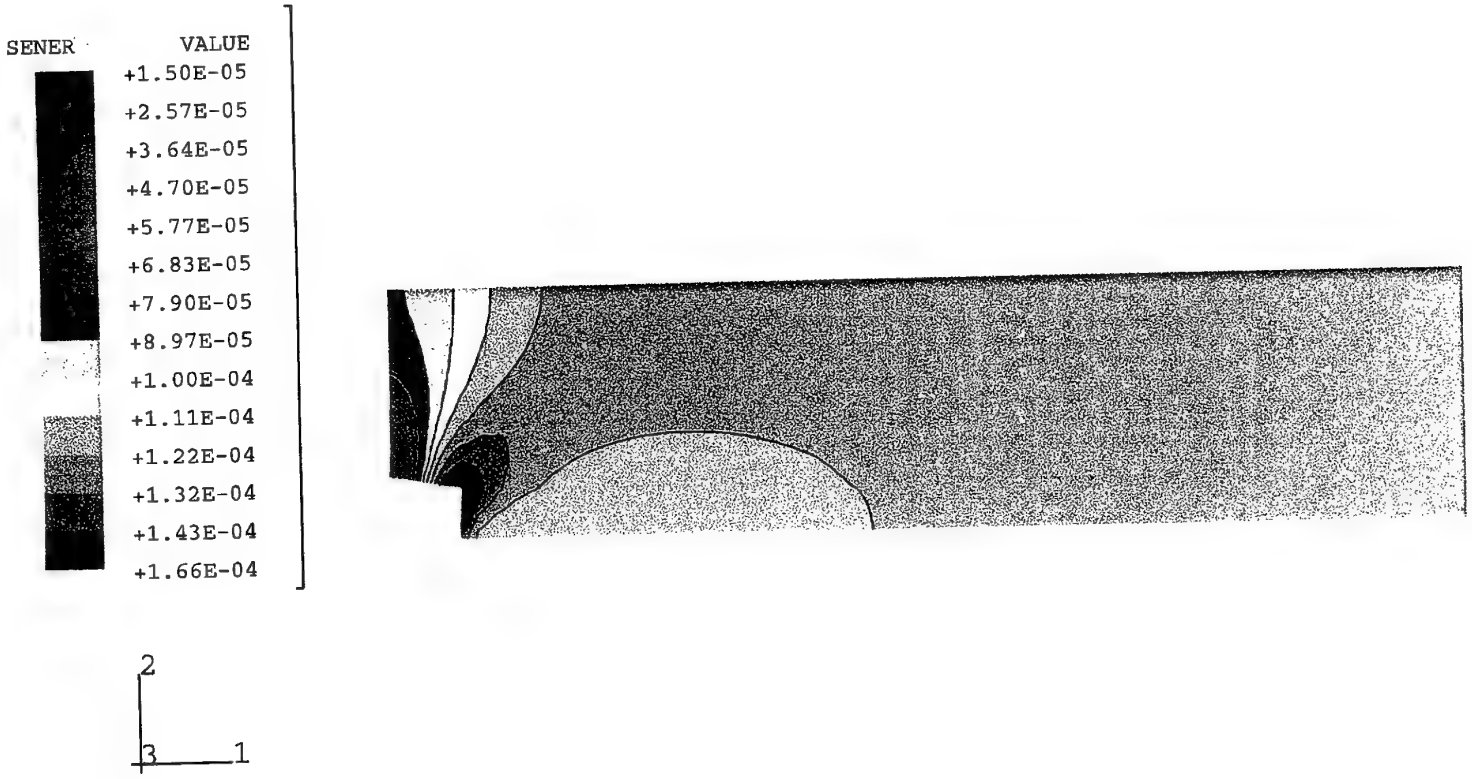

Fig. 31 Strain energy density, dW/dV, contours (in the deformed specimen configuration) for Figure 28. Values in kN.mm/mm^3. Applied displacement u_0=3.3295 mm. Case I.

Fig. 32 Strain energy density, dW/dV, contours (in the deformed specimen configuration) for Figure 29. Values in kN.mm/mm^3. Applied displacement u_0=3.3295 mm. Case I.

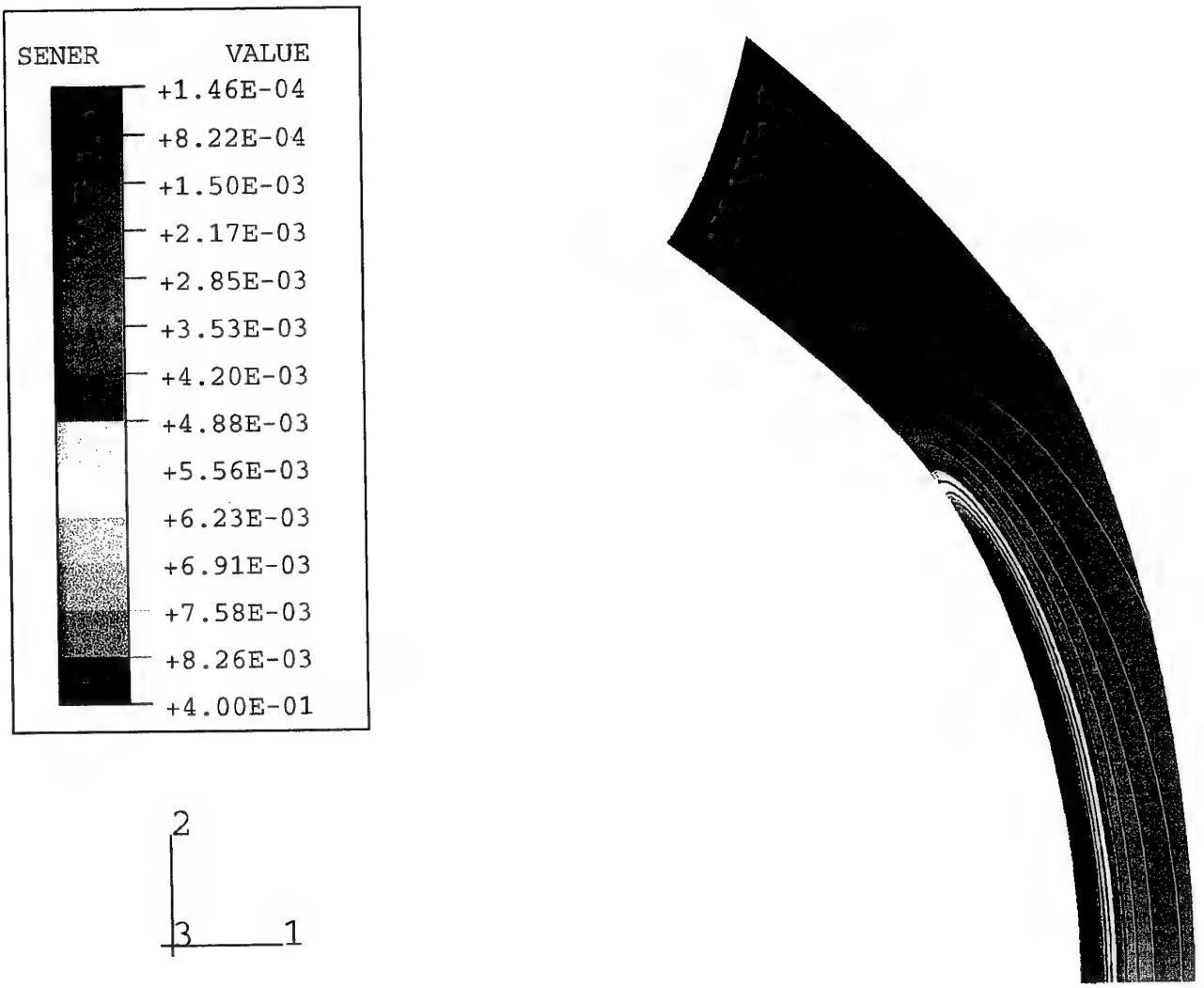

Fig. 33 Strain energy density, dW/dV, contours (in the deformed specimen configuration) for Figure 30. Values in kN.mm/mm^3. Applied displacement u_0=3.3295 mm. Case I.

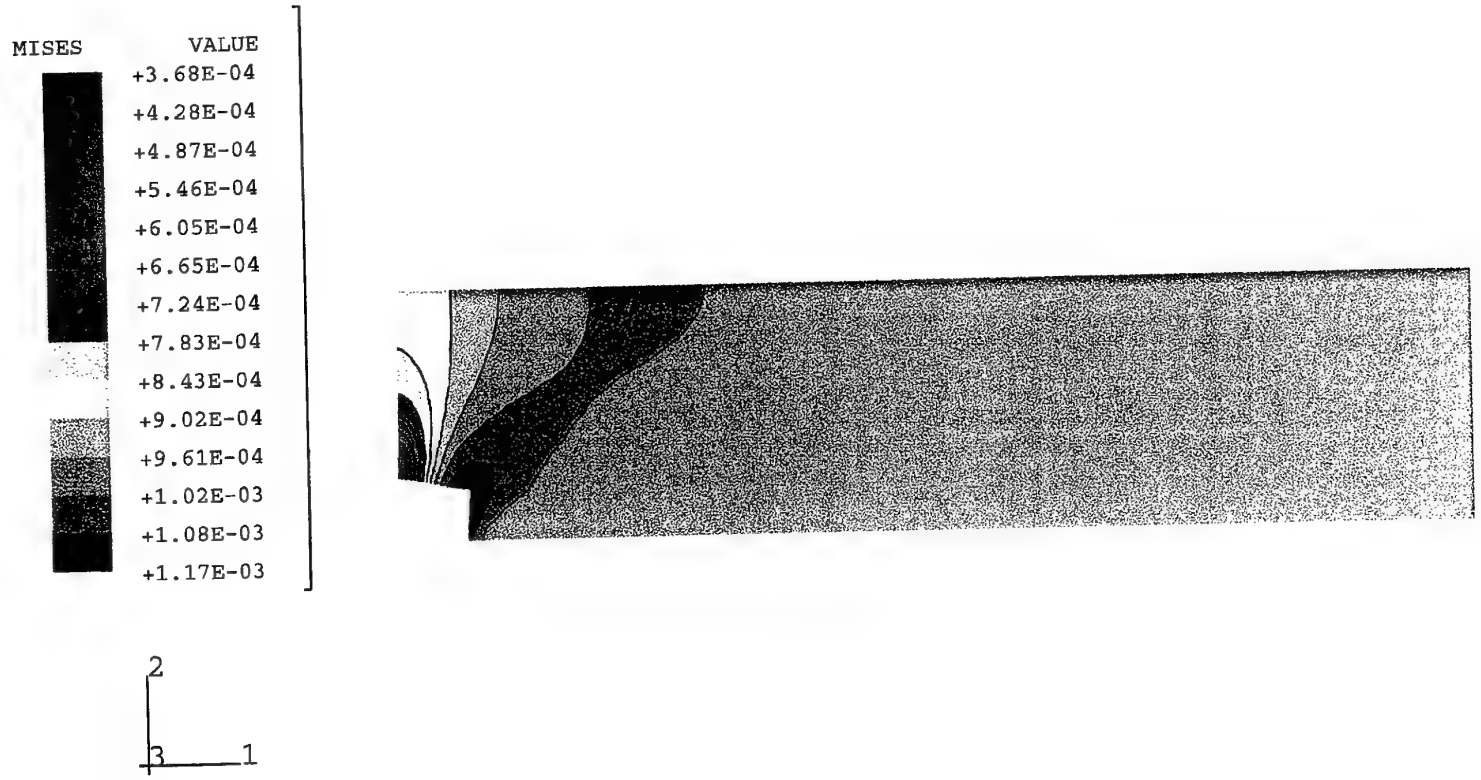

Fig. 34 Mises stress, σ_{eff}, contours (in the deformed specimen configuration) for Figure 28. Values in kN/mm^2. Applied displacement u_0=3.3295 mm. Case I.

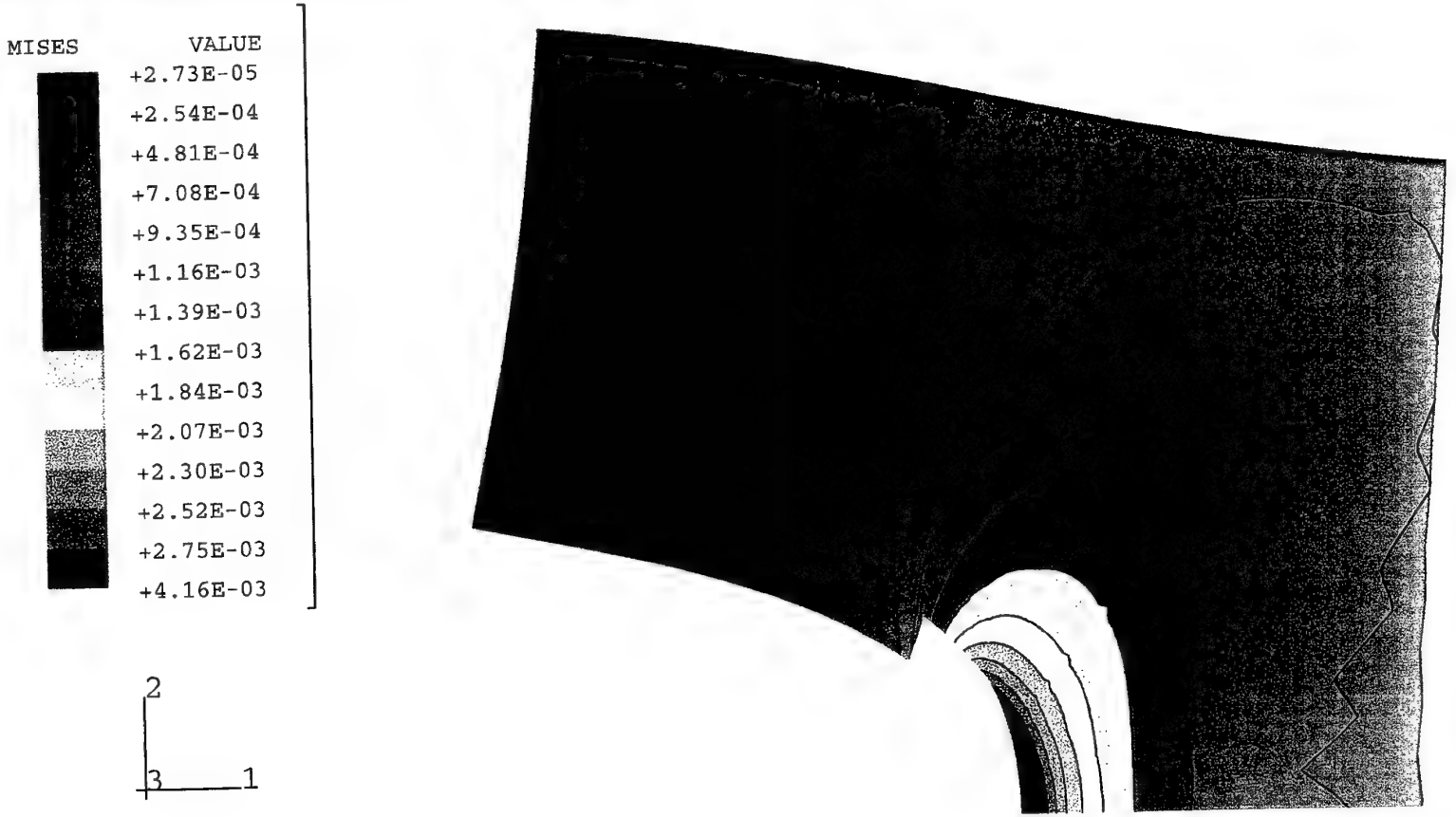

Fig. 35 Mises stress, σ_{eff}, contours (in the deformed specimen configuration) for Figure 29. Values in kN/mm^2. Applied displacement u_0=3.3295 mm. Case I.

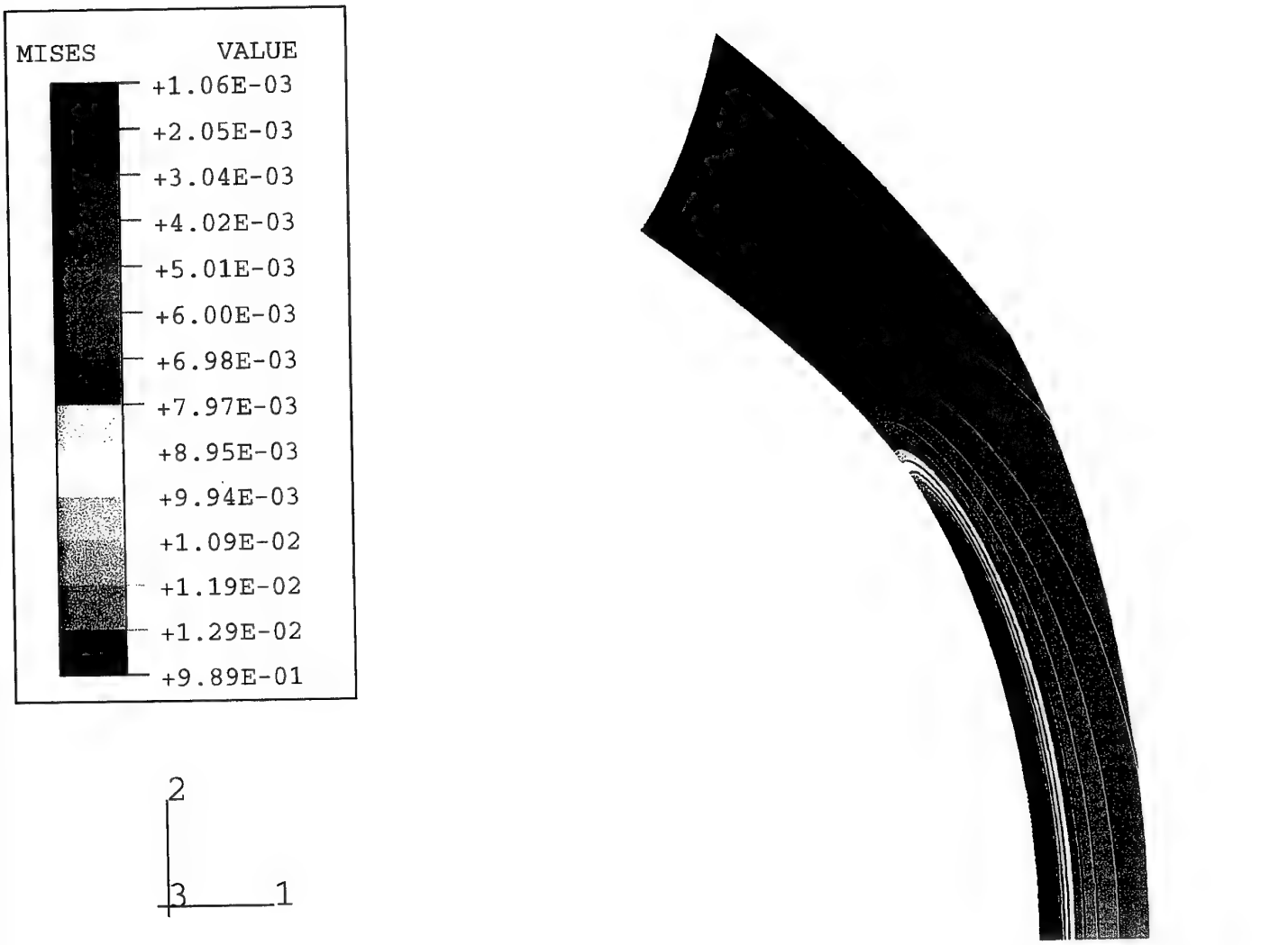

Fig. 36 Mises stress, σ_{eff}, contours (in the deformed specimen configuration) for Figure 30. Values in kN/mm^2. Applied displacement u_0=3.3295 mm. Case I.

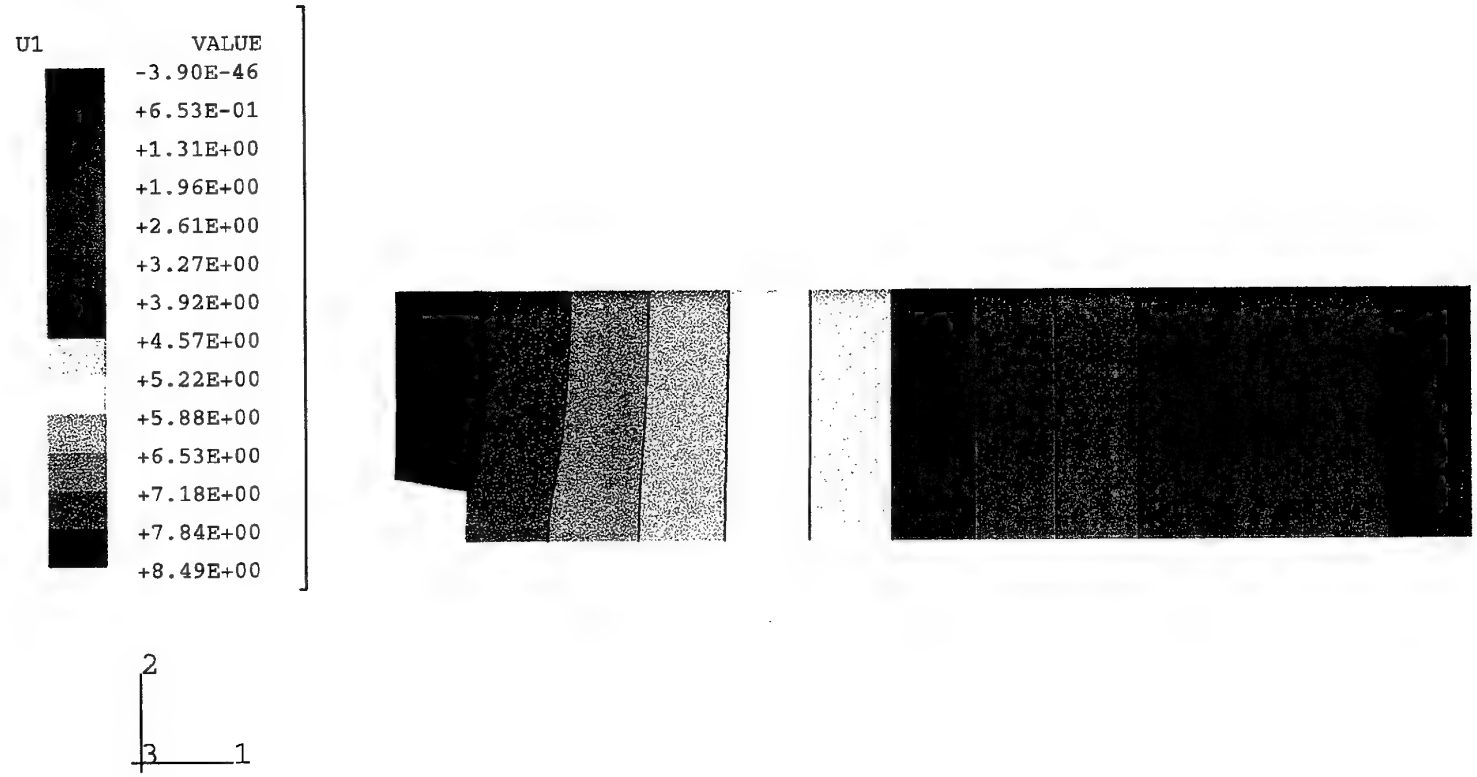

Fig. 37 Displacement along the crack axis direction, u_1, contours (in the deformed specimen configuration) for Figure 28. Values in mm. Applied displacement u_0=3.3295 mm. Case I.

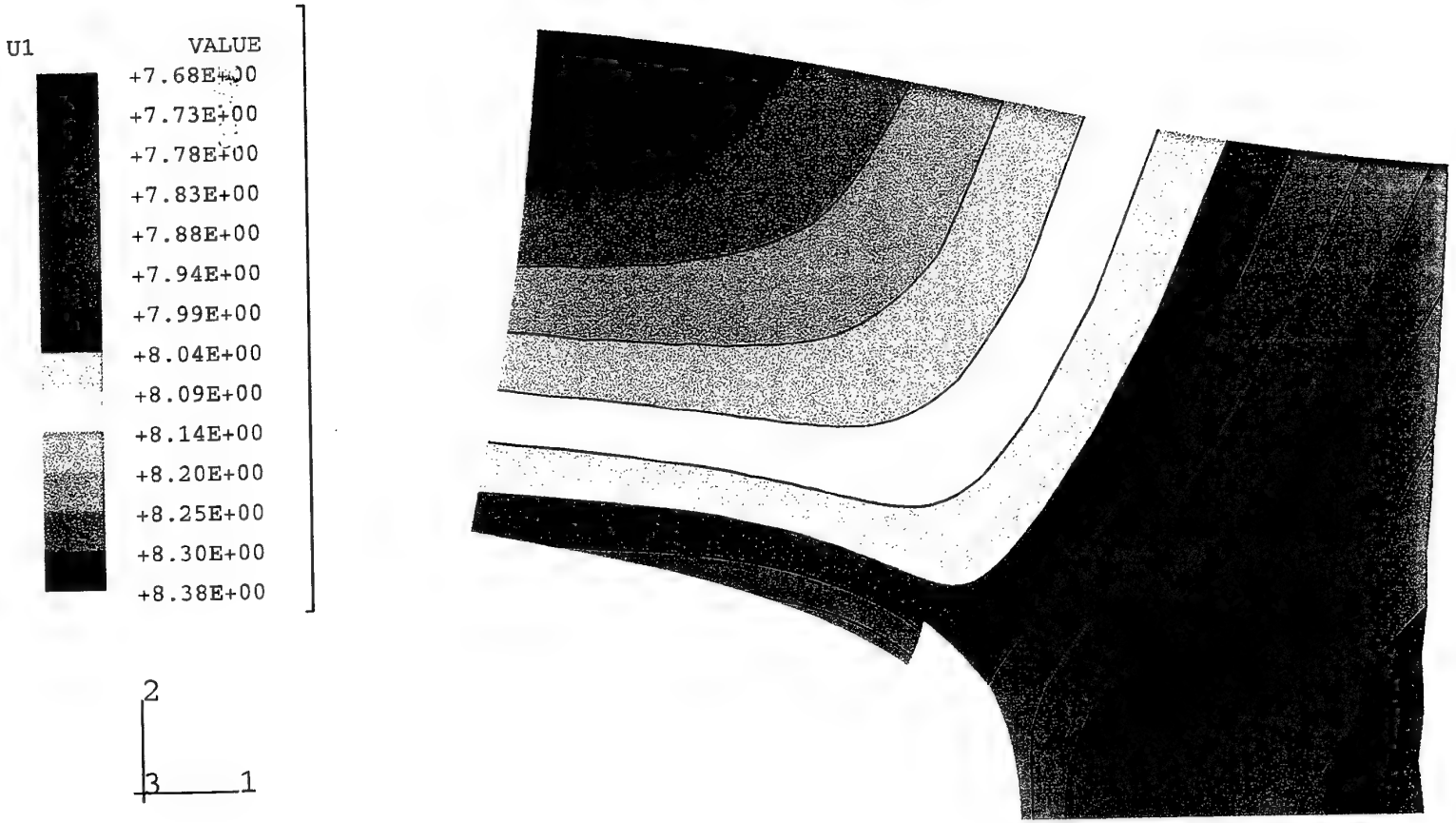

Fig. 38 Displacement along the crack axis direction, u_1, contours (in the deformed specimen configuration) for Figure 29. Values in mm. Applied displacement u_0=3.3295 mm. Case I.

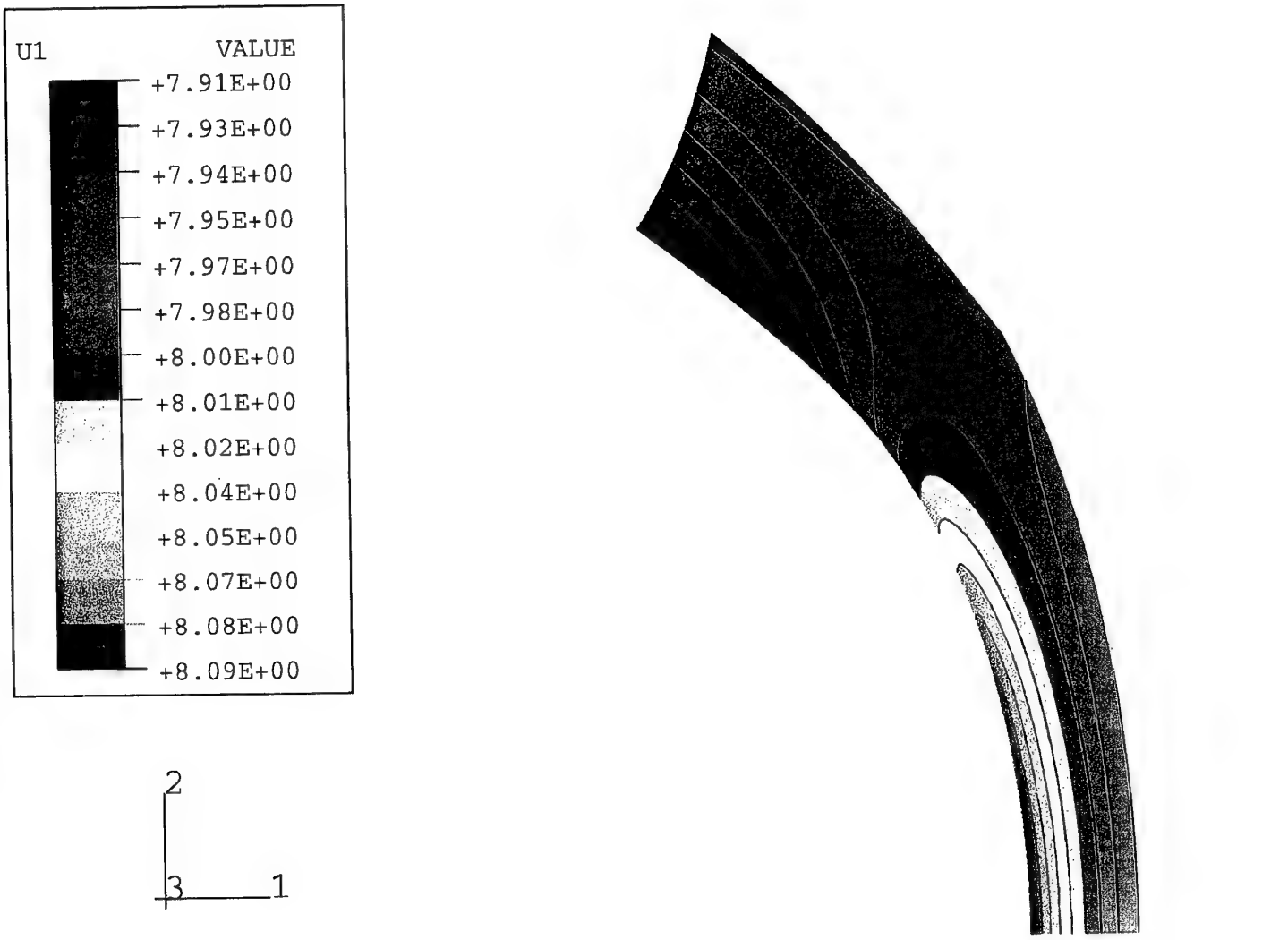

Fig. 39 Displacement along the crack axis direction, u_1, contours (in the deformed specimen configuration) for Figure 30. Values in mm. Applied displacement u_0=3.3295 mm. Case I.

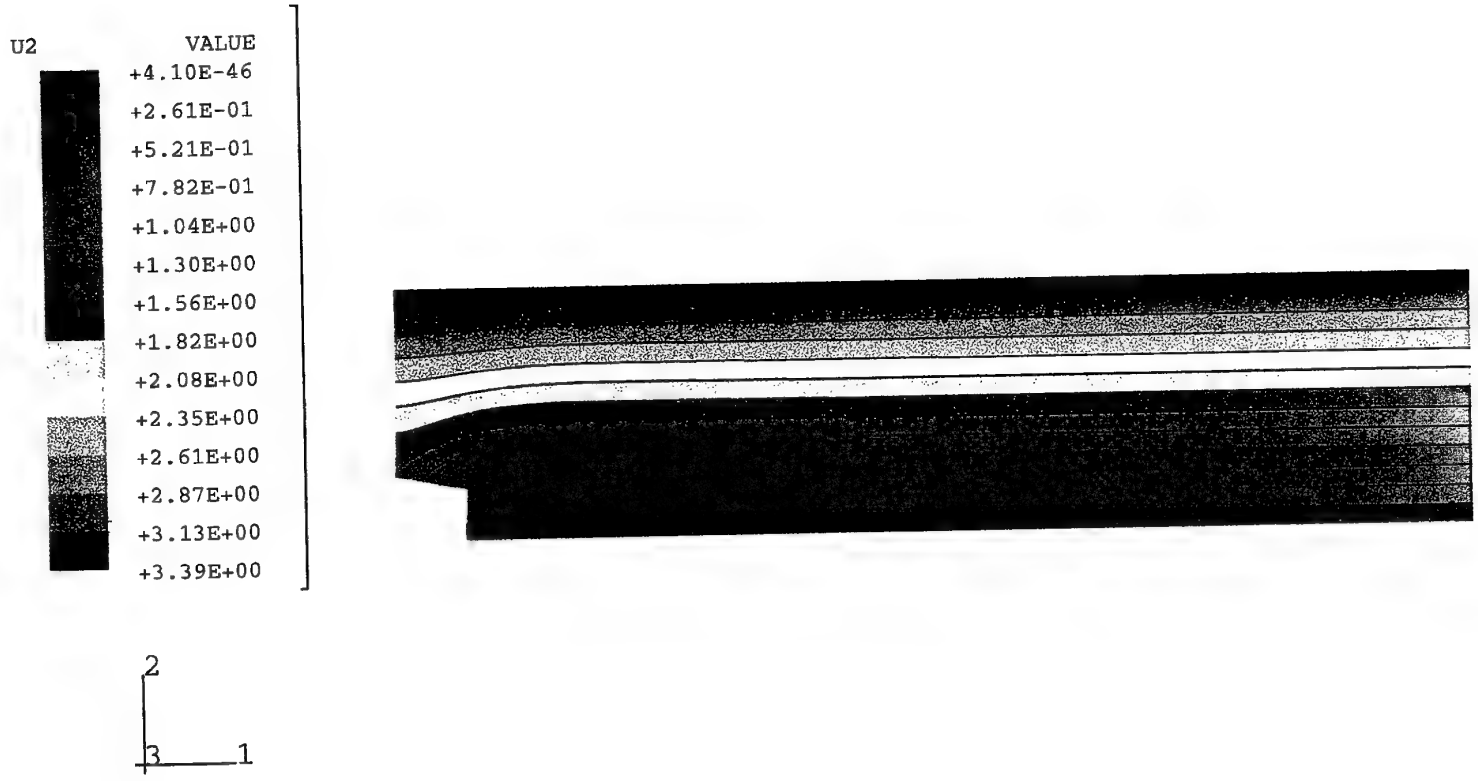

Fig. 40 Displacement along the perpendicular to the crack axis direction, u_2 contours (in the deformed specimen configuration) for Figure 28. Values in mm. Applied displacement u_0=3.3295 mm. Case I.

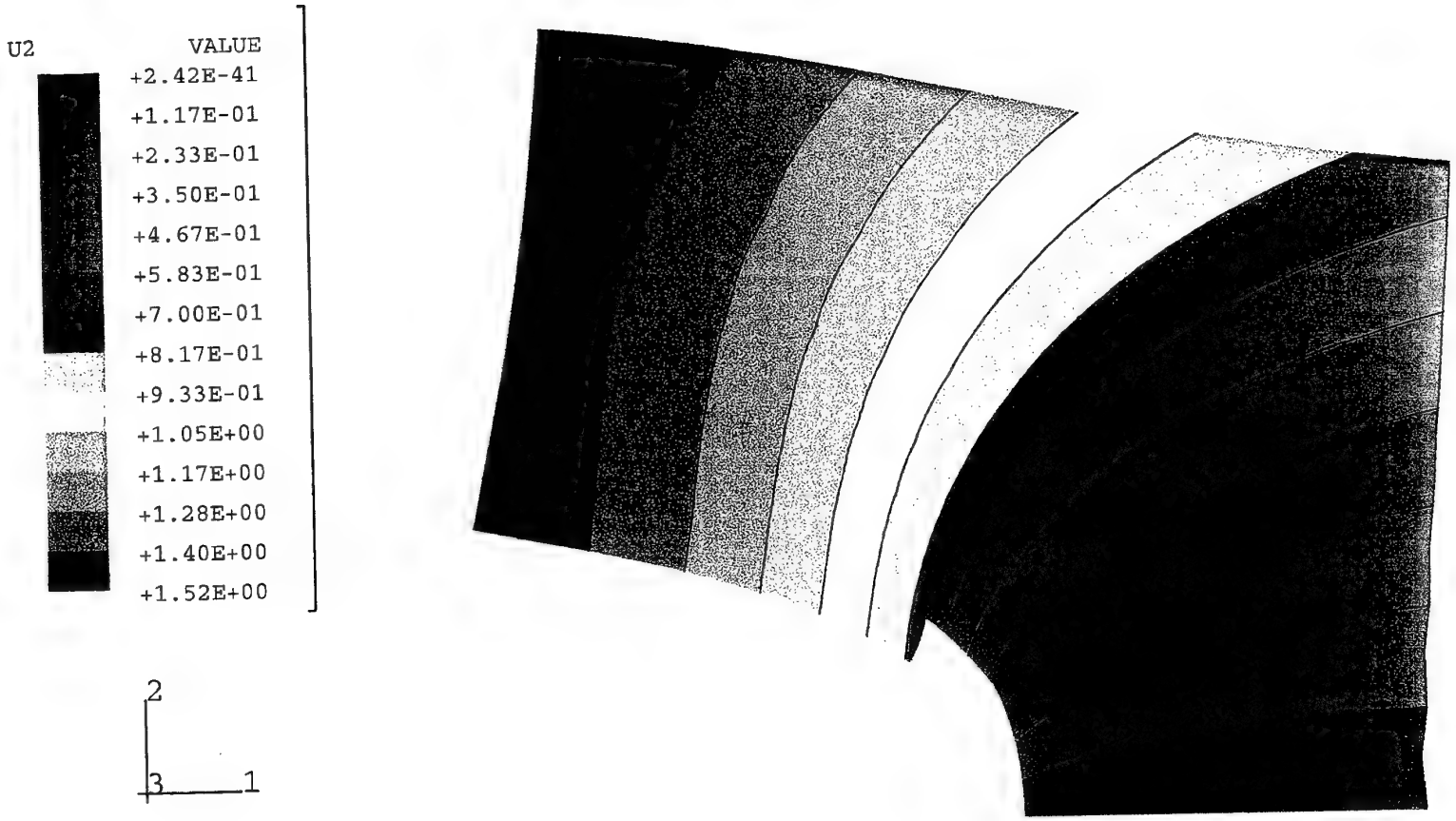

Fig. 41 Displacement along the perpendicular to the crack axis direction, u_2 contours (in the deformed specimen configuration) for Figure 29. Values in mm. Applied displacement u_0=3.3295 mm. Case I.

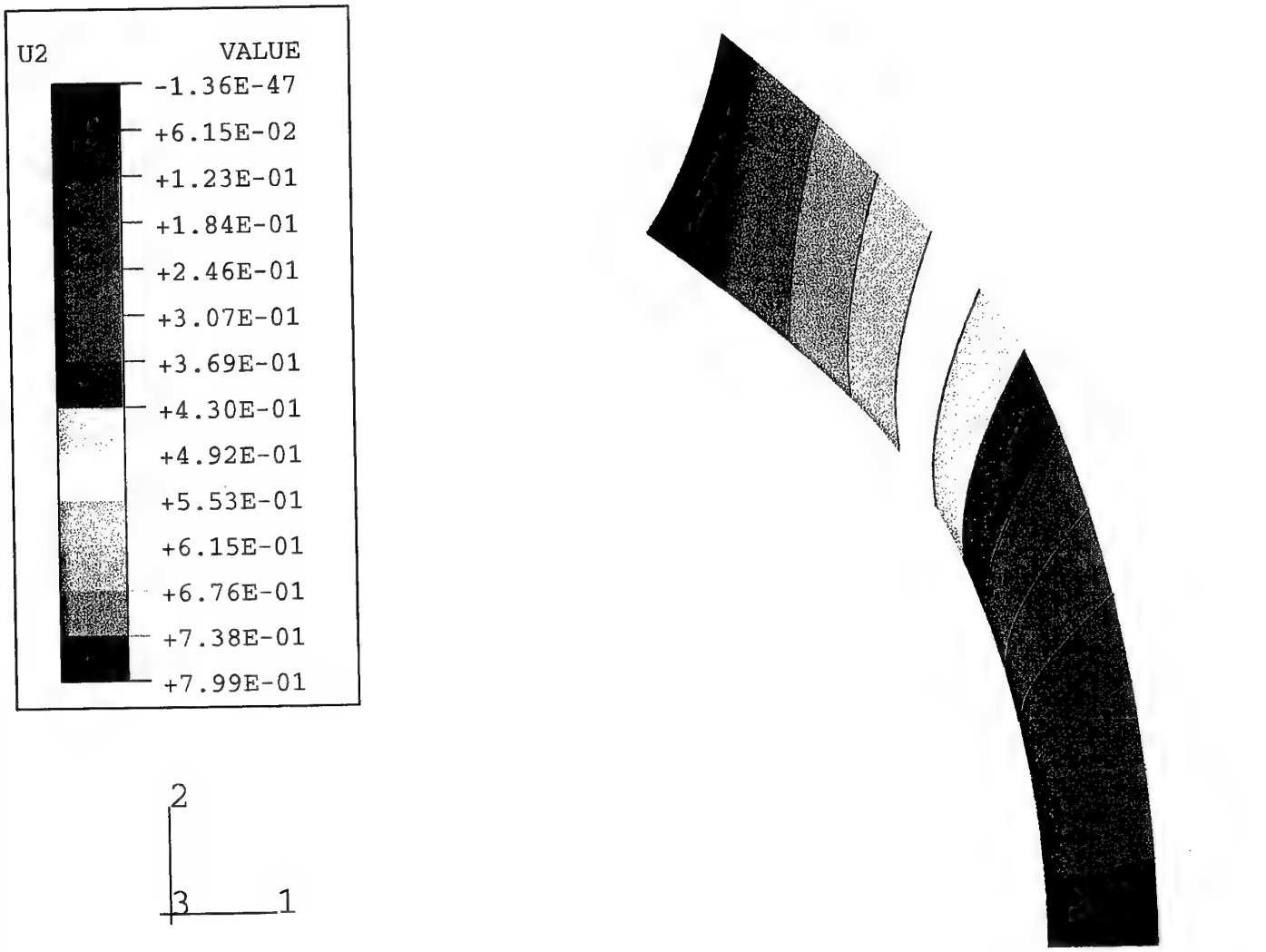

Fig. 42 Displacement along the perpendicular to the crack axis direction, u_2 contours (in the deformed specimen configuration) for Figure 30. Values in mm. Applied displacement u_0=3.3295 mm. Case I.

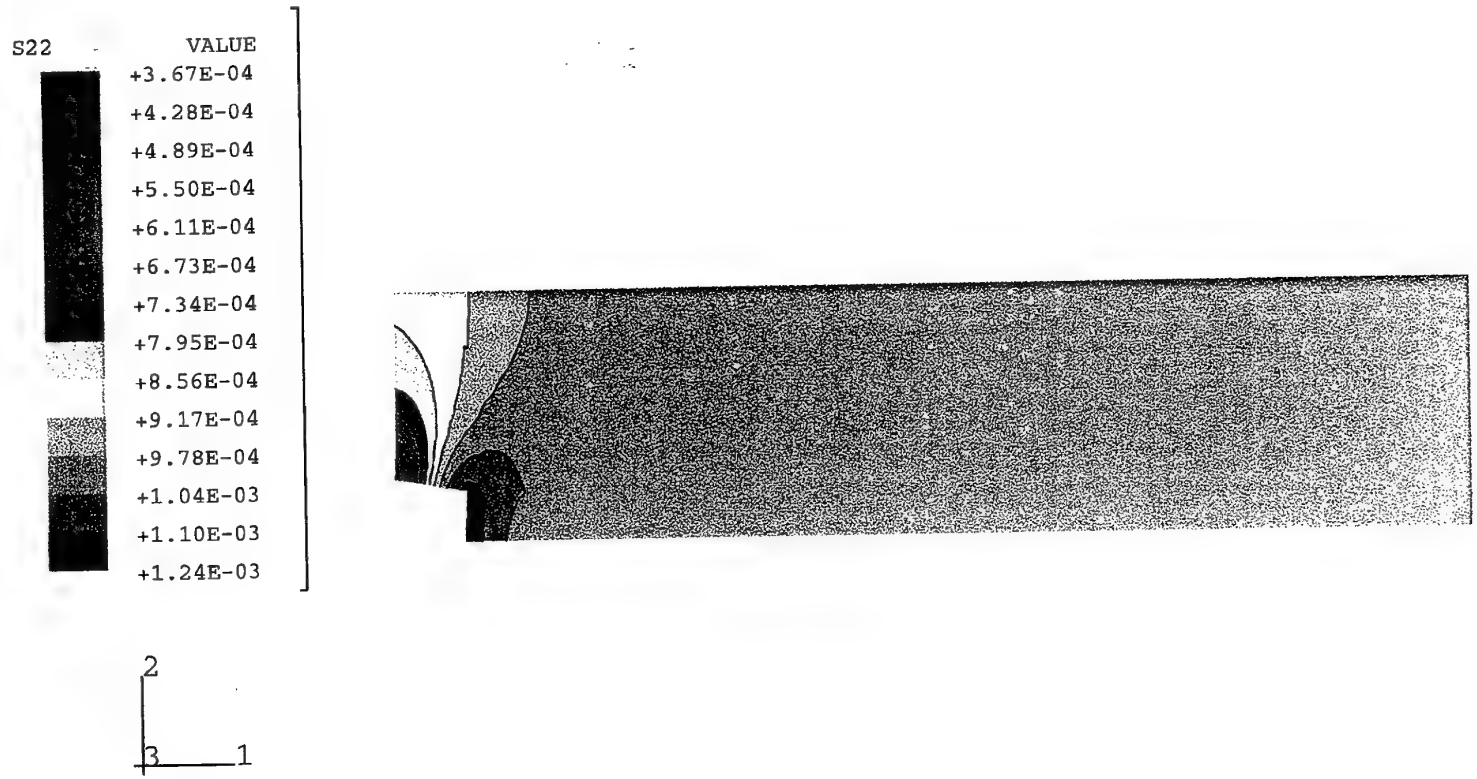

Fig. 43 Normal stress along the perpendicular to the crack axis direction, σ_{22}, contours (in the deformed specimen configuration) for Figure 28. Values in kN/mm^2. Applied displacement u_0=3.3295 mm. Case I.

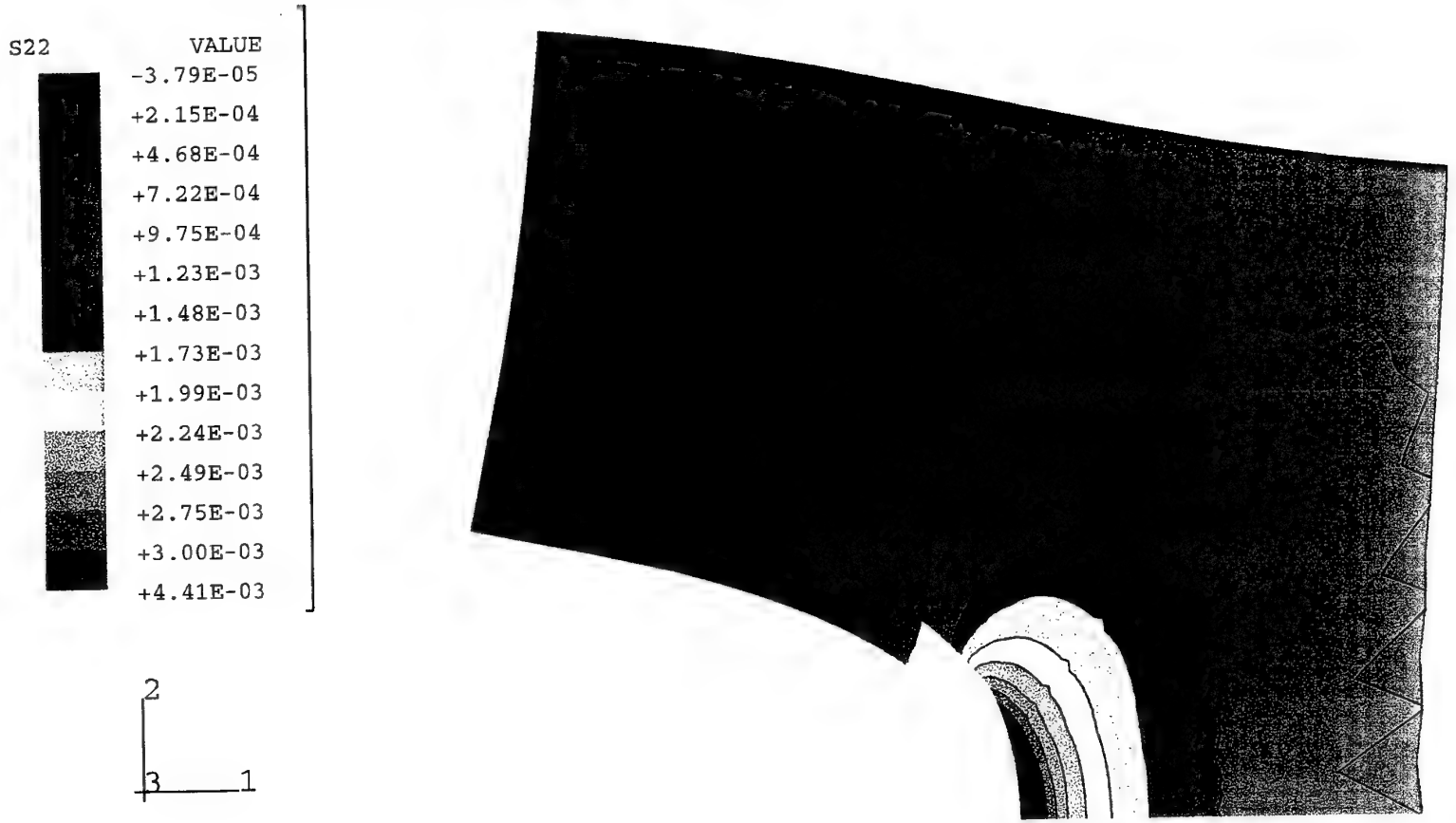

Fig. 44 Normal stress along the perpendicular to the crack axis direction, σ_{22}, contours (in the deformed specimen configuration) for Figure 29. Values in kN/mm^2. Applied displacement u_0=3.3295 mm. Case I.

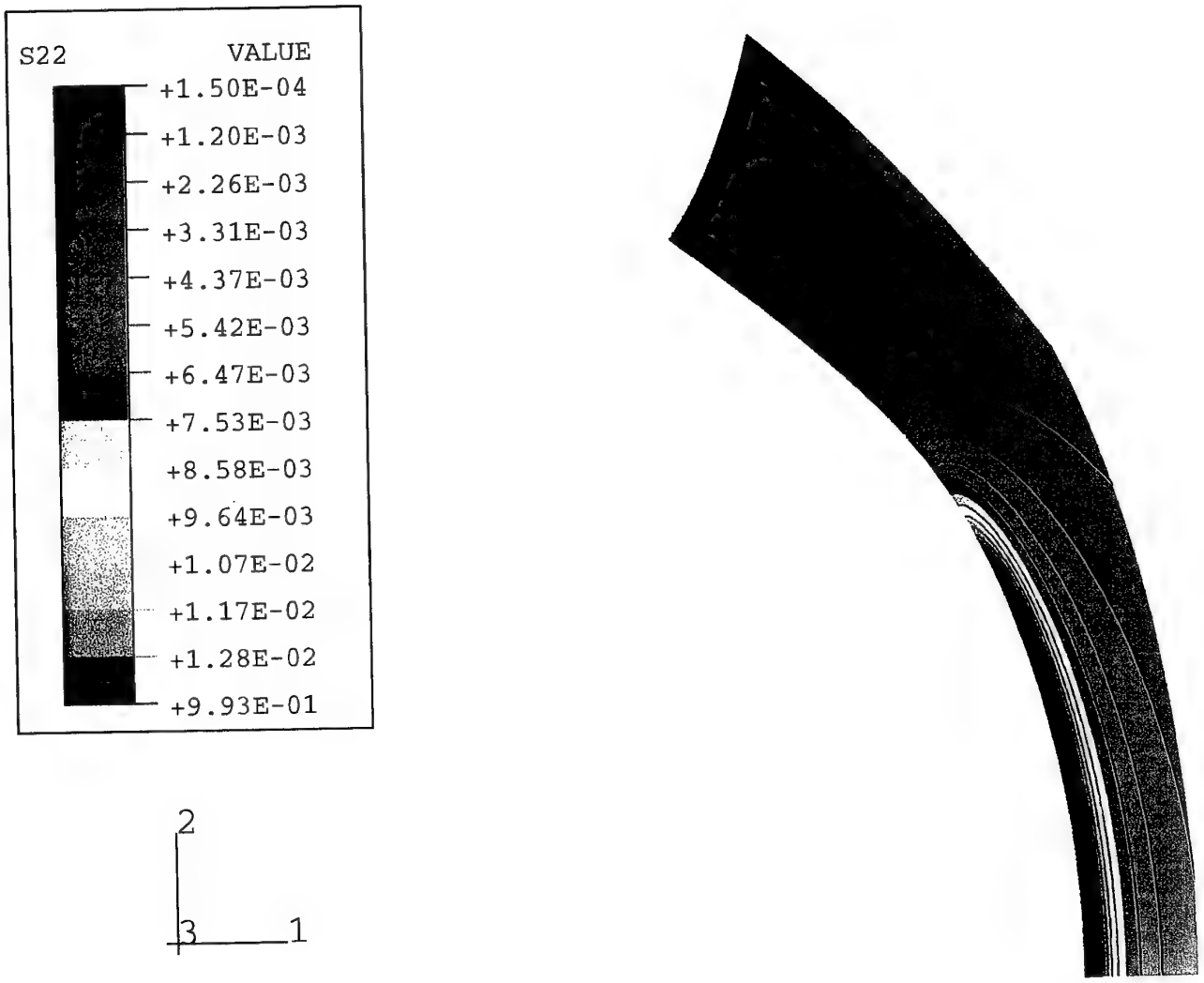

Fig. 45 Normal stress along the perpendicular to the crack axis direction, σ_{22}, contours (in the deformed specimen configuration) for Figure 30. Values in kN/mm^2. Applied displacement u_0=3.3295 mm. Case I.

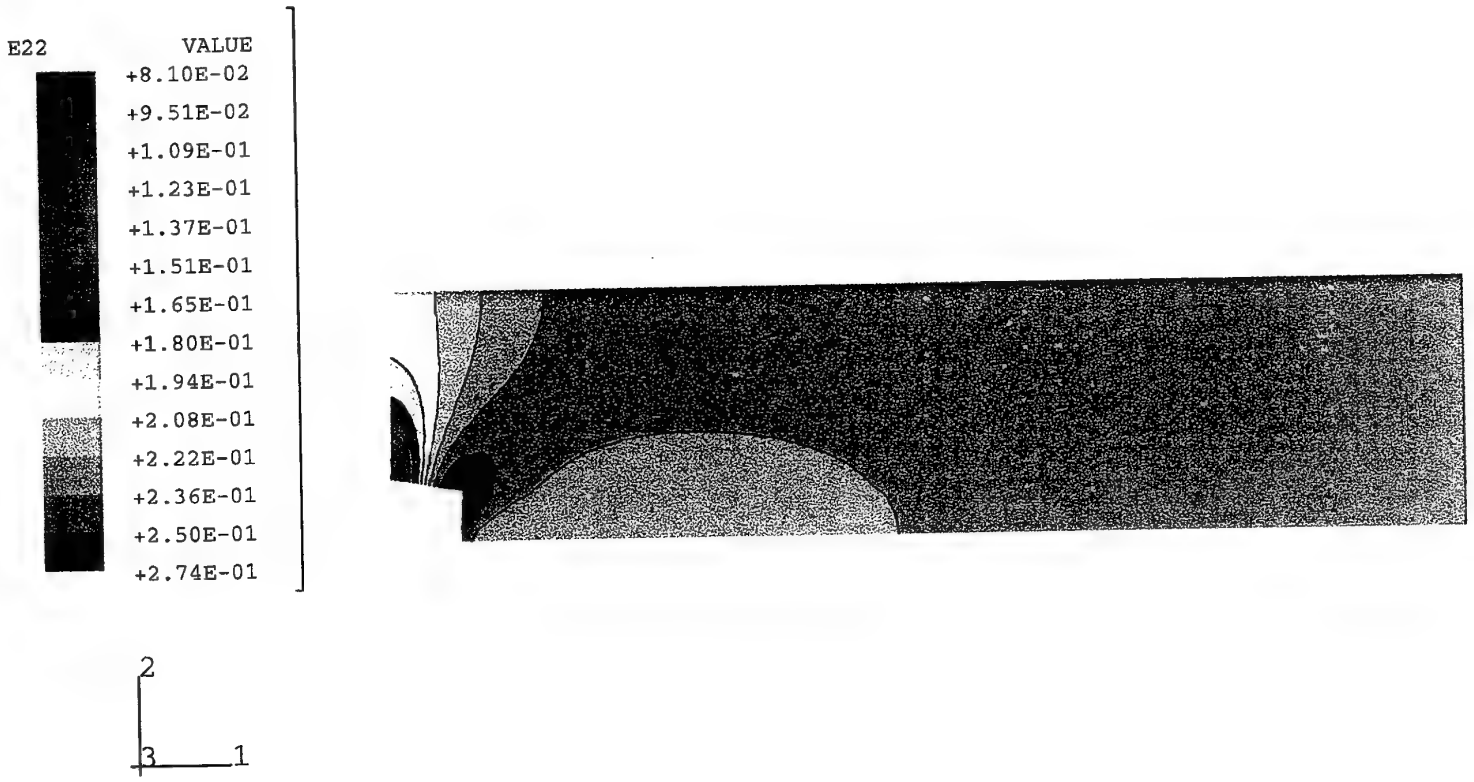

Fig. 46 Normal strain along the perpendicular to the crack axis direction, ε_{22}, contours (in the deformed specimen configuration) for Figure 28. Applied displacement u_0=3.3295 mm. Case I.

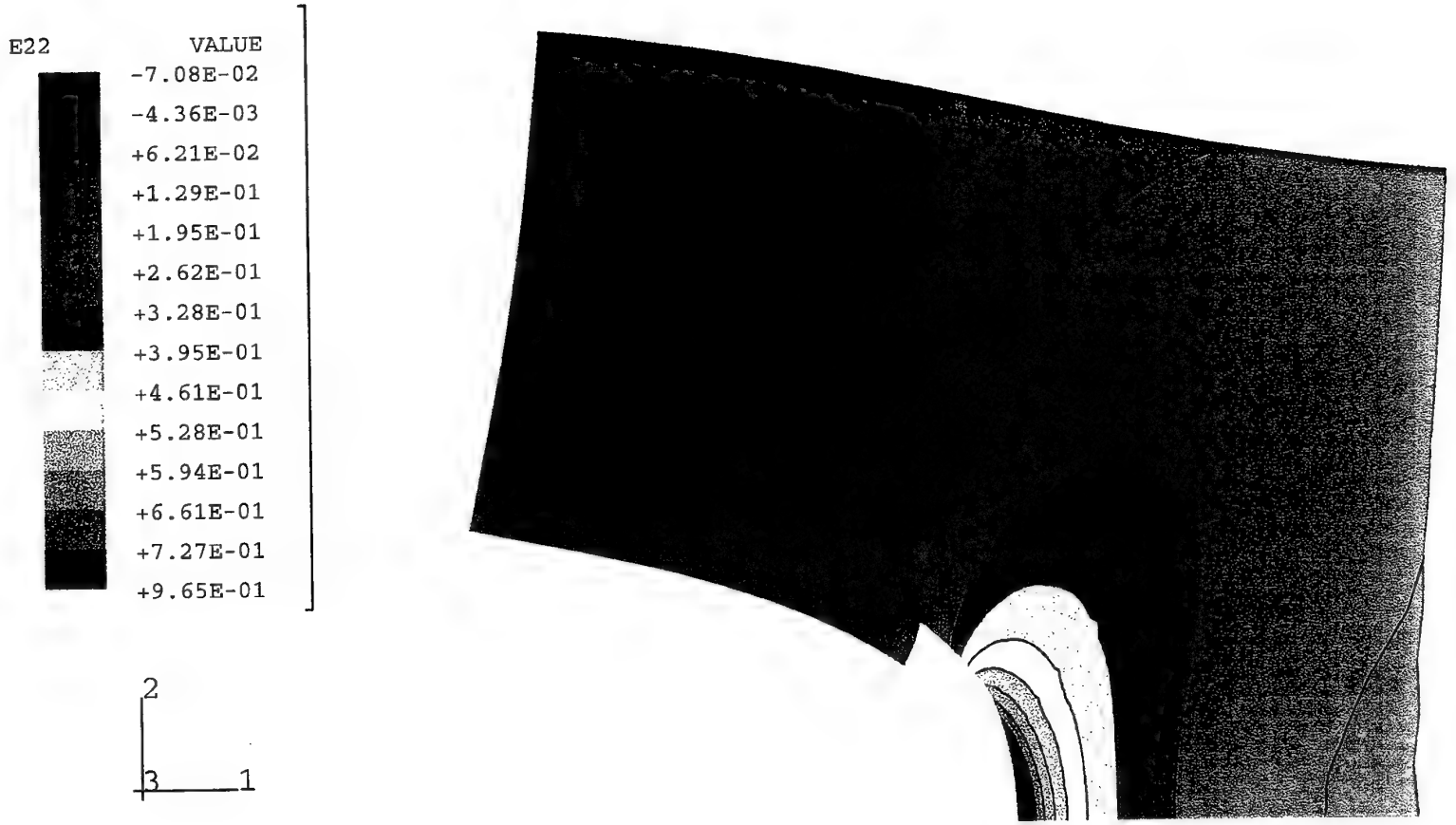

Fig. 47 Normal strain along the perpendicular to the crack axis direction, ε_{22}, contours (in the deformed specimen configuration) for Figure 29. Applied displacement u_0=3.3295 mm. Case I.

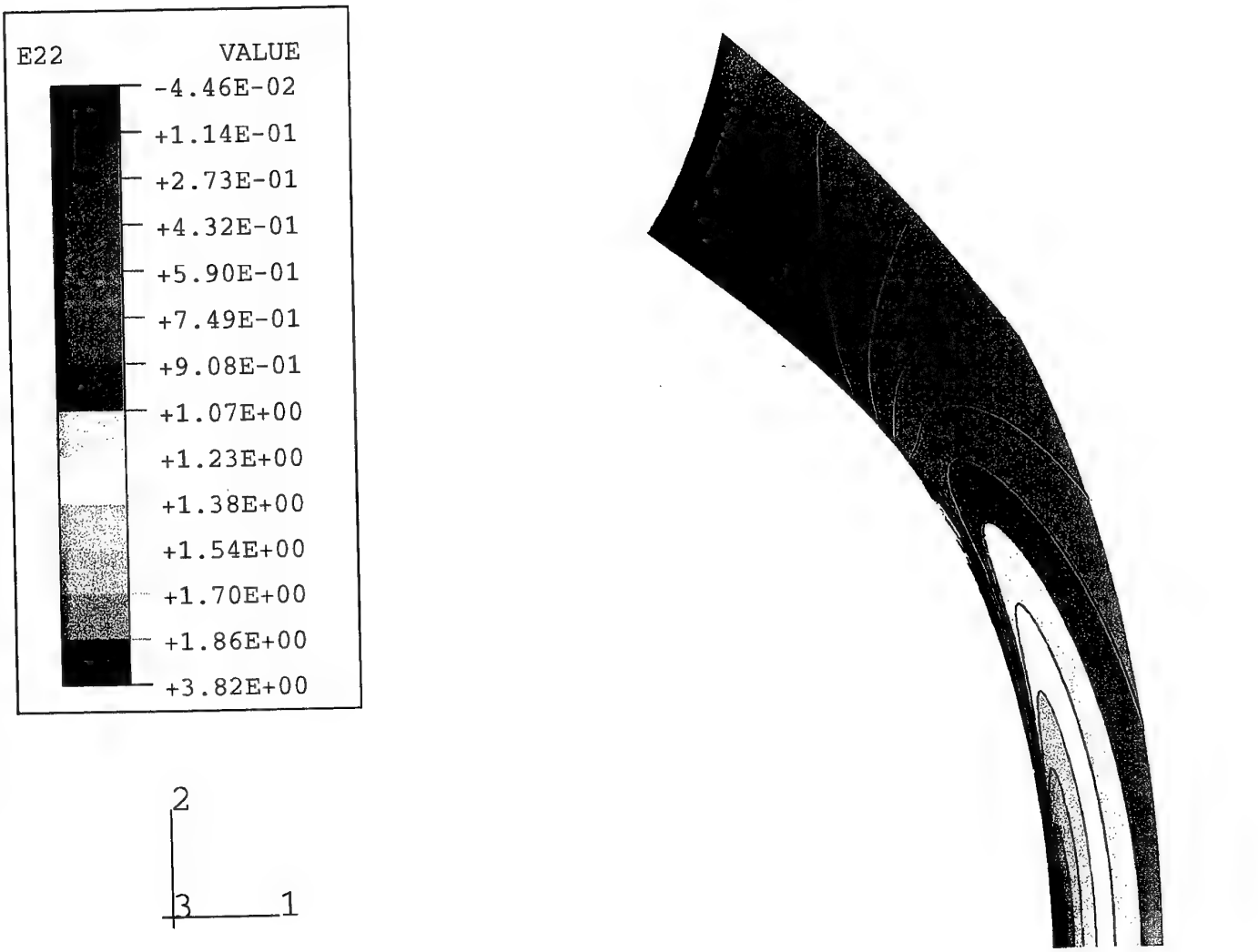

Fig. 48 Normal strain along the perpendicular to the crack axis direction, ε_{22}, contours (in the deformed specimen configuration) for Figure 30. Applied displacement u_0=3.3295 mm. Case I.

Case II

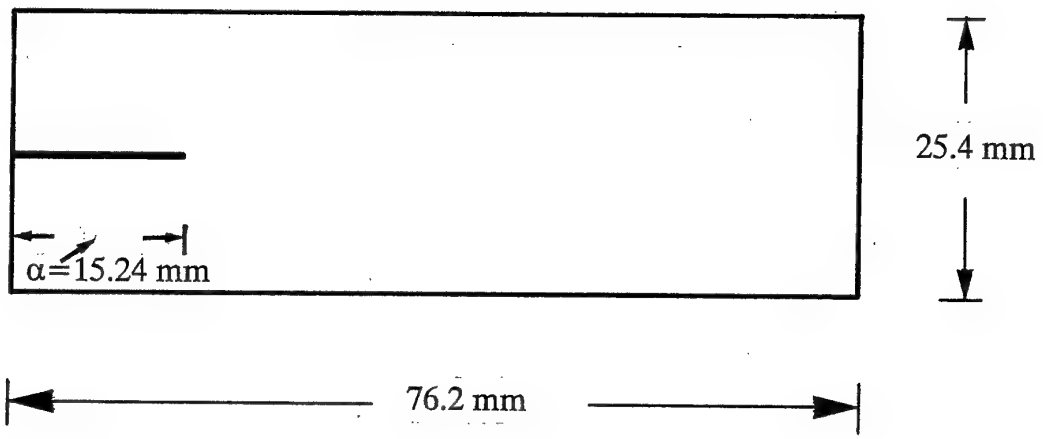

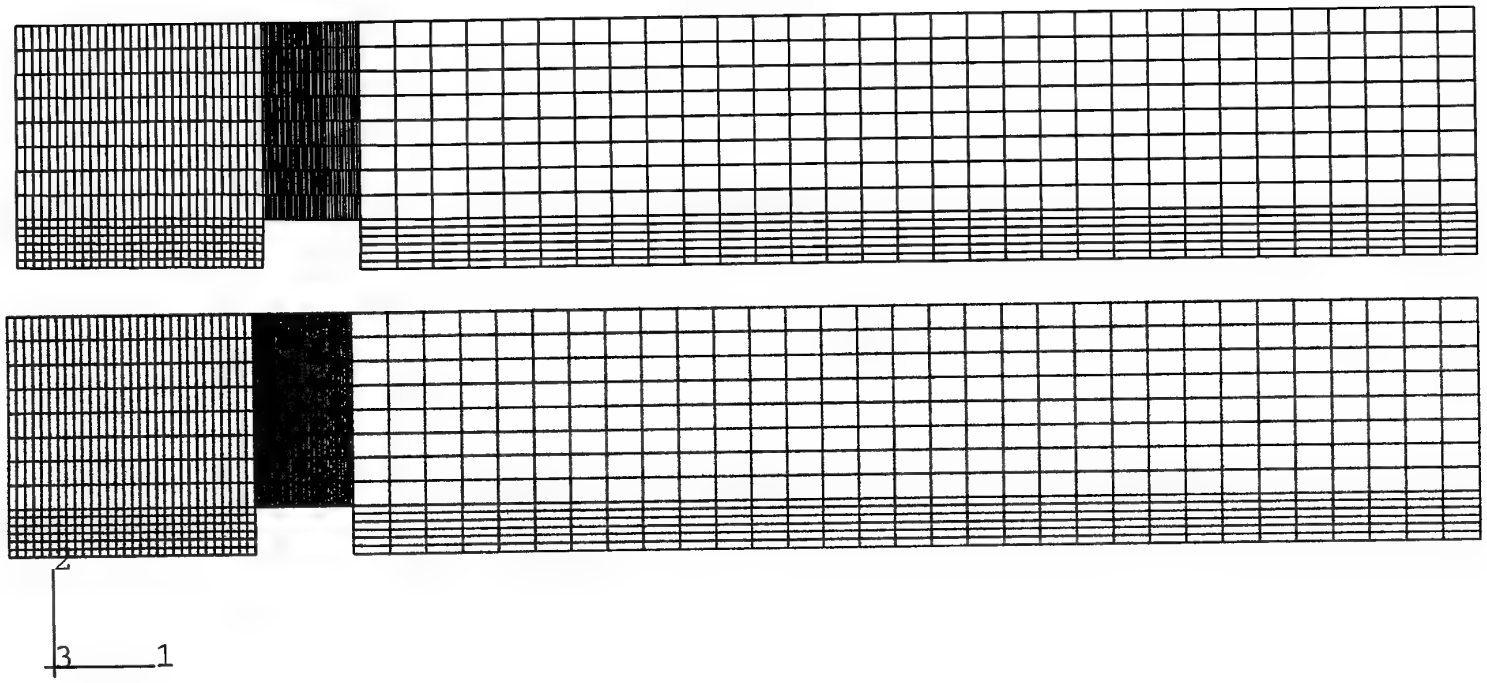

Fig. 49 Undeformed (in red) and deformed (in black) finite element grids for half specimen. Applied displacement u_0=0.2541 mm. Case II.

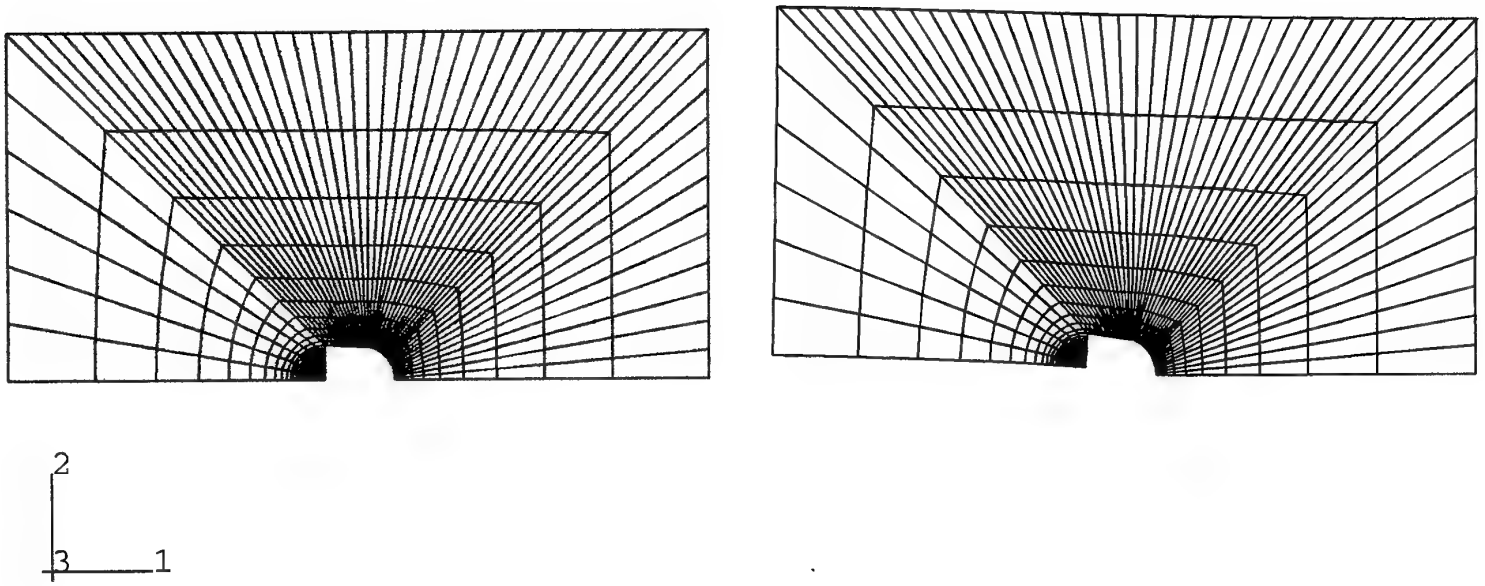

Fig. 50 Undeformed (in red) and deformed (in black) finite element grids for the missing part of Figure 49. Applied displacement u_0=0.2541 mm. Case II.

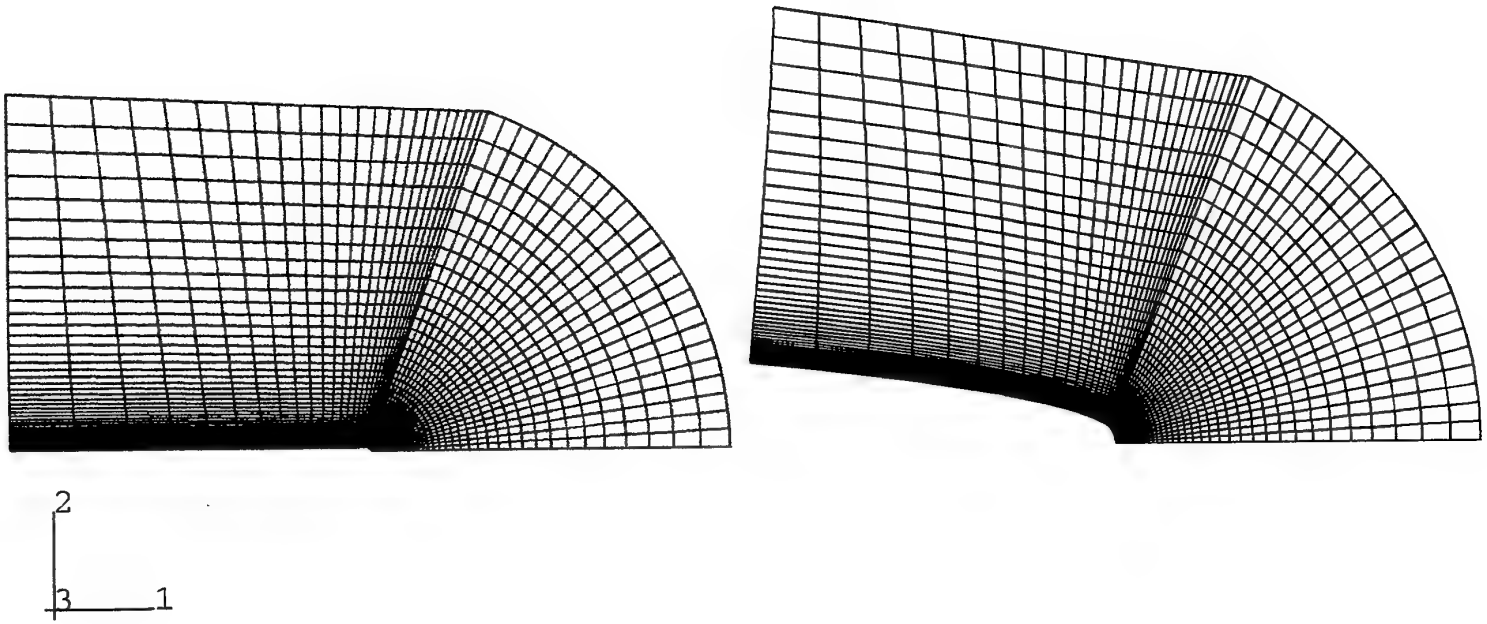

Fig. 51 Undeformed (in red) and deformed (in black) finite element grids for the missing part of Figure 50. Applied displacement u_0=0.2541 mm. Case II.

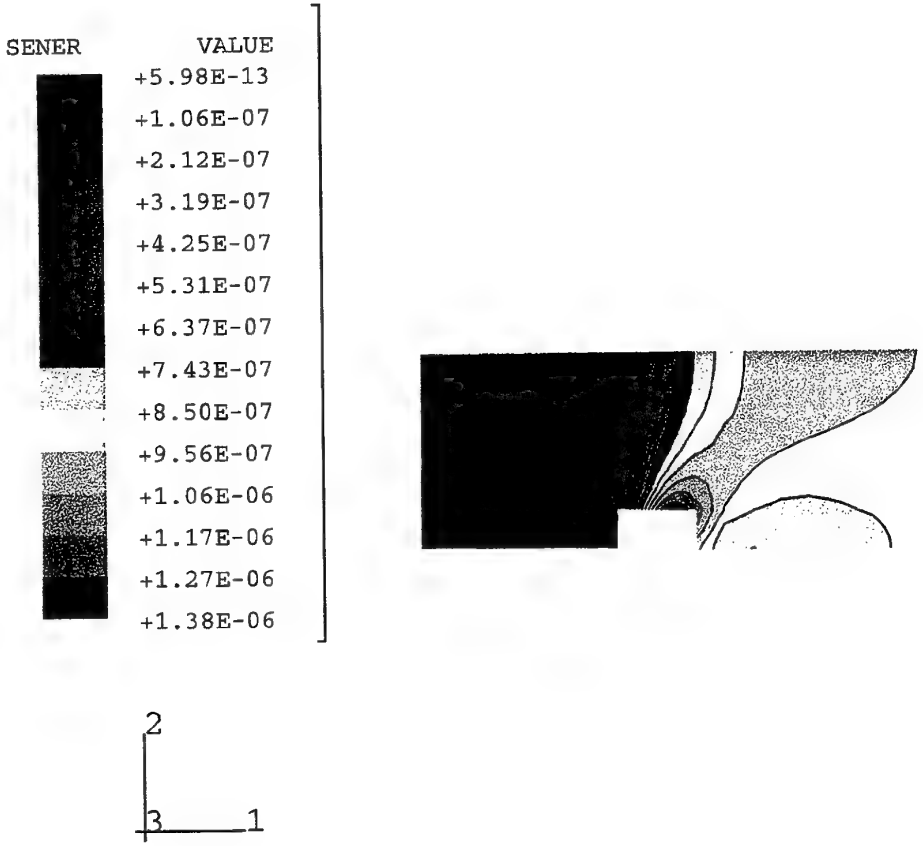

Fig. 52 Strain energy density, dW/dV, contours (in the deformed specimen configuration) for Figure 49. Values in kN.mm/mm^3. Applied displacement u_0=0.2541 mm. Case II.

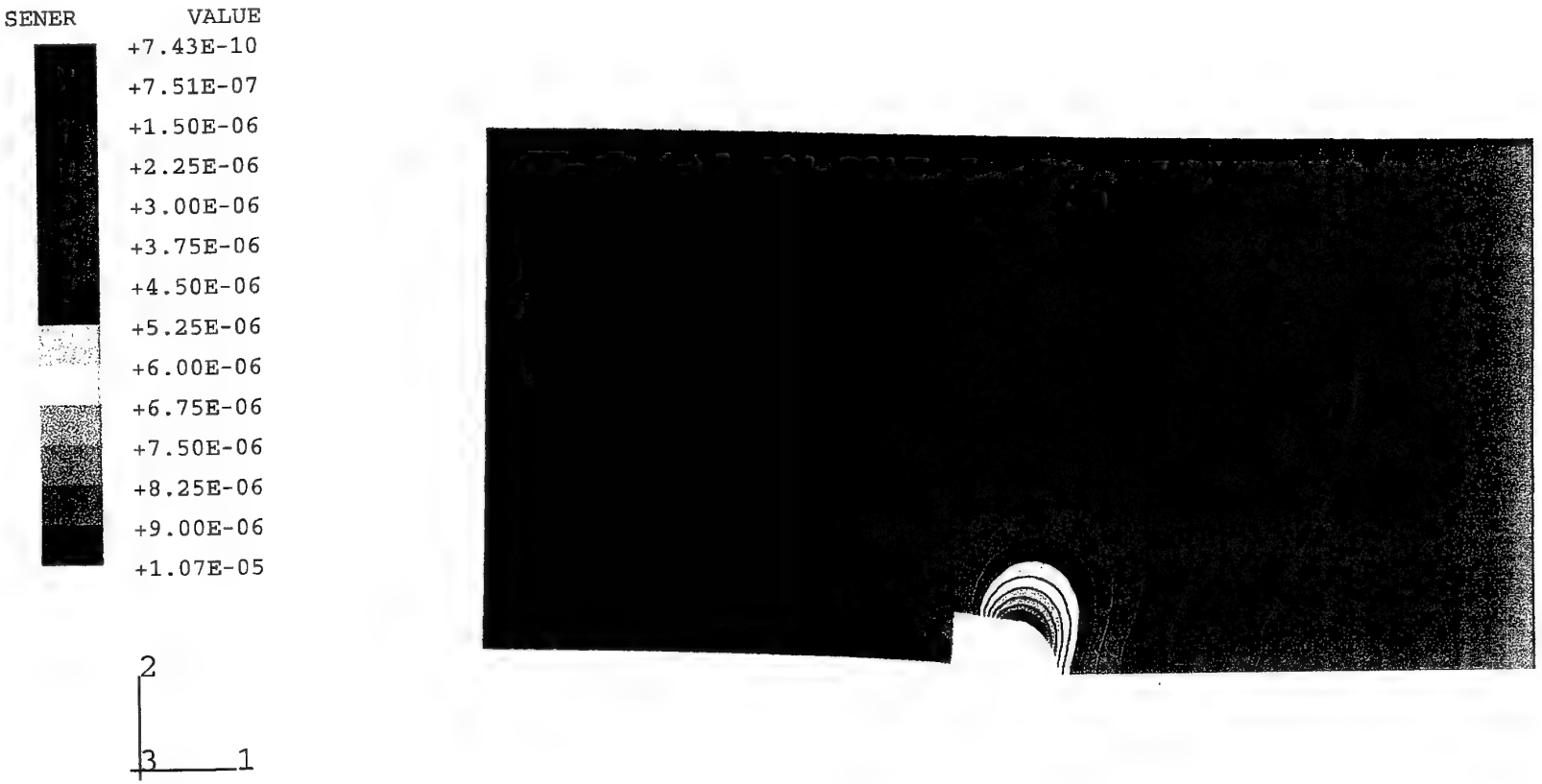

Fig. 53 Strain energy density, dW/dV, contours (in the deformed specimen configuration) for Figure 50. Values in kN.mm/mm^3. Applied displacement u_0=0.2541 mm. Case II.

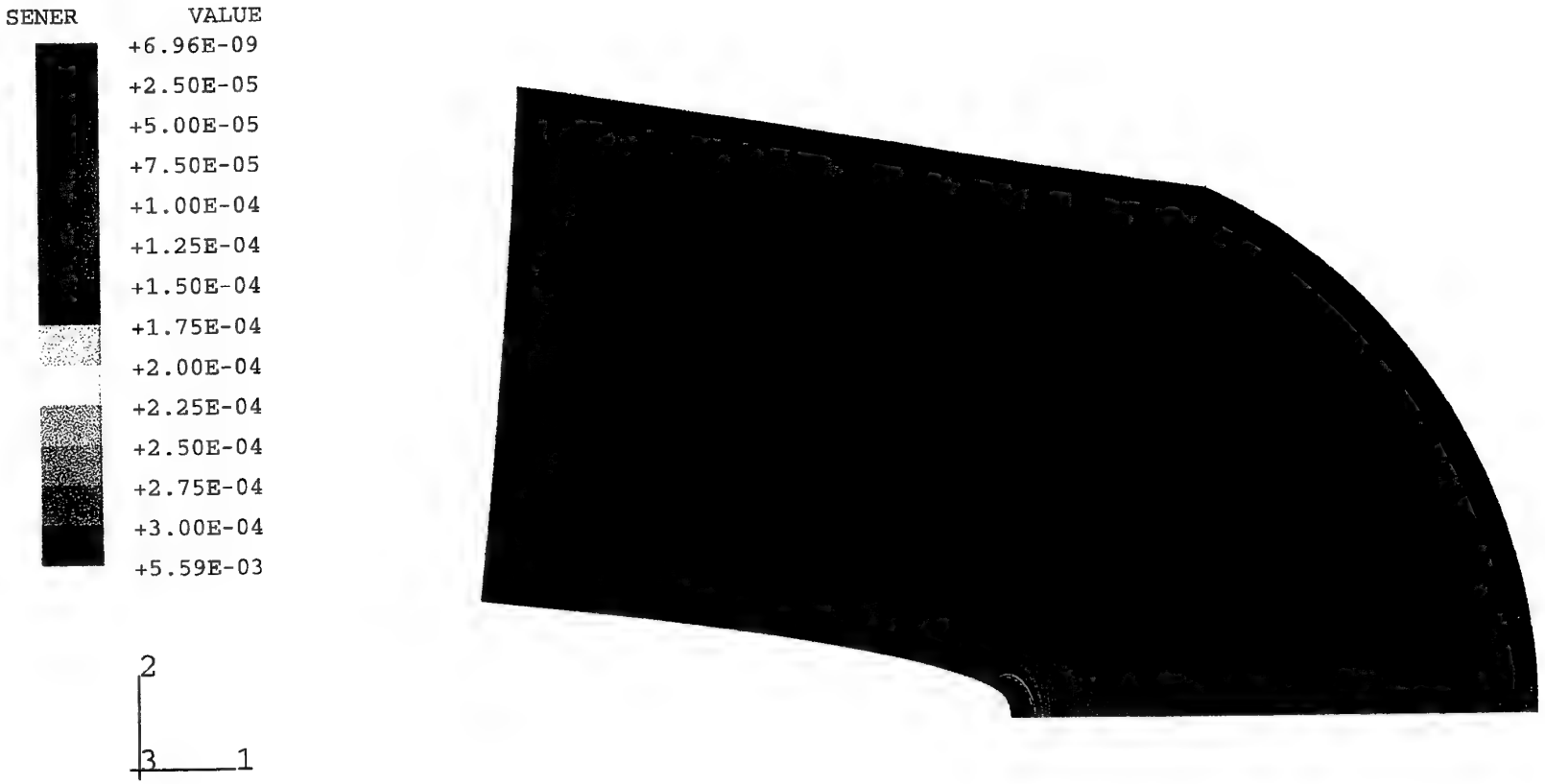

Fig. 54 Strain energy density, dW/dV, contours (in the deformed specimen configuration) for Figure 51. Values in kN.mm/mm^3. Applied displacement u_0=0.2541 mm. Case II.

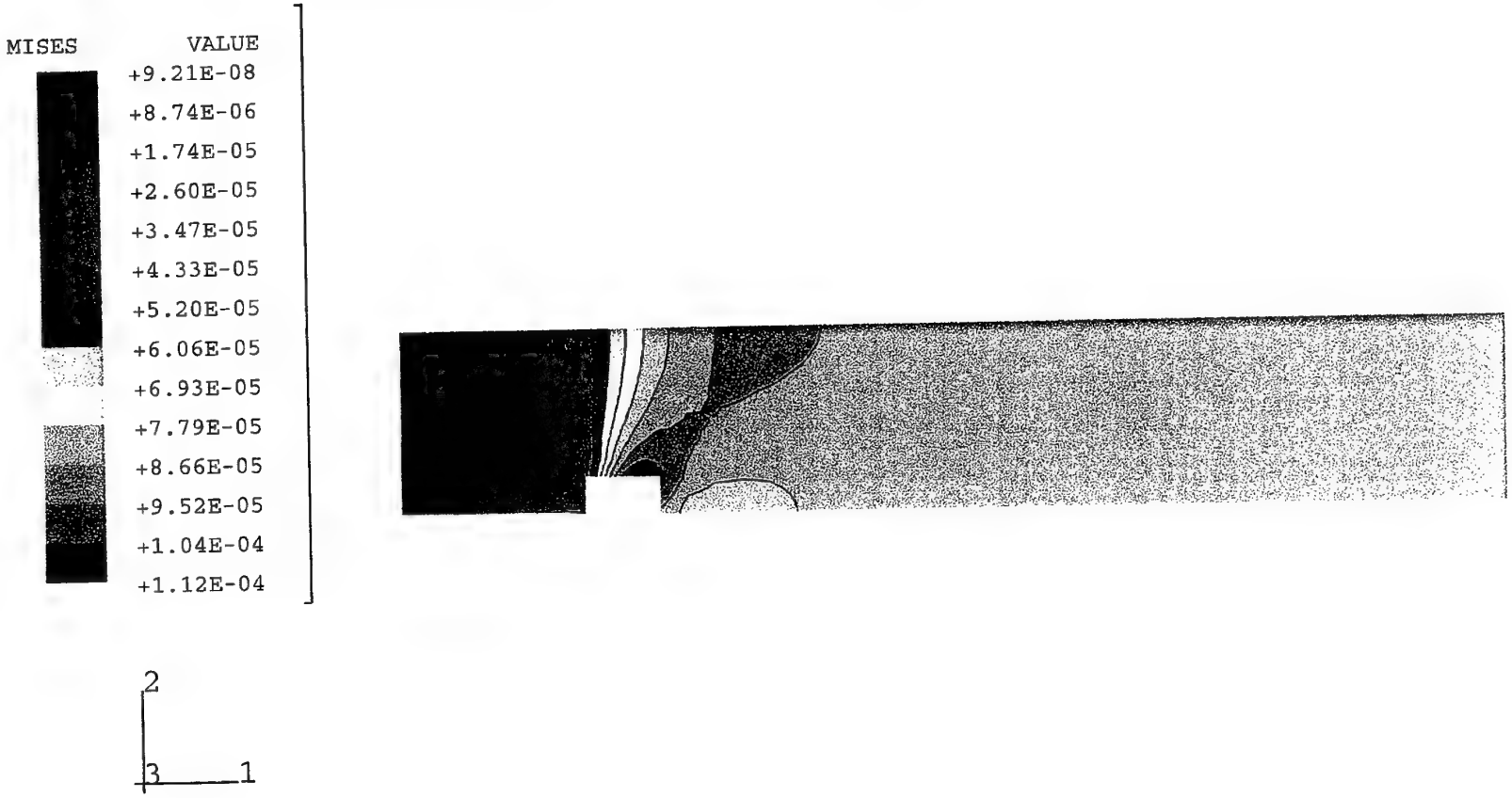

Fig. 55 Mises stress, σ_{eff}, contours (in the deformed specimen configuration) for Figure 49. Values in kN/mm^2. Applied displacement u_0=0.2541 mm. Case II.

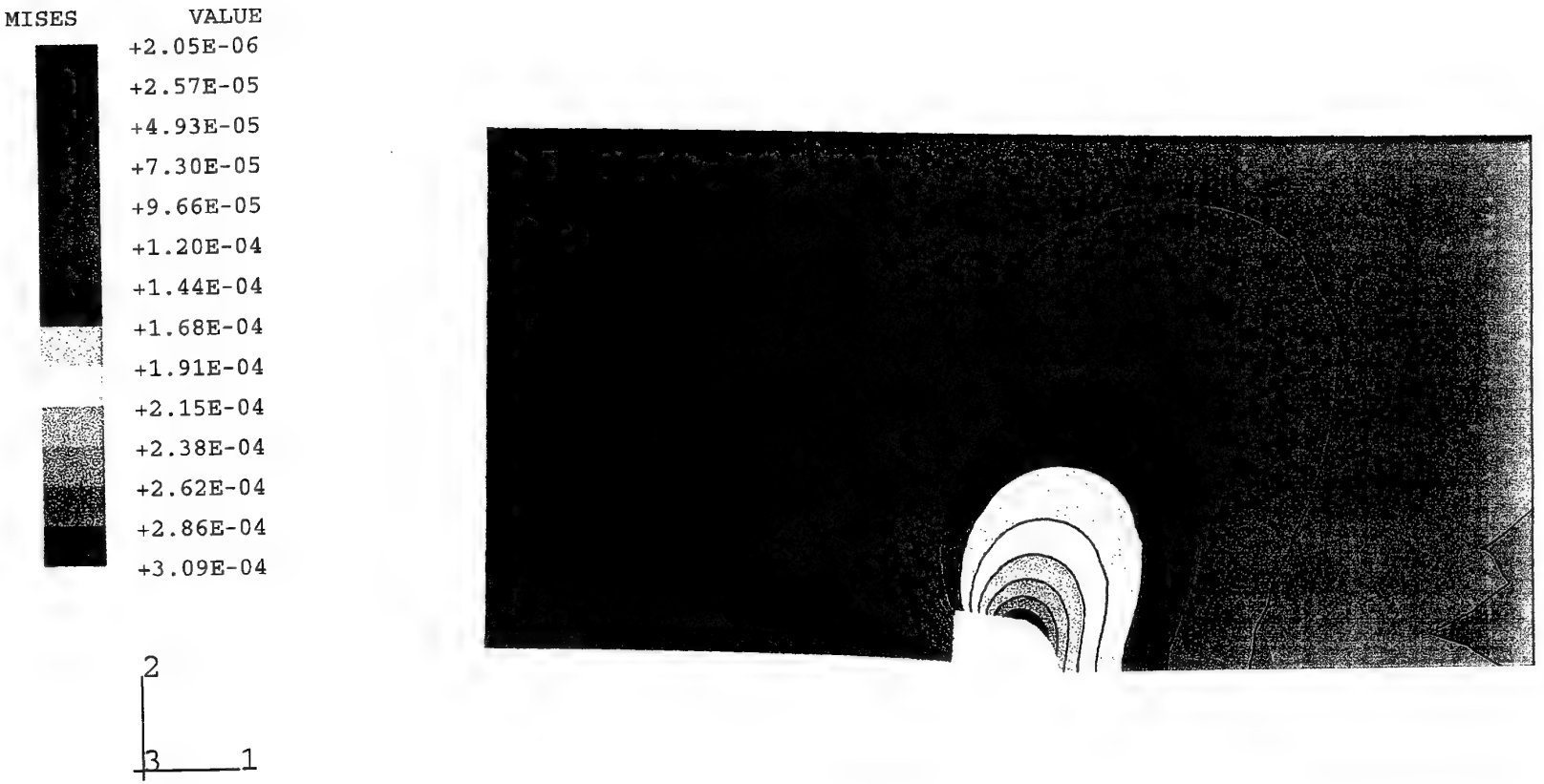

Fig. 56 Mises stress, σ_{eff}, contours (in the deformed specimen configuration) for Figure 50. Values in kN/mm^2. Applied displacement u_0=0.2541 mm. Case II.

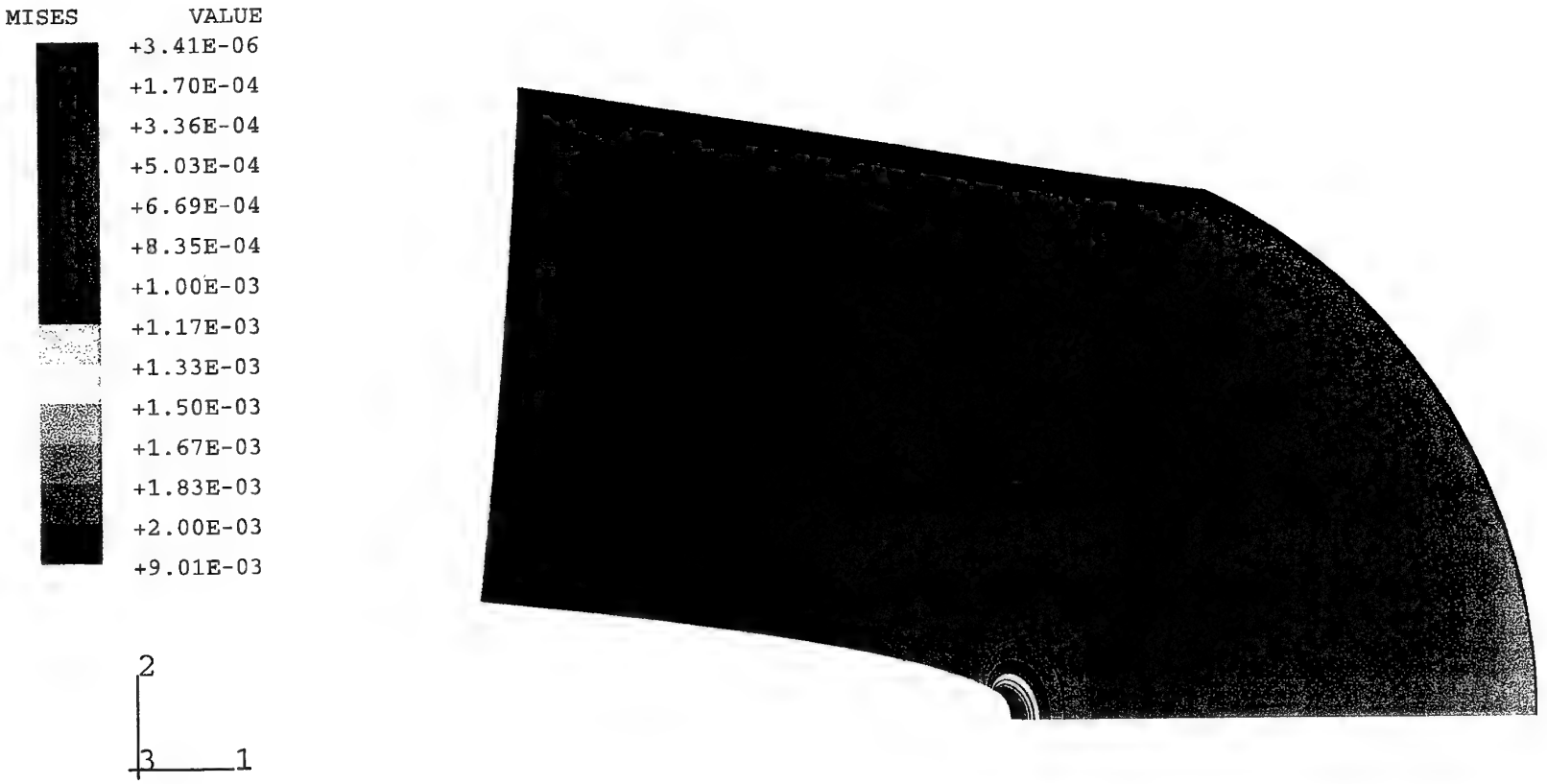

Fig. 57 Mises stress, σ_{eff}, contours (in the deformed specimen configuration) for Figure 51. Values in kN/mm^2. Applied displacement u_0=0.2541 mm. Case II.

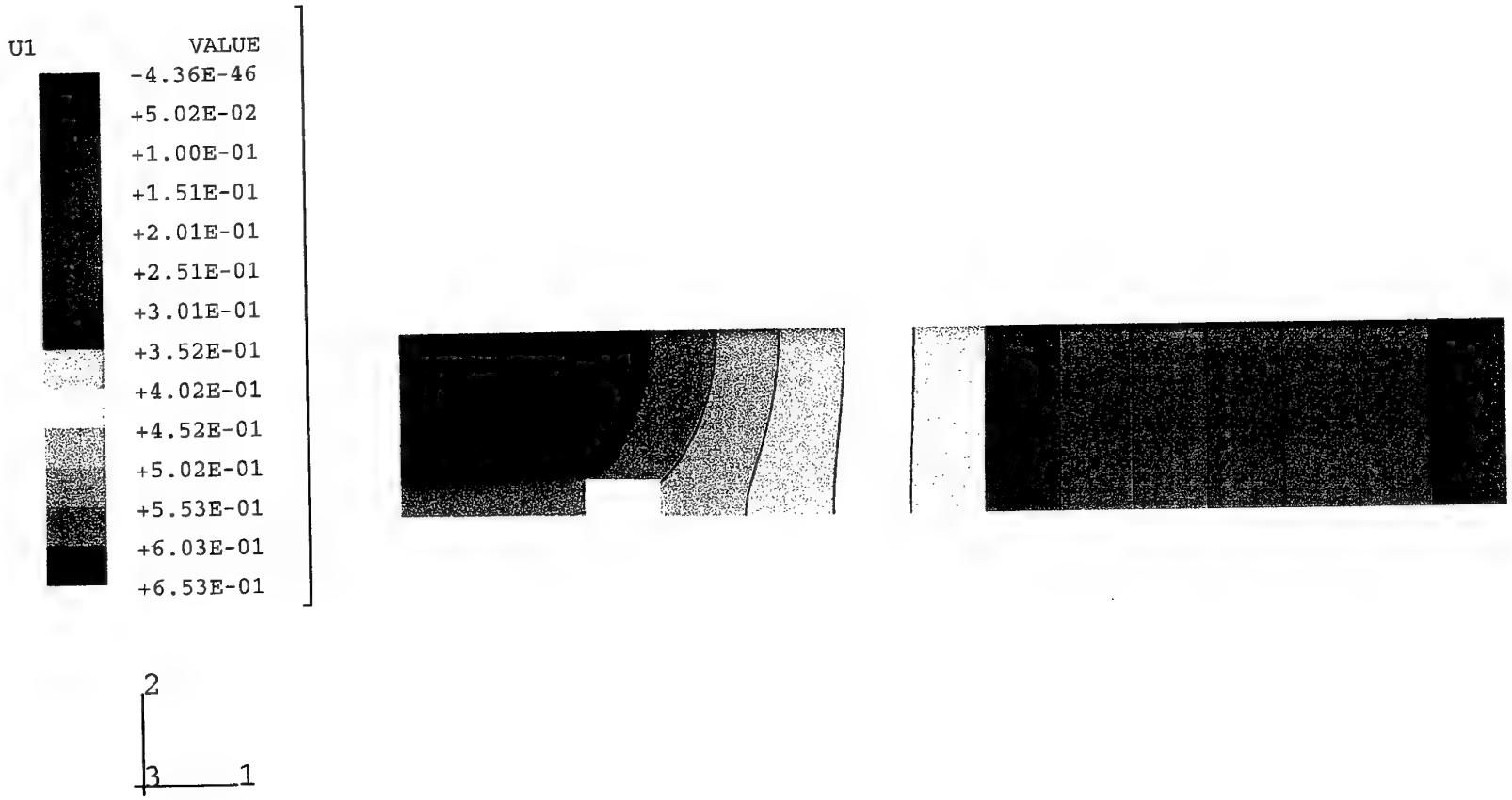

Fig. 58 Displacement along the crack axis direction, u_1, contours (in the deformed specimen configuration) for Figure 49. Values in mm. Applied displacement u_0=0.2541 mm. Case II.

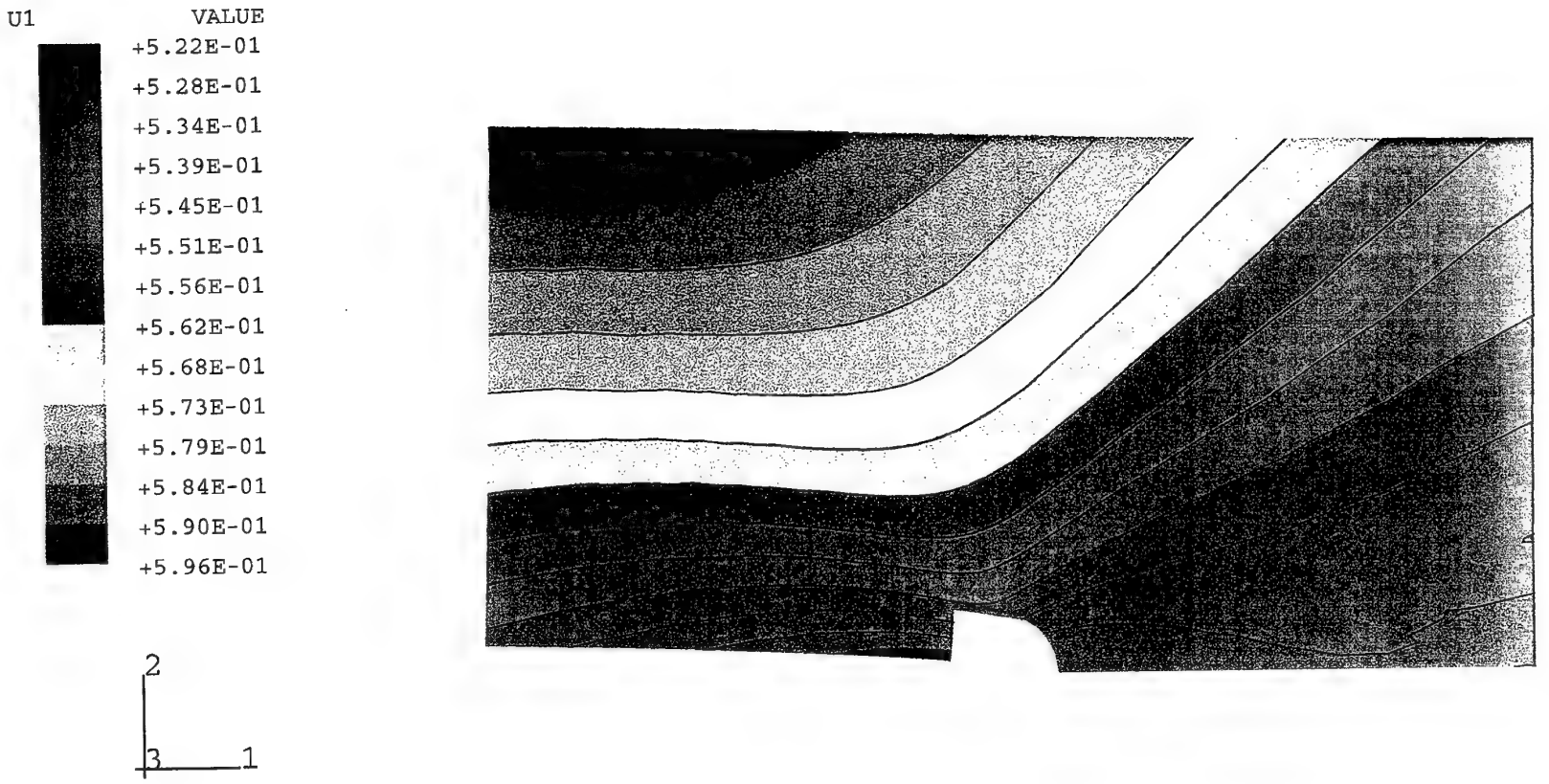

Fig. 59 Displacement along the crack axis direction, u_1, contours (in the deformed specimen configuration) for Figure 50. Values in mm. Applied displacement u_0=0.2541 mm. Case II.

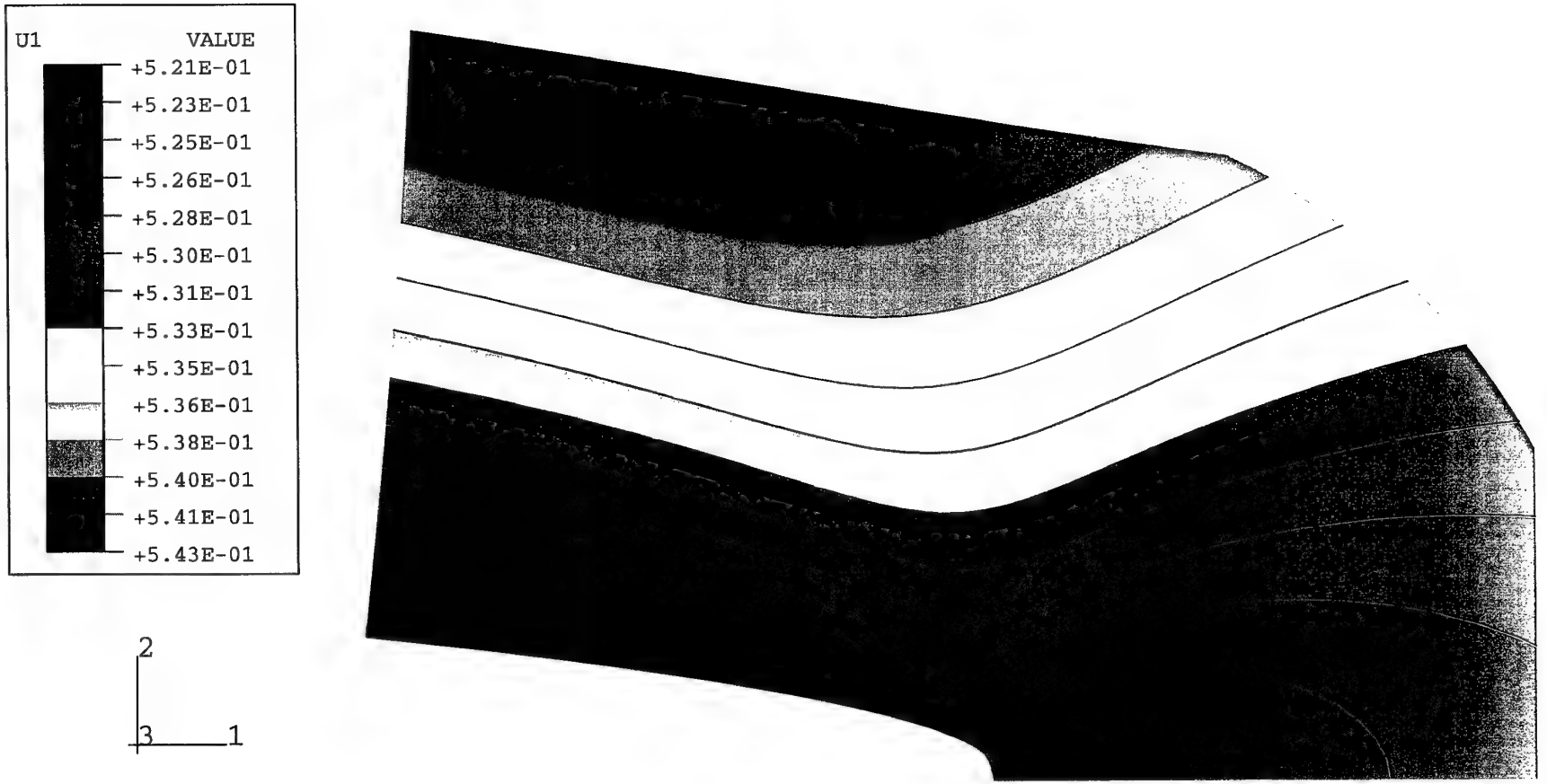

Fig. 60 Displacement along the crack axis direction, u_1, contours (in the deformed specimen configuration) for Figure 51. Values in mm. Applied displacement u_0=0.2541 mm. Case II.

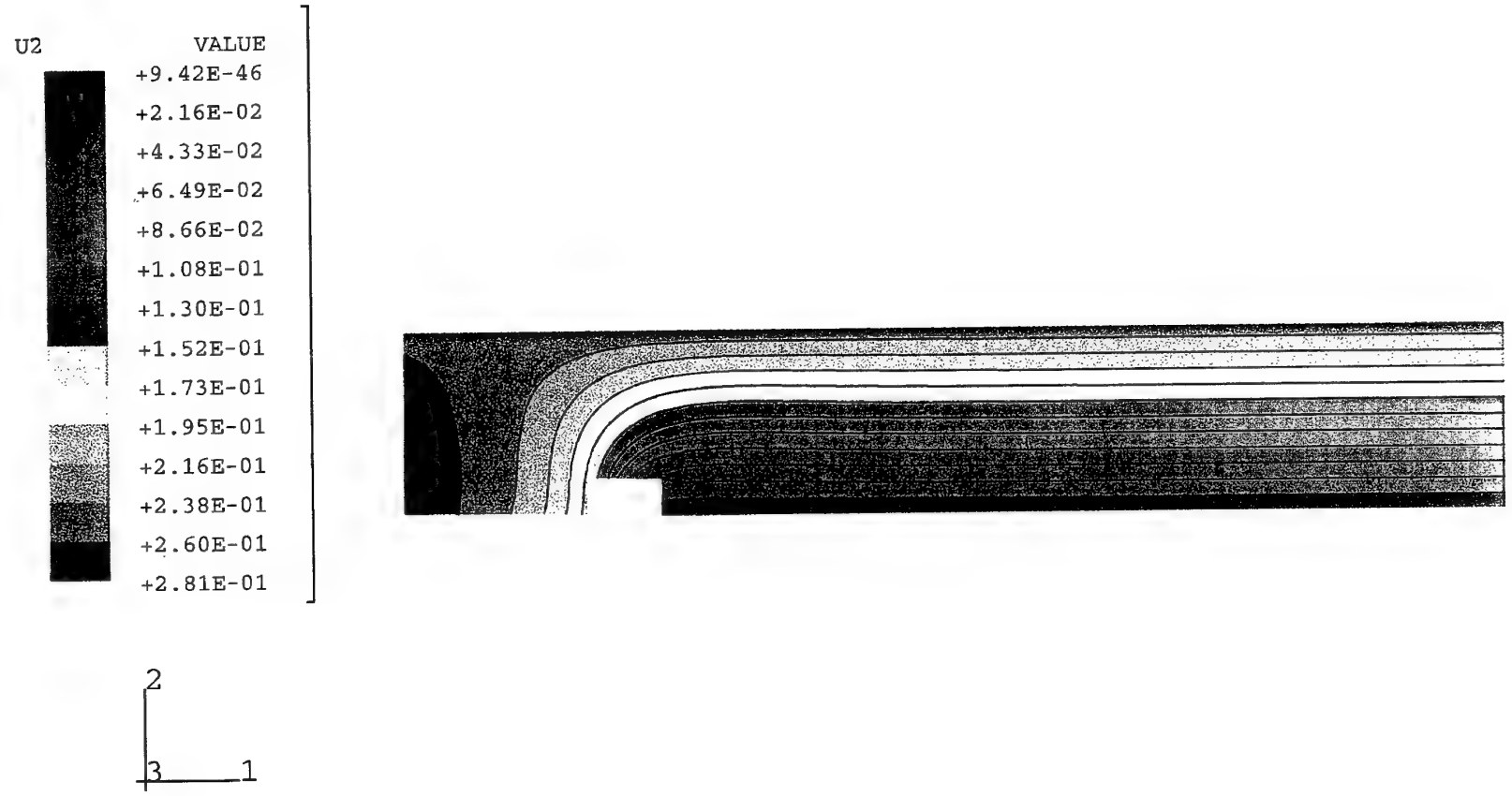

Fig. 61 Displacement along the perpendicular to the crack axis direction, u_2, contours (in the deformed specimen configuration) for Figure 49. Values in mm. Applied displacement u_0=0.2541 mm. Case II.

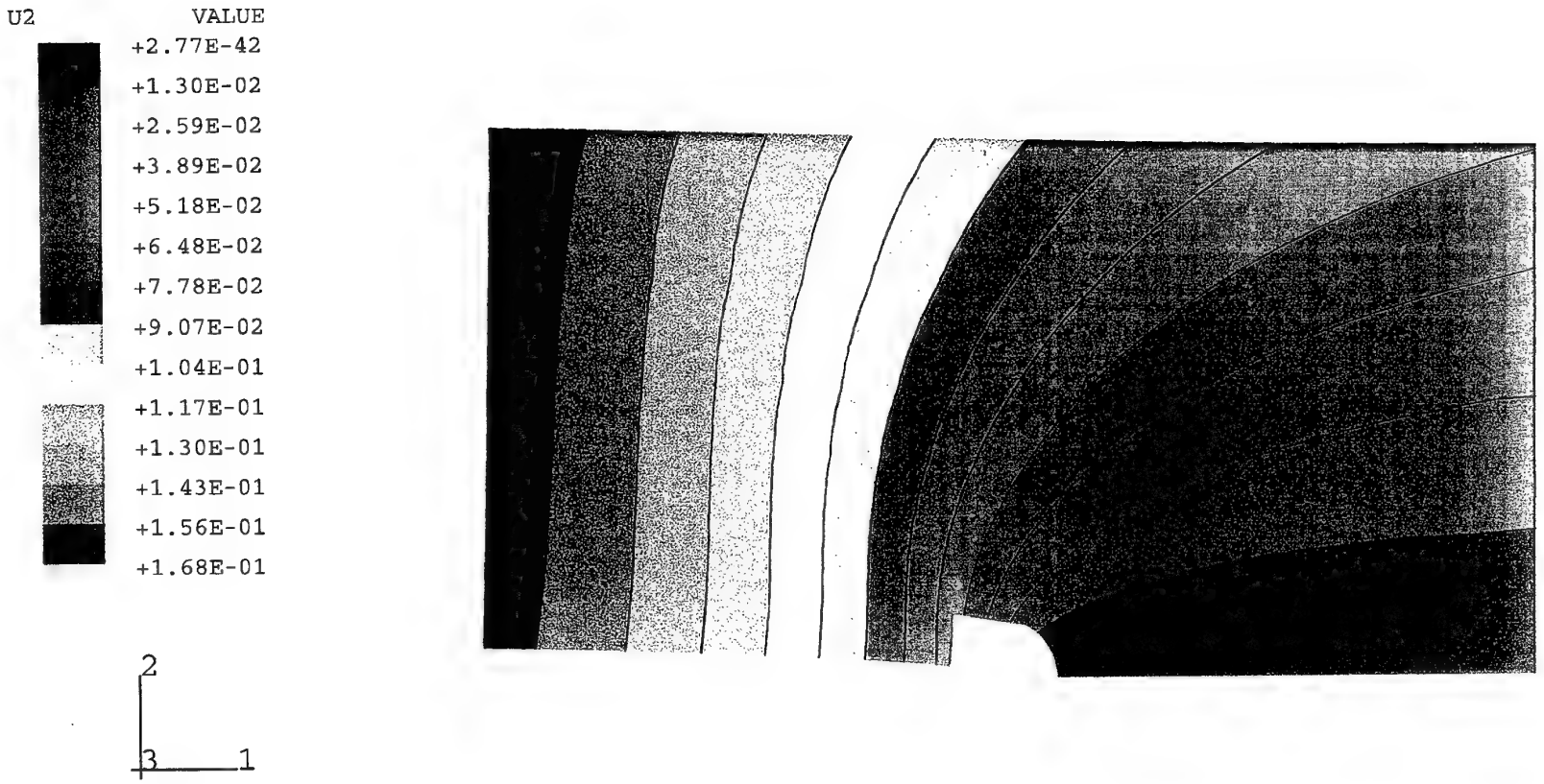

Fig. 62 Displacement along the perpendicular to the crack axis direction, u_2, contours (in the deformed specimen configuration) for Figure 50. Values in mm. Applied displacement u_0=0.2541 mm. Case II.

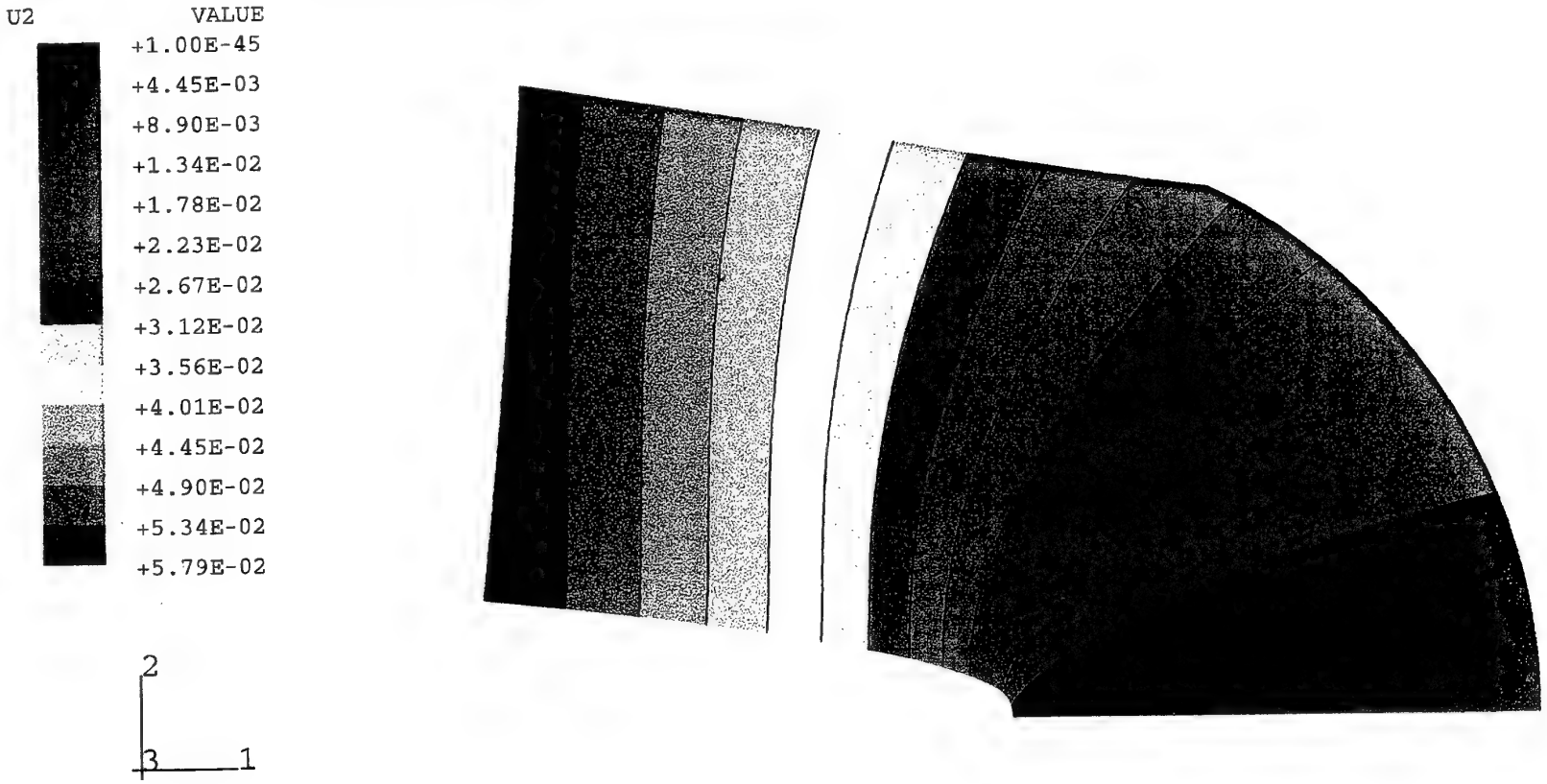

Fig. 63 Displacement along the perpendicular to the crack axis direction, u_2, contours (in the deformed specimen configuration) for Figure 51. Values in mm. Applied displacement u_0=0.2541 mm. Case II.

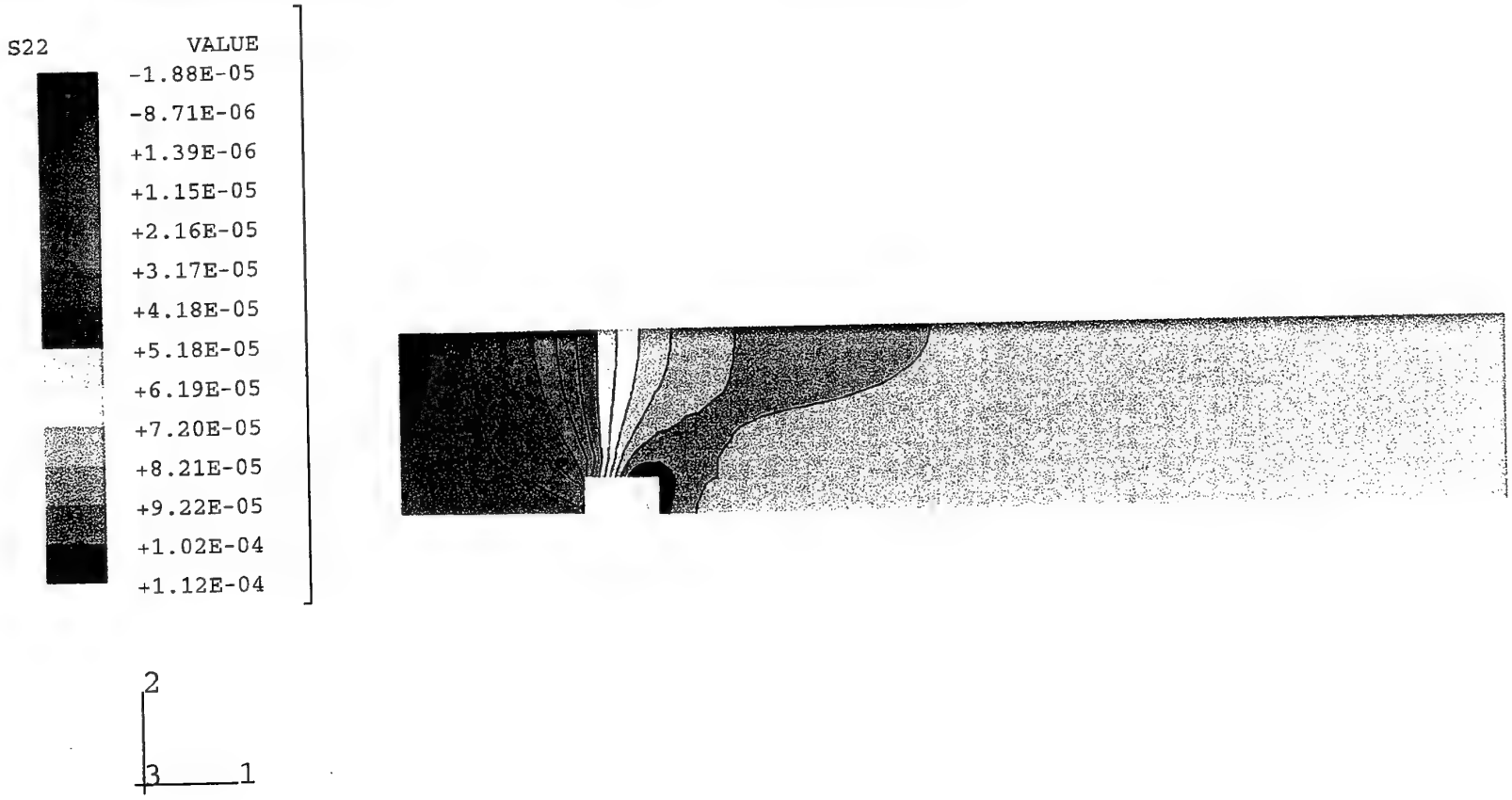

Fig. 64 Normal stress along the perpendicular to the crack axis direction, σ_{22}, contours (in the deformed specimen configuration) for Figure 49. Values in kN/mm^2. Applied displacement u_0=0.2541 mm. Case II.

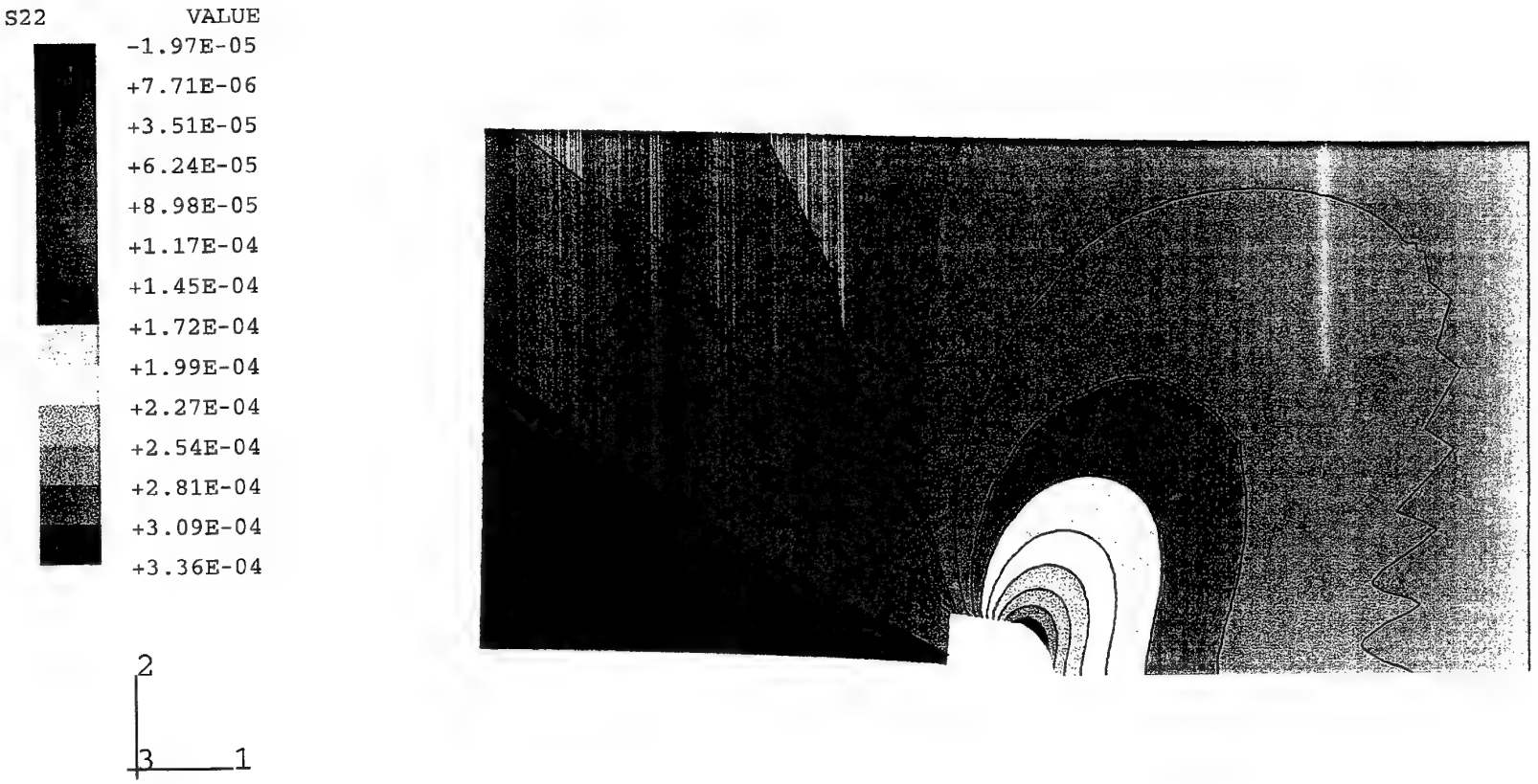

Fig. 65 Normal stress along the perpendicular to the crack axis direction, σ_{22}, contours (in the deformed specimen configuration) for Figure 50. Values in kN/mm^2. Applied displacement u_0=0.2541 mm. Case II.

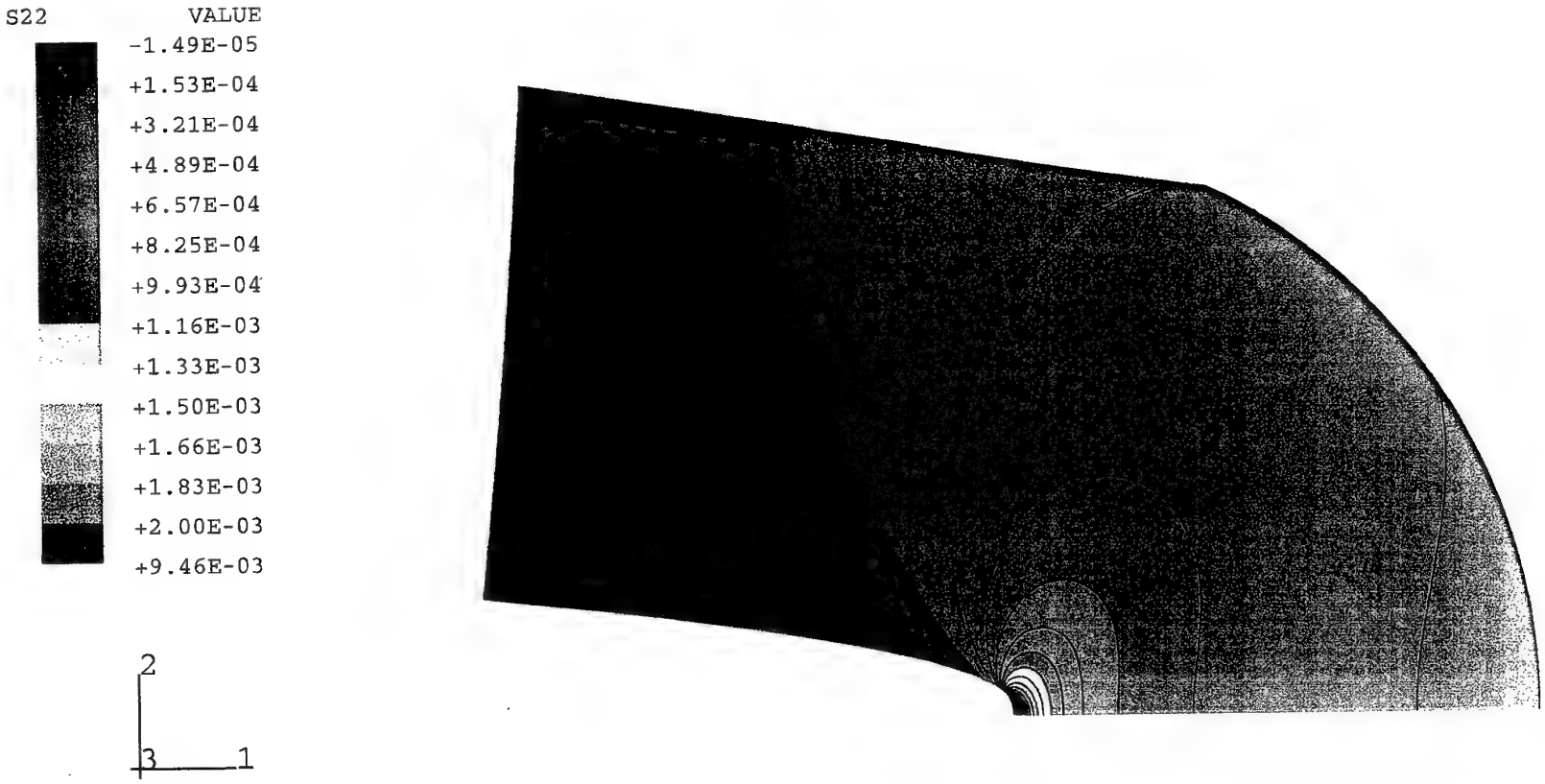

Fig. 66 Normal stress along the perpendicular to the crack axis direction, σ_{22}, contours (in the deformed specimen configuration) for Figure 51. Values in kN/mm^2 Applied displacement u_0=0.2541 mm. Case II.

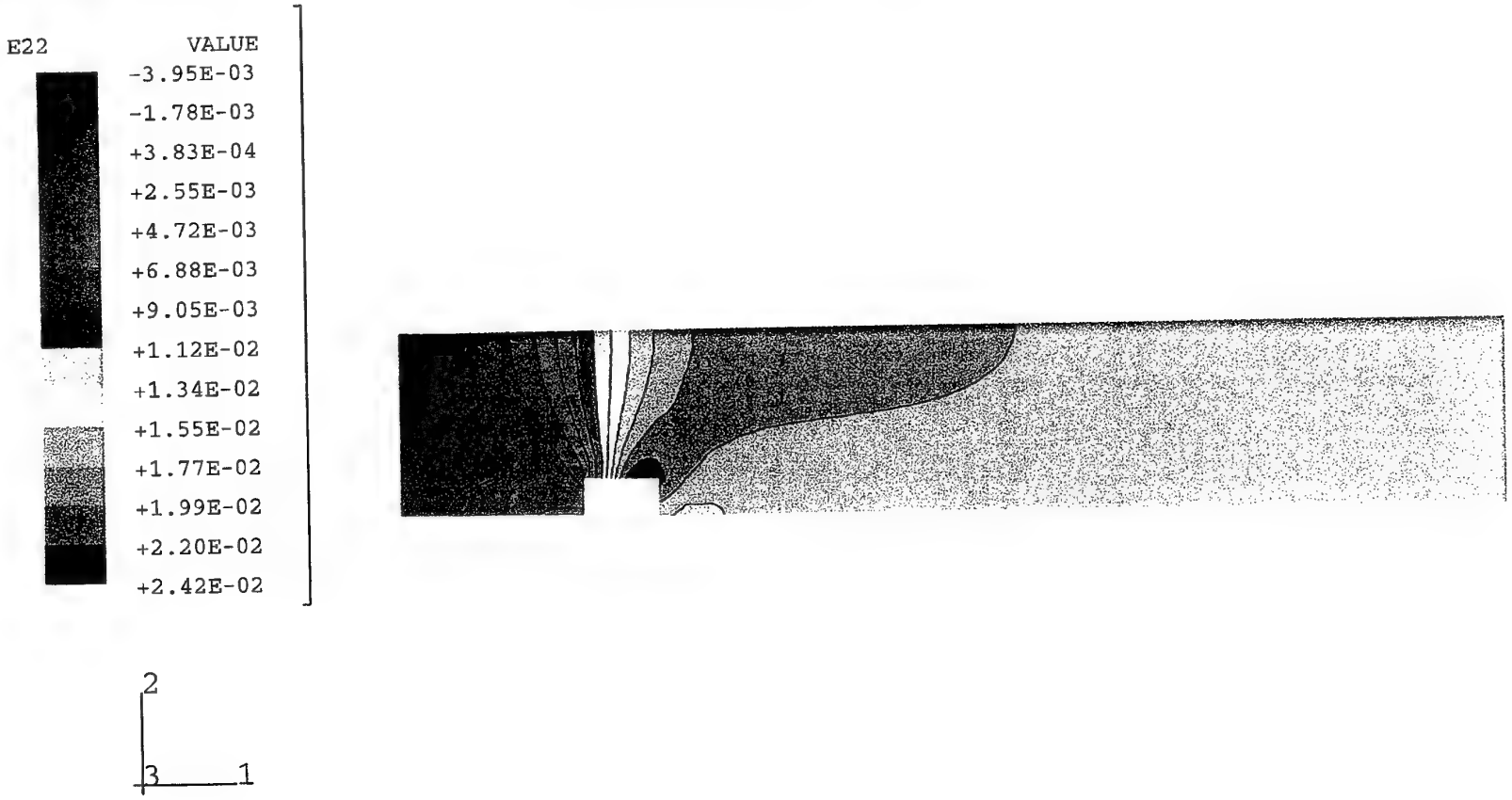

Fig. 67 Normal strain along the perpendicular to the crack axis direction, ε_{22}, contours (in the deformed specimen configuration) for Figure 49. Applied displacement u_0=0.2541 mm. Case II.

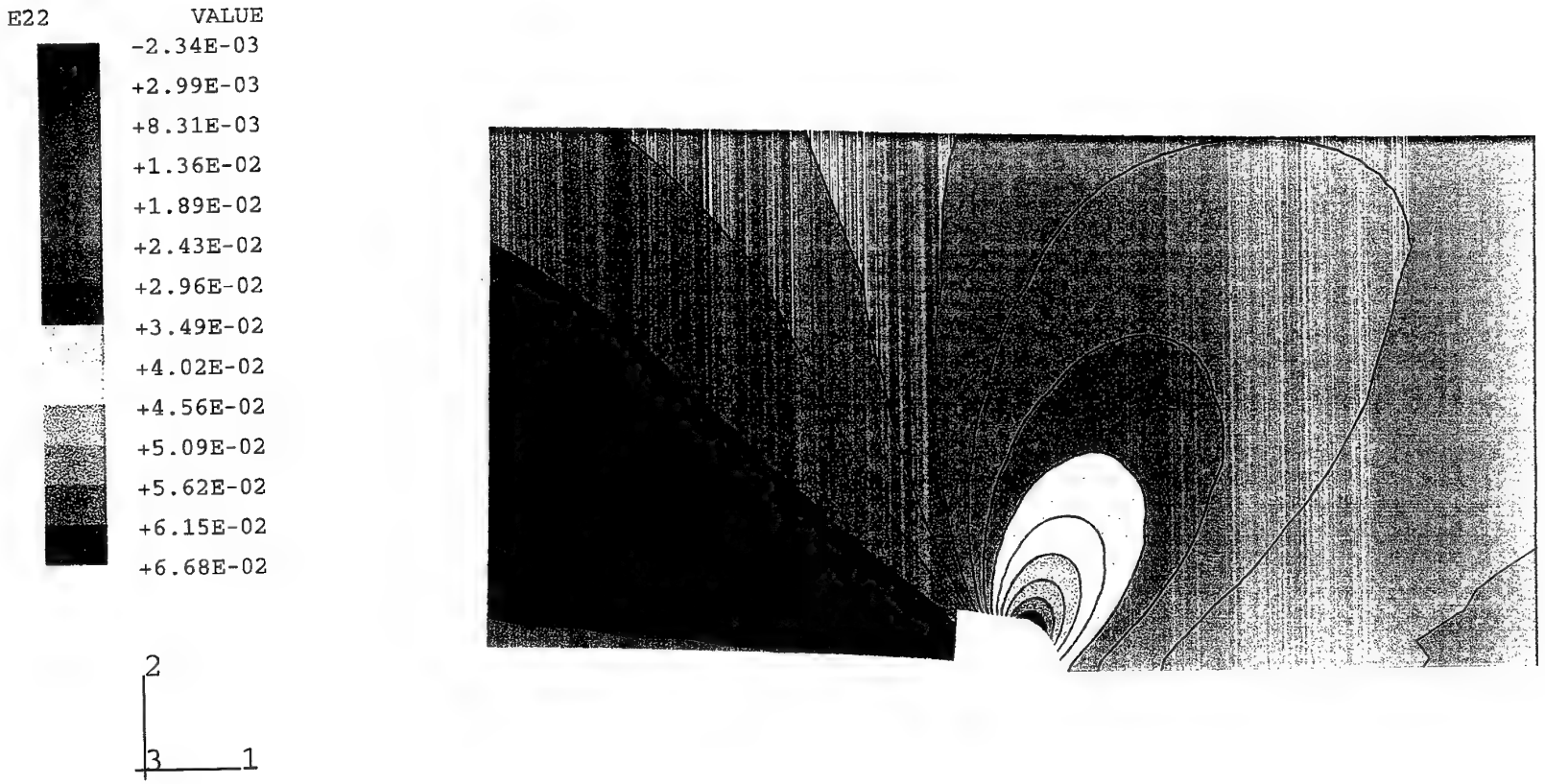

Fig. 68 Normal strain along the perpendicular to the crack axis direction, ε_{22}, contours (in the deformed specimen configuration) for Figure 50. Applied displacement u_0=0.2541 mm. Case II.

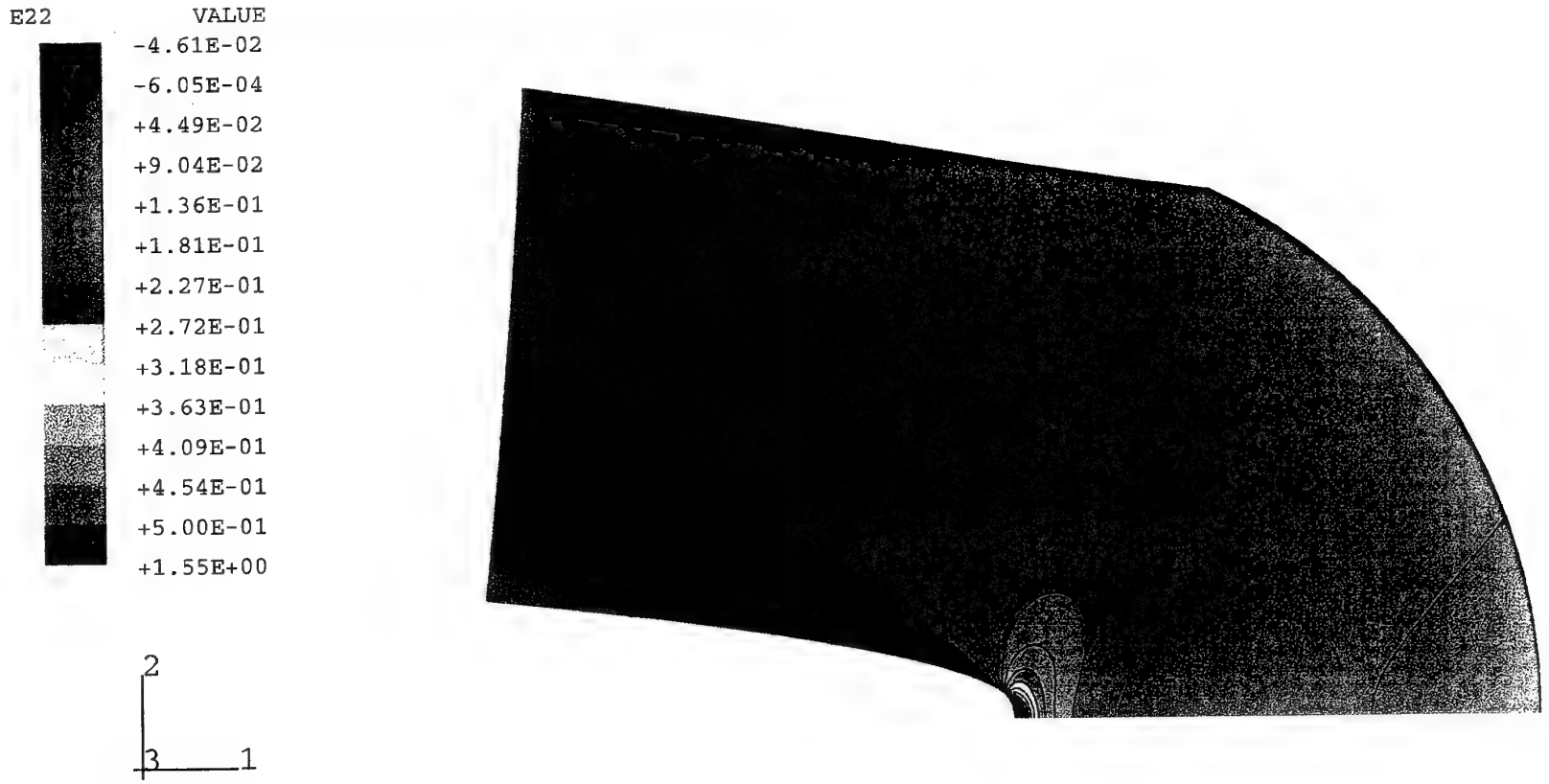

Fig. 69 Normal strain along the perpendicular to the crack axis direction, ε_{22}, contours (in the deformed specimen configuration) for Figure 51. Applied displacement u_0=0.2541 mm. Case II.

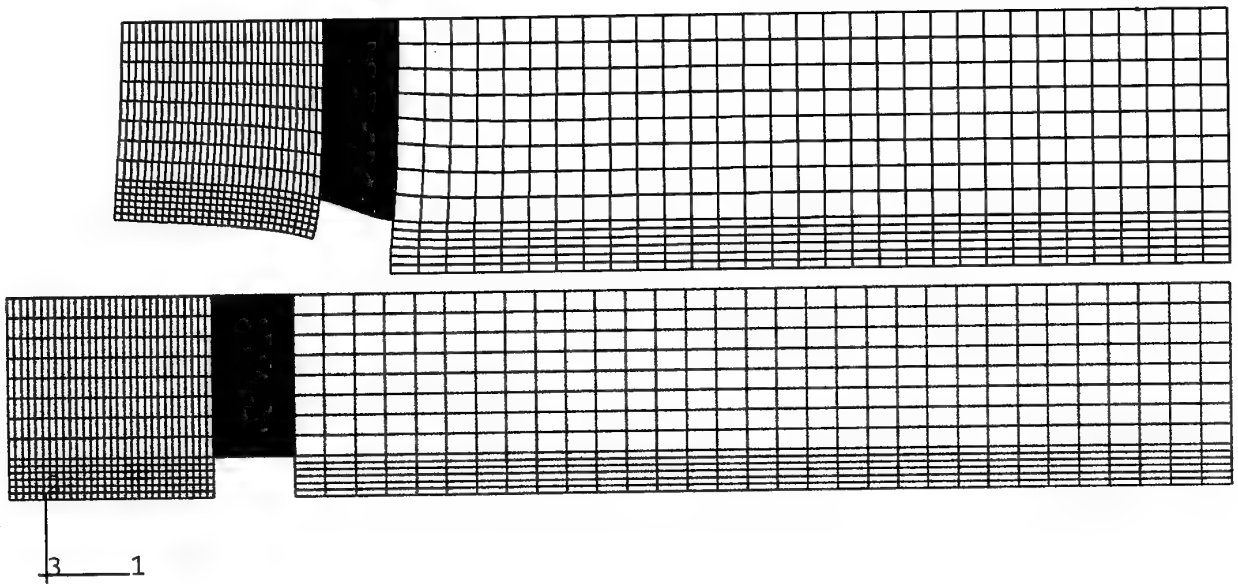

Fig. 70 Undeformed (in red) and deformed (in black) finite element grids for half specimen. Applied displacement u_0=3.3295 mm. Case II.

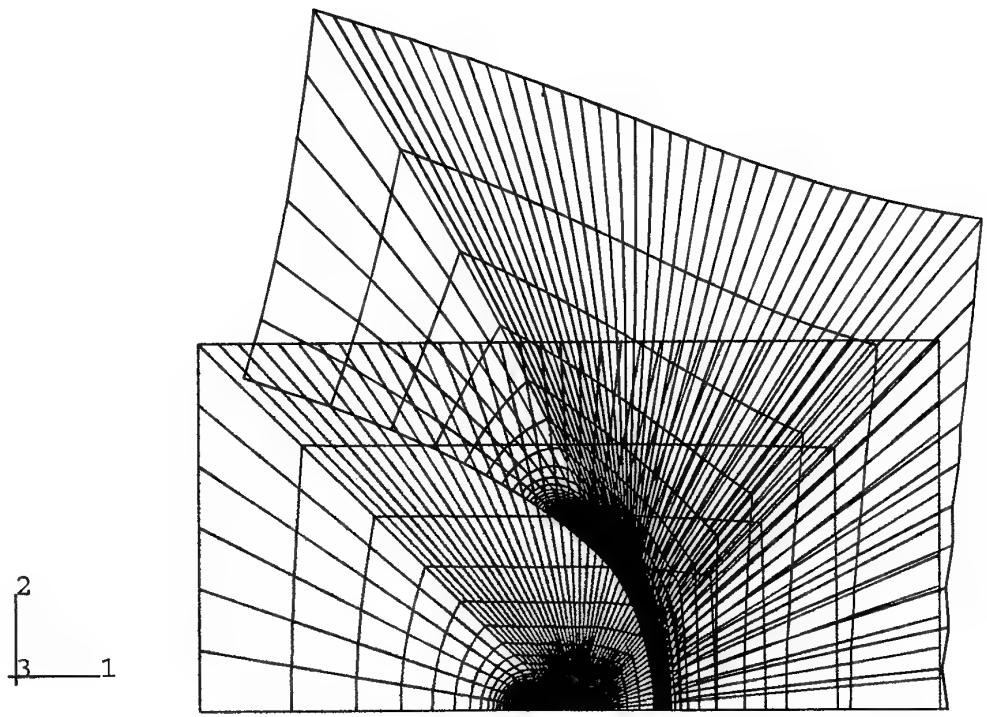

Fig. 71 Undeformed (in red) and deformed (in black) finite element grids for the missing part of Figure 70. Applied displacement u_0=3.3295 mm. Case II.

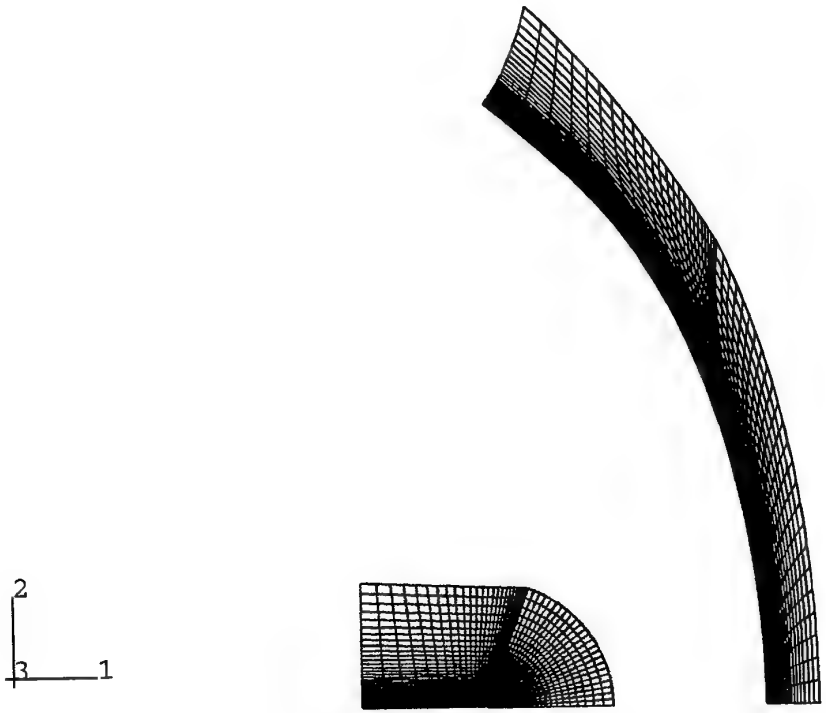

Fig. 72 Undeformed (in red) and deformed (in black) finite element grids for the missing part of Figure 71. Applied displacement u_0=3.3295 mm. Case II.

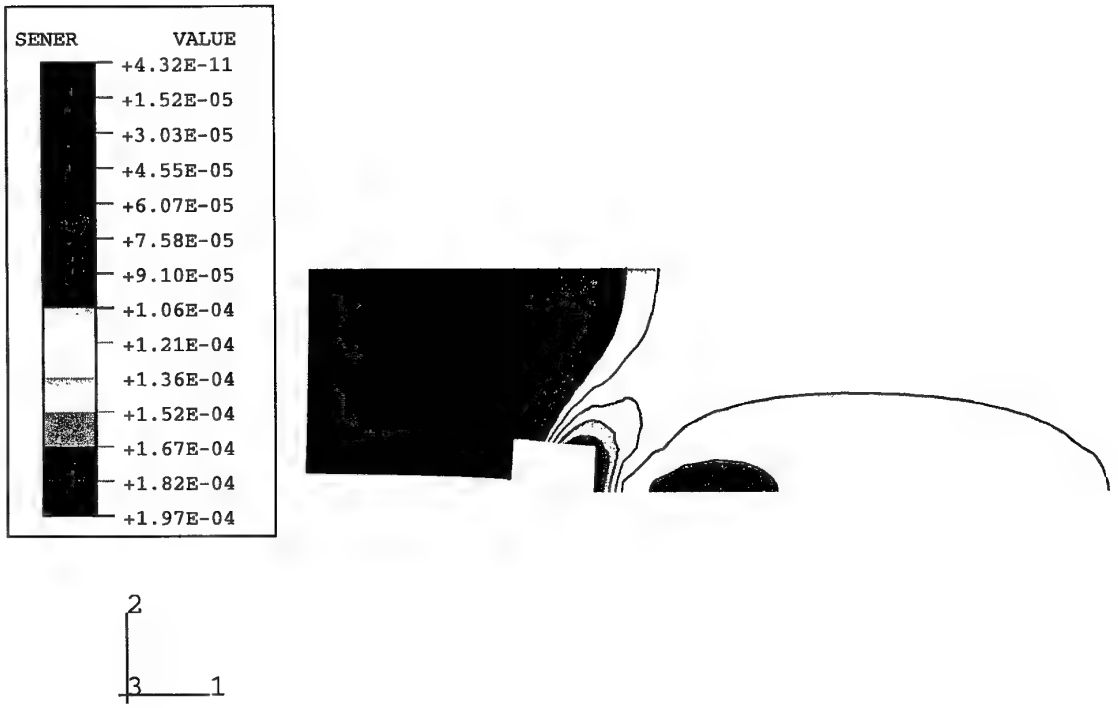

Fig. 73 Strain energy density, dW/dV, contours (in the deformed specimen configuration) for Figure 70. Values in kN.mm/mm^3. Applied displacement u_0=3.3295 mm. Case II.

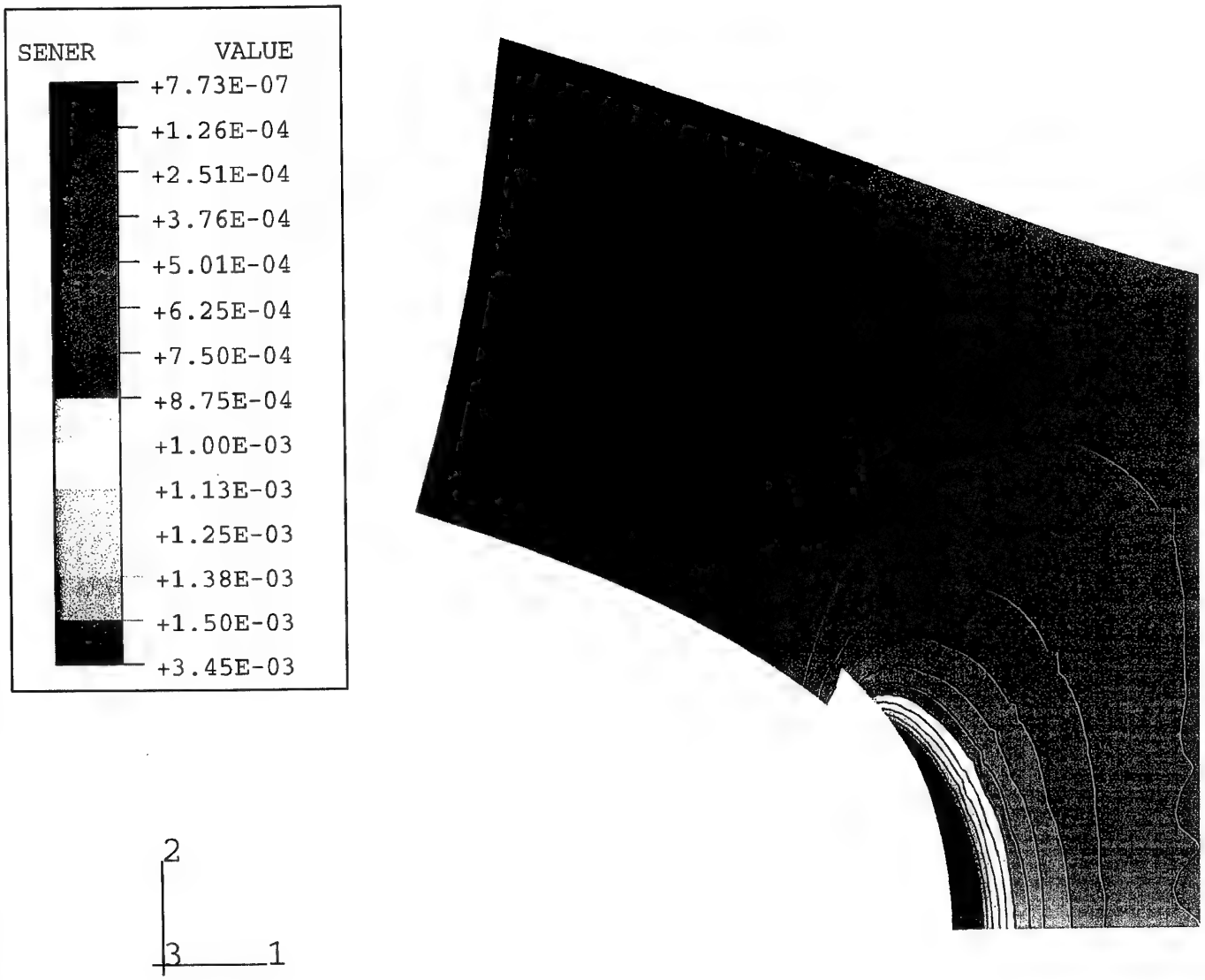

Fig. 74 Strain energy density, dW/dV, contours (in the deformed specimen configuration) for Figure 71. Values in kN.mm/mm^3. Applied displacement u_0=3.3295 mm. Case II.

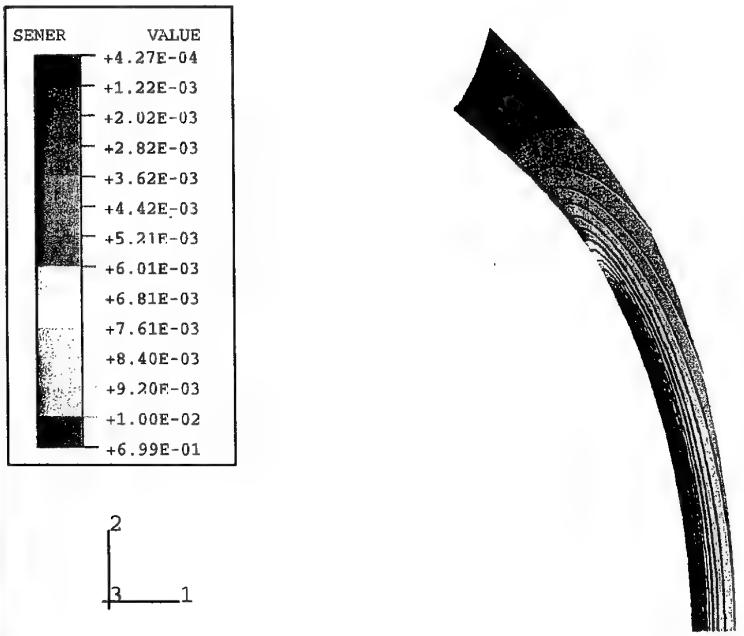

Fig. 75 Strain energy density, dW/dV, contours (in the deformed specimen configuration) for Figure 72. Values in kN.mm/mm^3. Applied displacement u_0=3.3295 mm. Case II.

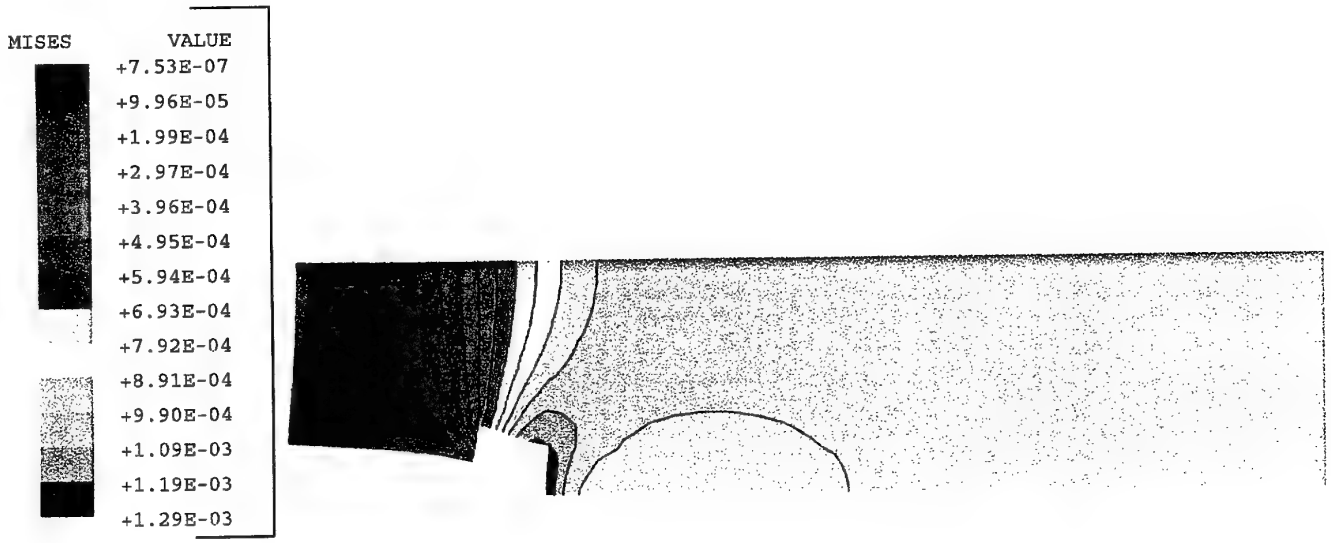

Fig. 76 Mises stress, σ_{eff}, contours (in the deformed specimen configuration) for Figure 70. Values in kN/mm^2. Applied displacement u_0=3.3295 mm. Case II.

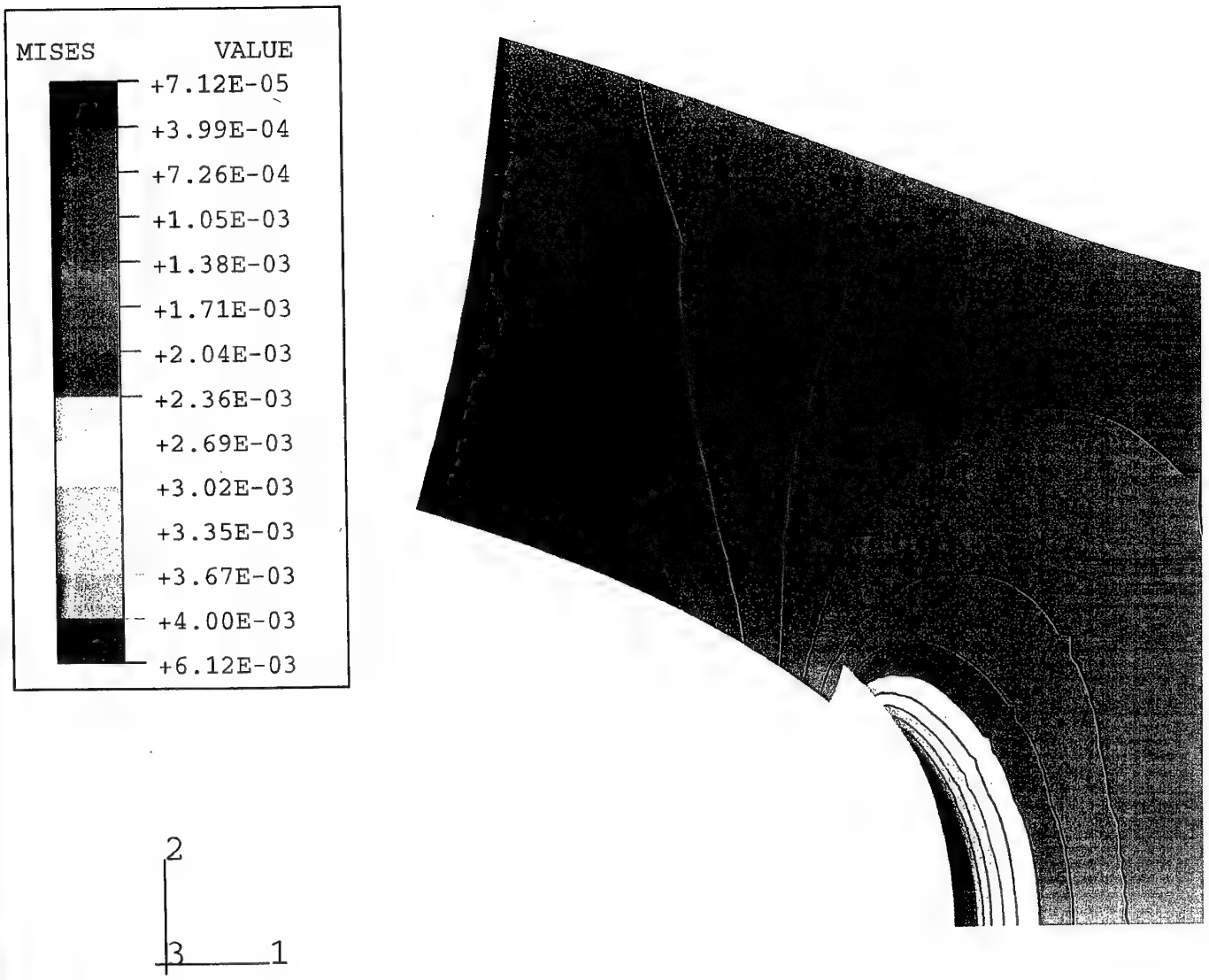

Fig. 77 Mises stress, σ_{eff}, contours (in the deformed specimen configuration) for Figure 71. Values in kN/mm^2. Applied displacement u_0=3.3295 mm. Case II.

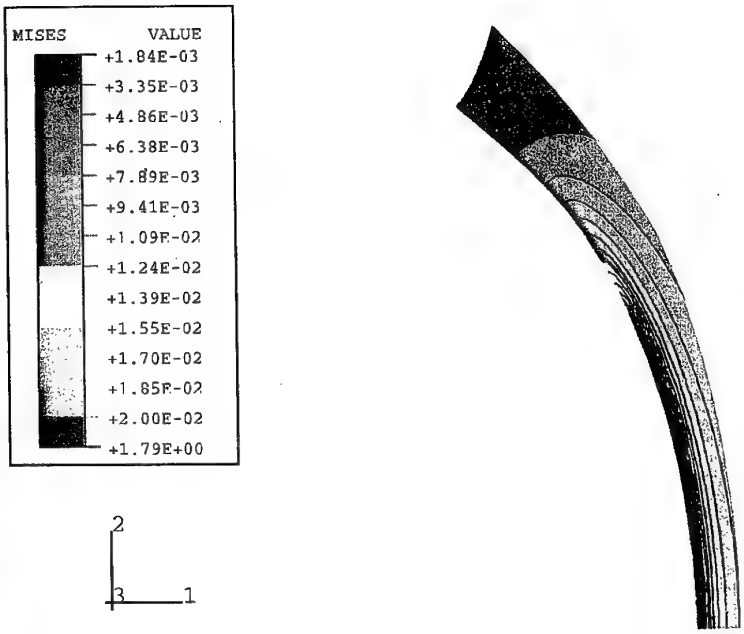

Fig. 78 Mises stress, σ_{eff}, contours (in the deformed specimen configuration) for Figure 72. Values in kN/mm^2. Applied displacement u_0=3.3295 mm. Case II.

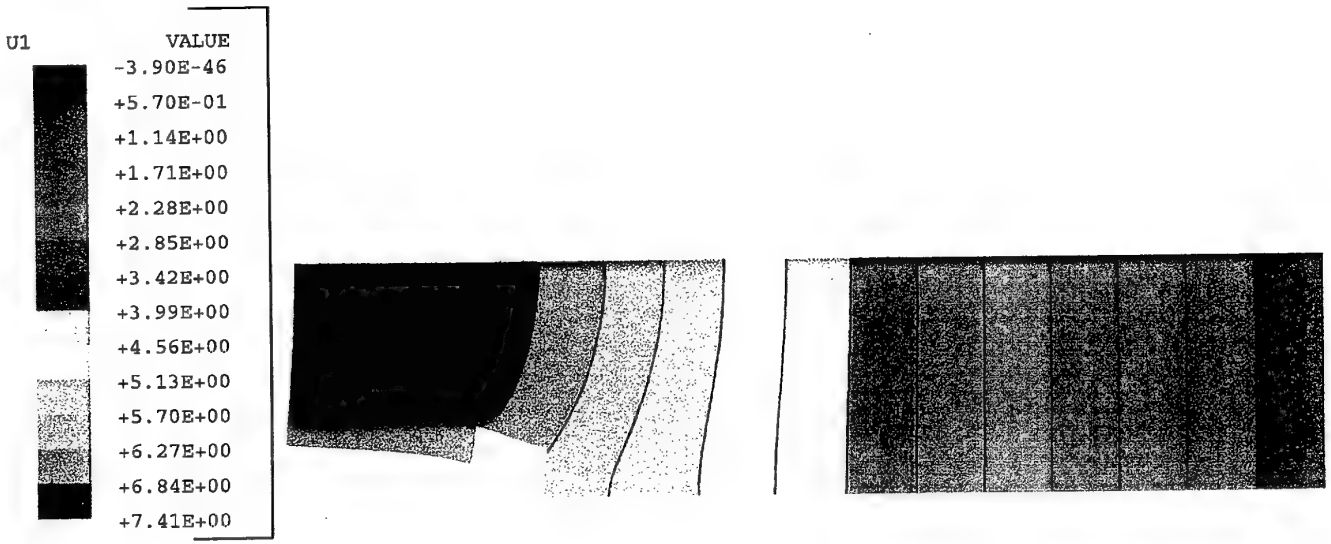

Fig. 79 Displacement along the crack axis direction, u_1, contours (in the deformed specimen configuration) for Figure 70. Values in mm. Applied displacement u_0=3.3295 mm. Case II.

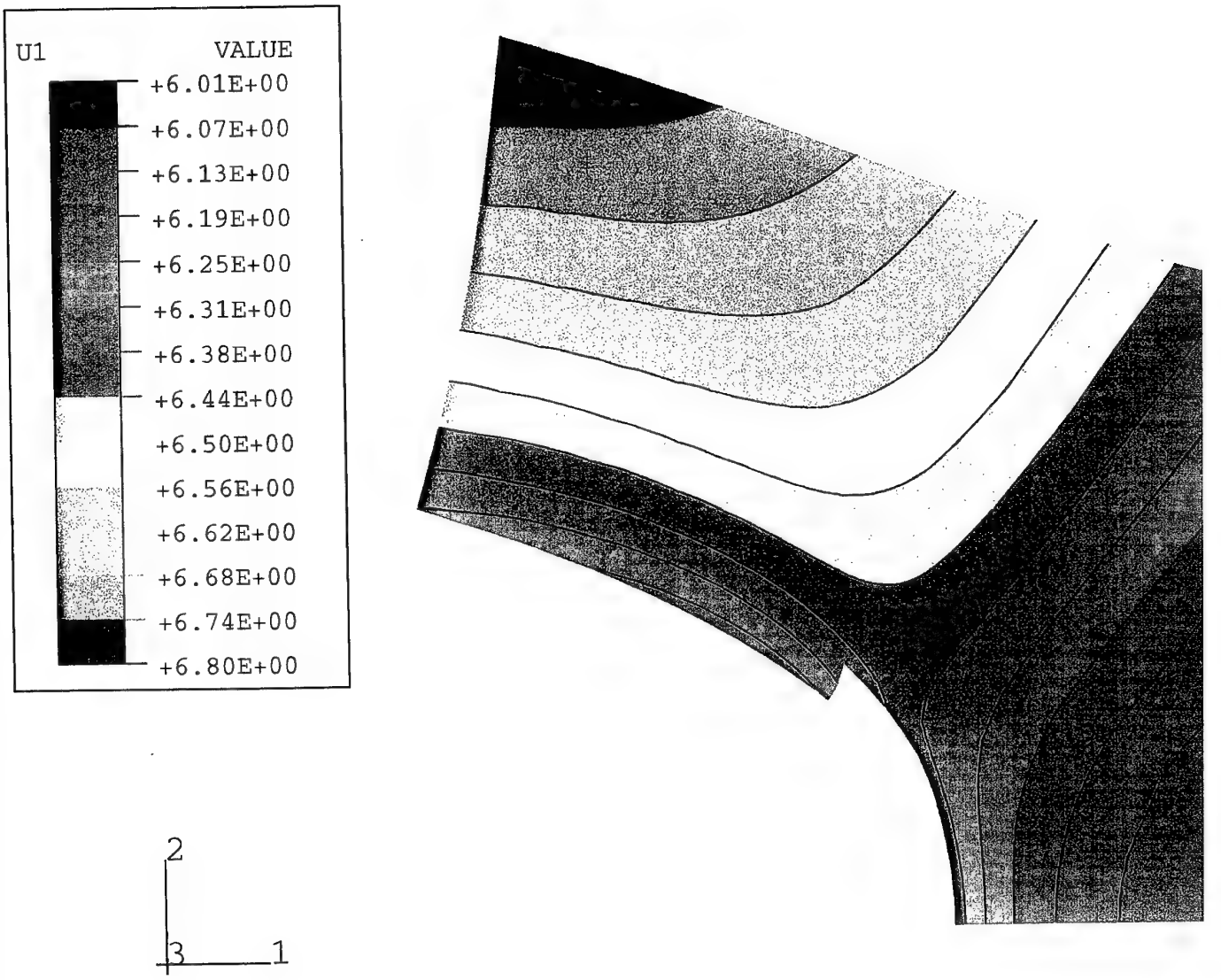

Fig. 80 Displacement along the crack axis direction, u_1, contours (in the deformed specimen configuration) for Figure 71. Values in mm. Applied displacement u_0=3.3295 mm. Case II.

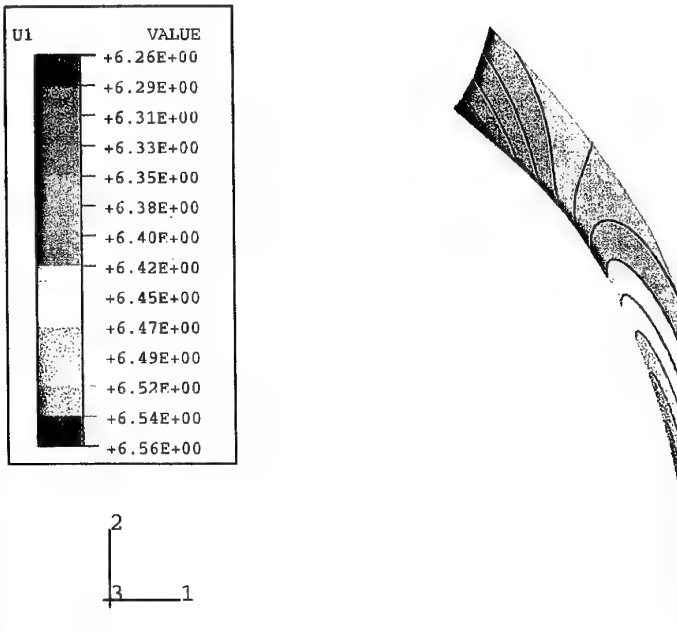

Fig. 81 Displacement along the crack axis direction, u_1, contours (in the deformed specimen configuration) for Figure 72. Values in mm. Applied displacement u_0=3.3295 mm. Case II.

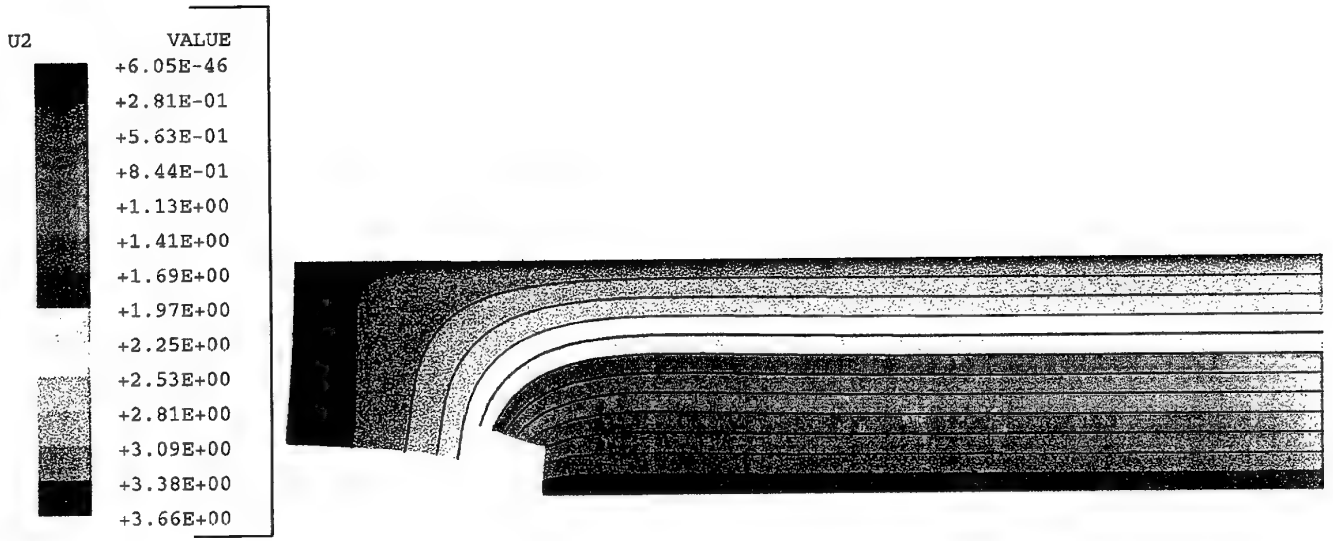

Fig. 82 Displacement along the perpendicular to the crack axis direction, u_2 contours (in the deformed specimen configuration) for Figure 70. Values in mm. Applied displacement u_0=3.3295 mm. Case II.

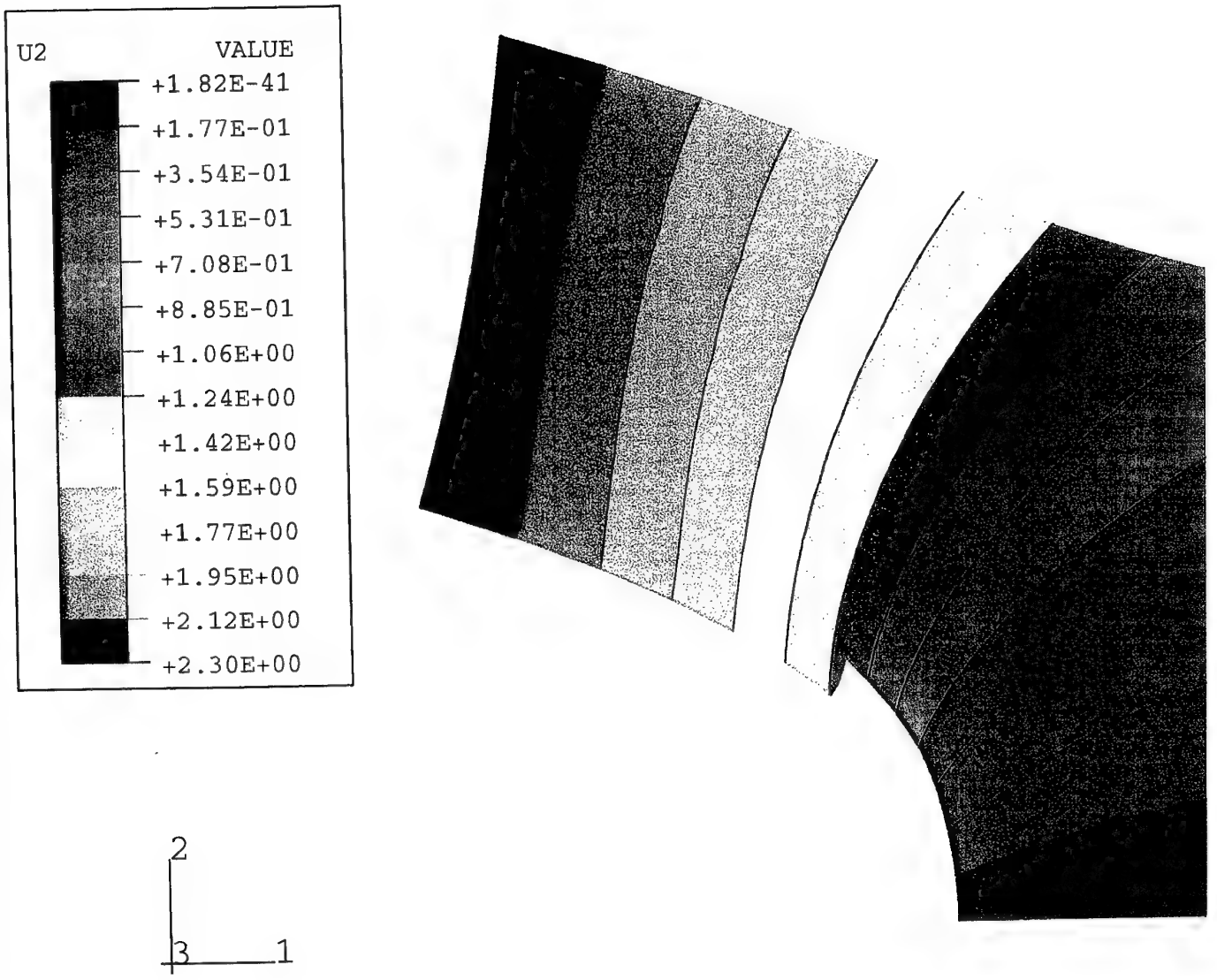

Fig. 83 Displacement along the perpendicular to the crack axis direction, u_2 contours (in the deformed specimen configuration) for Figure 71. Values in mm. Applied displacement u_0=3.3295 mm. Case II.

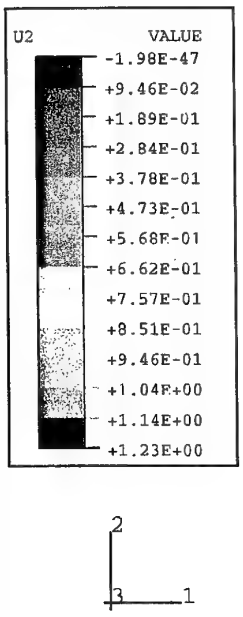

Fig. 84 Displacement along the perpendicular to the crack axis direction, u_2 contours (in the deformed specimen configuration) for Figure 72. Values in mm. Applied displacement u_0=3.3295 mm. Case II.

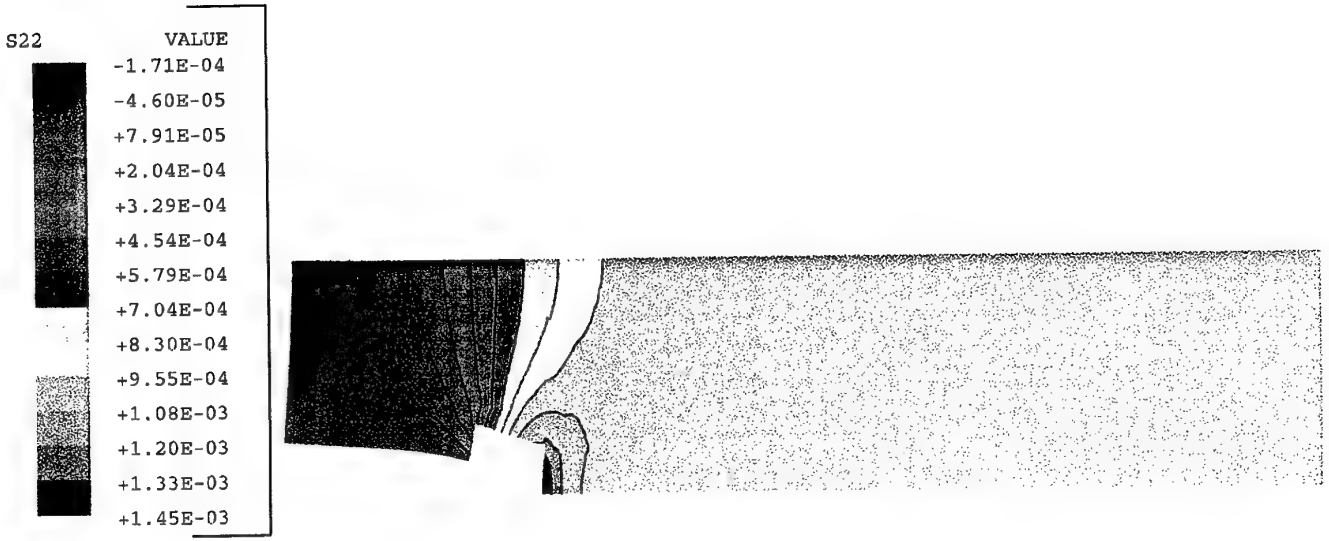

Fig. 85 Normal stress along the perpendicular to the crack axis direction, σ_{22}, contours (in the deformed specimen configuration) for Figure 70. Values in kN/mm^2. Applied displacement u_0=3.3295 mm. Case II.

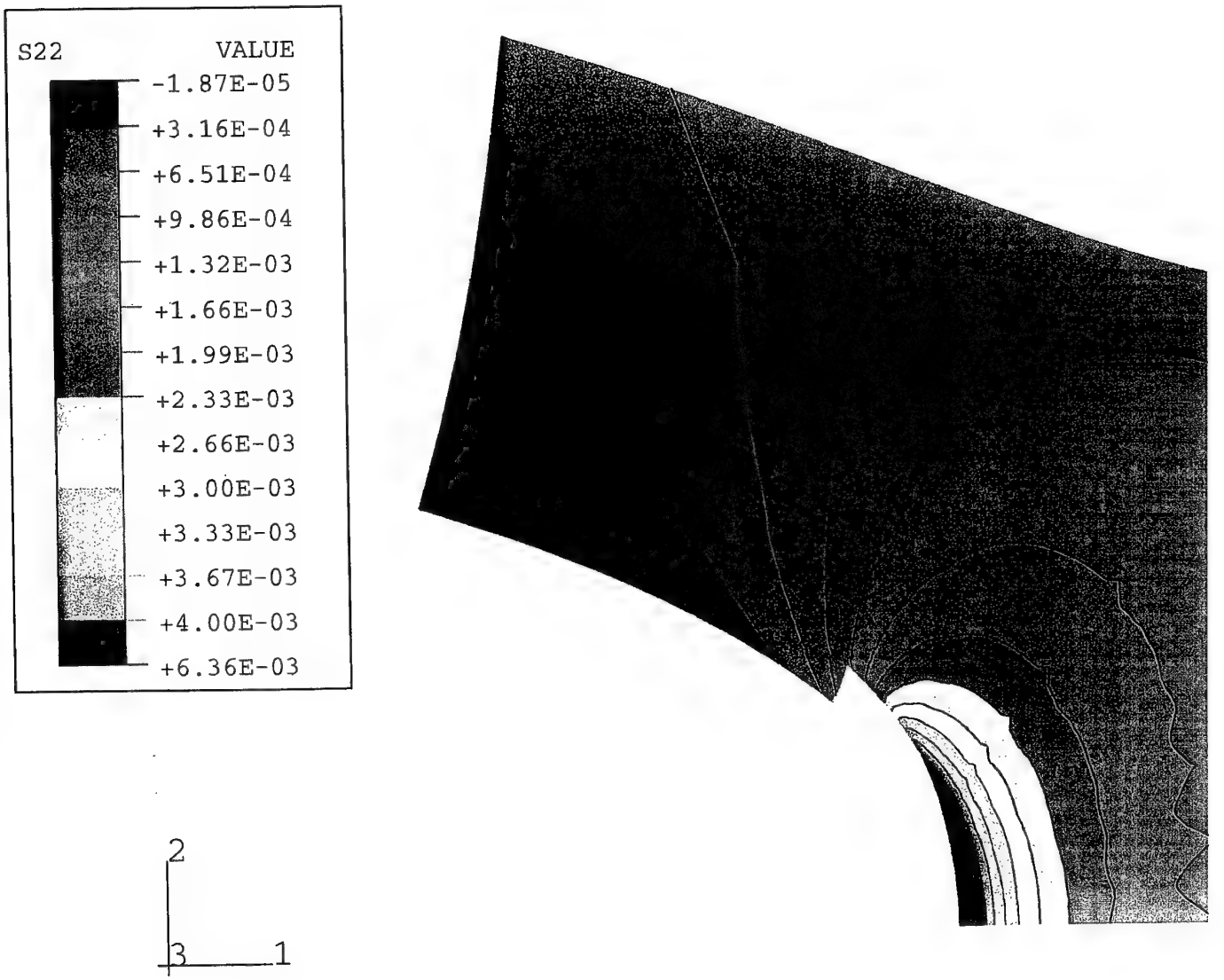

Fig. 86 Normal stress along the perpendicular to the crack axis direction, σ_{22}, contours (in the deformed specimen configuration) for Figure 71. Values in kN/mm^2. Applied displacement u_0=3.3295 mm. Case II.

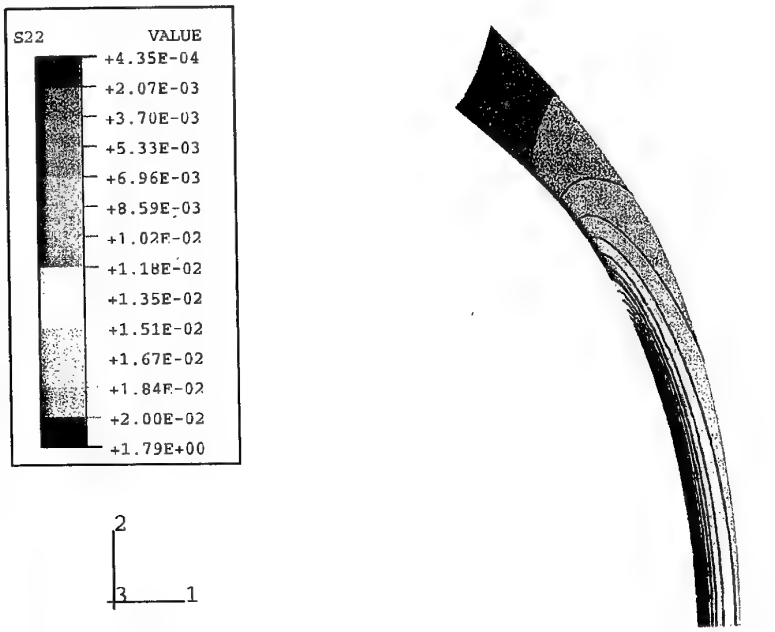

Fig. 87 Normal stress along the perpendicular to the crack axis direction, σ_{22}, contours (in the deformed specimen configuration) for Figure 72. Values in kN/mm^2. Applied displacement u_0=3.3295 mm. Case II.

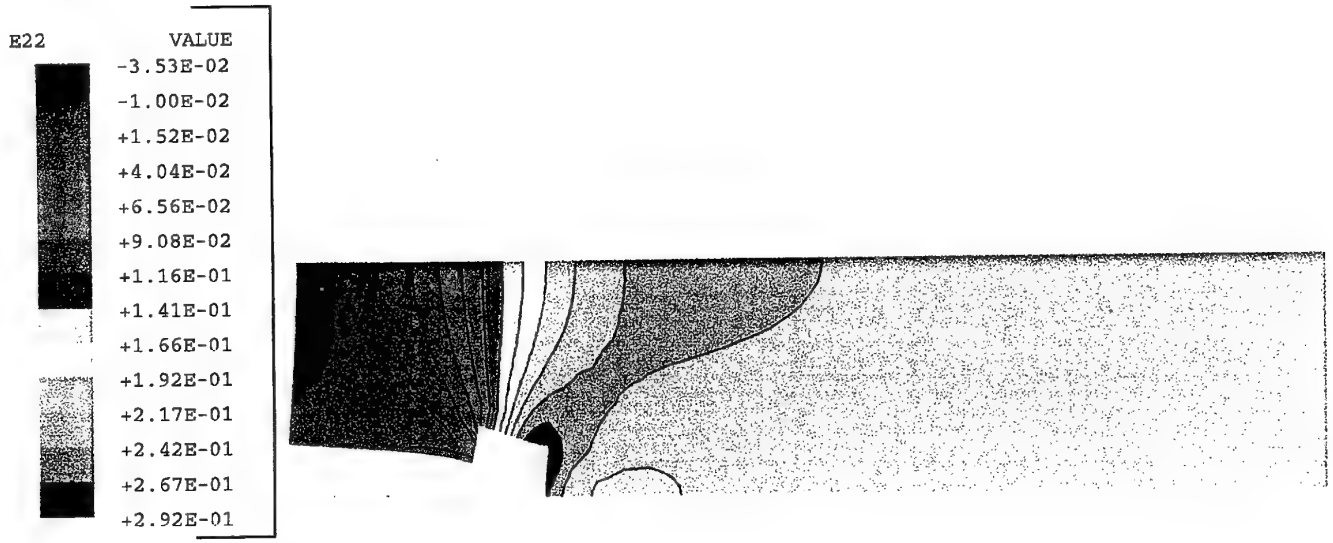

Fig. 88 Normal strain along the perpendicular to the crack axis direction, ε_{22}, contours (in the deformed specimen configuration) for Figure 70. Applied displacement u_0=3.3295 mm. Case II.

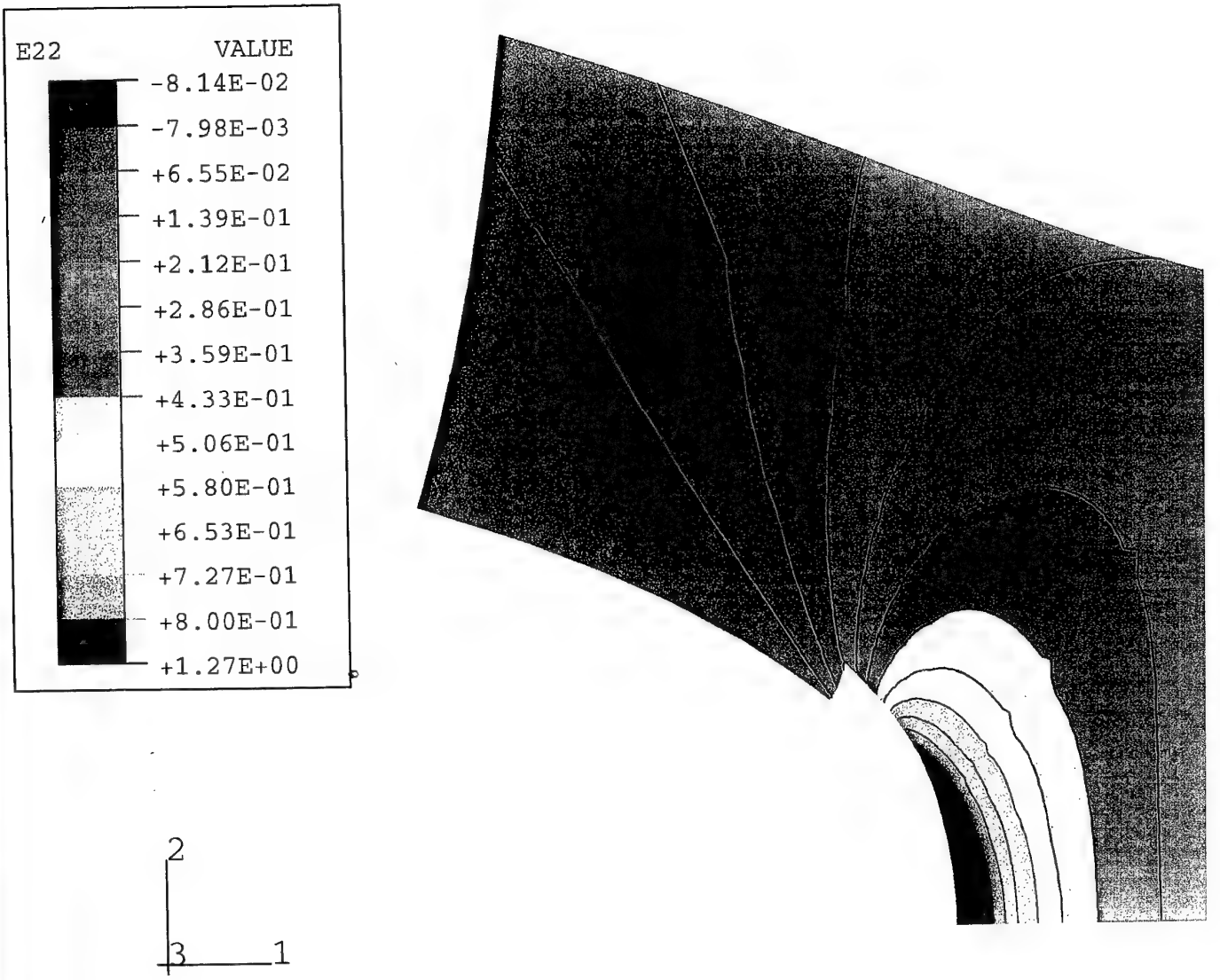

Fig. 89 Normal strain along the perpendicular to the crack axis direction, ε_{22}, contours (in the deformed specimen configuration) for Figure 71. Applied displacement u_0=3.3295 mm. Case II.

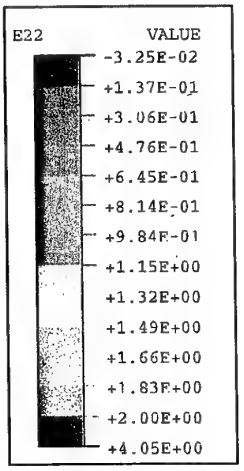

Fig. 90 Normal strain along the perpendicular to the crack axis direction, ε_{22}, contours (in the deformed specimen configuration) for Figure 72. Applied displacement u_0=3.3295 mm. Case II.

Case III

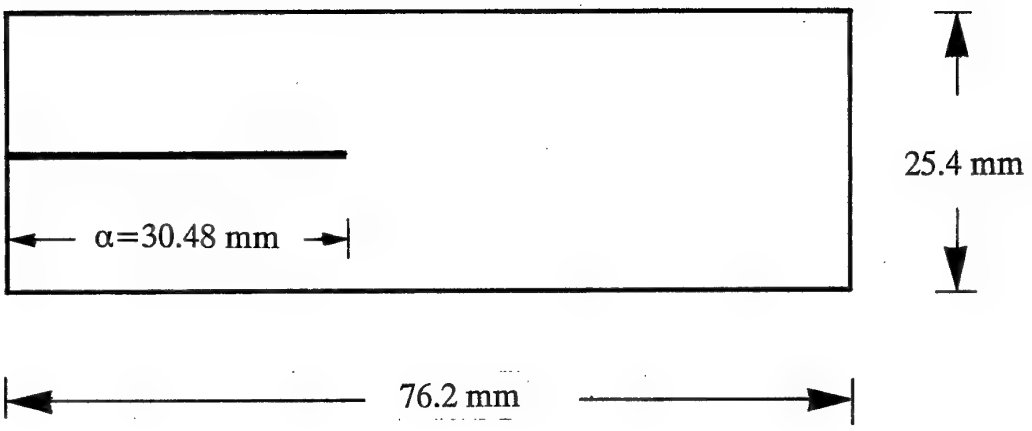

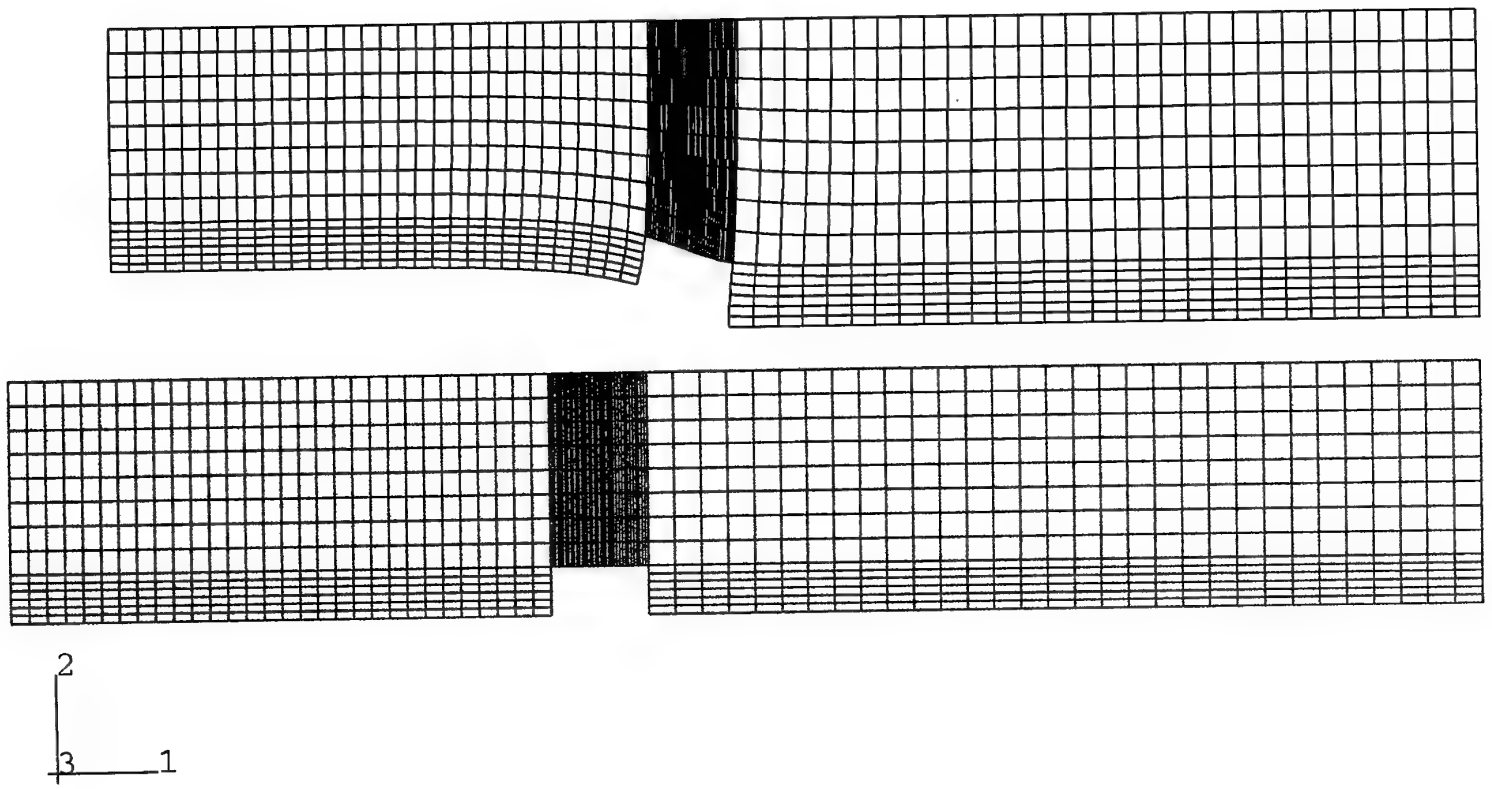

Fig. 91 Undeformed (in red) and deformed (in black) finite element grids for half specimen. Applied displacement u_0=0.2541 mm. Case III.

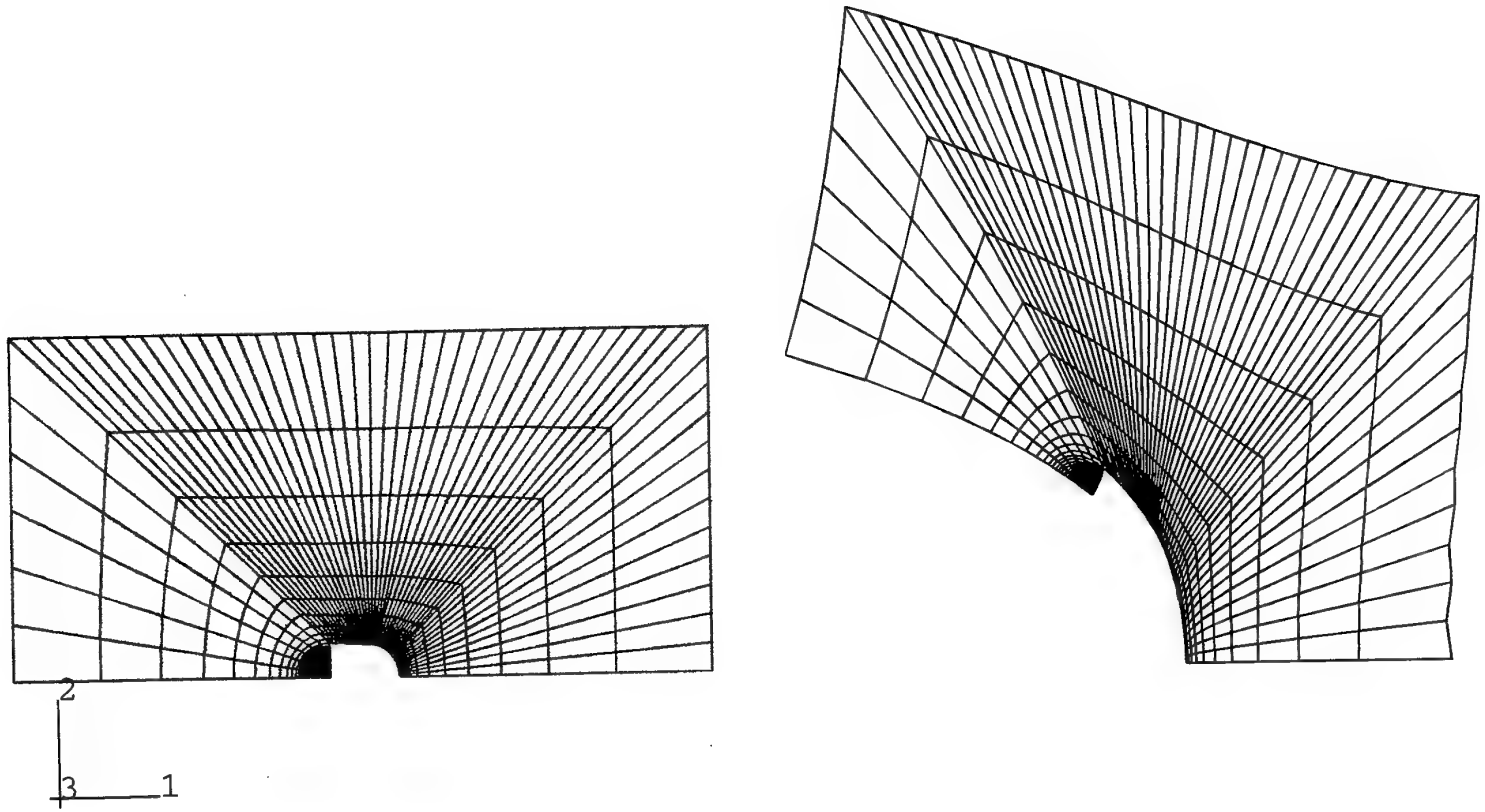

Fig. 92 Undeformed (in red) and deformed (in black) finite element grids for the missing part of Figure 91. Applied displacement u_0=0.2541 mm. Case III.

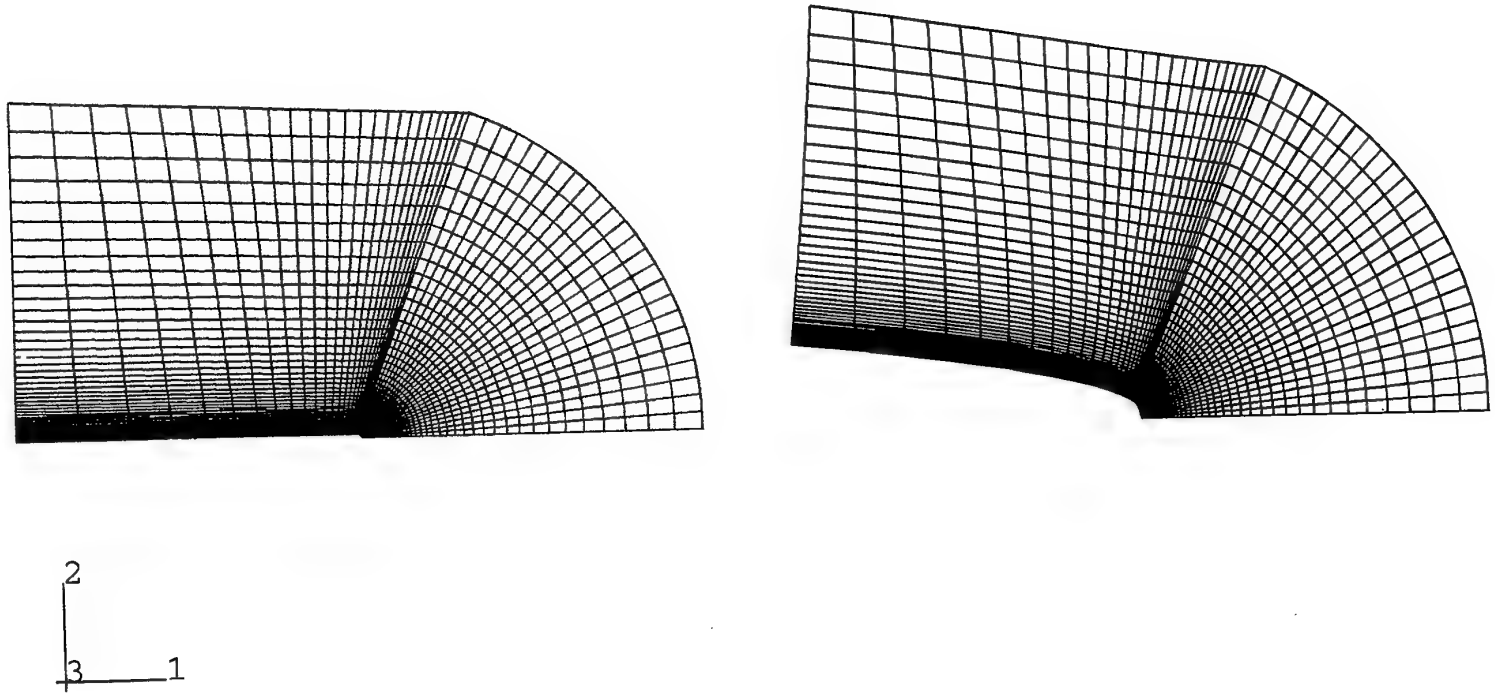

Fig. 93 Undeformed (in red) and deformed (in black) finite element grids for the missing part of Figure 92. Applied displacement u_0=0.2541 mm. Case III.

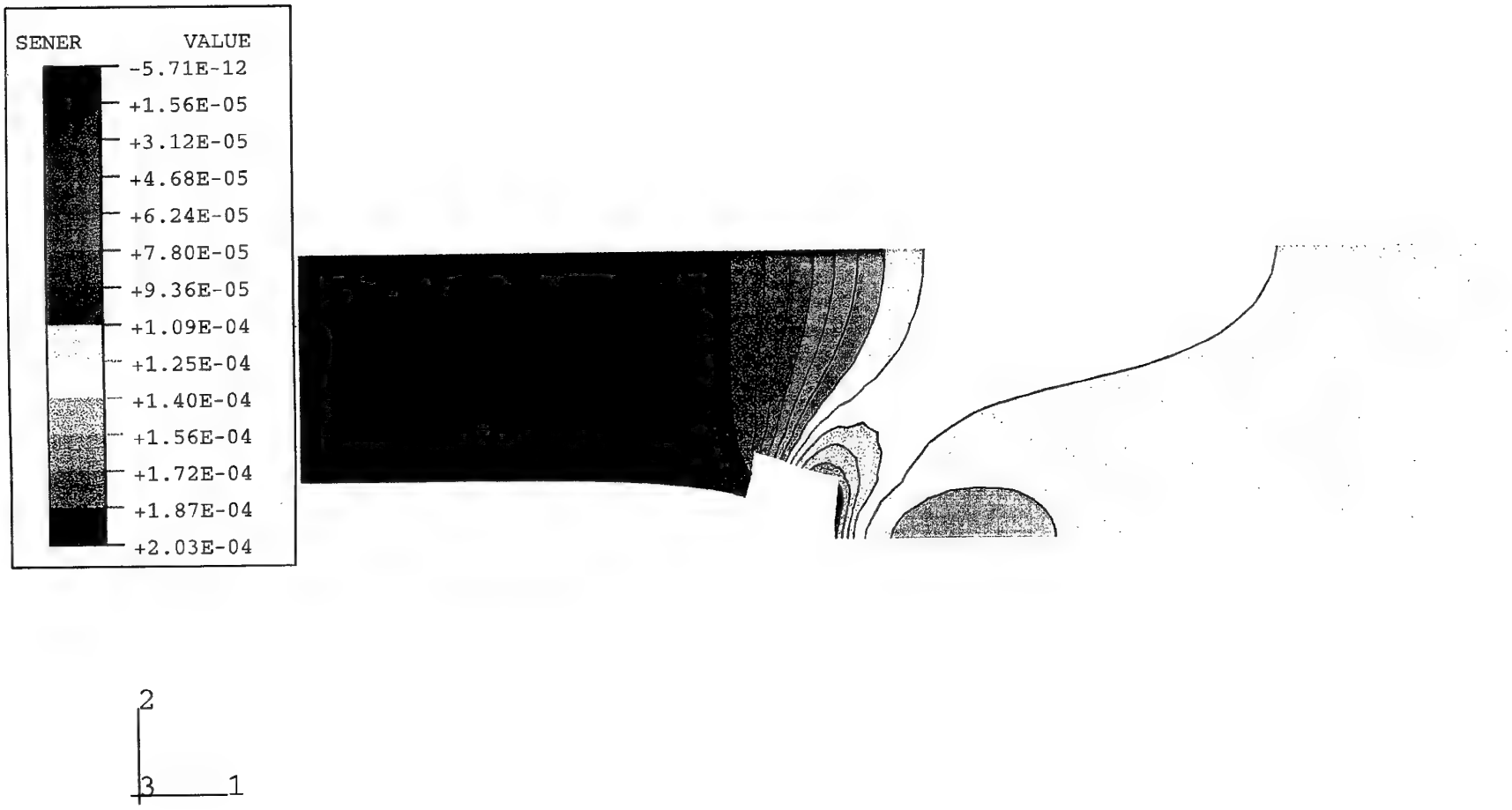

Fig. 94 Strain energy density, dW/dV, contours (in the deformed specimen configuration) for Figure 91. Values in kN.mm/mm^3. Applied displacement u_0=0.2541 mm. Case III.

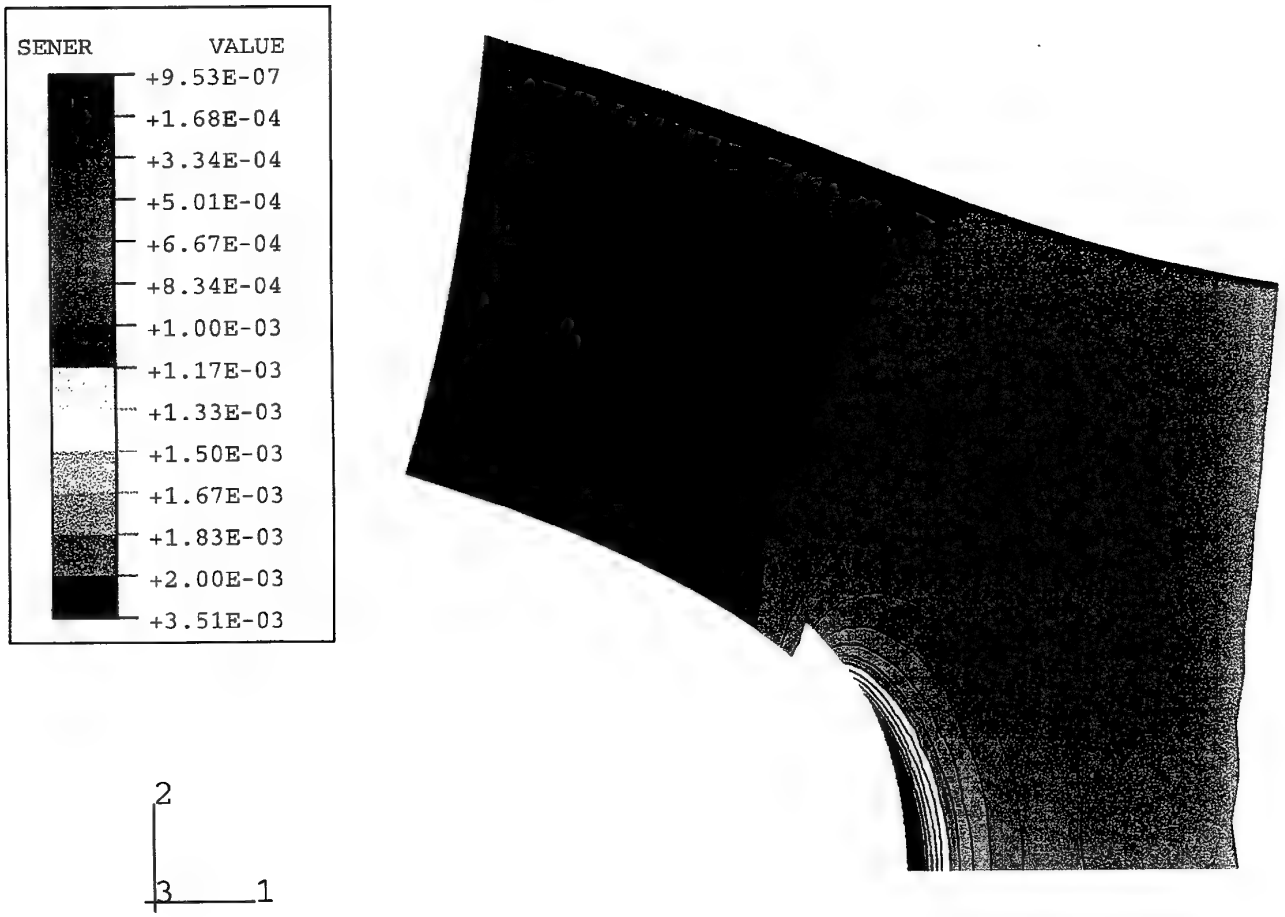

Fig. 95 Strain energy density, dW/dV, contours (in the deformed specimen configuration) for Figure 92. Values in kN.mm/mm^3. Applied displacement u_0=0.2541 mm. Case III.

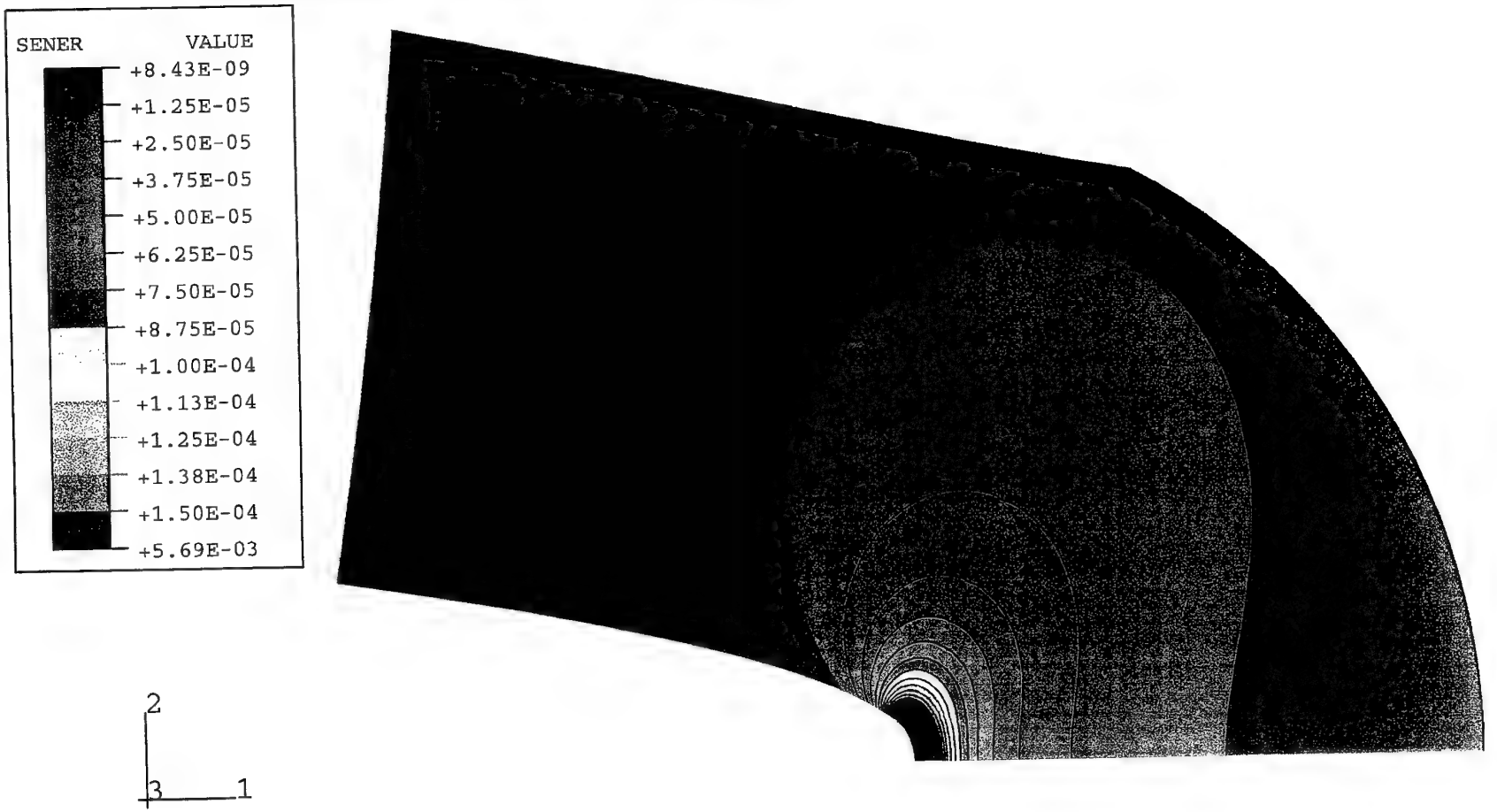

Fig. 96 Strain energy density, dW/dV, contours (in the deformed specimen configuration) for Figure 93. Values in kN.mm/mm^3. Applied displacement u_0=0.2541 mm. Case III.

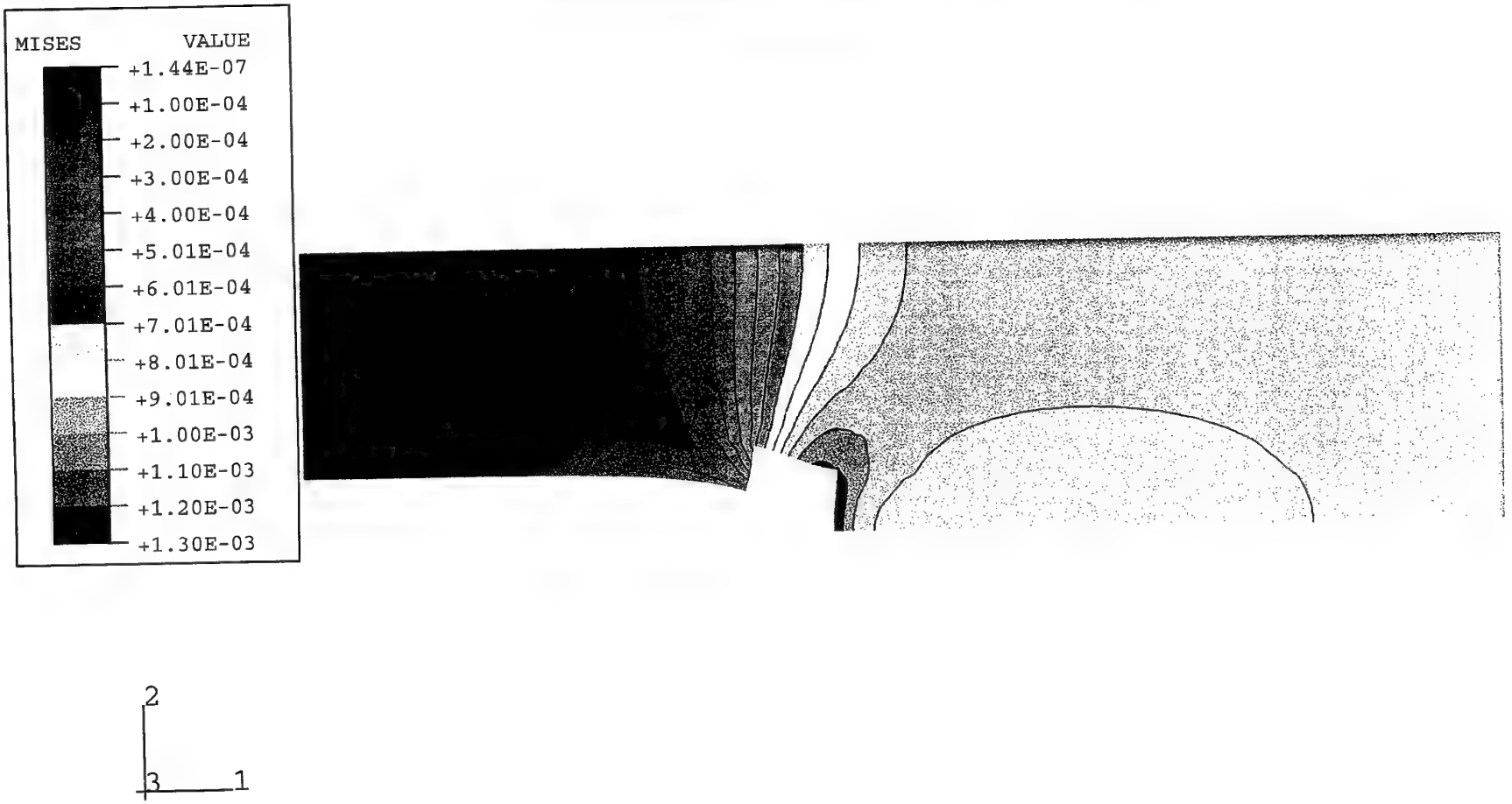

Fig. 97 Mises stress, σ_{eff}, contours (in the deformed specimen configuration) for Figure 91. Values in kN/mm^2. Applied displacement u_0=0.2541 mm. Case III.

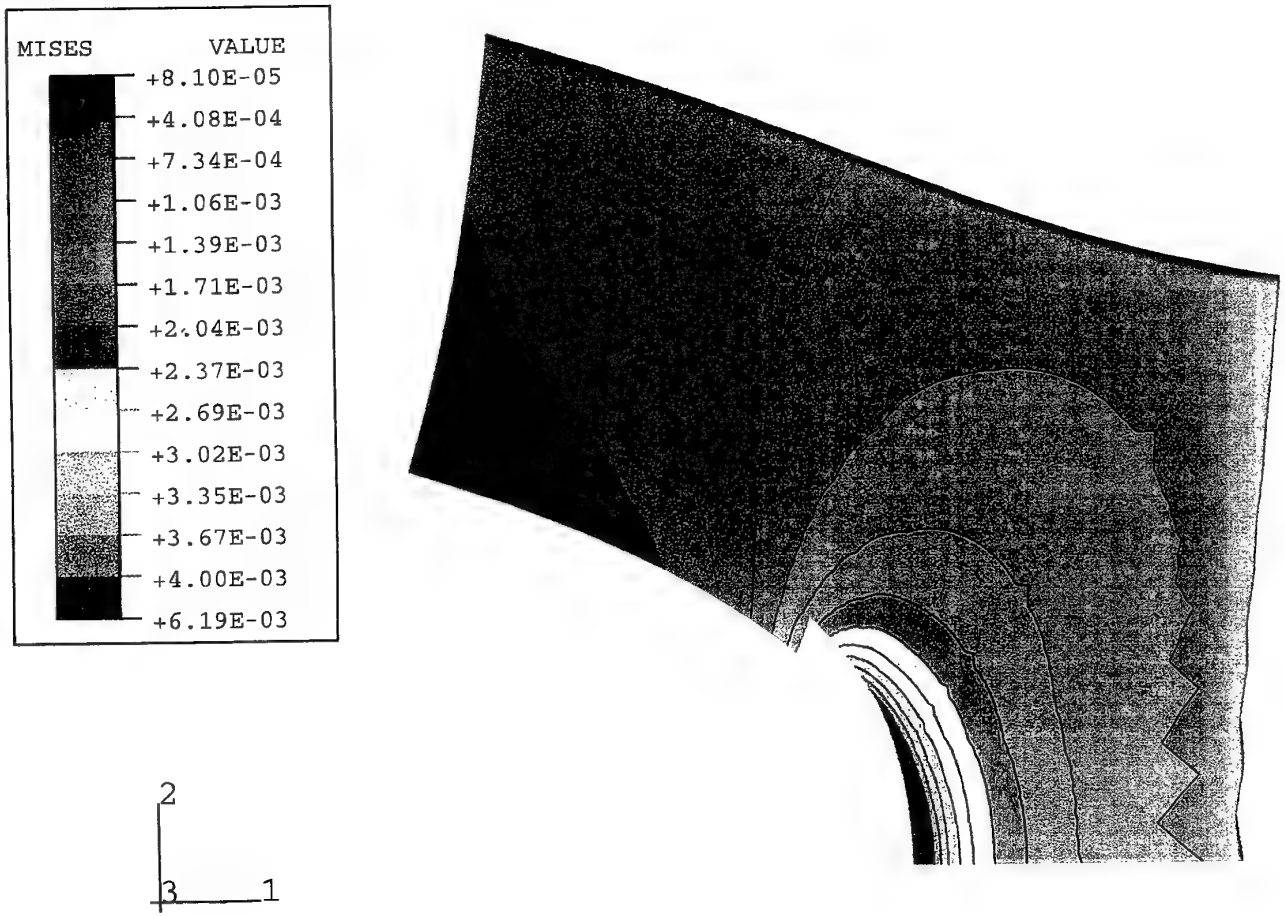

Fig. 98 Mises stress, σ_{eff}, contours (in the deformed specimen configuration) for Figure 92. Values in kN/mm^2. Applied displacement u_0=0.2541 mm. Case III.

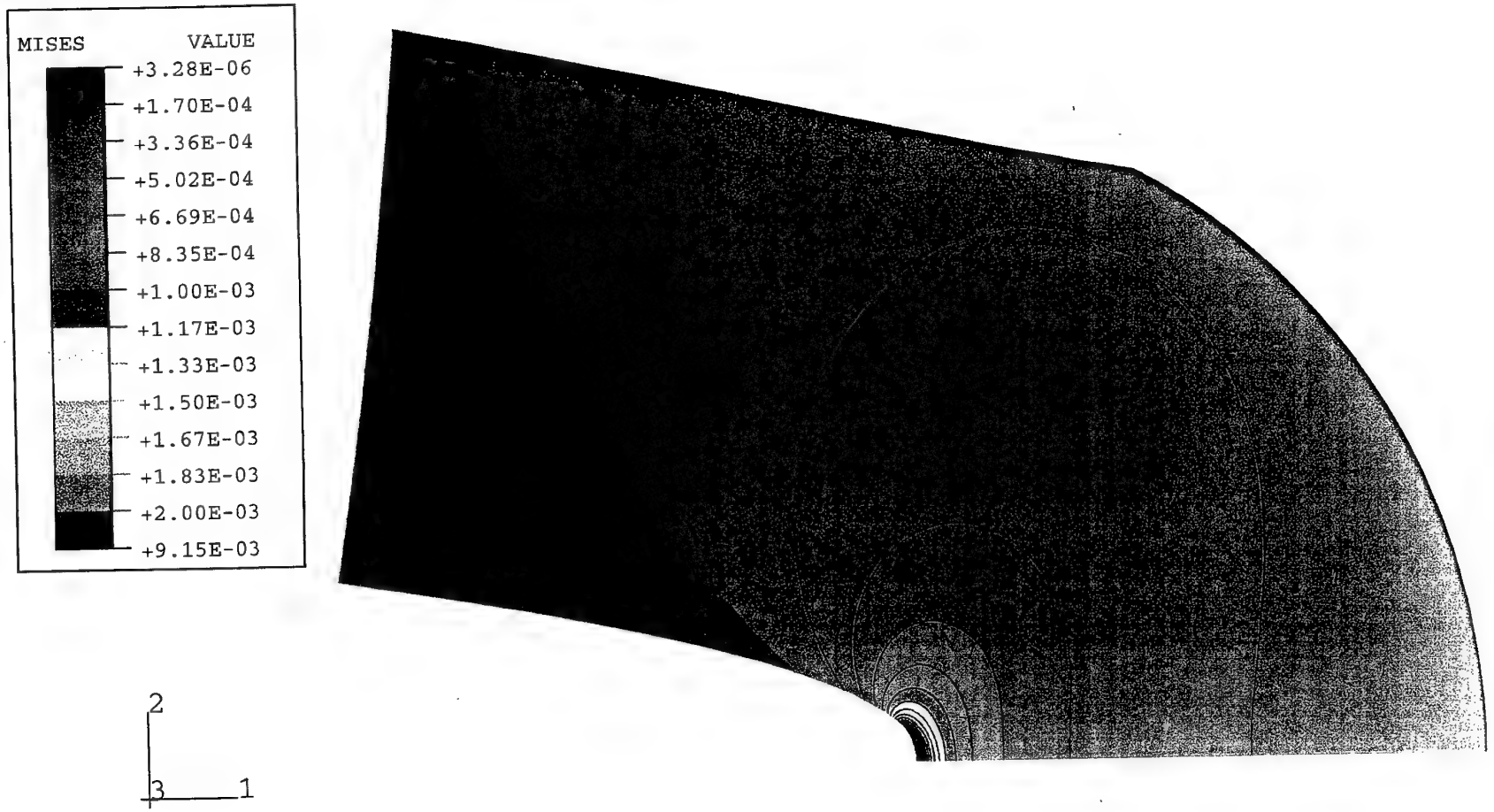

Fig. 99 Mises stress, σ_{eff}, contours (in the deformed specimen configuration) for Figure 93. Values in kN/mm^2. Applied displacement u_0=0.2541 mm. Case III.

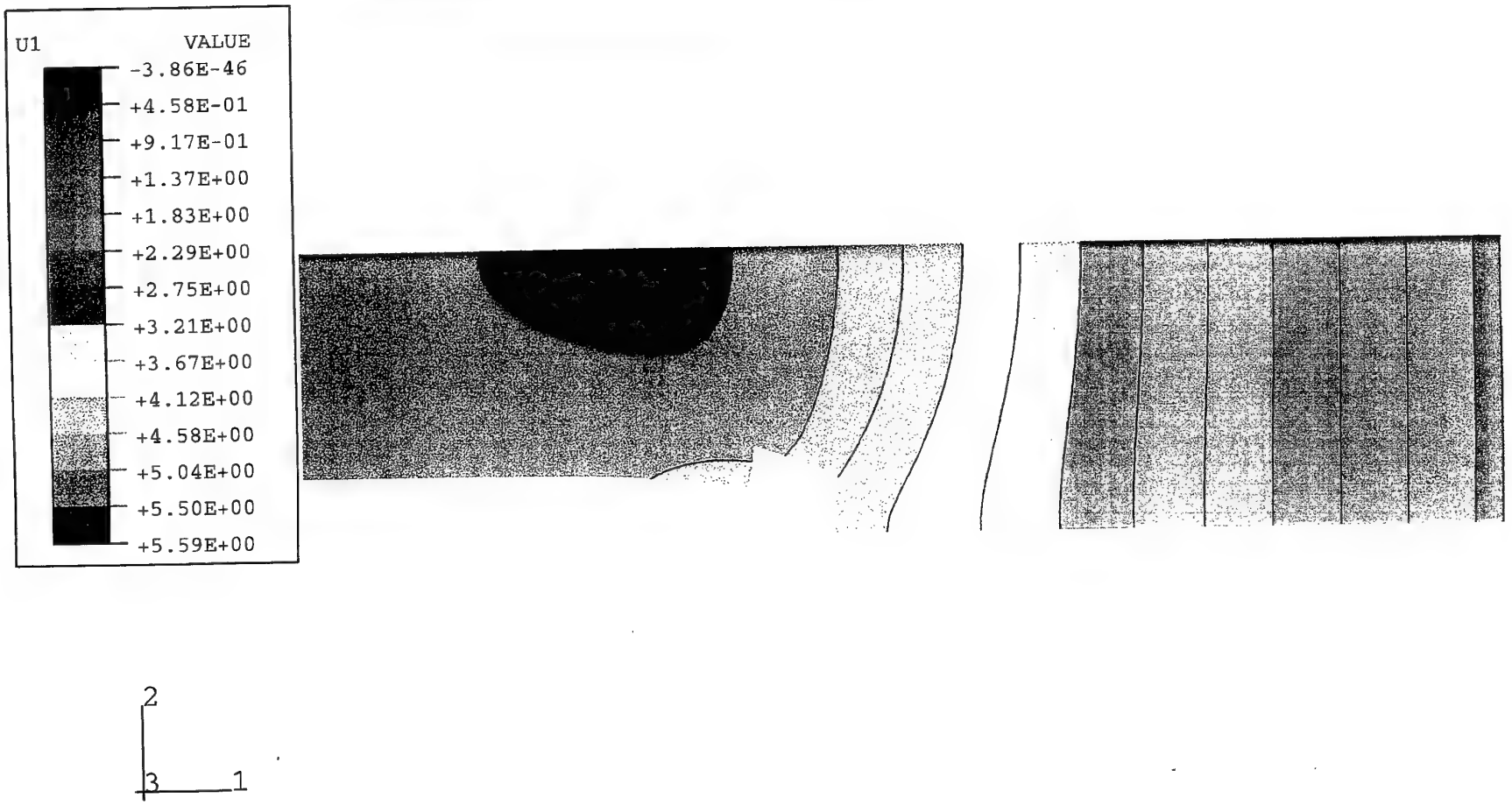

Fig. 100 Displacement along the crack axis direction, u_1, contours (in the deformed specimen configuration) for Figure 91. Values in mm. Applied displacement u_0=0.2541 mm. Case III.

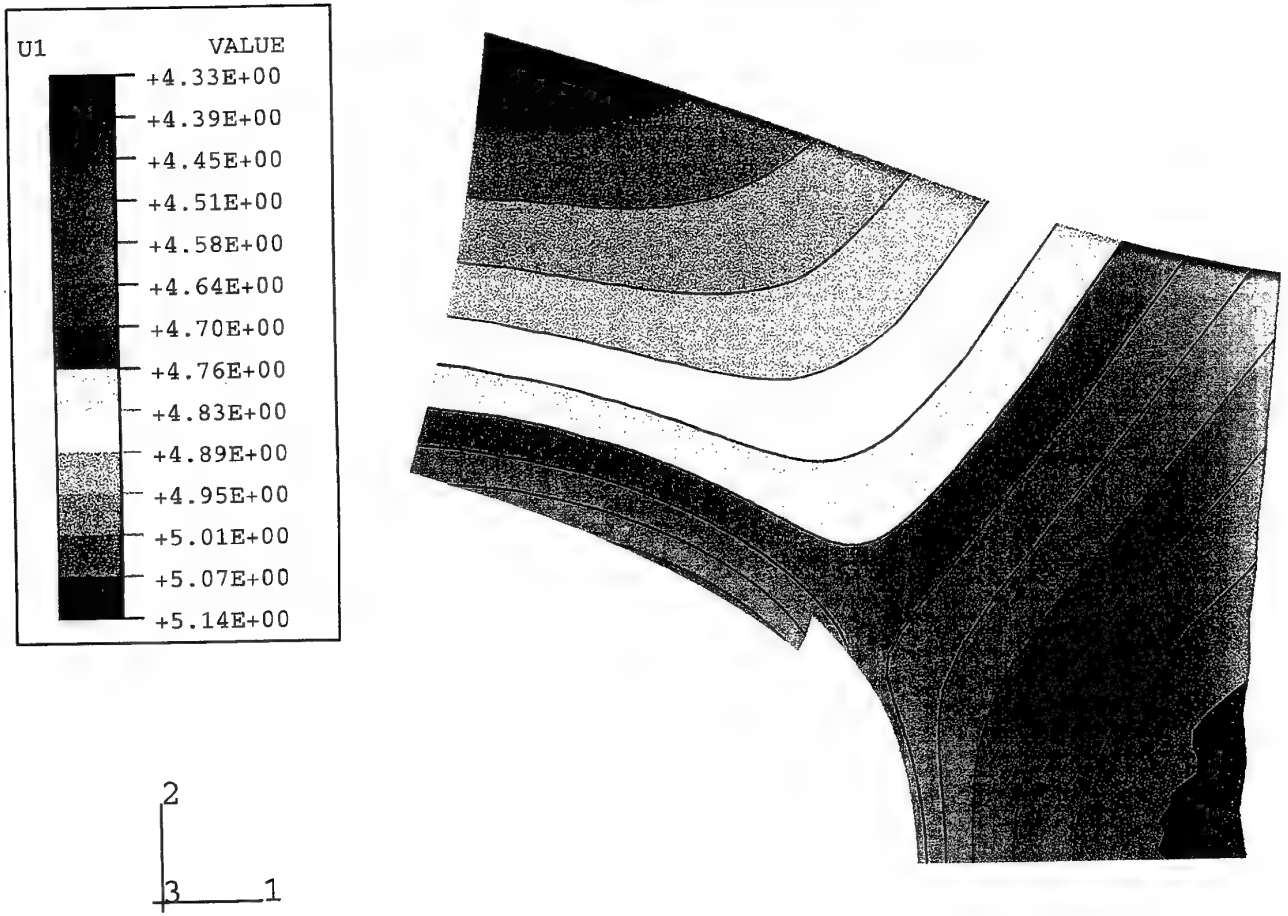

Fig. 101 Displacement along the crack axis direction, u_1, contours (in the deformed specimen configuration) for Figure 92. Values in mm. Applied displacement u_0=0.2541 mm. Case III.

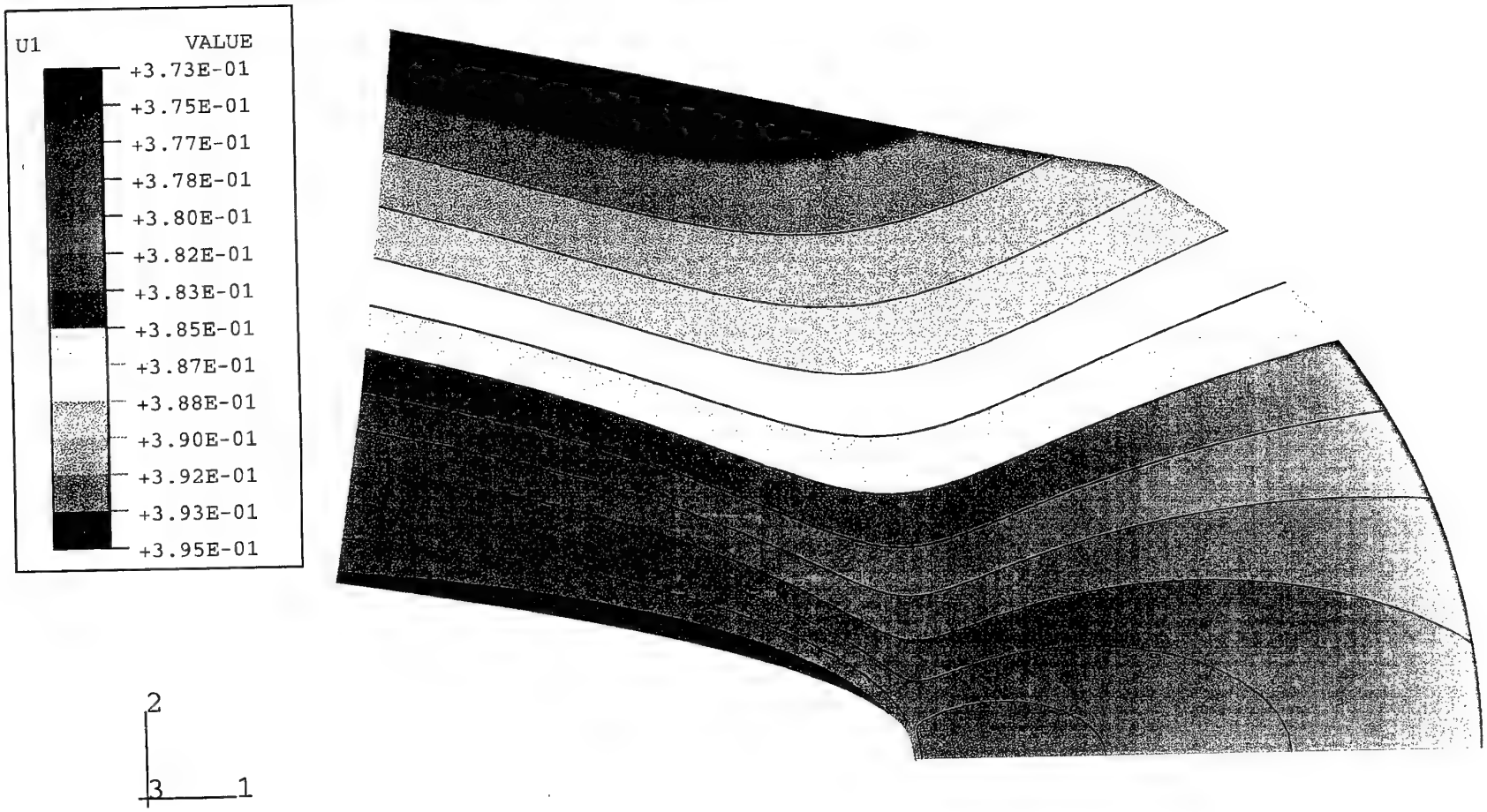

Fig. 102 Displacement along the crack axis direction, u_1, contours (in the deformed specimen configuration) for Figure 93. Values in mm. Applied displacement u_0=0.2541 mm. Case III.

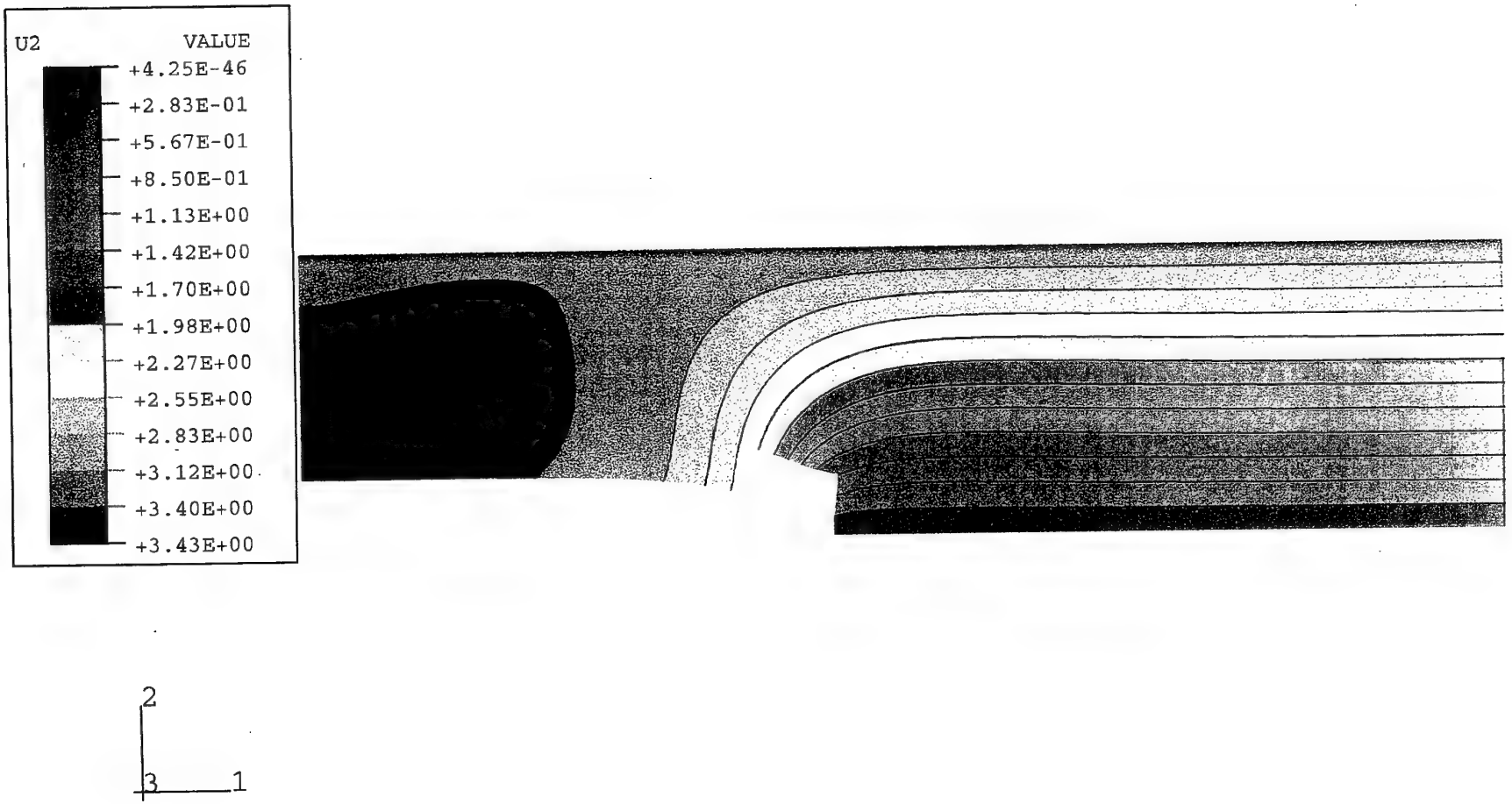

Fig. 103 Displacement along the perpendicular to the crack axis direction, u_2, contours (in the deformed specimen configuration) for Figure 91. Values in mm. Applied displacement u_0=0.2541 mm. Case III.

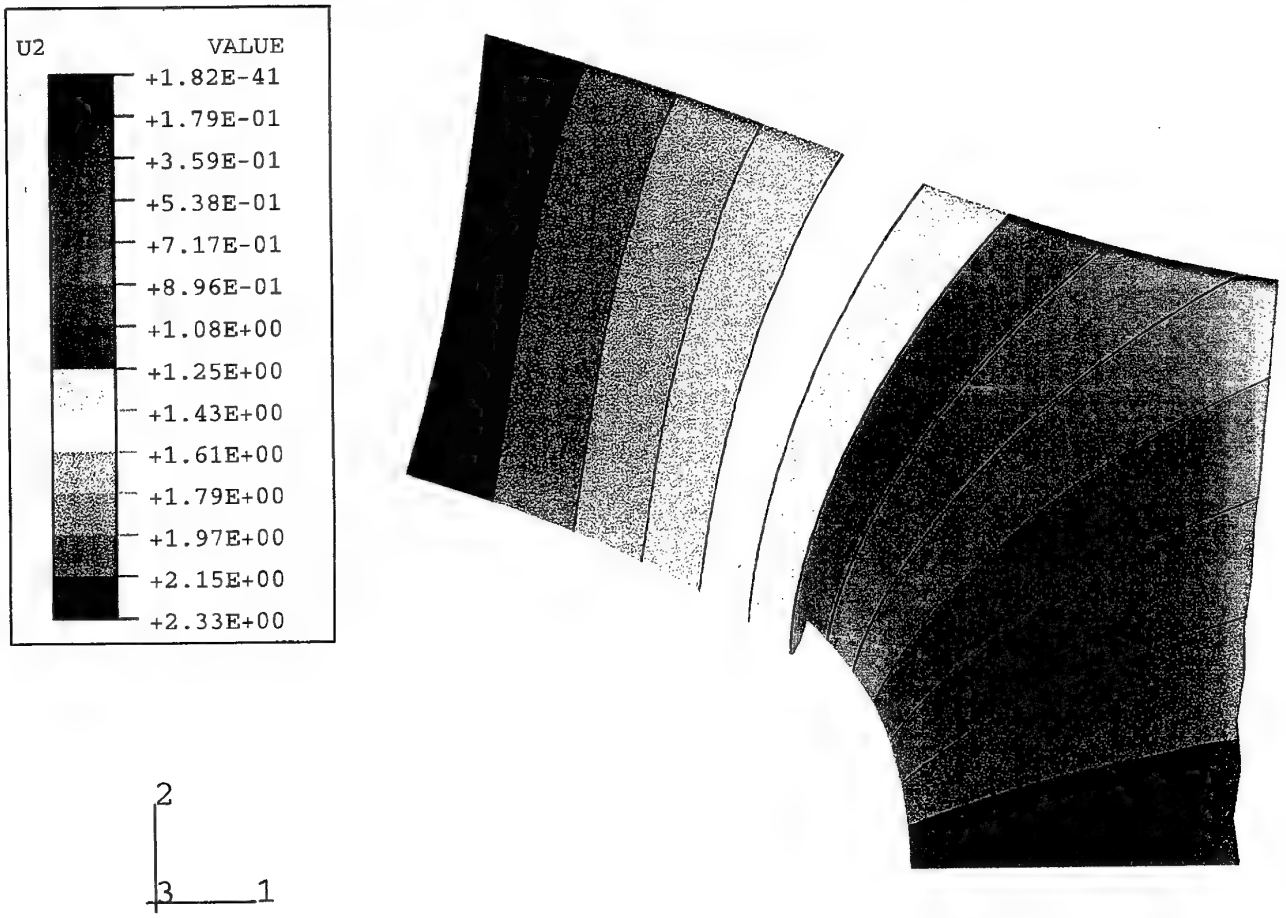

Fig. 104 Displacement along the perpendicular to the crack axis direction, u_2, contours (in the deformed specimen configuration) for Figure 92. Values in mm. Applied displacement u_0=0.2541 mm. Case III.

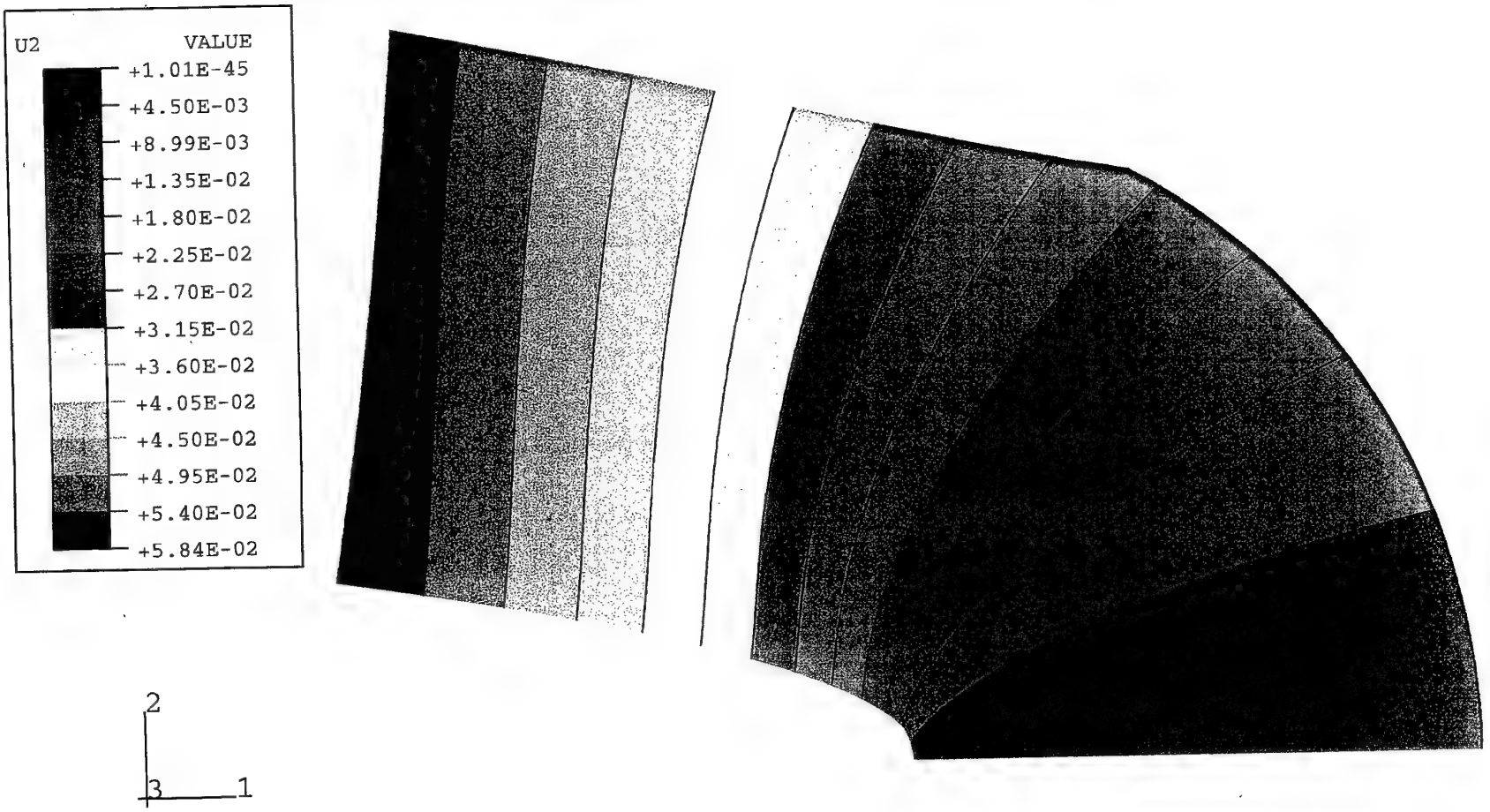

Fig. 105 Displacement along the perpendicular to the crack axis direction, u_2, contours (in the deformed specimen configuration) for Figure 93. Values in mm. Applied displacement u_0=0.2541 mm. Case III.

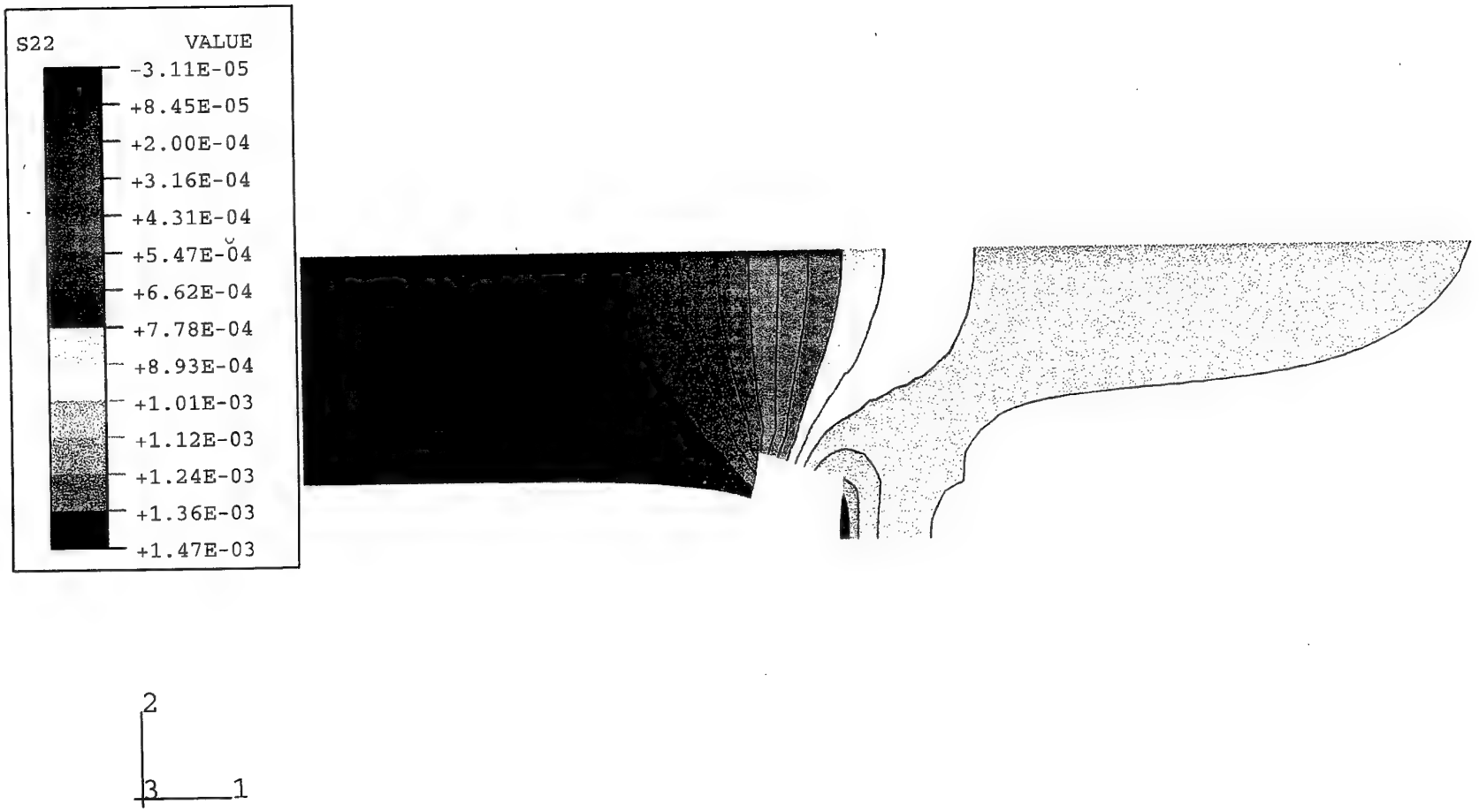

Fig. 106 Normal stress along the perpendicular to the crack axis direction, σ_{22}, contours (in the deformed specimen configuration) for Figure 91. Values in kN/mm^2. Applied displacement u_0=0.2541 mm. Case III.

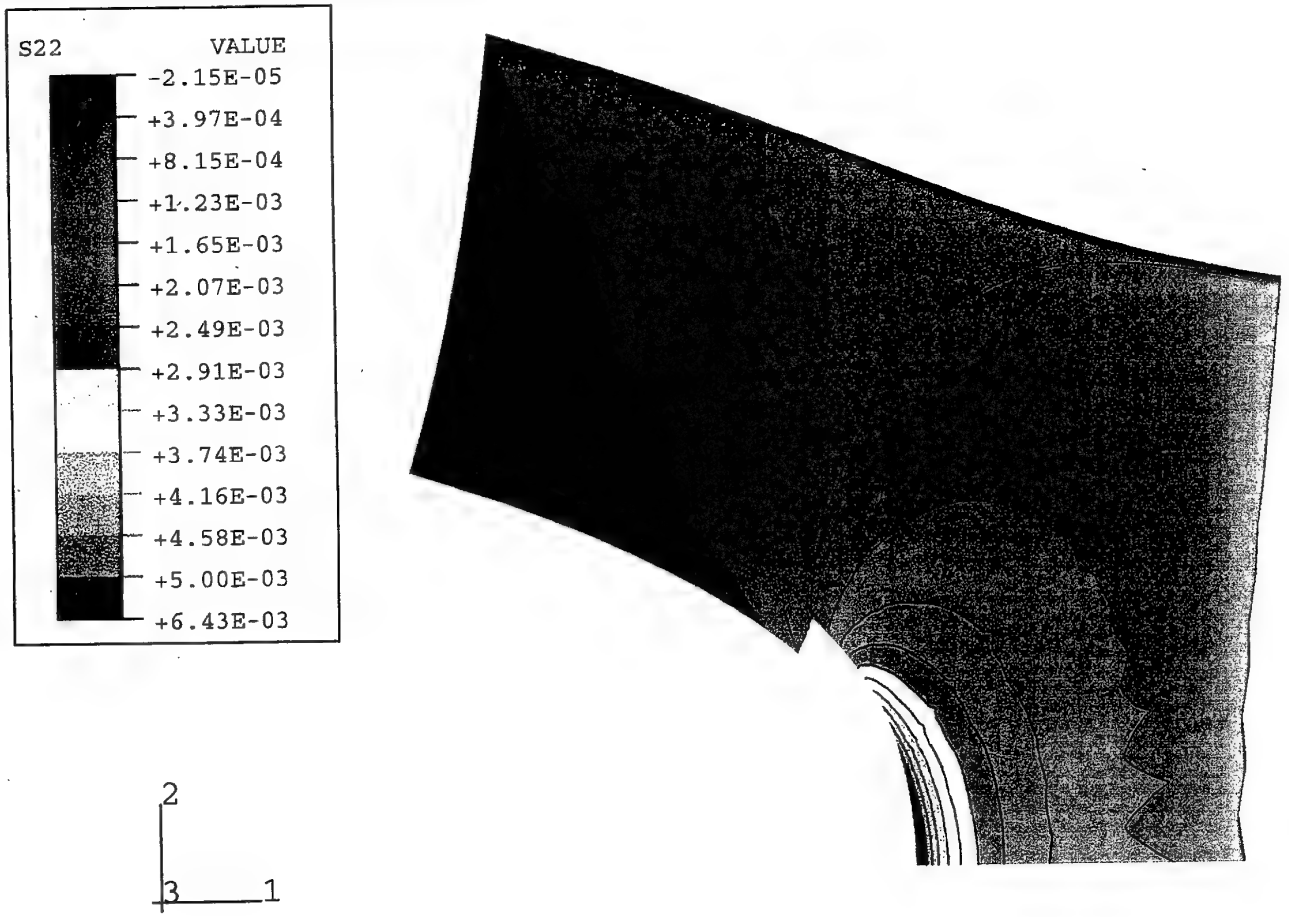

Fig. 107 Normal stress along the perpendicular to the crack axis direction, σ_{22}, contours (in the deformed specimen configuration) for Figure 92. Values in kN/mm^2. Applied displacement u_0=0.2541 mm. Case III.

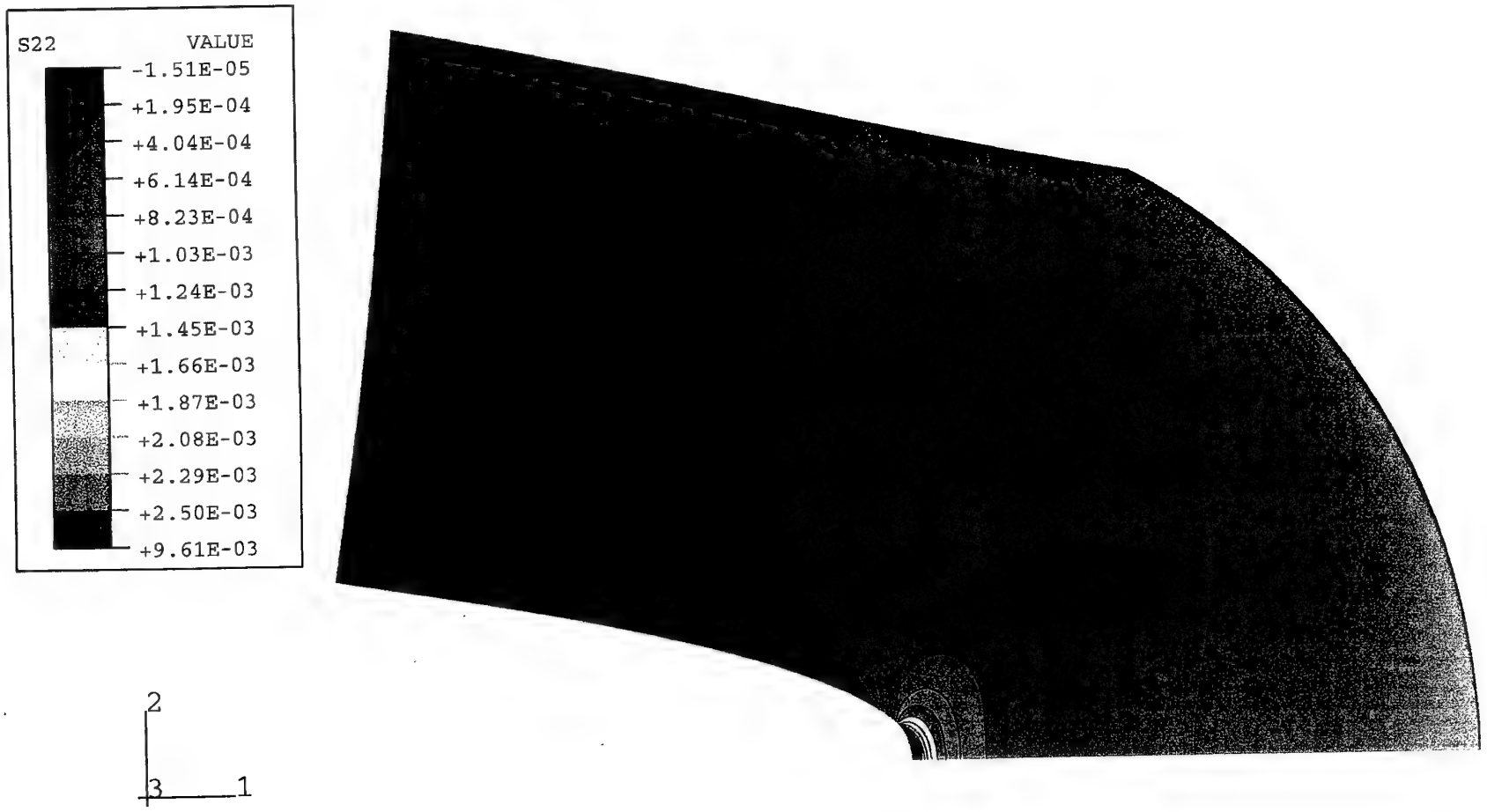

Fig. 108 Normal stress along the perpendicular to the crack axis direction, σ_{22}, contours (in the deformed specimen configuration) for Figure 93. Values in kN/mm^2 Applied displacement u_0=0.2541 mm. Case III.

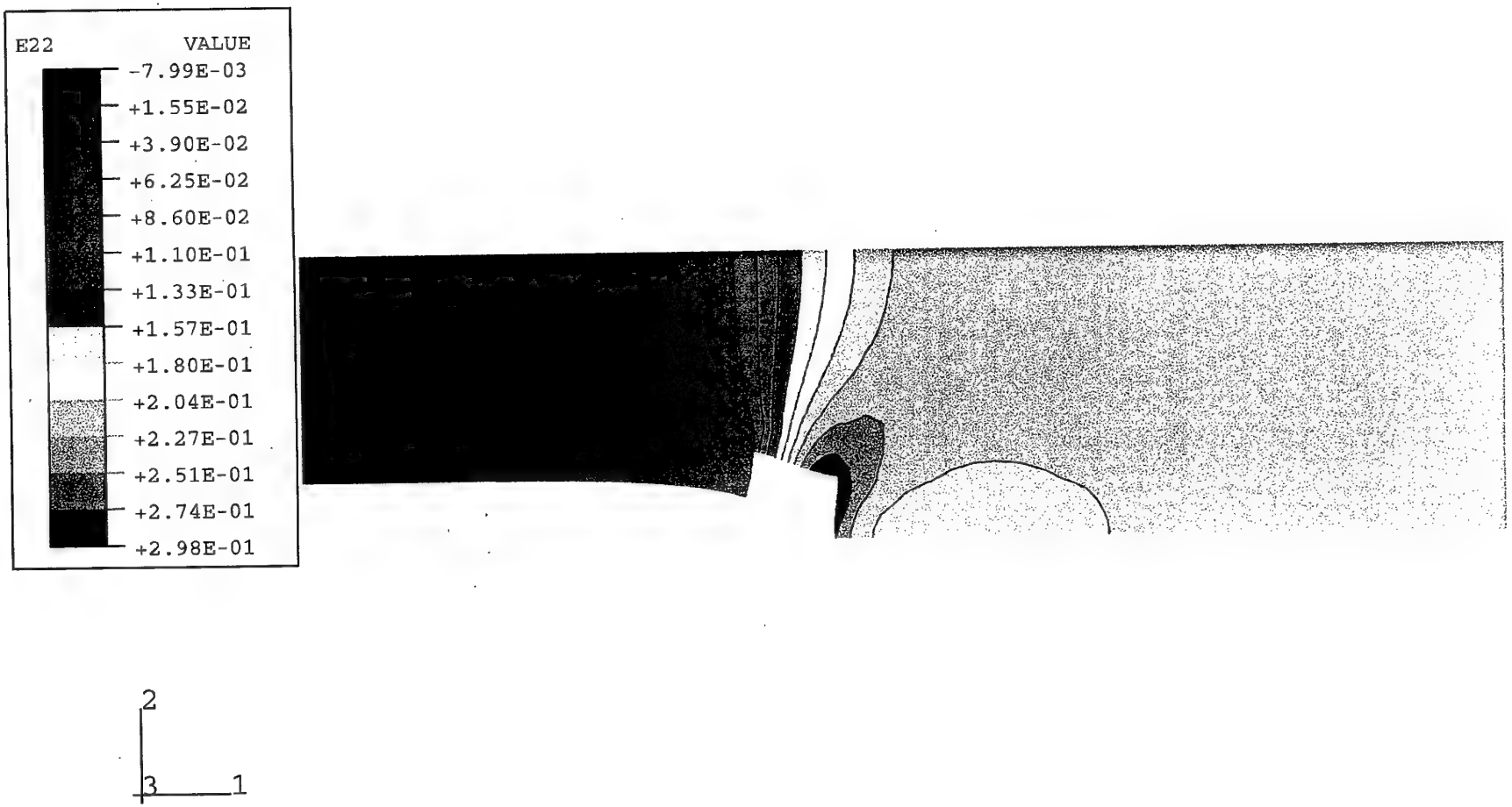

Fig. 109 Normal strain along the perpendicular to the crack axis direction, ε_{22}, contours (in the deformed specimen configuration) for Figure 91. Applied displacement u_0=0.2541 mm. Case III.

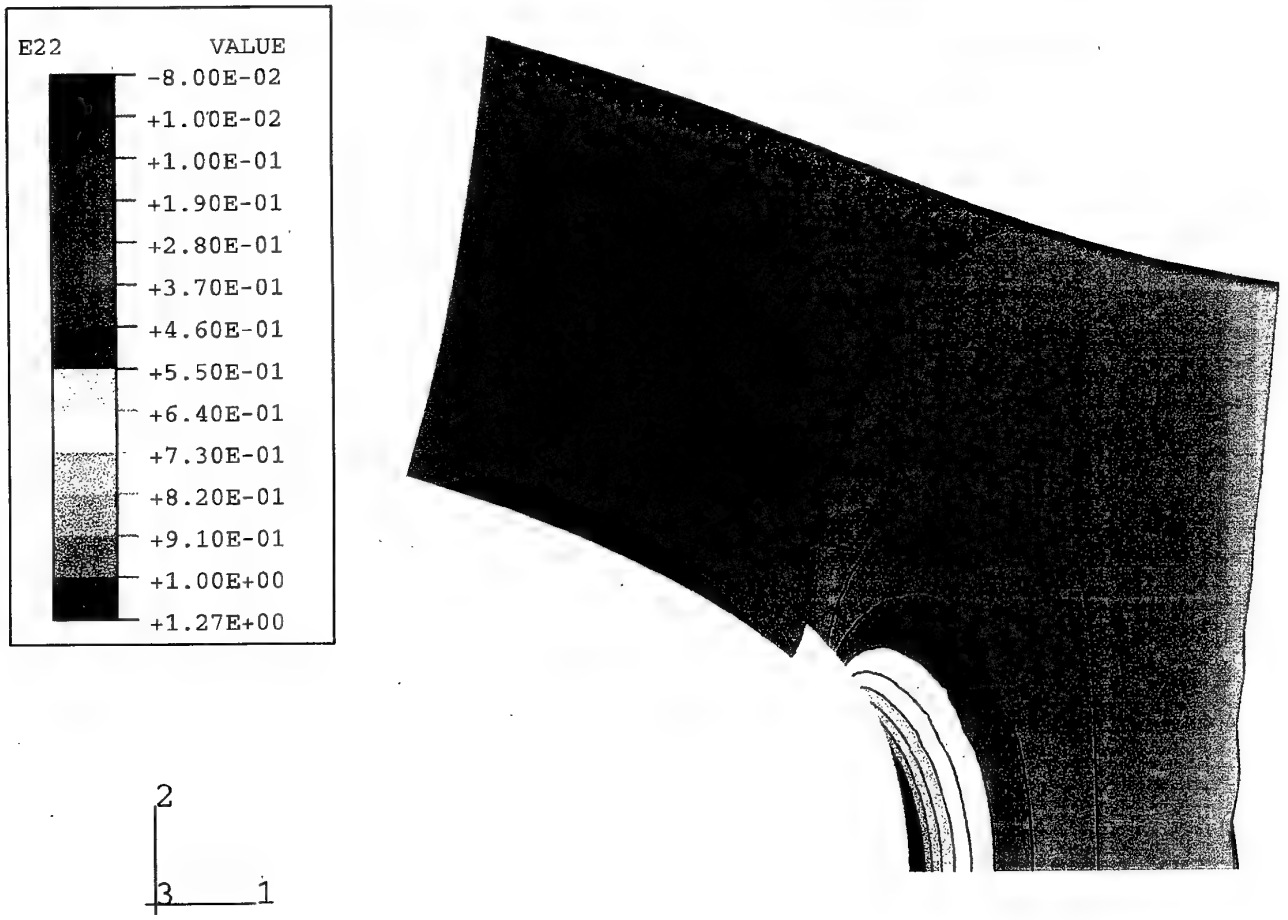

Fig. 110 Normal strain along the perpendicular to the crack axis direction, ε_{22}, contours (in the deformed specimen configuration) for Figure 92. Applied displacement u_0=0.2541 mm. Case III.

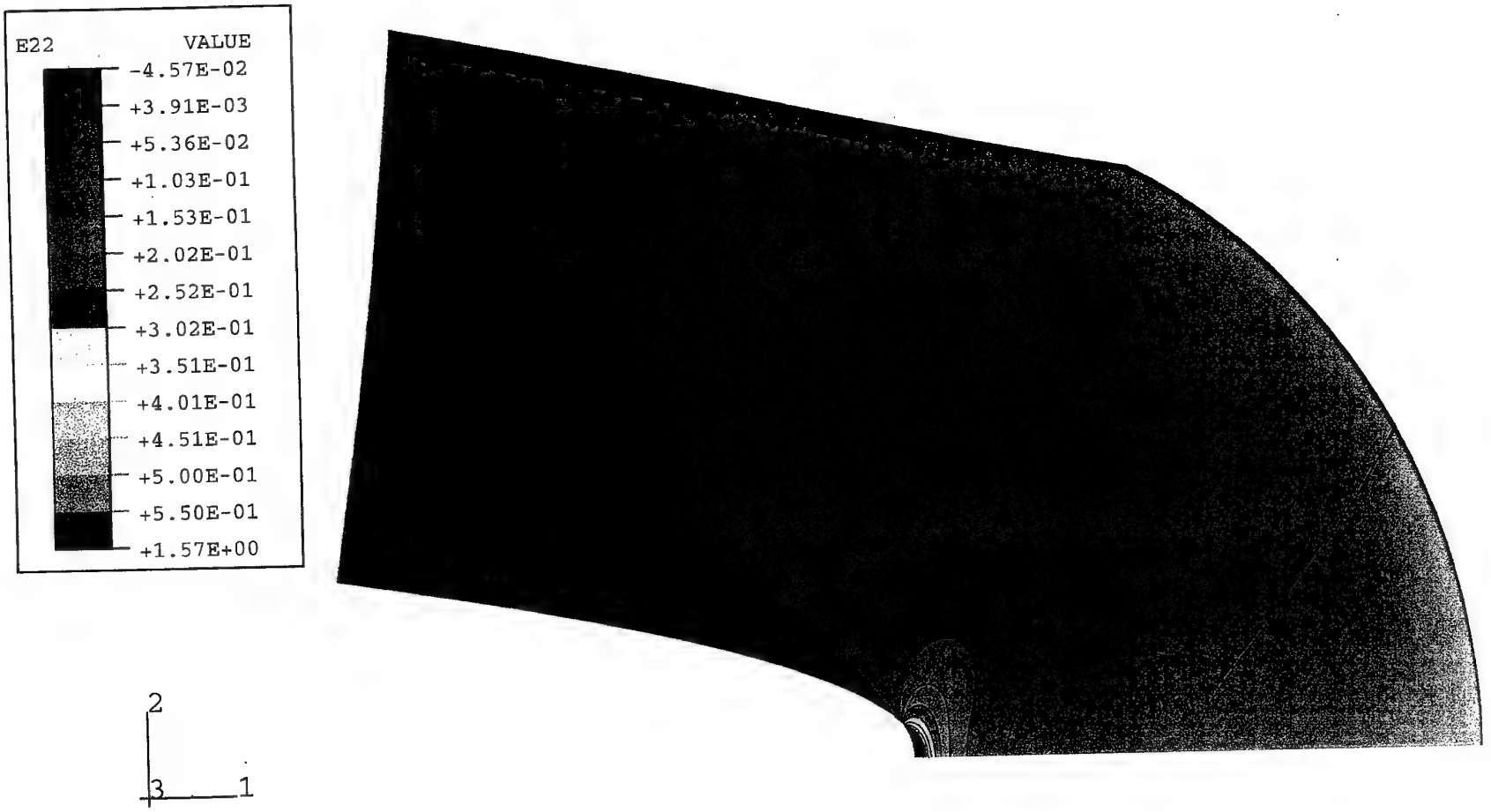

Fig. 111 Normal strain along the perpendicular to the crack axis direction, ε_{22}, contours (in the deformed specimen configuration) for Figure 93. Applied displacement u_0=0.2541 mm. Case III.

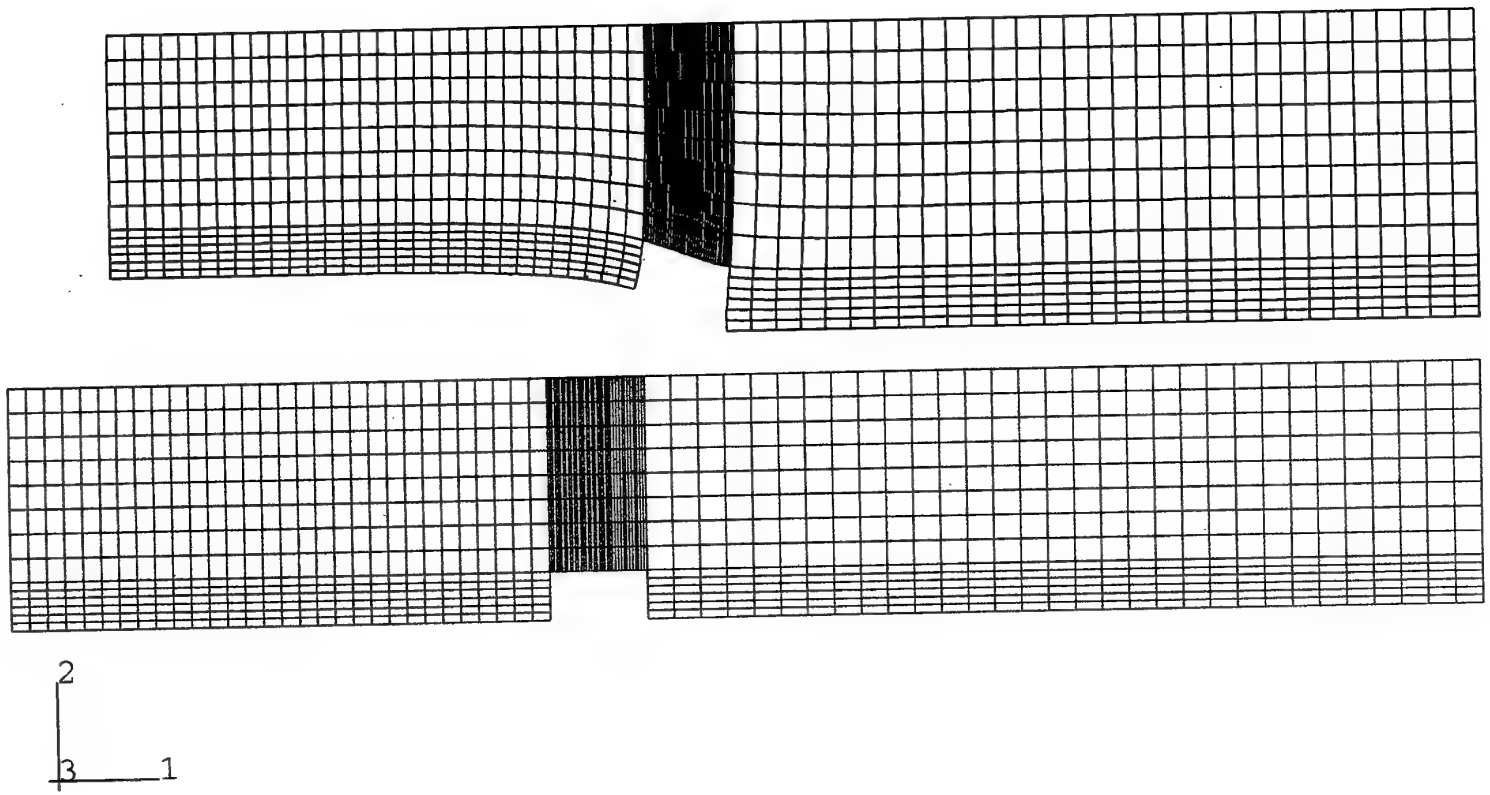

Fig. 112 Undeformed (in red) and deformed (in black) finite element grids for half specimen. Applied displacement u_0=3.3295 mm. Case III.

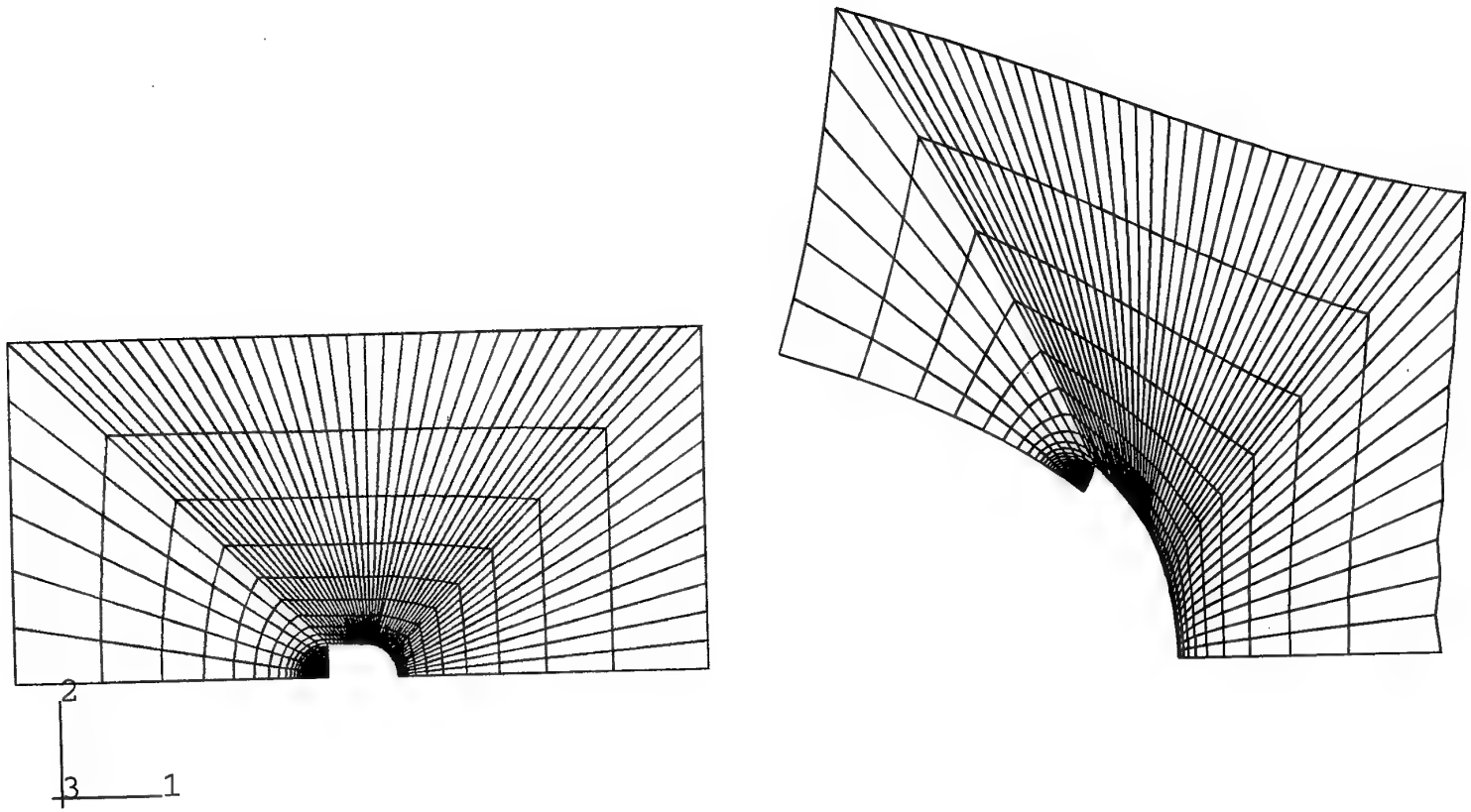

Fig. 113 Undeformed (in red) and deformed (in black) finite element grids for the missing part of Figure 112. Applied displacement u_0=3.3295 mm. Case III.

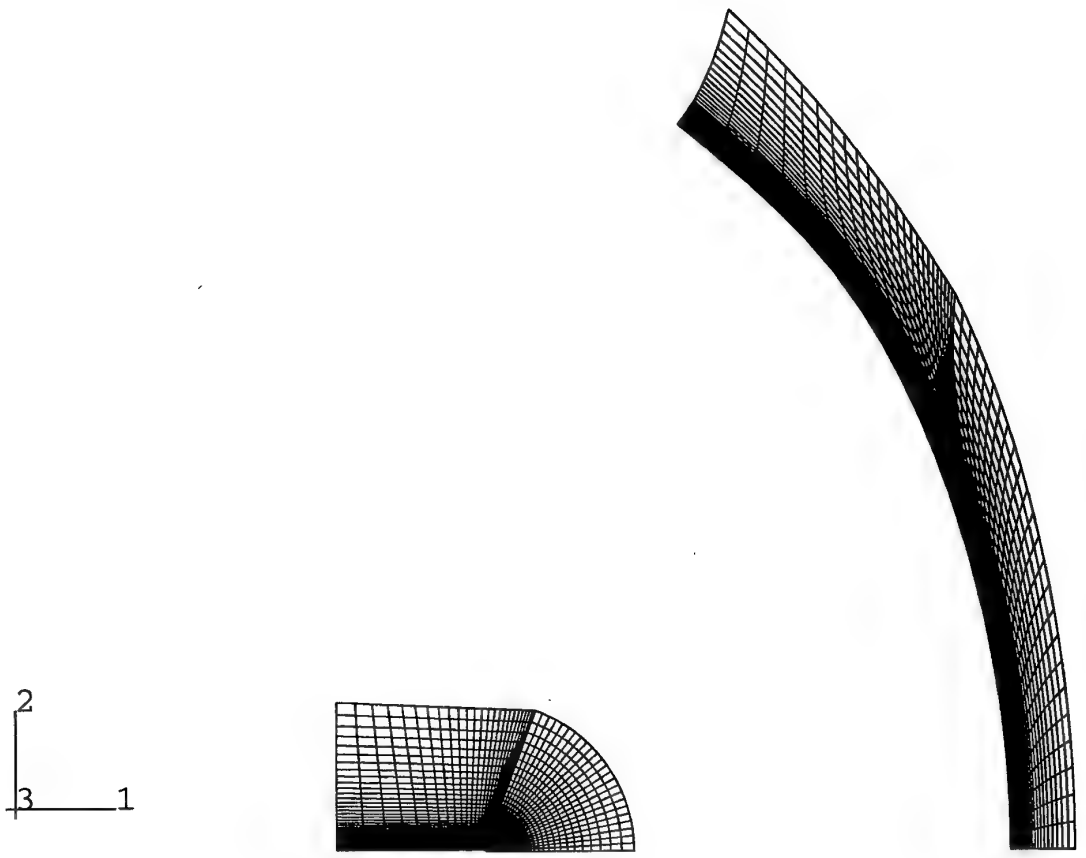

Fig. 114 Undeformed (in red) and deformed (in black) finite element grids for the missing part of Figure 113. Applied displacement u_0=3.3295 mm. Case III.

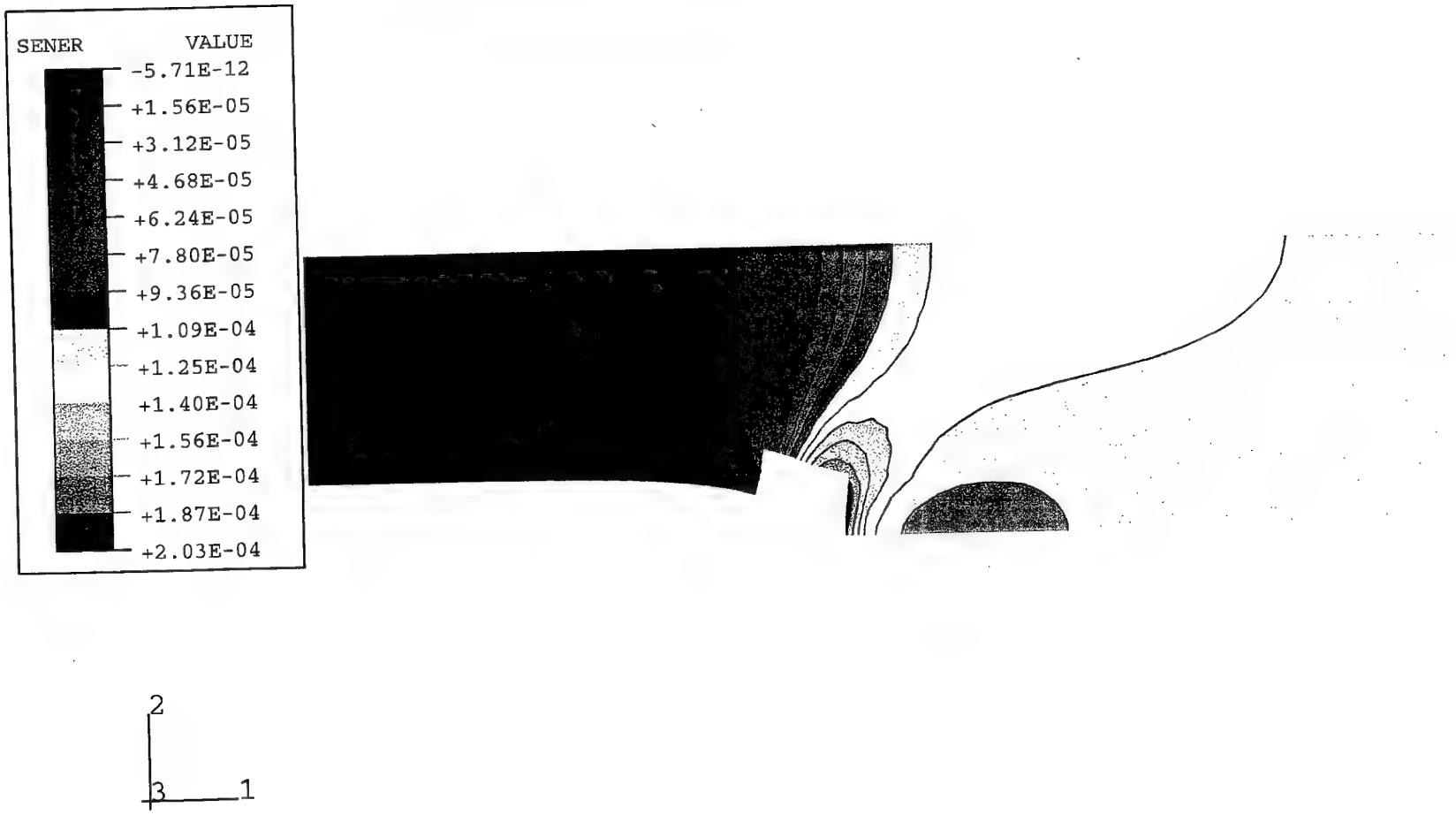

Fig. 115 Strain energy density, dW/dV, contours (in the deformed specimen configuration) for Figure 112. Values in kN.mm/mm^3. Applied displacement u_0=3.3295 mm. Case III.

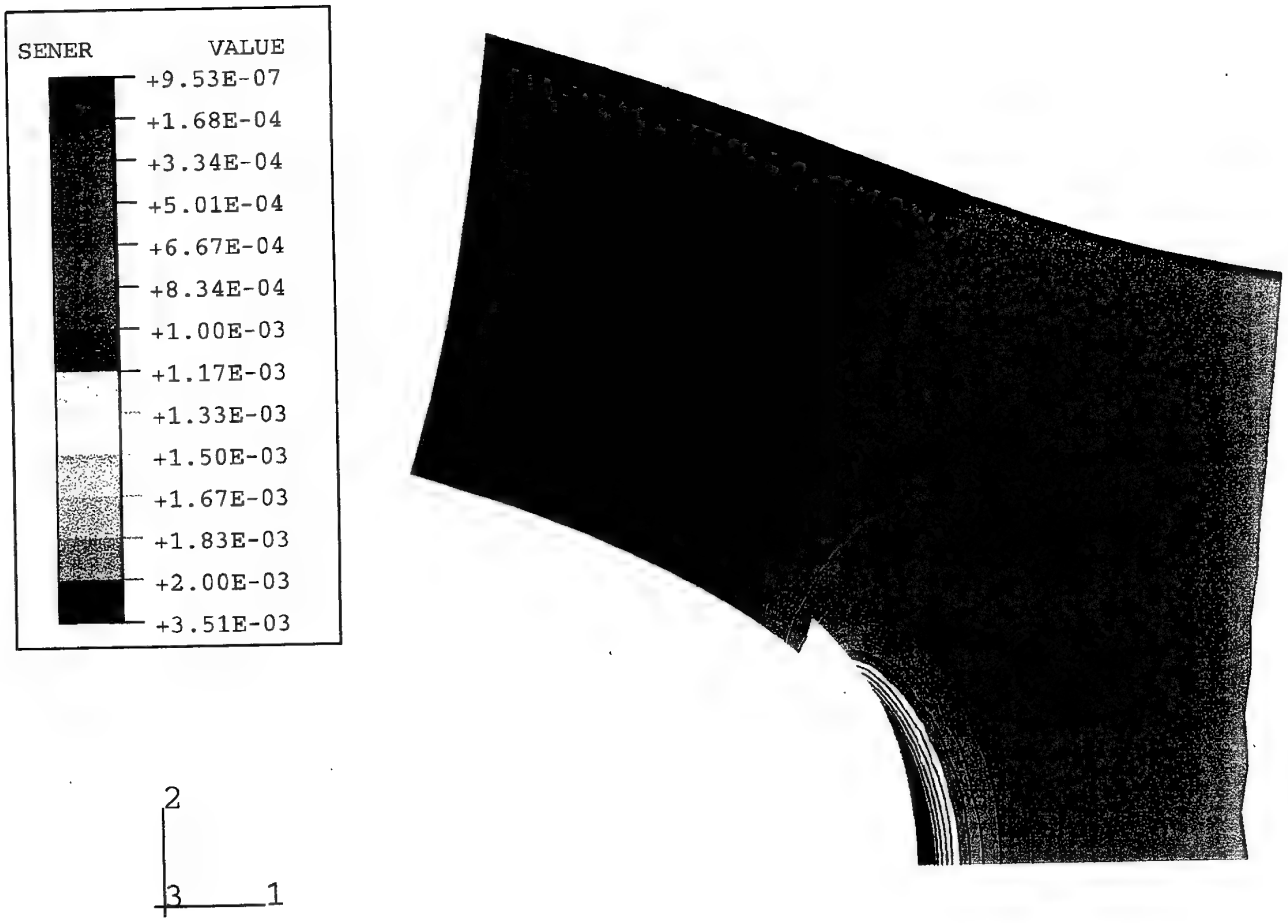

Fig. 116 Strain energy density, dW/dV, contours (in the deformed specimen configuration) for Figure 113. Values in kN.mm/mm^3. Applied displacement u_0=3.3295 mm. Case III.

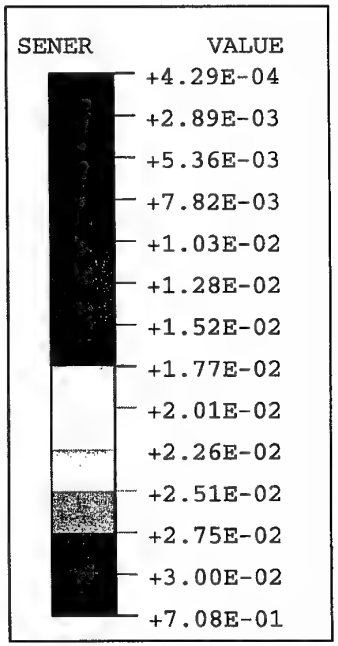

Fig. 117 Strain energy density, dW/dV, contours (in the deformed specimen configuration) for Figure 114. Values in kN.mm/mm^3. Applied displacement u_0=3.3295 mm. Case III.

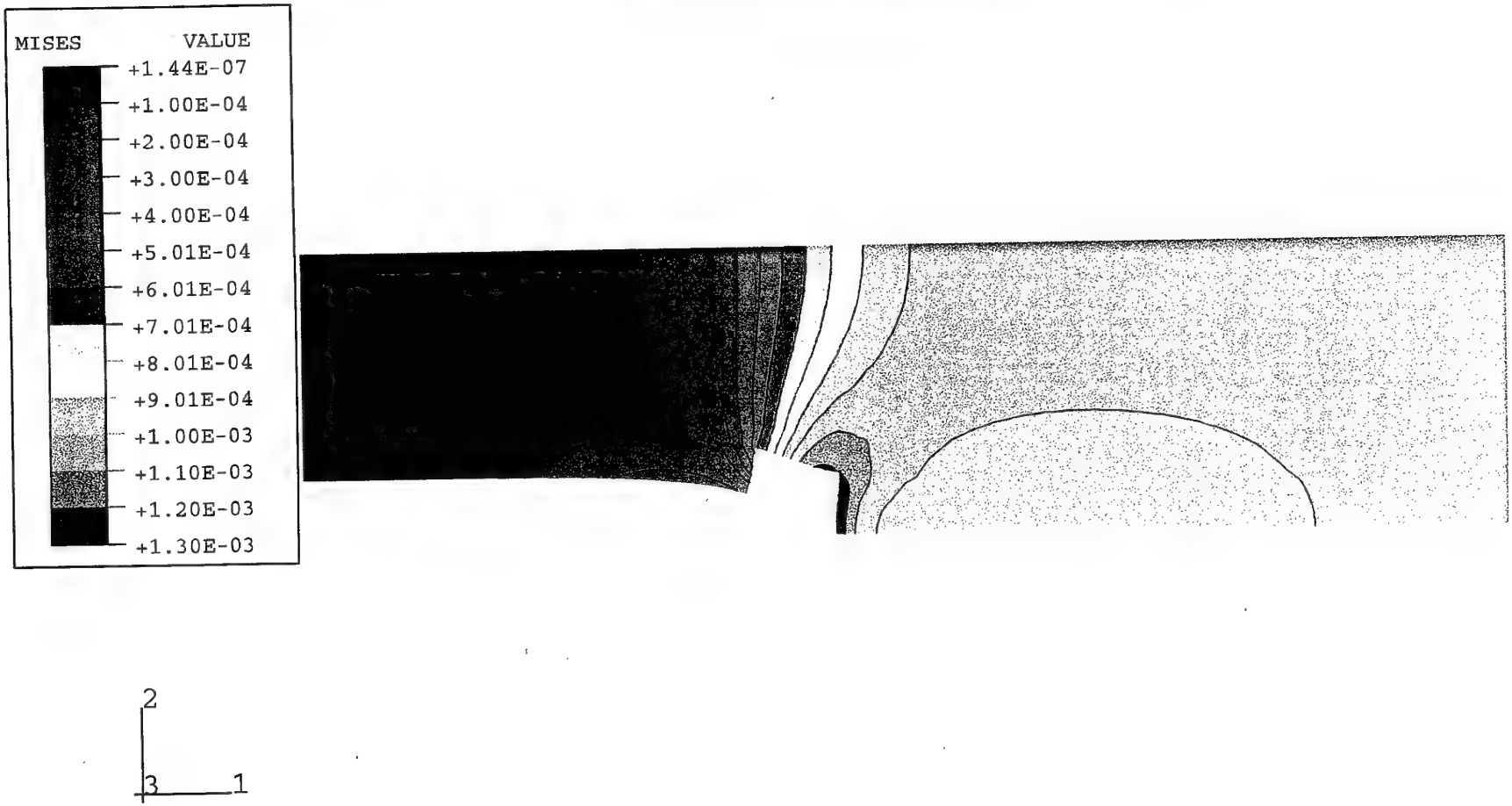

Fig. 118 Mises stress, σ_{eff}, contours (in the deformed specimen configuration) for Figure 112. Values in kN/mm^2. Applied displacement u_0=3.3295 mm. Case III.

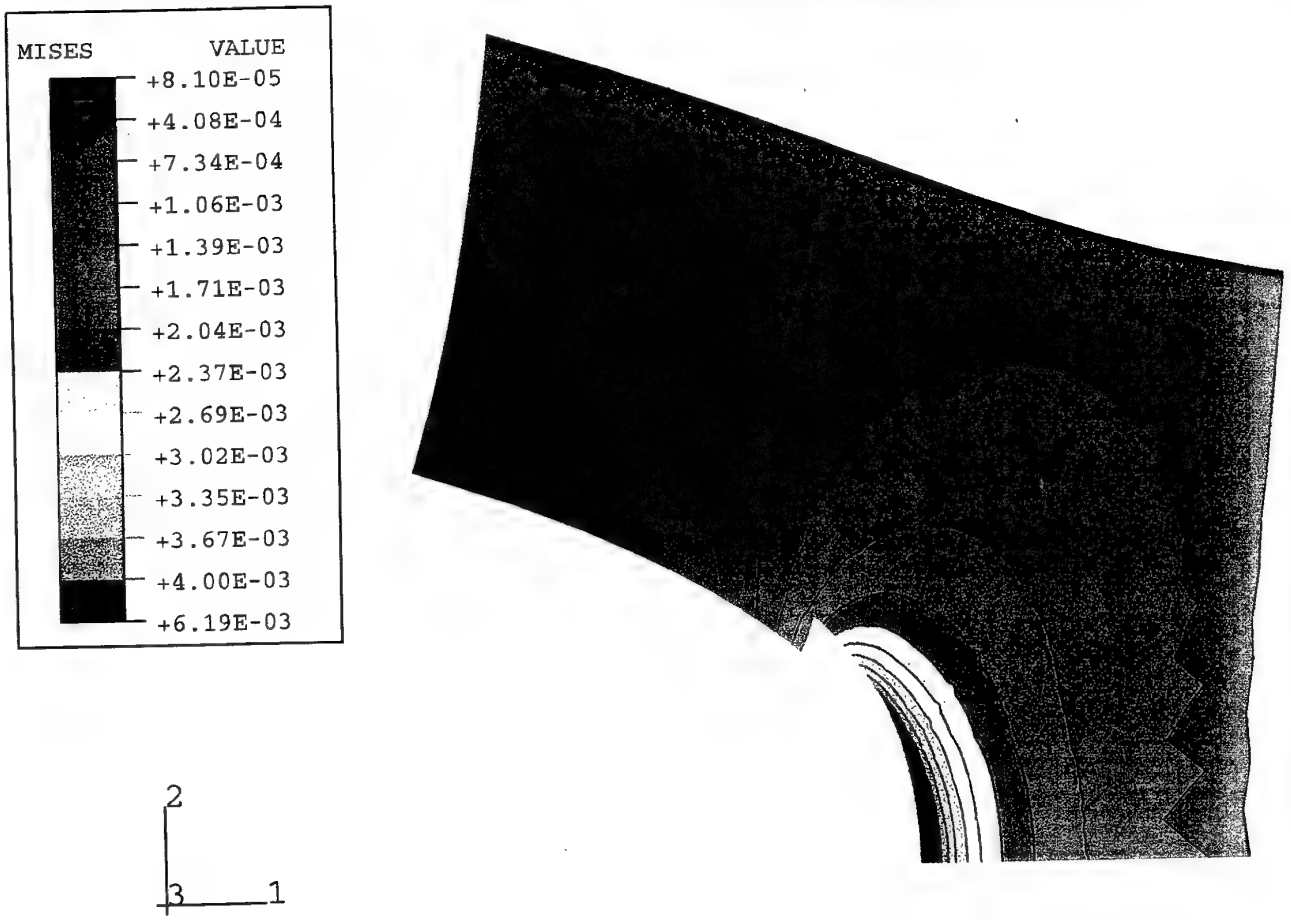

Fig. 119 Mises stress, σ_{eff}, contours (in the deformed specimen configuration) for Figure 113. Values in kN/mm^2. Applied displacement u_0=3.3295 mm. Case III.

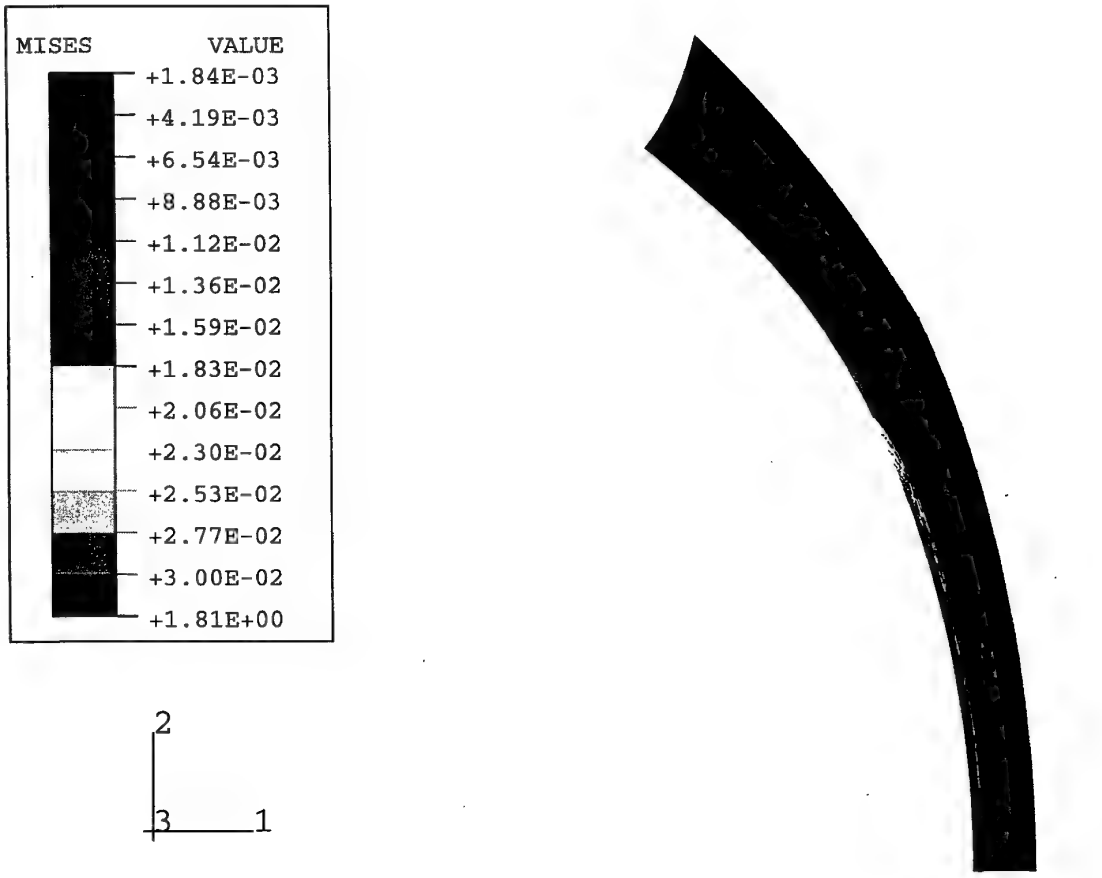

Fig. 120 Mises stress, σ_{eff}, contours (in the deformed specimen configuration) for Figure 114. Values in kN/mm^2. Applied displacement u_0=3.3295 mm. Case III.

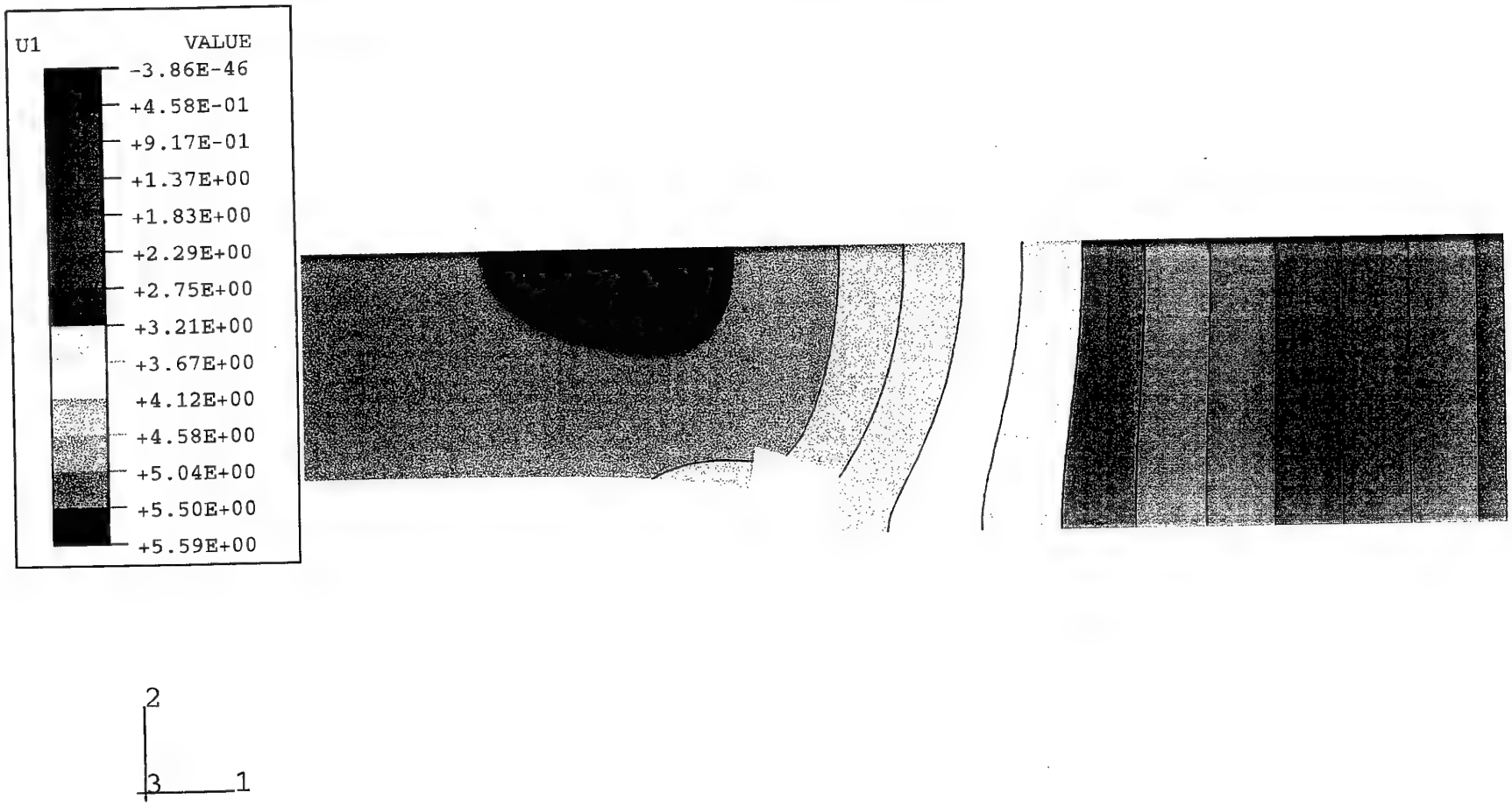

Fig. 121 Displacement along the crack axis direction, u_1, contours (in the deformed specimen configuration) for Figure 112. Values in mm. Applied displacement u_0=3.3295 mm. Case III.

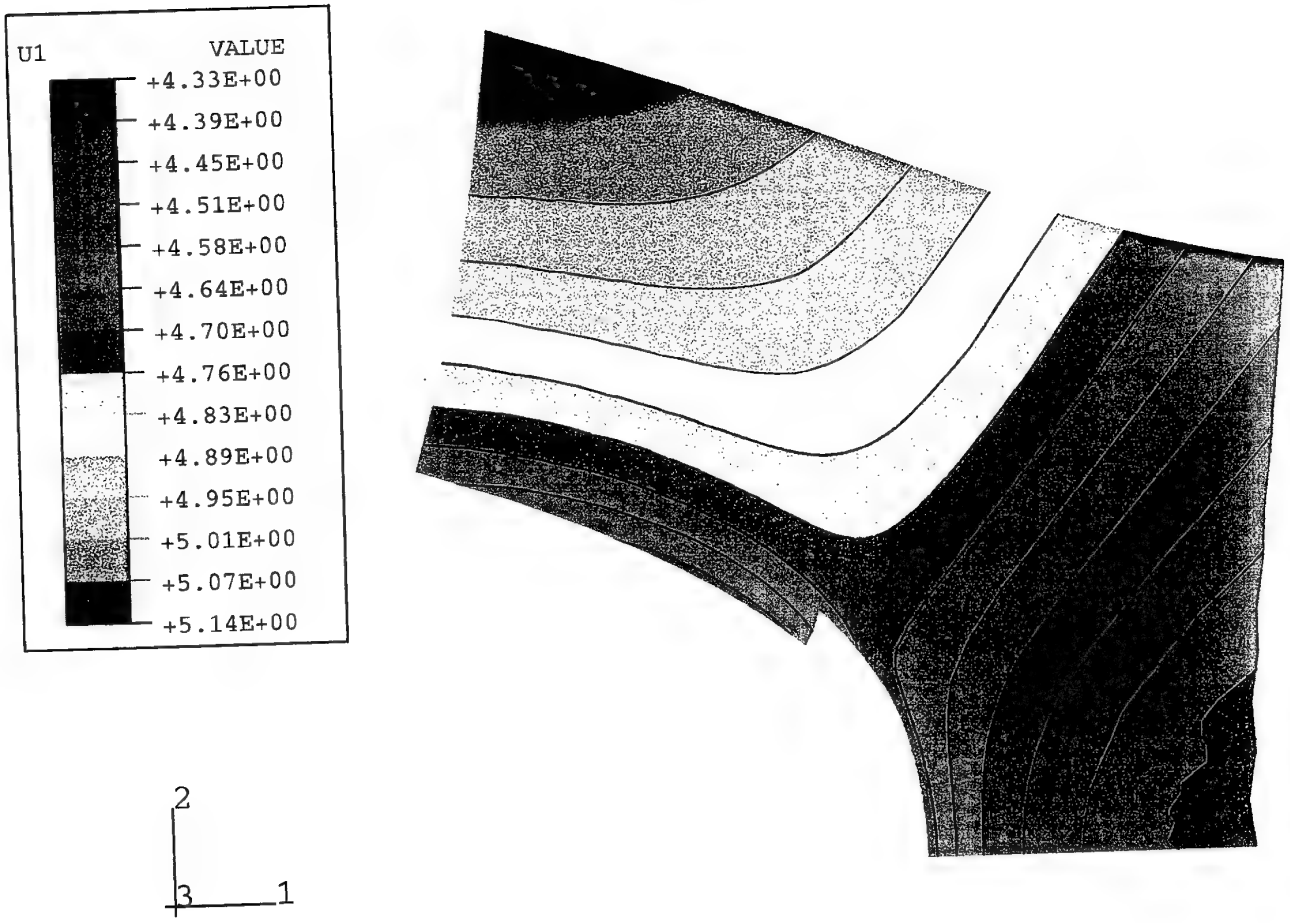

Fig. 122 Displacement along the crack axis direction, u_1, contours (in the deformed specimen configuration) for Figure 113. Values in mm. Applied displacement u_0=3.3295 mm. Case III.

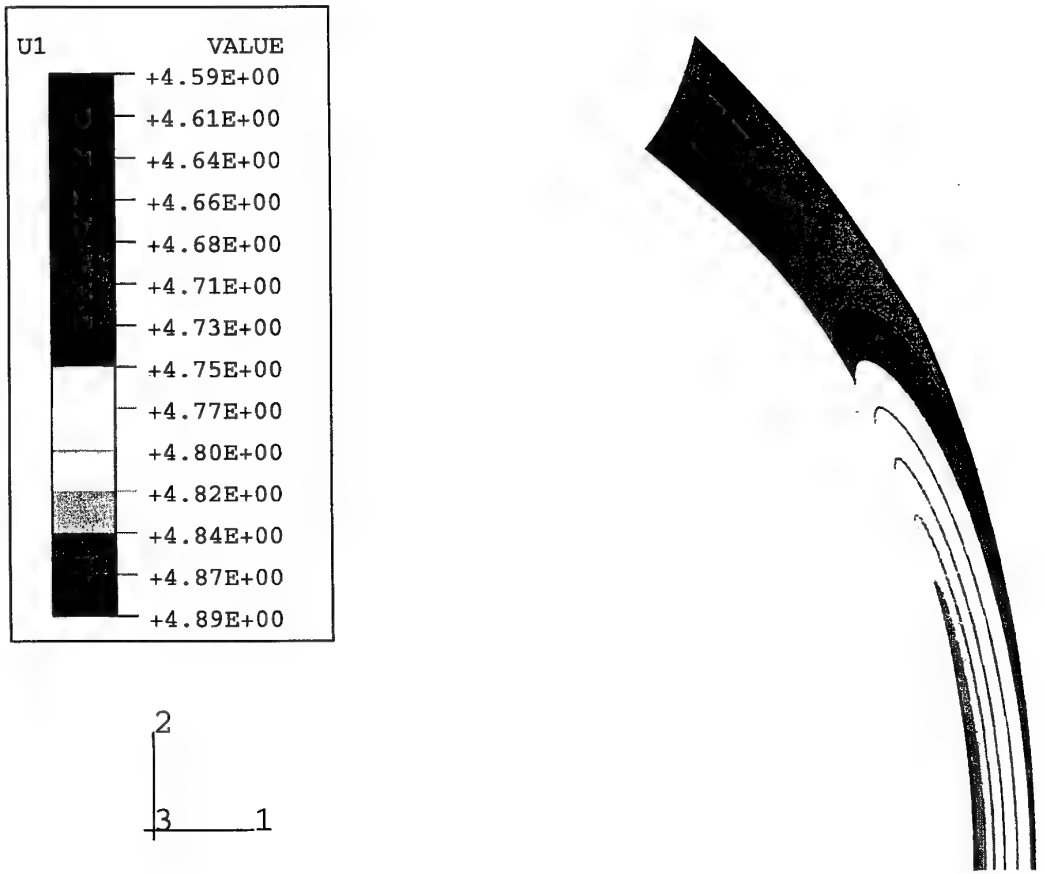

Fig. 123 Displacement along the crack axis direction, u_1, contours (in the deformed specimen configuration) for Figure 114. Values in mm. Applied displacement u_0=3.3295 mm. Case III.

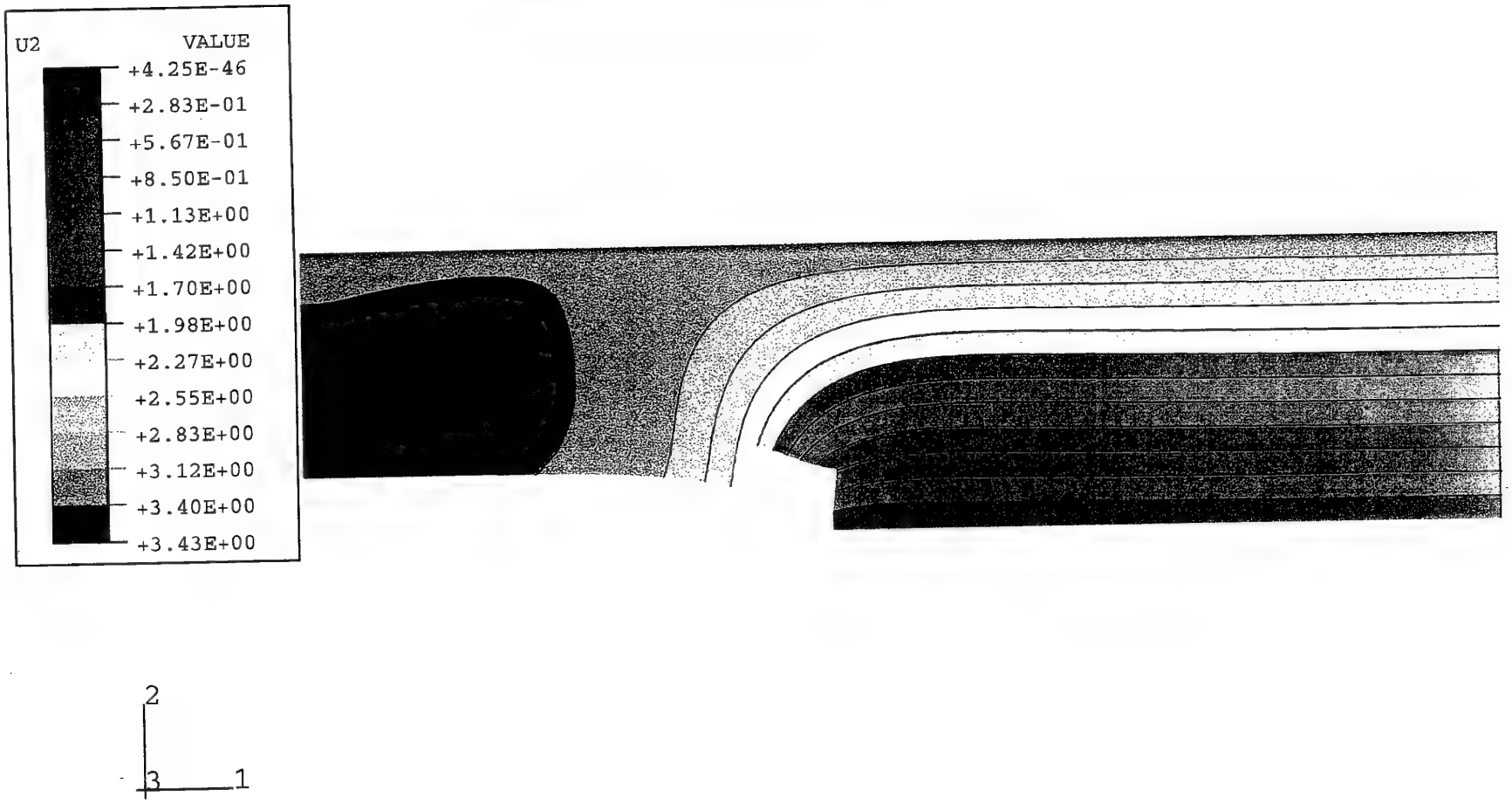

Fig. 124 Displacement along the perpendicular to the crack axis direction, u_2 contours (in the deformed specimen configuration) for Figure 112. Values in mm. Applied displacement u_0=3.3295 mm. Case III.

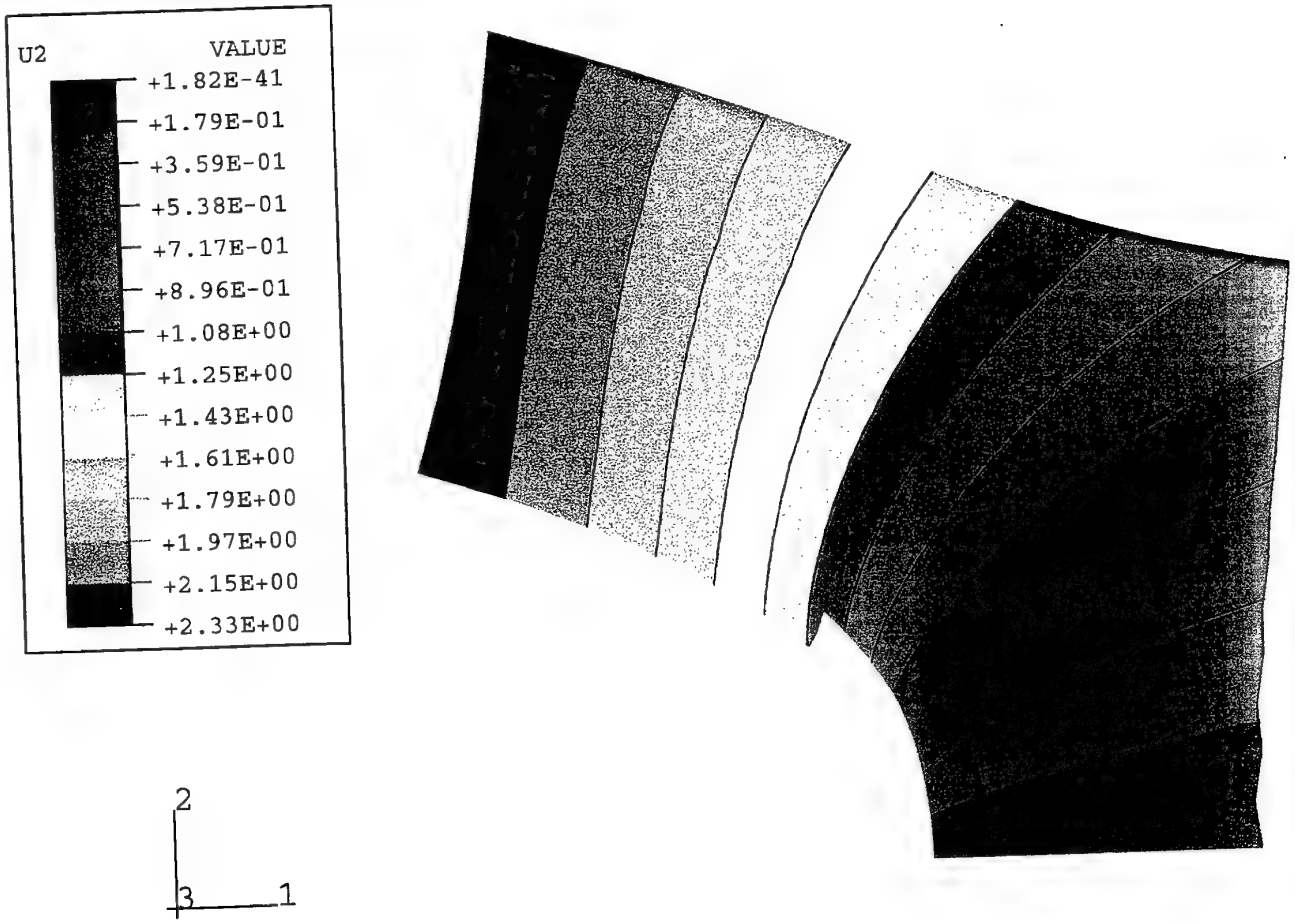

Fig. 125 Displacement along the perpendicular to the crack axis direction, u_2 contours (in the deformed specimen configuration) for Figure 113. Values in mm. Applied displacement u_0=3.3295 mm. Case III.

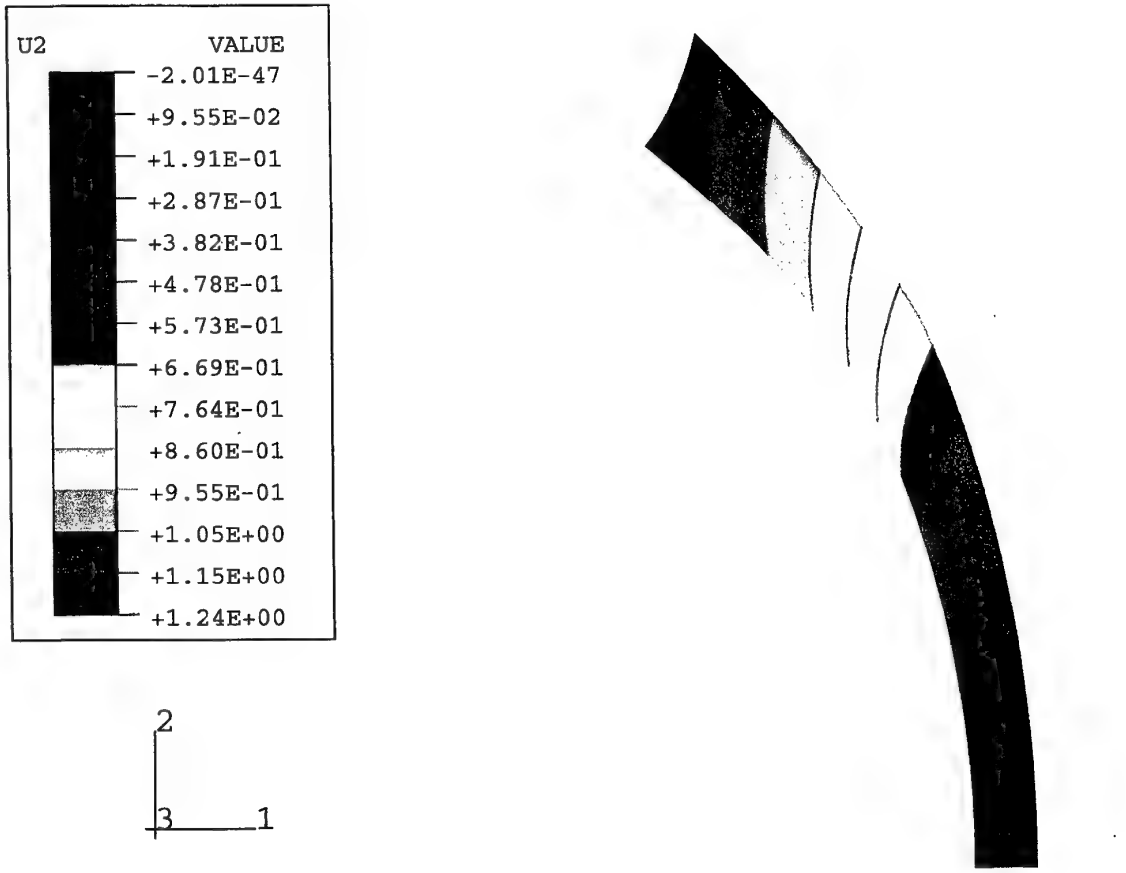

Fig. 126 Displacement along the perpendicular to the crack axis direction, u_2 contours (in the deformed specimen configuration) for Figure 114. Values in mm. Applied displacement u_0=3.3295 mm. Case III.

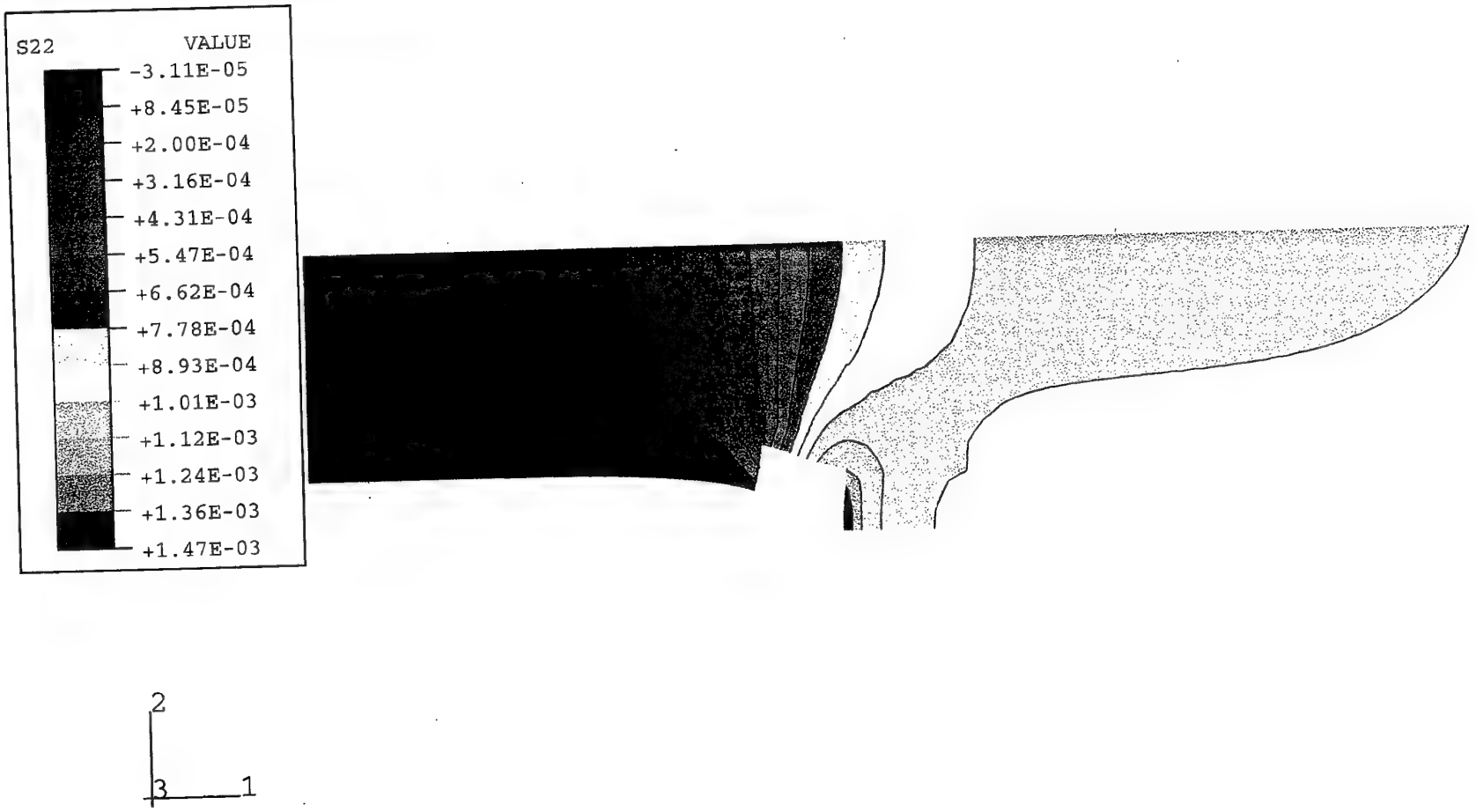

Fig. 127 Normal stress along the perpendicular to the crack axis direction, σ_{22}, contours (in the deformed specimen configuration) for Figure 112. Values in kN/mm^2. Applied displacement u_0=3.3295 mm. Case III.

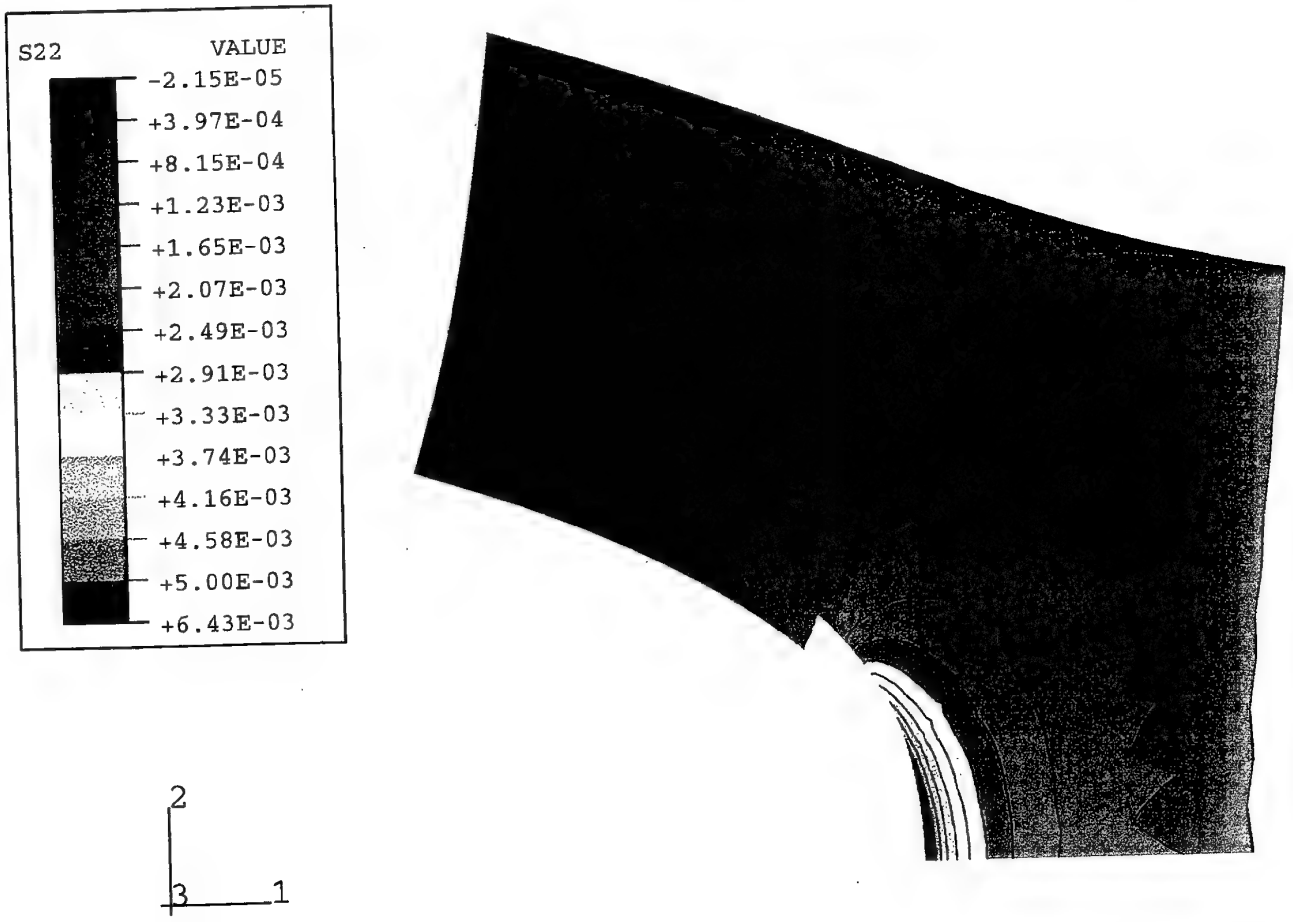

Fig. 128 Normal stress along the perpendicular to the crack axis direction, σ_{22}, contours (in the deformed specimen configuration) for Figure 113. Values in kN/mm^2. Applied displacement u_0=3.3295 mm. Case III.

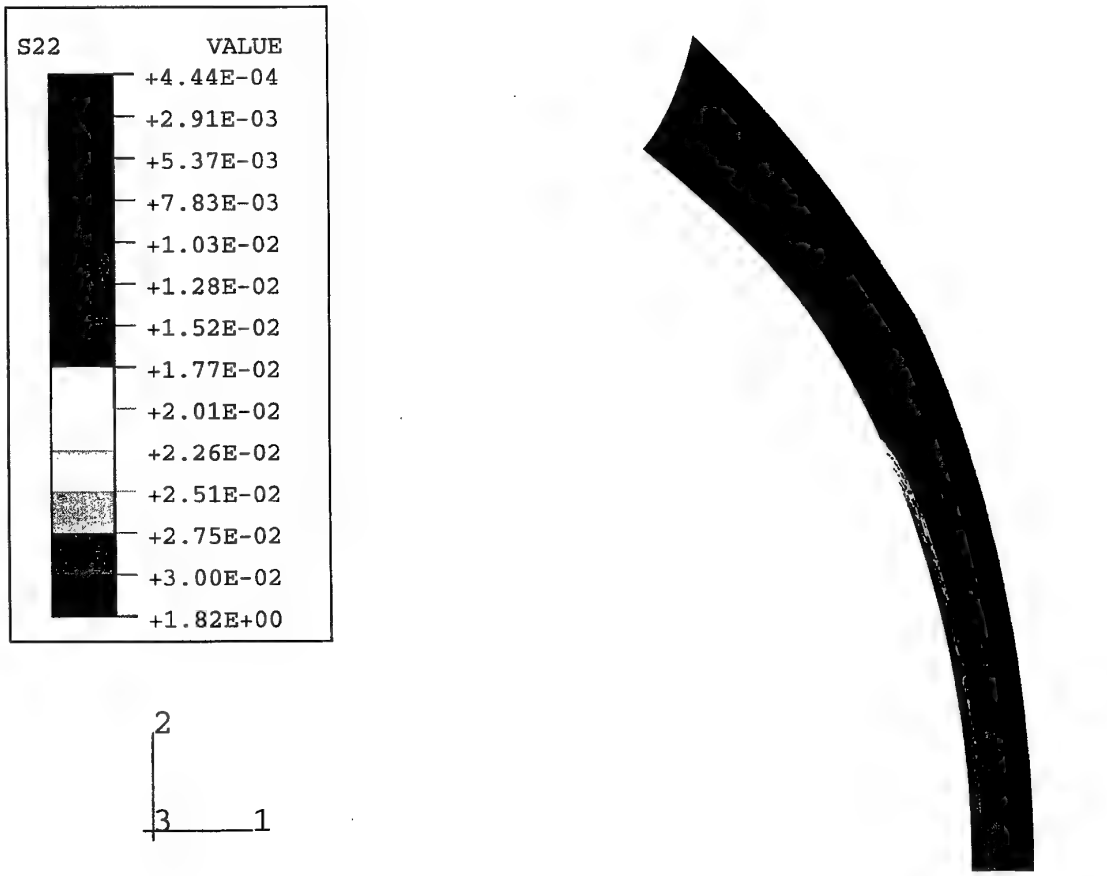

Fig. 129 Normal stress along the perpendicular to the crack axis direction, σ_{22}, contours (in the deformed specimen configuration) for Figure 114. Values in kN/mm^2. Applied displacement u_0=3.3295 mm. Case III.

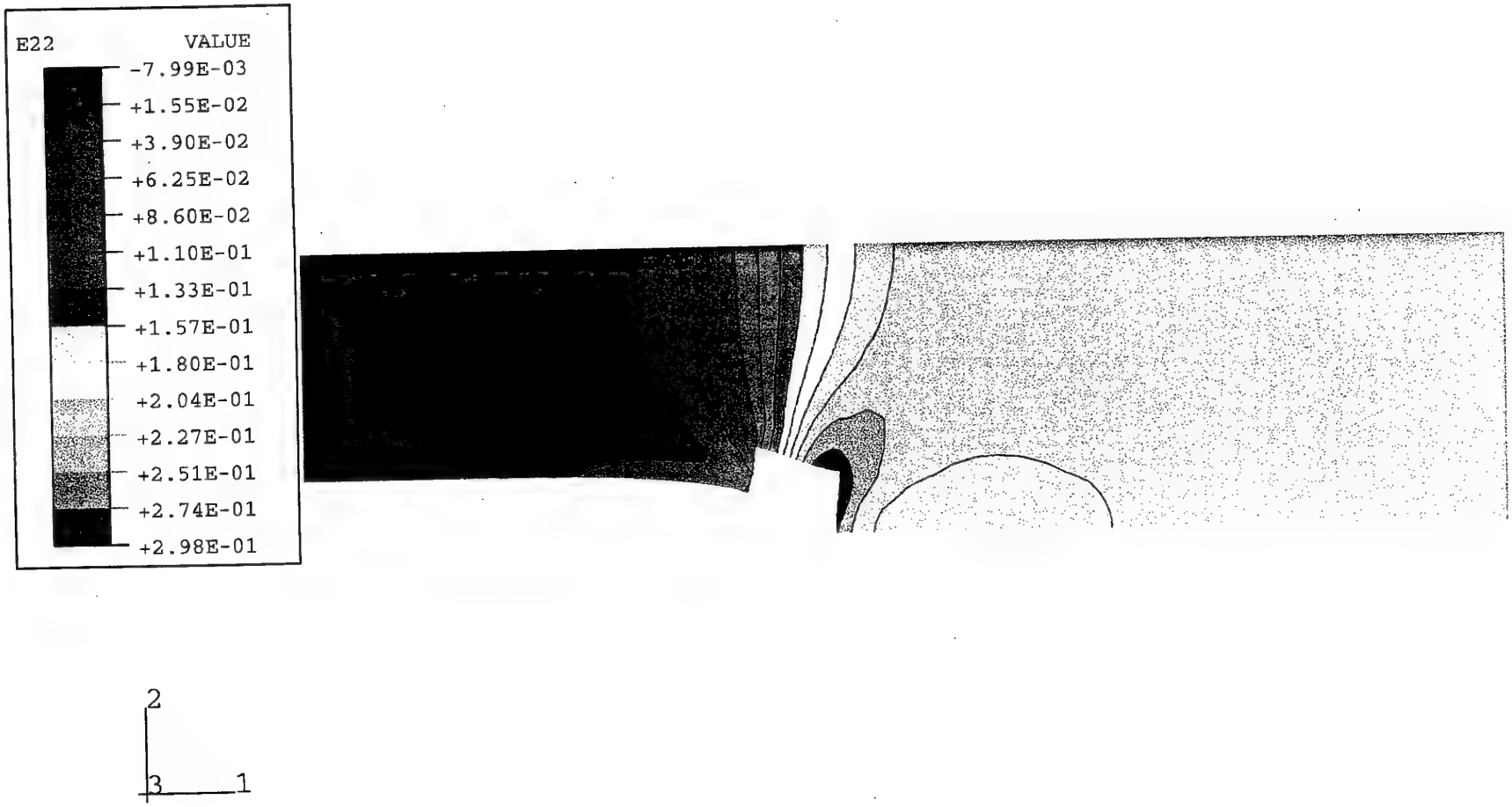

Fig. 130 Normal strain along the perpendicular to the crack axis direction, ε_{22}, contours (in the deformed specimen configuration) for Figure 112. Applied displacement u_0=3.3295 mm. Case III.

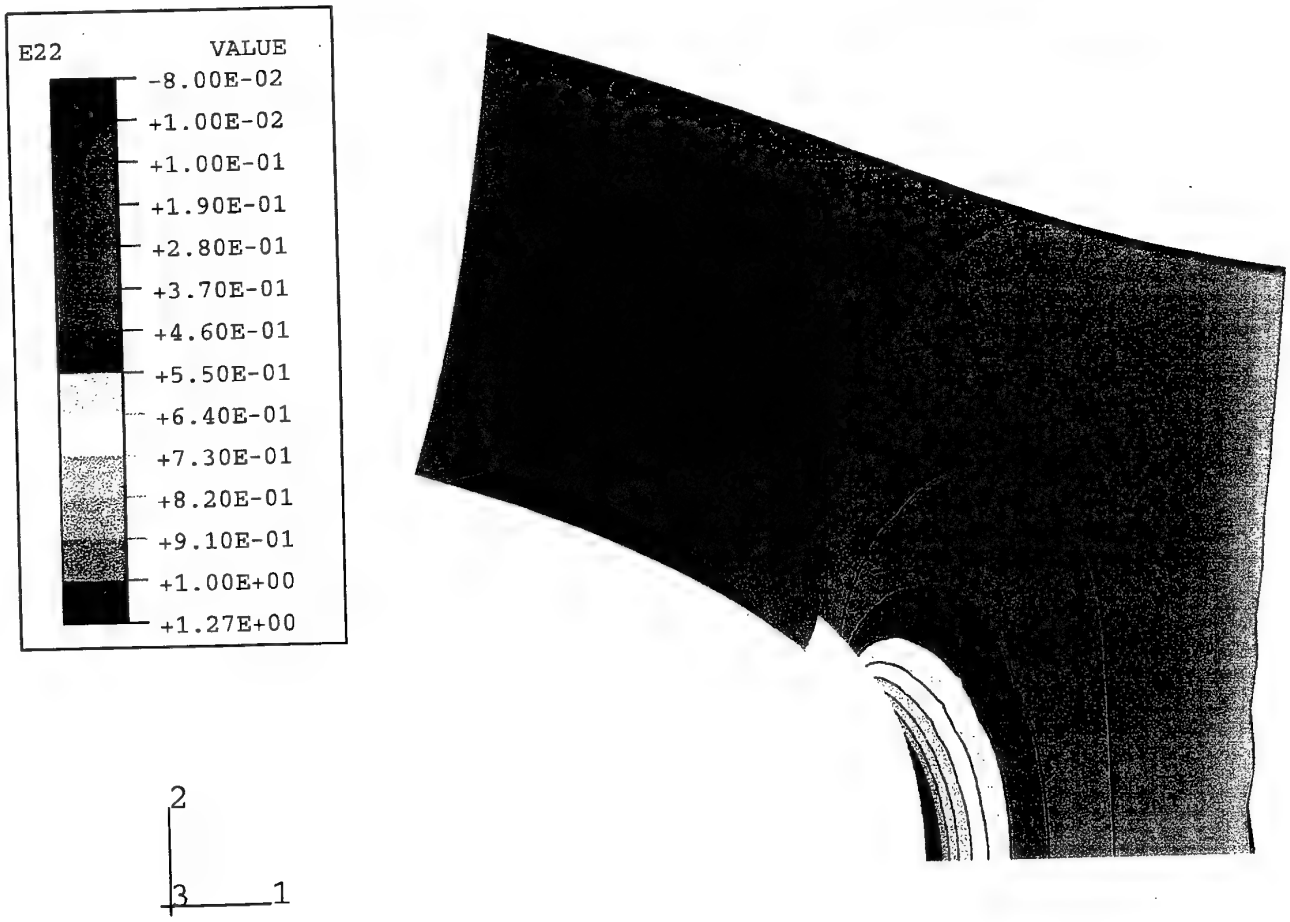

Fig. 131 Normal strain along the perpendicular to the crack axis direction, ε_{22}, contours (in the deformed specimen configuration) for Figure 113. Applied displacement u_0=3.3295 mm. Case III.

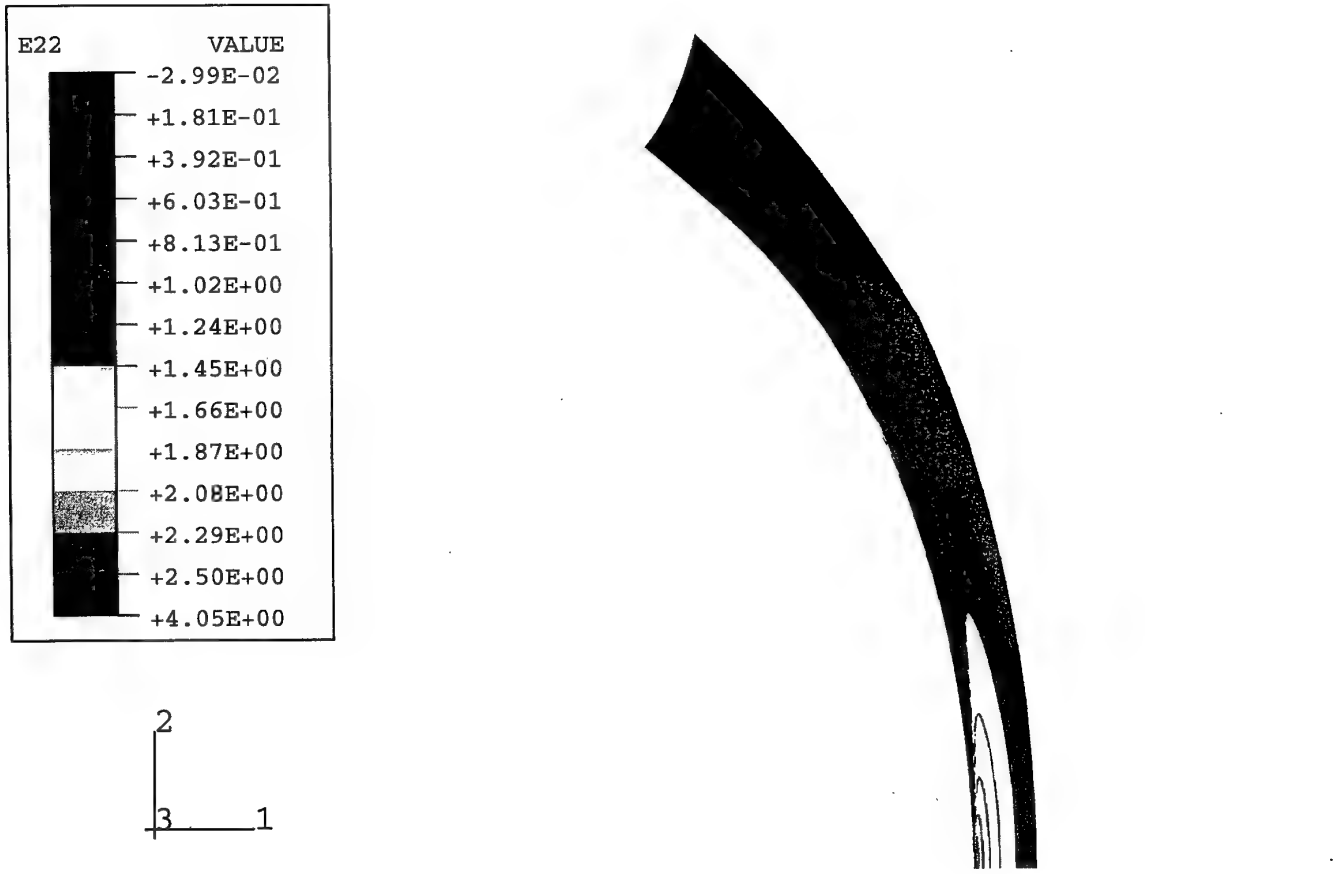

Fig. 132 Normal strain along the perpendicular to the crack axis direction, ε_{22}, contours (in the deformed specimen configuration) for Figure 114. Applied displacement u_0=3.3295 mm. Case III.

Case IV

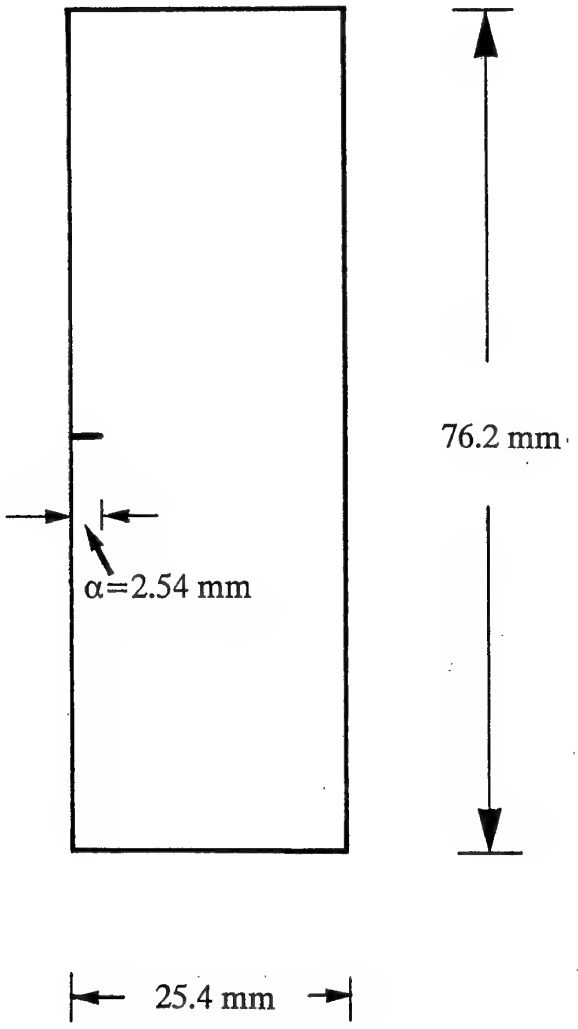

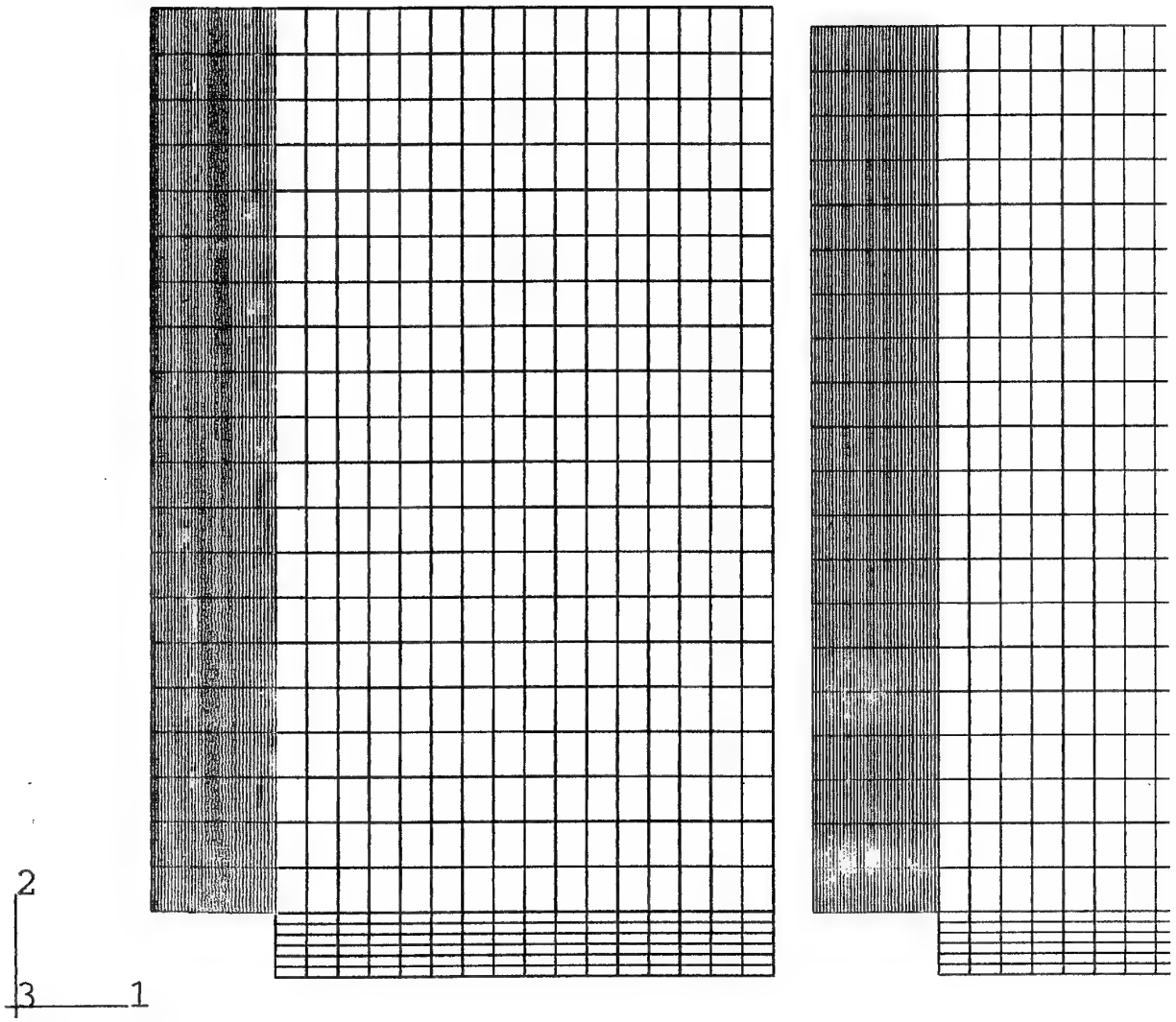

Fig. 133 Undeformed (in red) and deformed (in black) finite element grids for half specimen. Applied displacement u_0=0.7623 mm. Case IV.

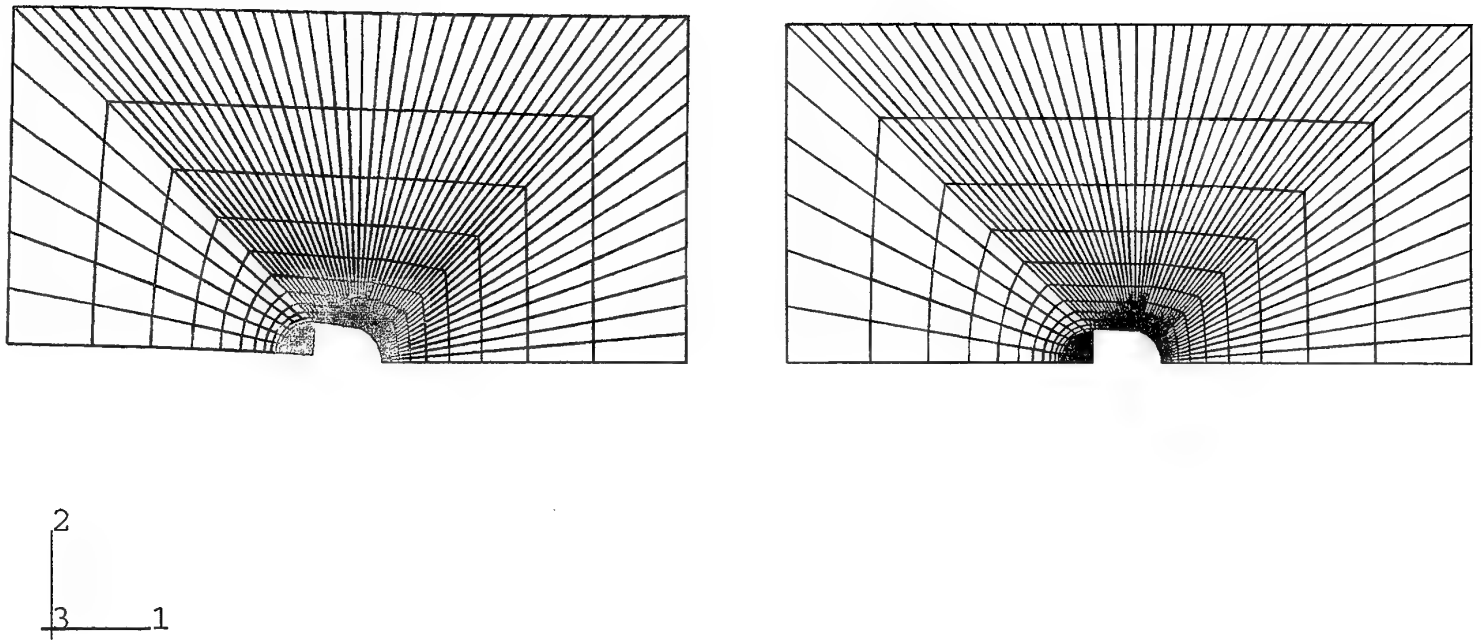

Fig. 134 Undeformed (in red) and deformed (in black) finite element grids for the missing part of Figure 133. Applied displacement u_0=0.7623 mm. Case IV.

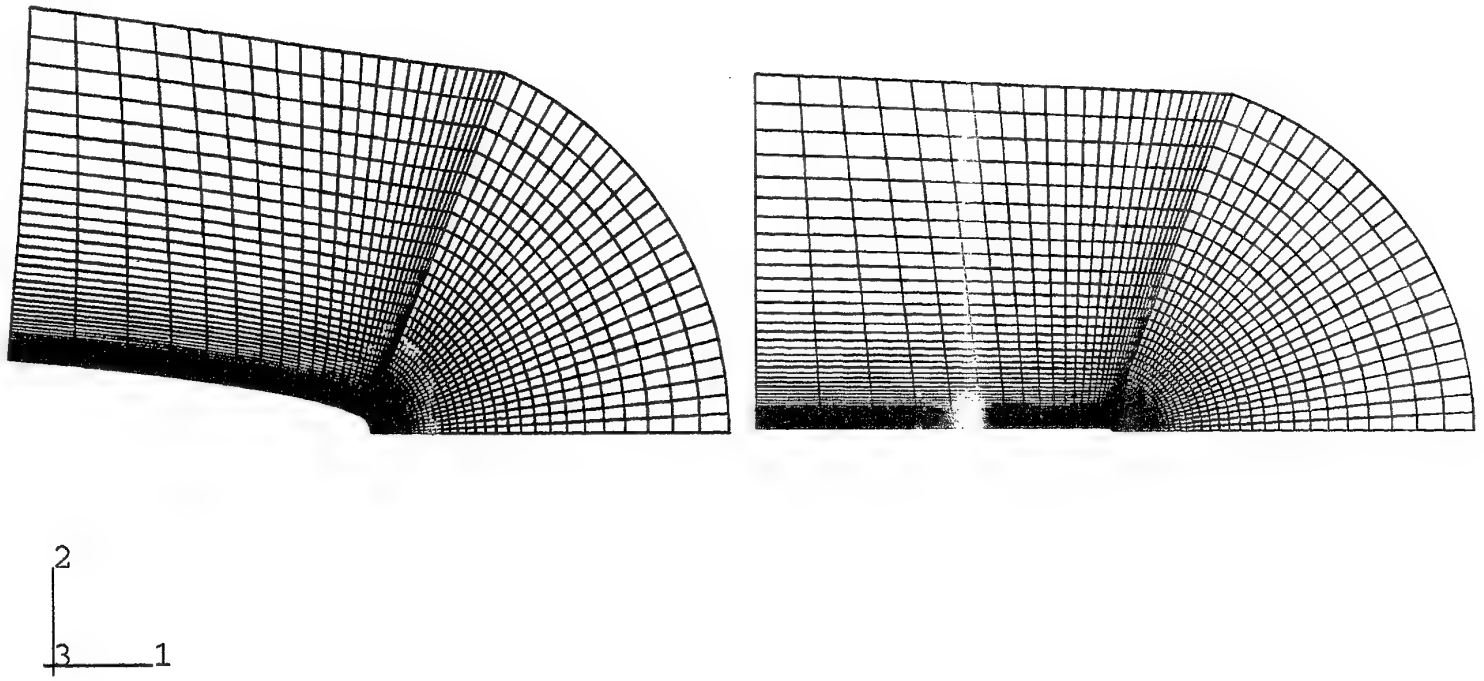

Fig. 135 Undeformed (in red) and deformed (in black) finite element grids for the missing part of Figure 134. Applied displacement u_0=0.7623 mm. Case IV.

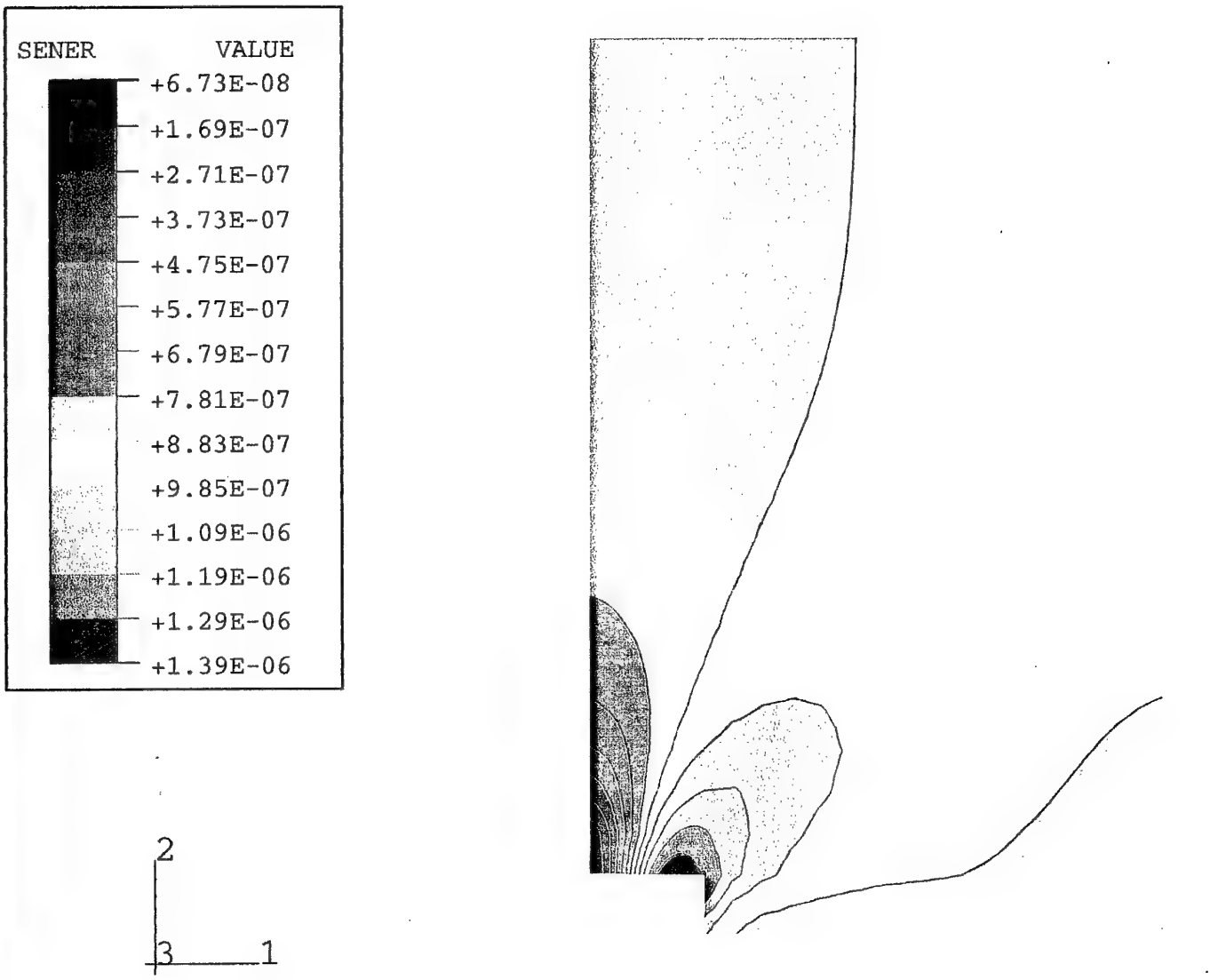

Fig. 136 Strain energy density, dW/dV, contours (in the deformed specimen configuration) for Figure 133. Values in kN.mm/mm^3. Applied displacement u_0=0.7623 mm. Case IV.

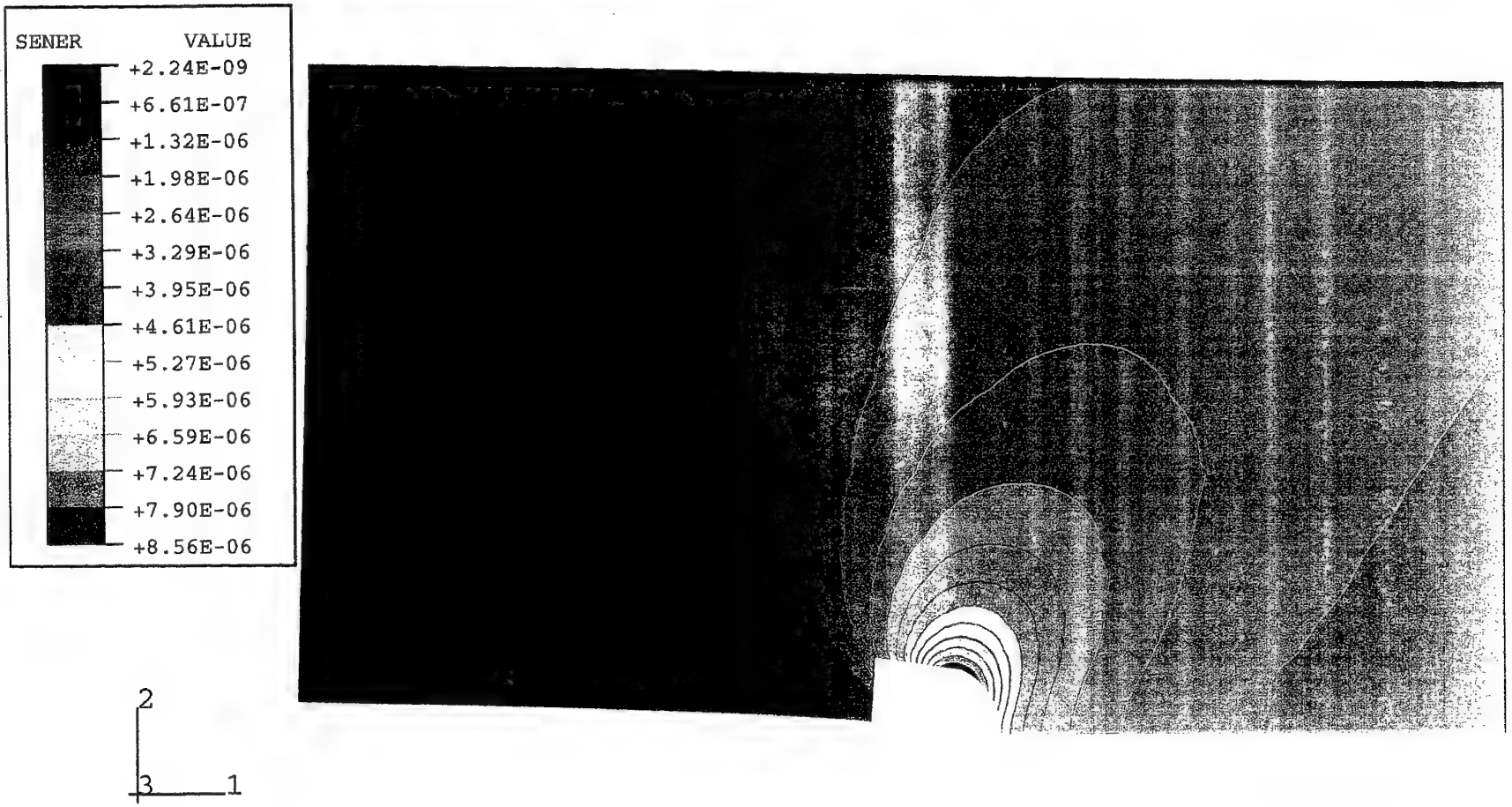

Fig. 137 Strain energy density, dW/dV, contours (in the deformed specimen configuration) for Figure 134. Values in kN.mm/mm^3. Applied displacement u_0=0.7623 mm. Case IV.

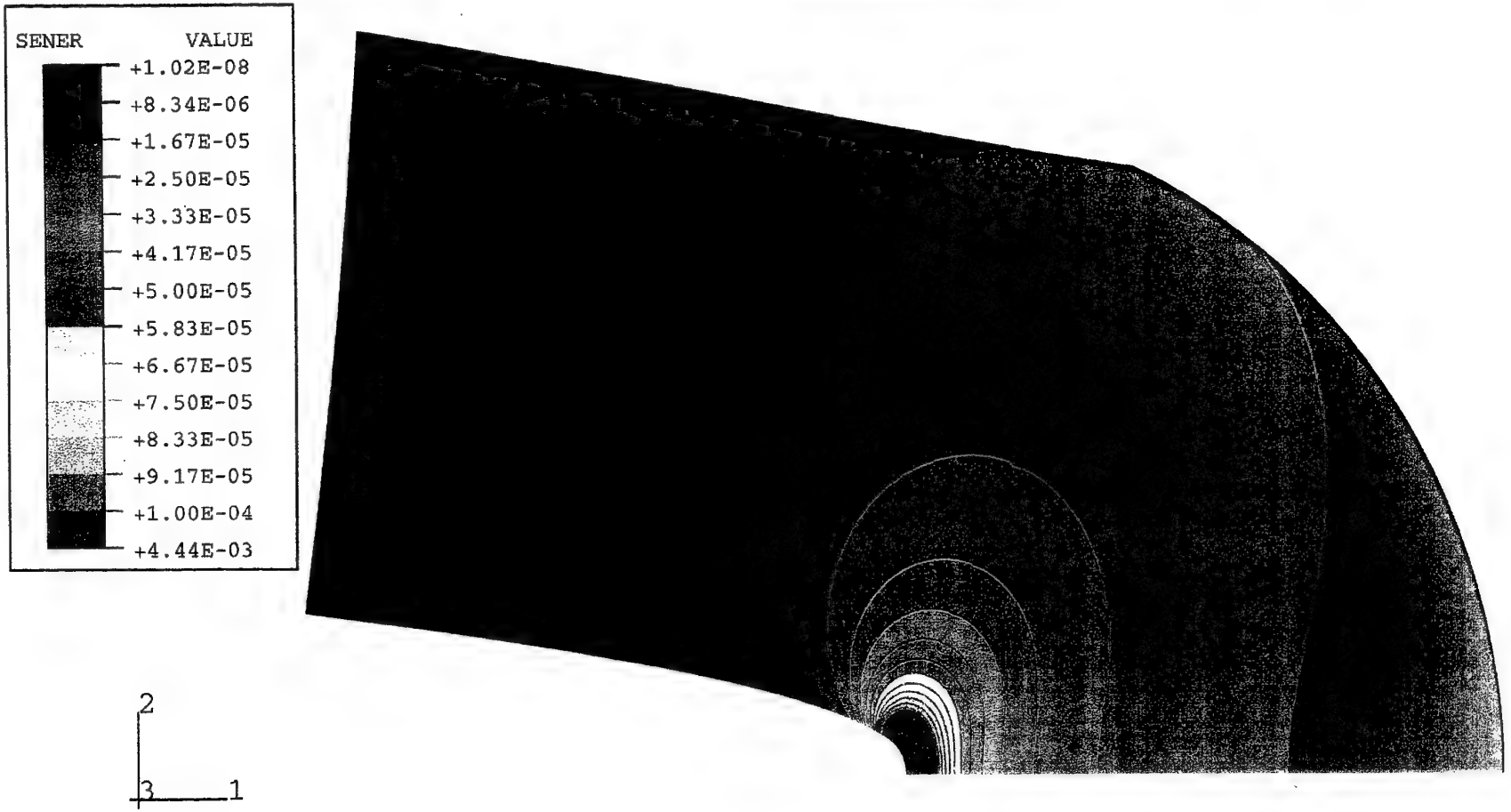

Fig. 138 Strain energy density, dW/dV, contours (in the deformed specimen configuration) for Figure 135. Values in kN.mm/mm^3. Applied displacement u_0=0.7623 mm. Case IV.

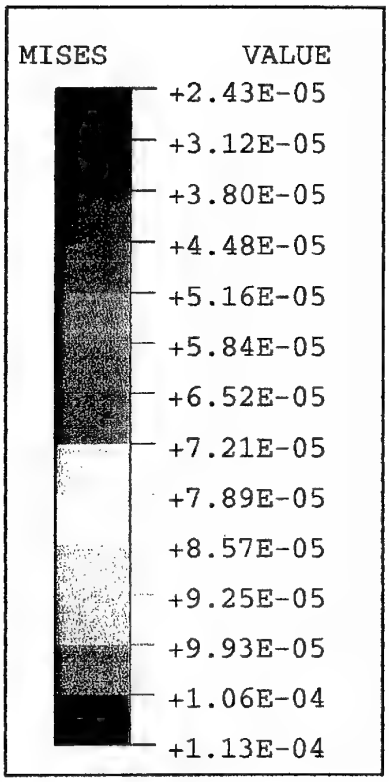

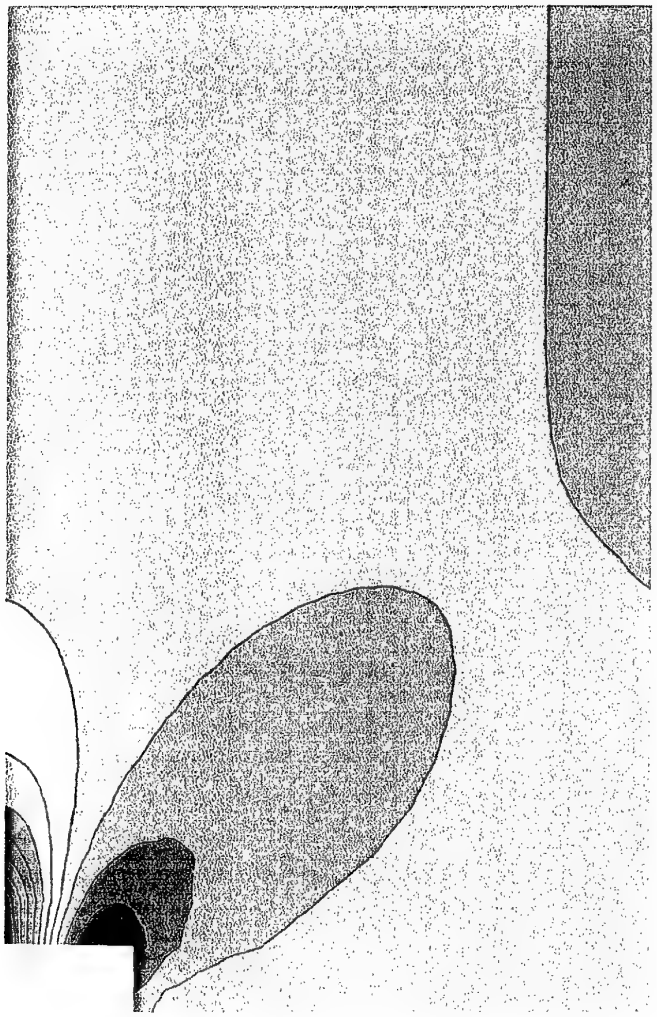

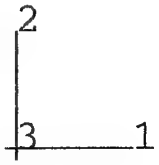

Fig. 139 Mises stress, σ_{eff}, contours (in the deformed specimen configuration) for Figure 133. Values in kN/mm^2. Applied displacement u_0=0.7623 mm. Case IV.

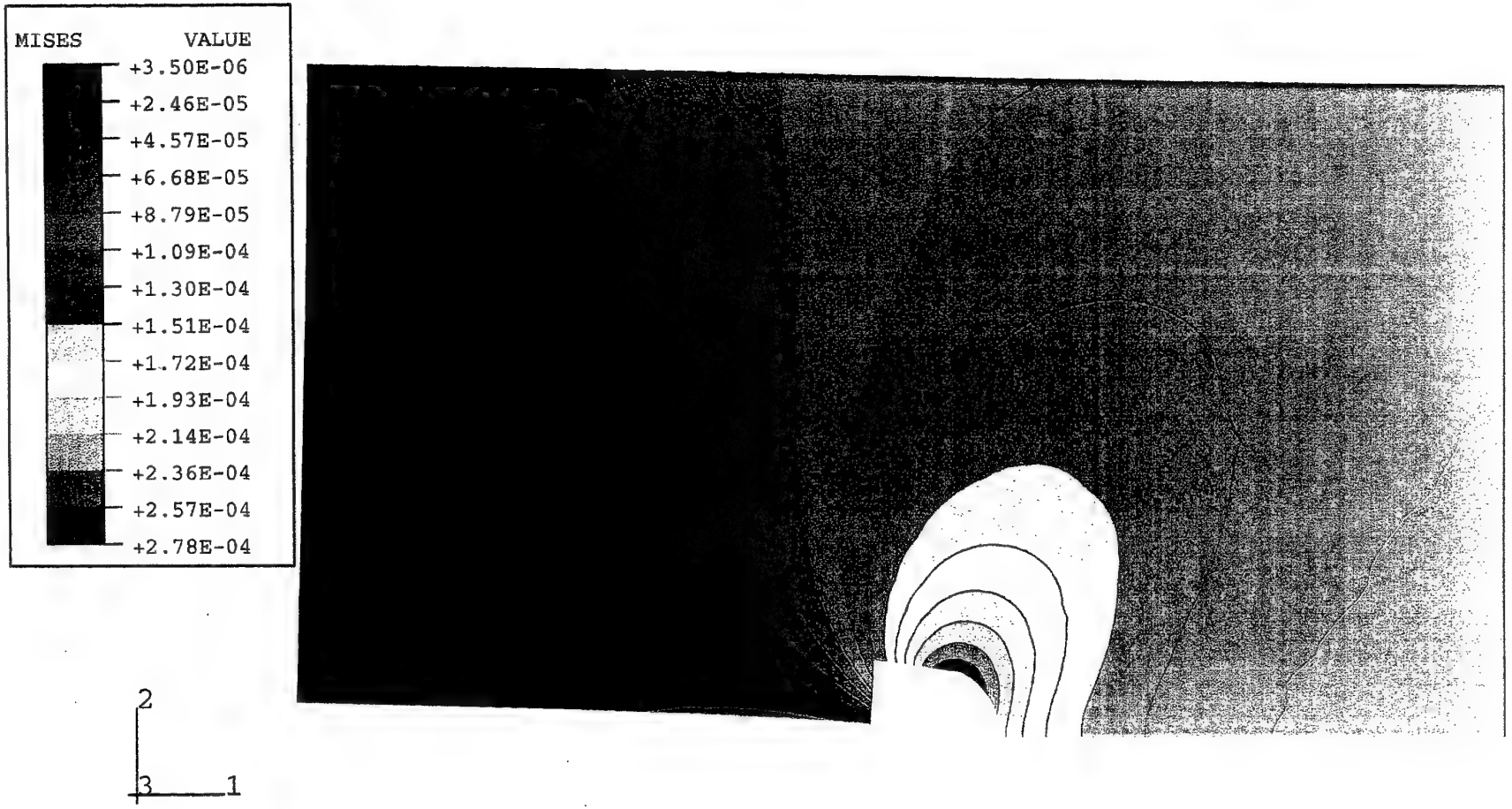

Fig. 140 Mises stress, σ_{eff}, contours (in the deformed specimen configuration) for Figure 134. Values in kN/mm^2. Applied displacement u_0=0.7623 mm. Case IV.

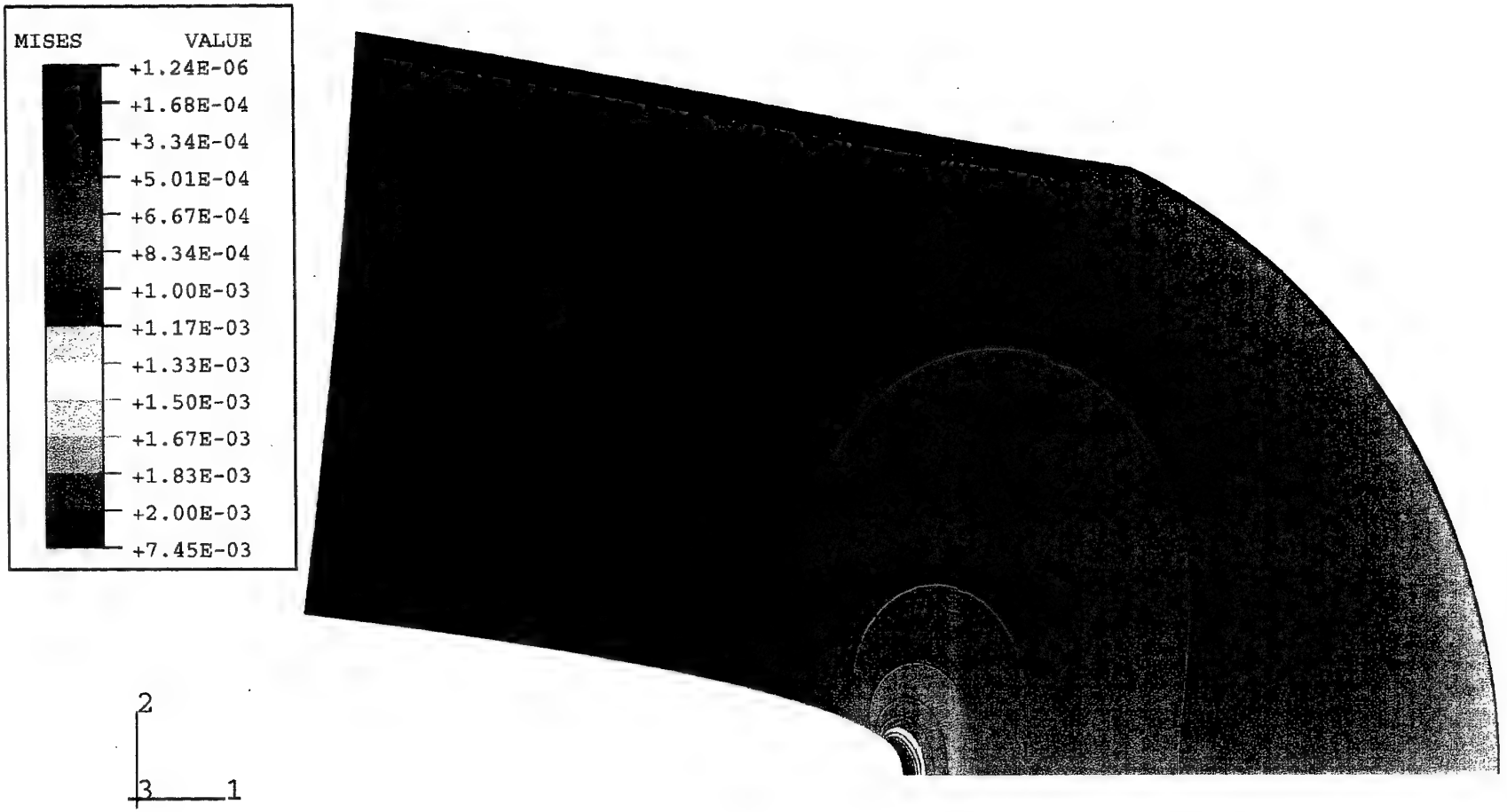

Fig. 141 Mises stress, σ_{eff}, contours (in the deformed specimen configuration) for Figure 135. Values in kN/mm^2. Applied displacement u_0=0.7623 mm. Case IV.

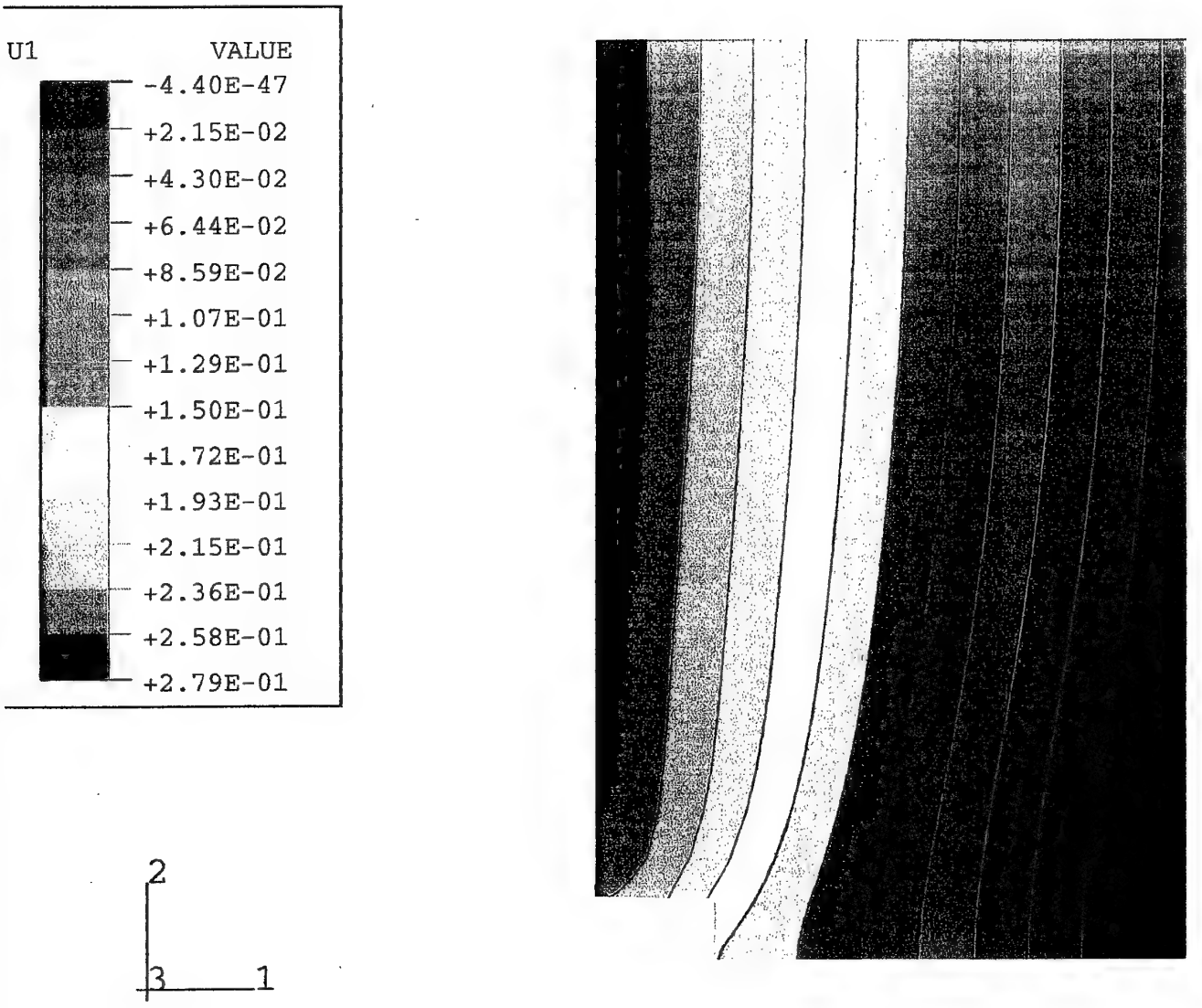

Fig. 142 Displacement along the crack axis direction, u_1, contours (in the deformed specimen configuration) for Figure 133. Values in mm. Applied displacement u_0=0.7623 mm. Case IV.

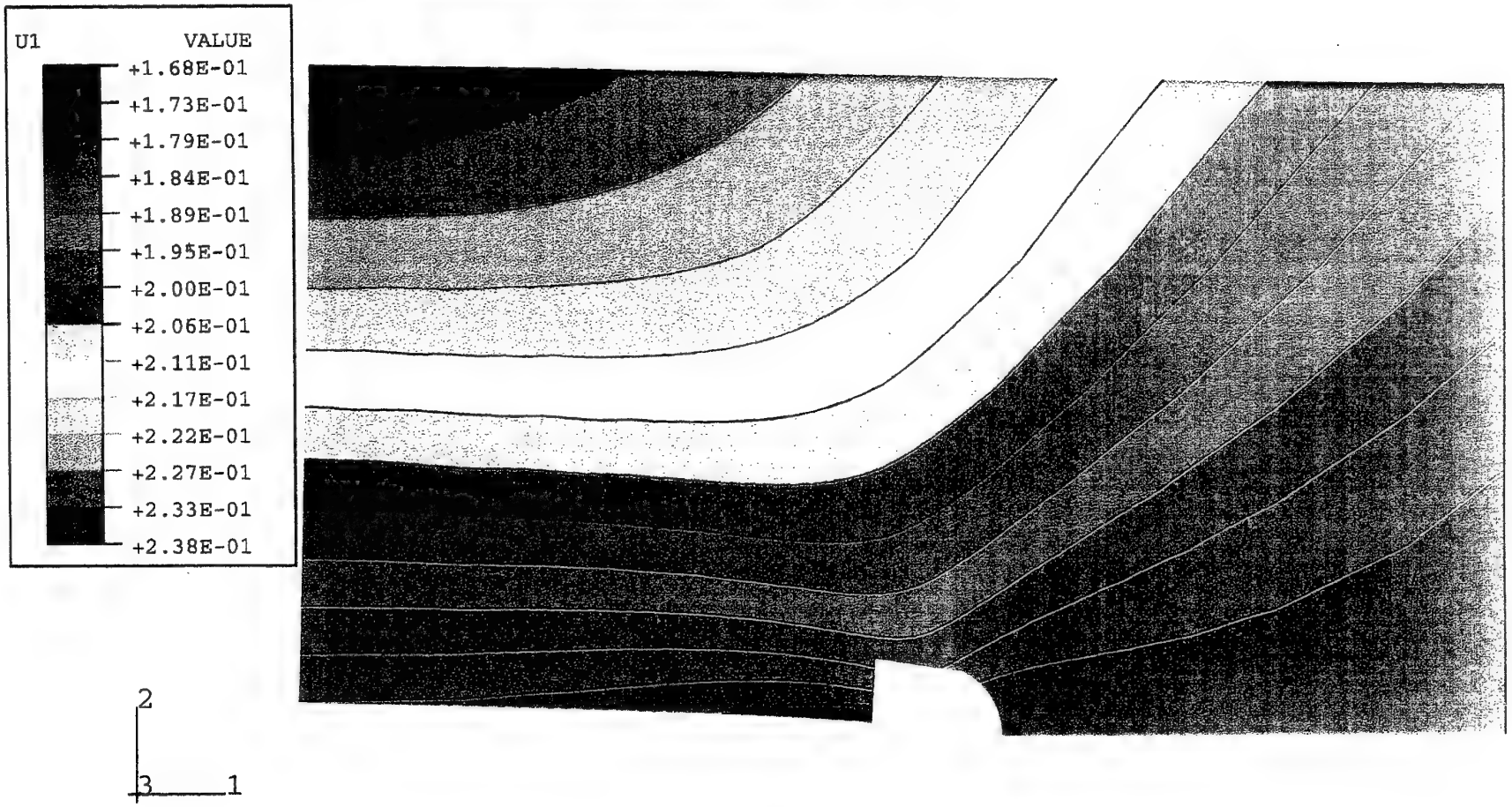

Fig. 143 Displacement along the crack axis direction, u_1, contours (in the deformed specimen configuration) for Figure 134. Values in mm. Applied displacement u_0=0.7623 mm. Case IV.

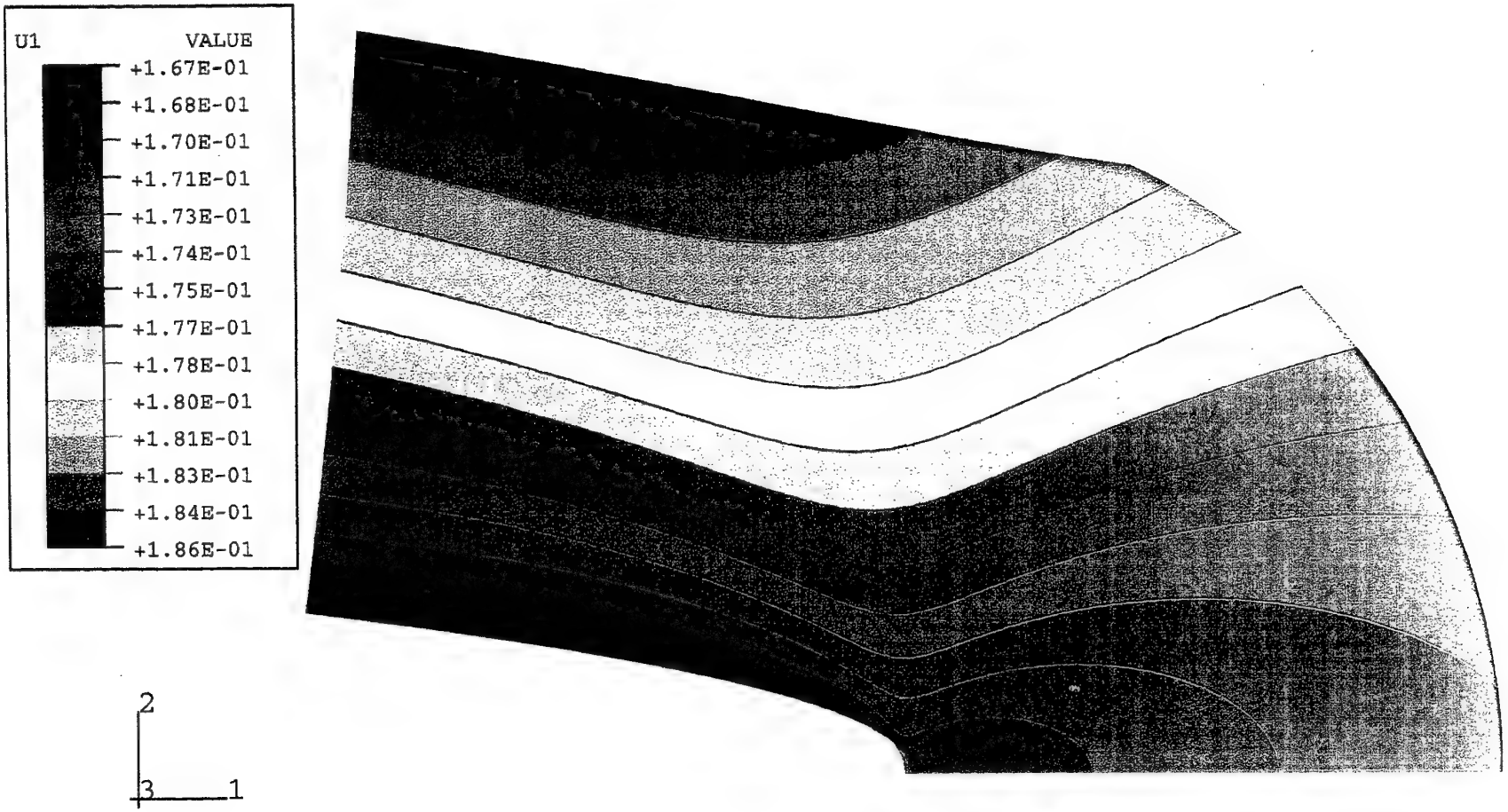

Fig. 144 Displacement along the crack axis direction, u_1, contours (in the deformed specimen configuration) for Figure 135. Values in mm. Applied displacement u_0=0.7623 mm. Case IV.

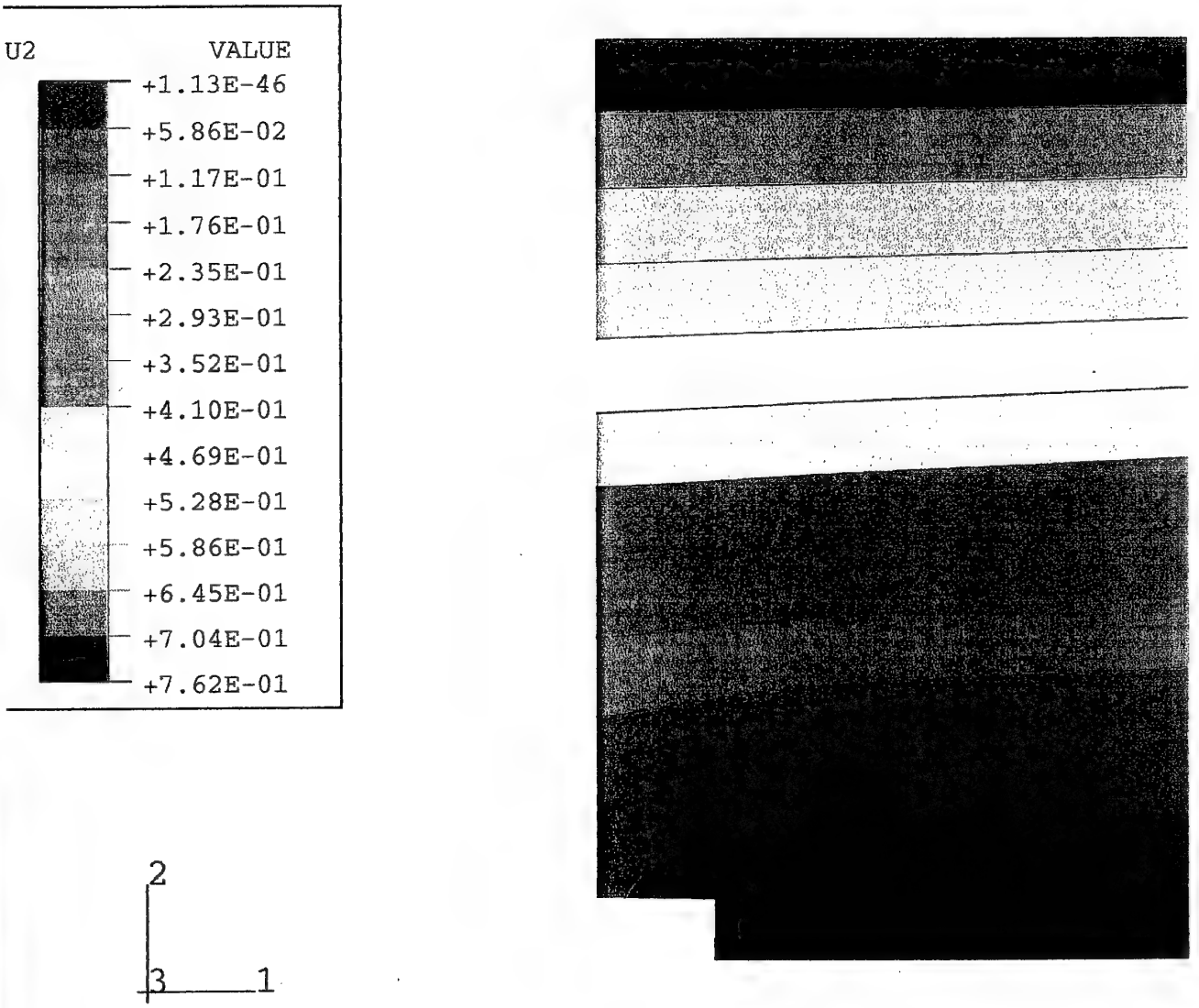

Fig. 145 Displacement along the perpendicular to the crack axis direction, u_2, contours (in the deformed specimen configuration) for Figure 133. Values in mm. Applied displacement u_0=0.7623 mm. Case IV.

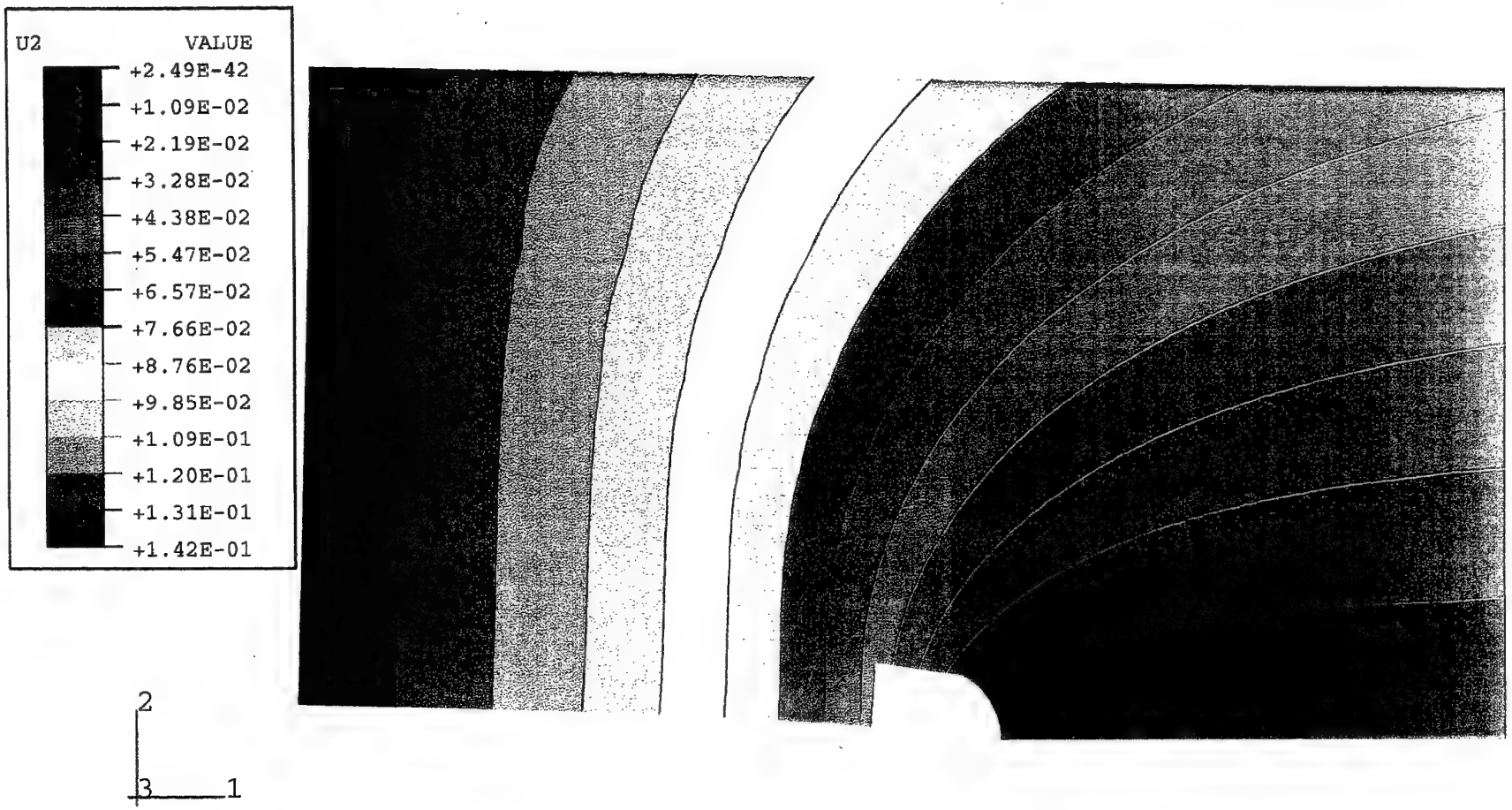

Fig. 146 Displacement along the perpendicular to the crack axis direction, u_2, contours (in the deformed specimen configuration) for Figure 134. Values in mm. Applied displacement u_0=0.7623 mm. Case IV.

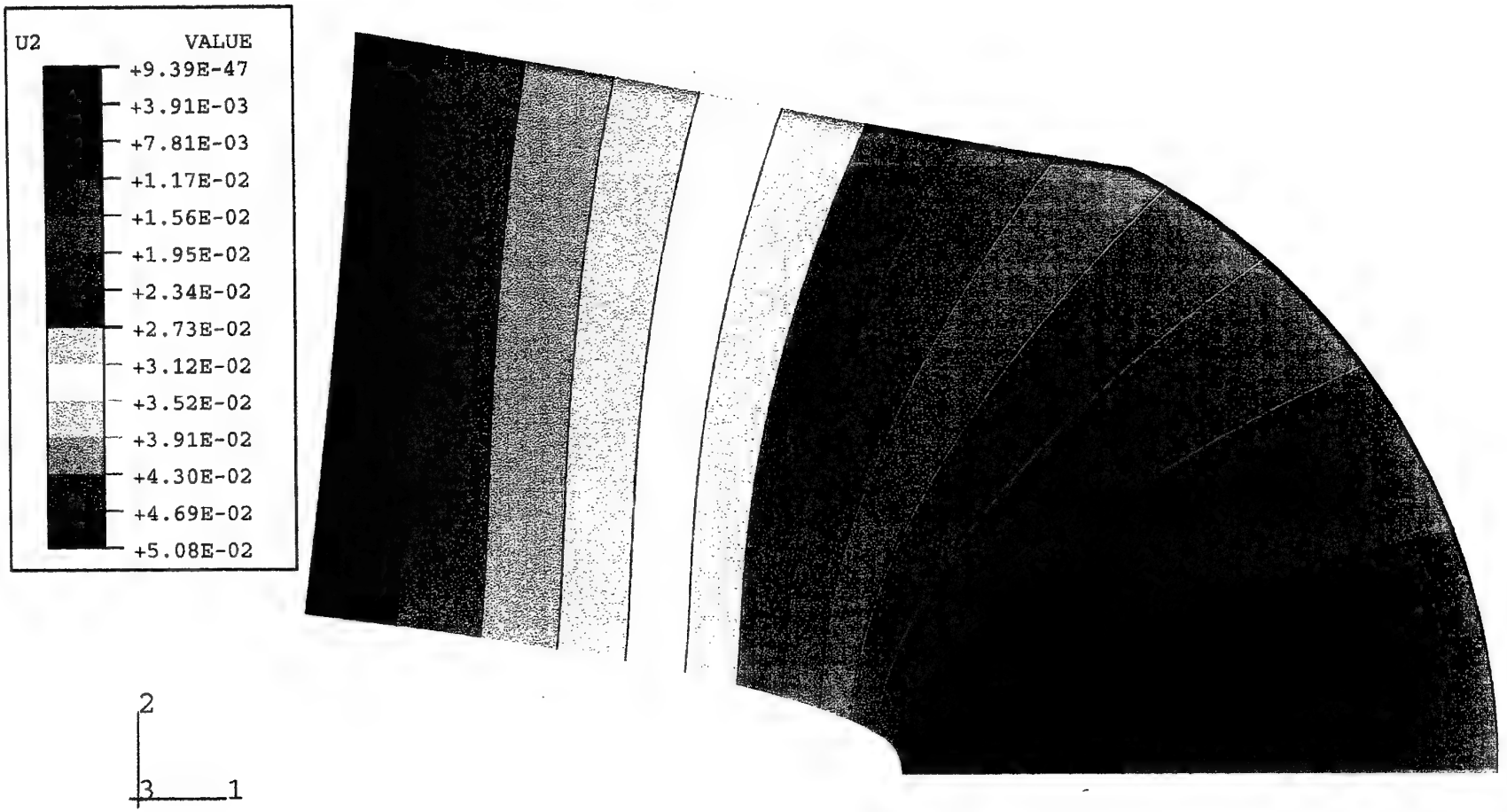

Fig. 147 Displacement along the perpendicular to the crack axis direction, u_2, contours (in the deformed specimen configuration) for Figure 135. Values in mm. Applied displacement u_0=0.7623 mm. Case IV.

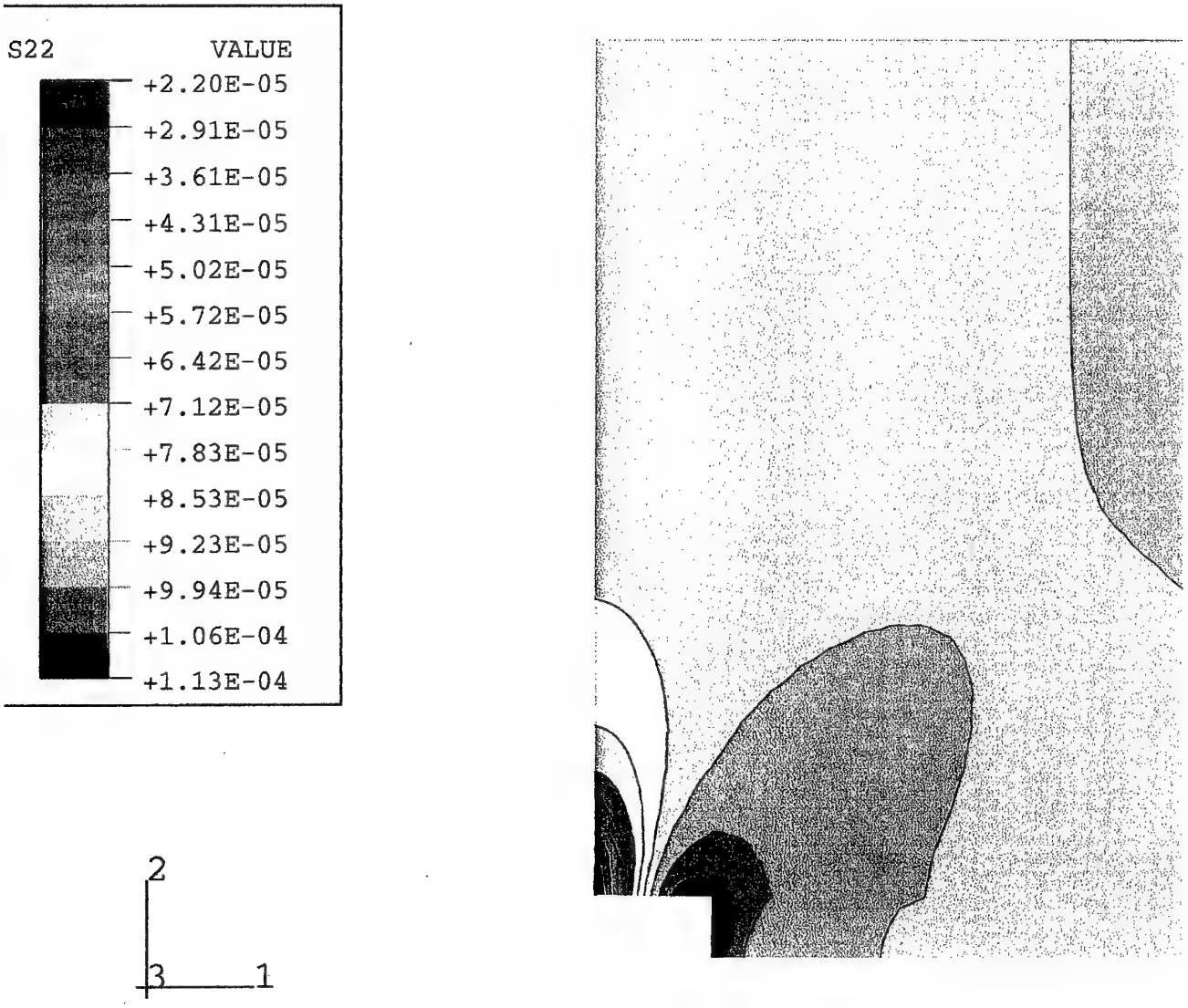

Fig. 148 Normal stress along the perpendicular to the crack axis direction, σ_{22}, contours (in the deformed specimen configuration) for Figure 133. Values in kN/mm^2. Applied displacement u_0=0.7623 mm. Case IV.

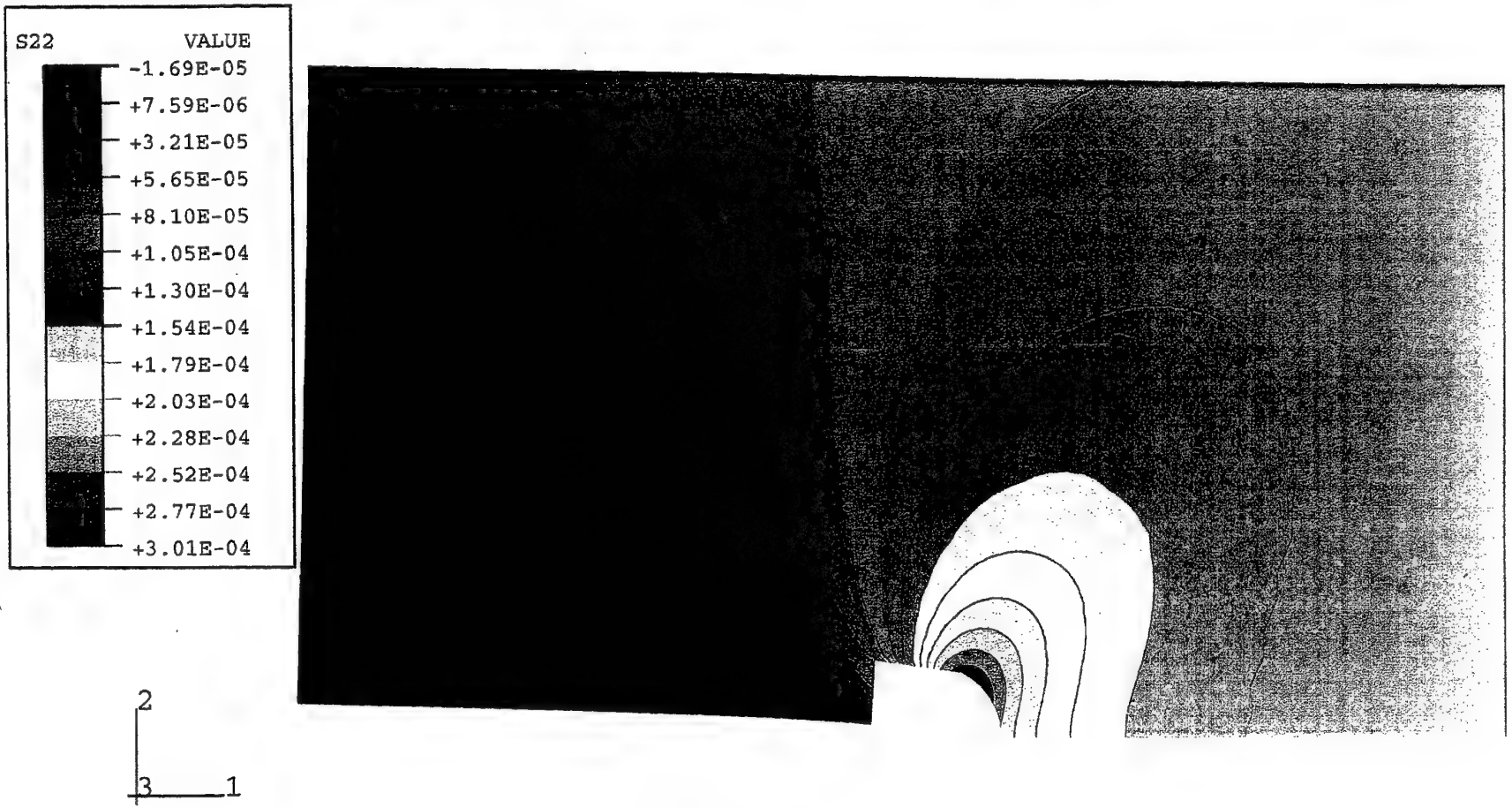

Fig. 149 Normal stress along the perpendicular to the crack axis direction, σ_{22}, contours (in the deformed specimen configuration) for Figure 134. Values in kN/mm^2. Applied displacement u_0=0.7623 mm. Case IV.

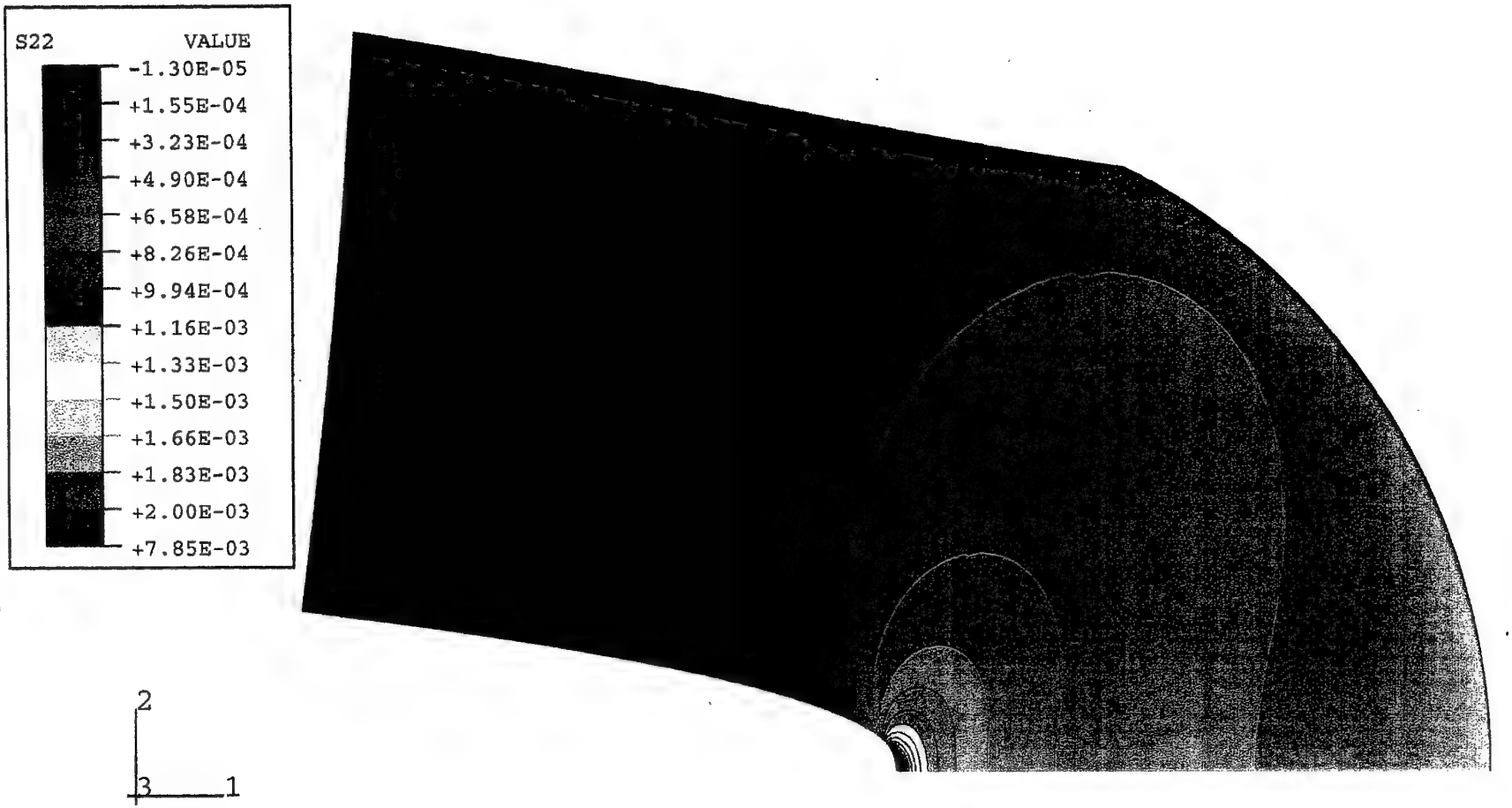

Fig. 150 Normal stress along the perpendicular to the crack axis direction, σ_{22}, contours (in the deformed specimen configuration) for Figure 135. Values in kN/mm^2 Applied displacement u_0=0.7623 mm. Case IV.

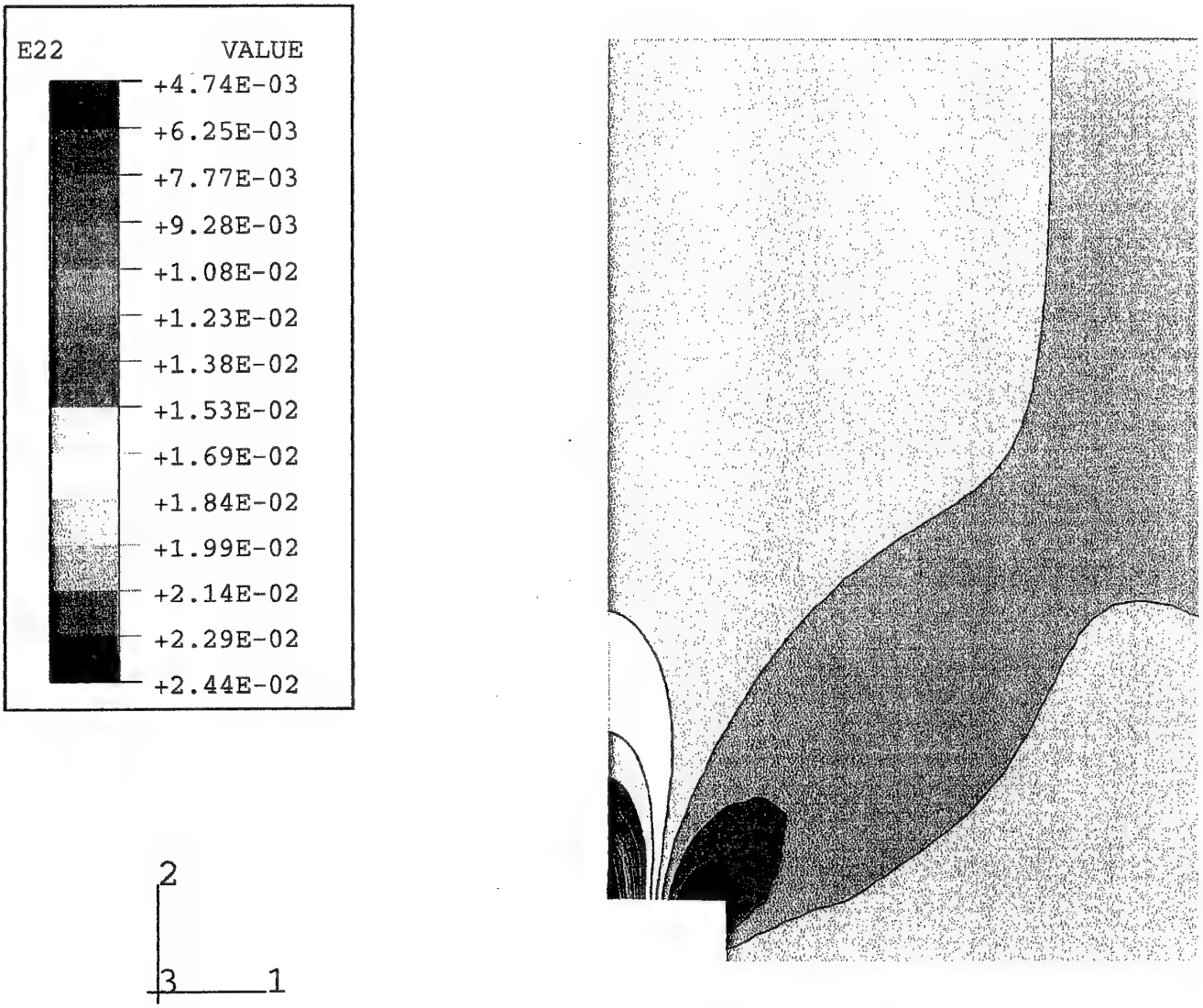

Fig. 151 Normal strain along the perpendicular to the crack axis direction, ε_{22}, contours (in the deformed specimen configuration) for Figure 133. Applied displacement u_0=0.7623 mm. Case IV.

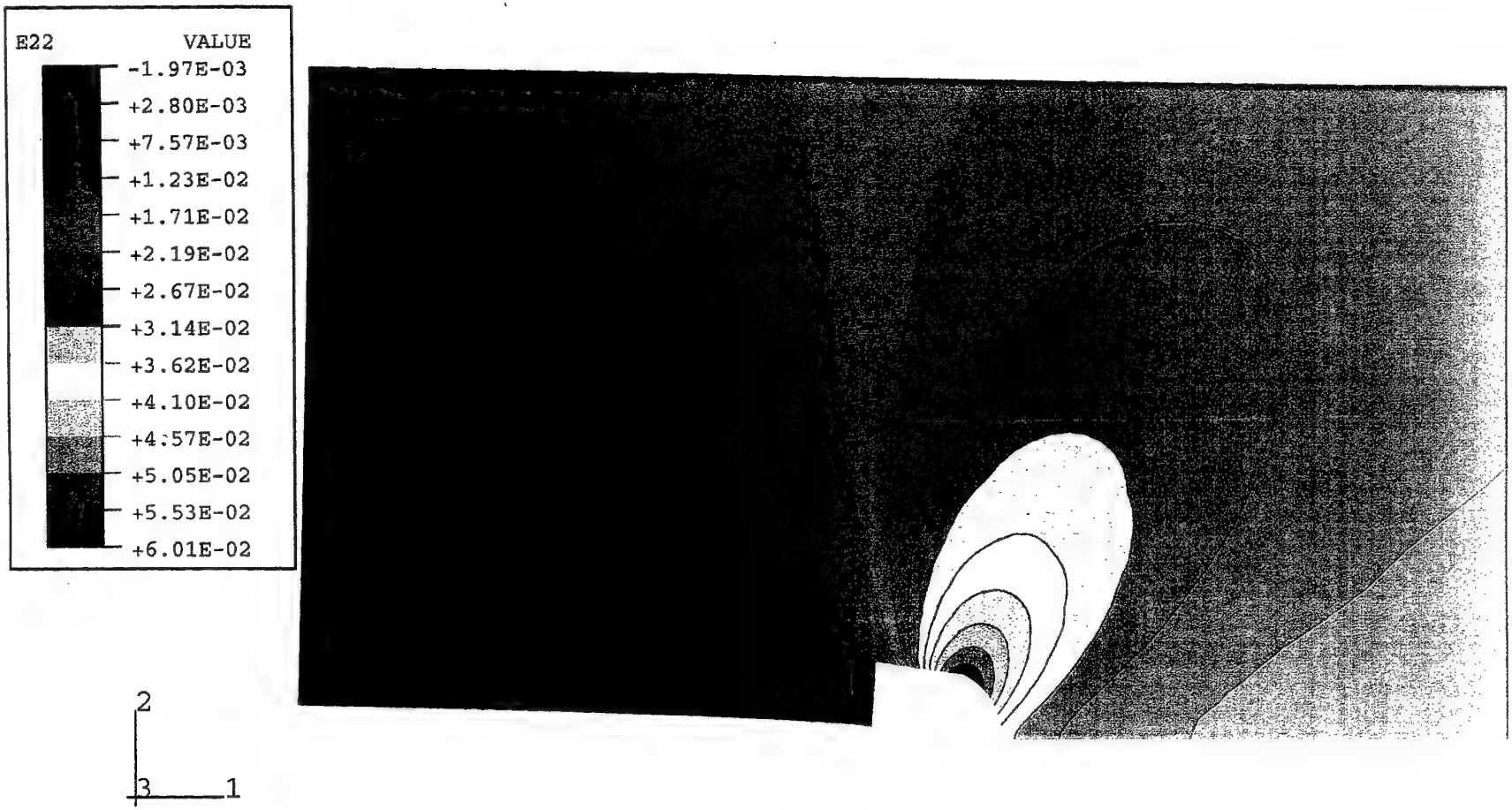

Fig. 152 Normal strain along the perpendicular to the crack axis direction, ε_{22}, contours (in the deformed specimen configuration) for Figure 134. Applied displacement u_0=0.7623 mm. Case IV.

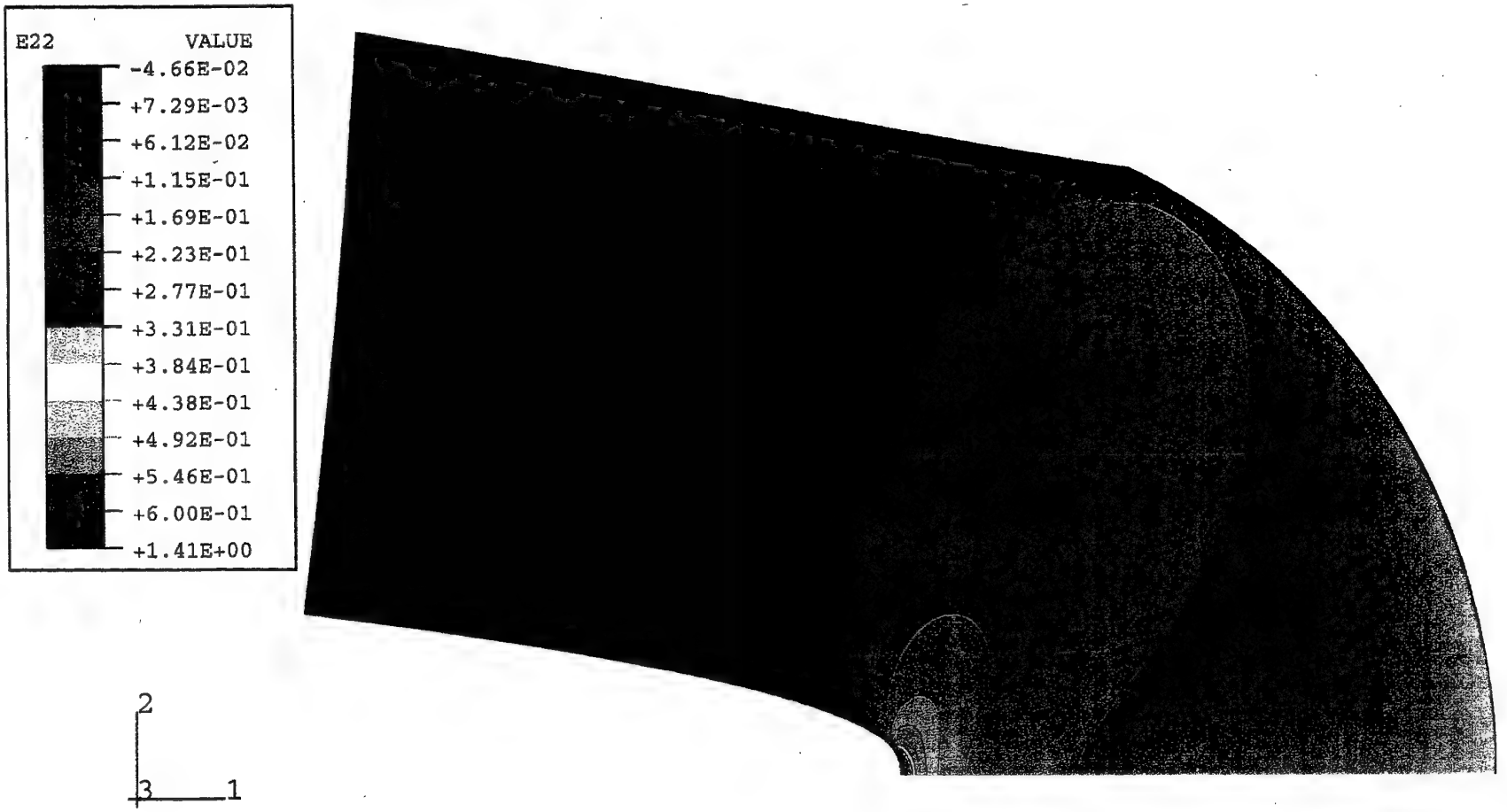

Fig. 153 Normal strain along the perpendicular to the crack axis direction, ε_{22}, contours (in the deformed specimen configuration) for Figure 135. Applied displacement u_0=0.7623 mm. Case IV.

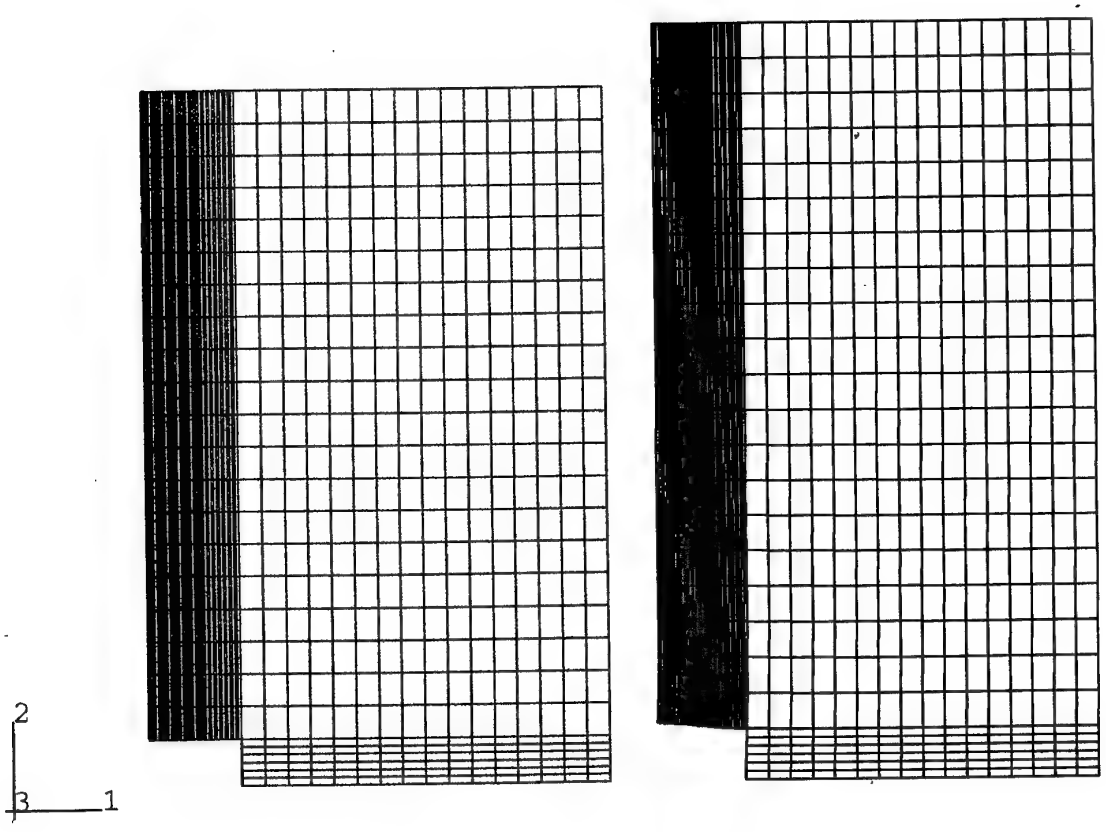

Fig. 154 Undeformed (in red) and deformed (in black) finite element grids for half specimen. Applied displacement u_0=3.3295 mm. Case IV.

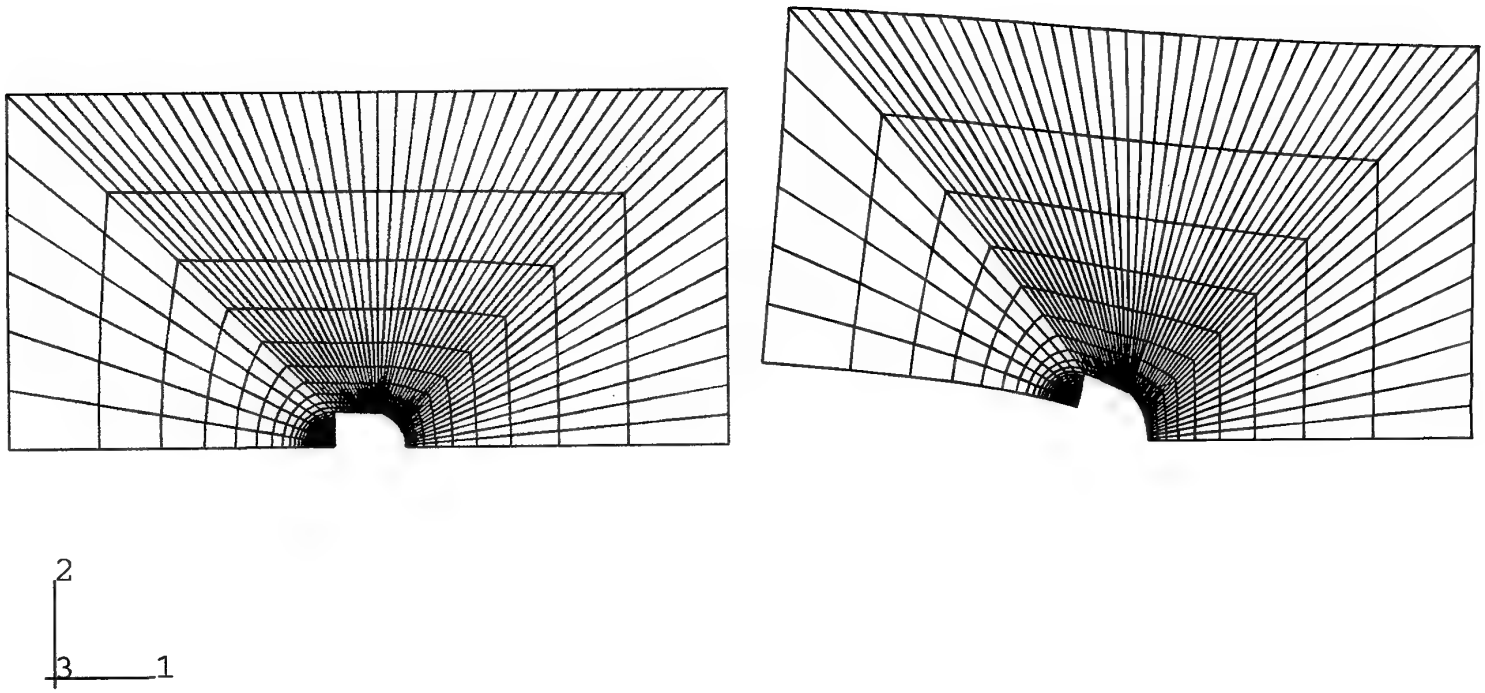

Fig. 155 Undeformed (in red) and deformed (in black) finite element grids for the missing part of Figure 154. Applied displacement u_0=3.3295 mm. Case IV.

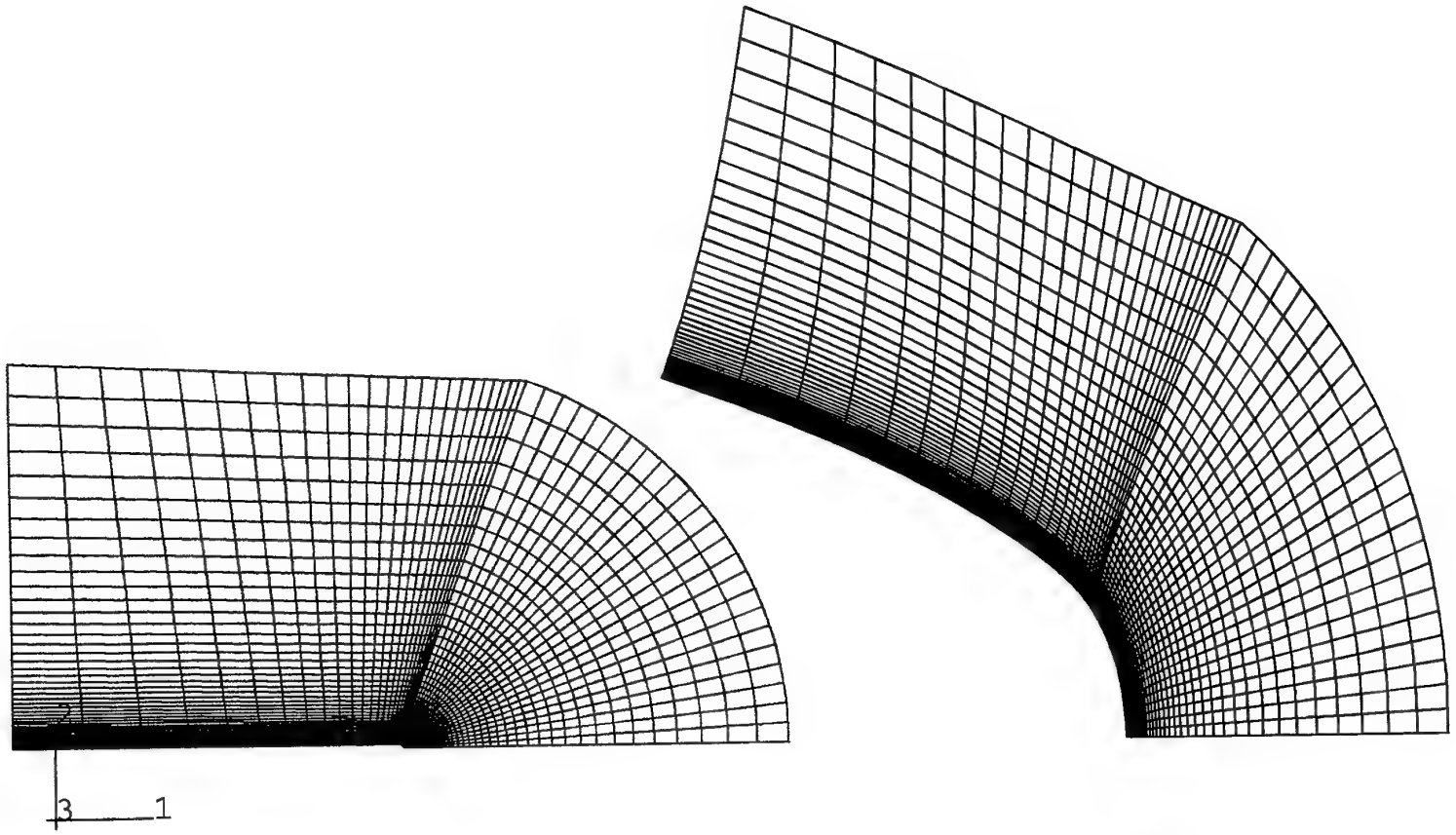

Fig. 156 Undeformed (in red) and deformed (in black) finite element grids for the missing part of Figure 155. Applied displacement u_0=3.3295 mm. Case IV.

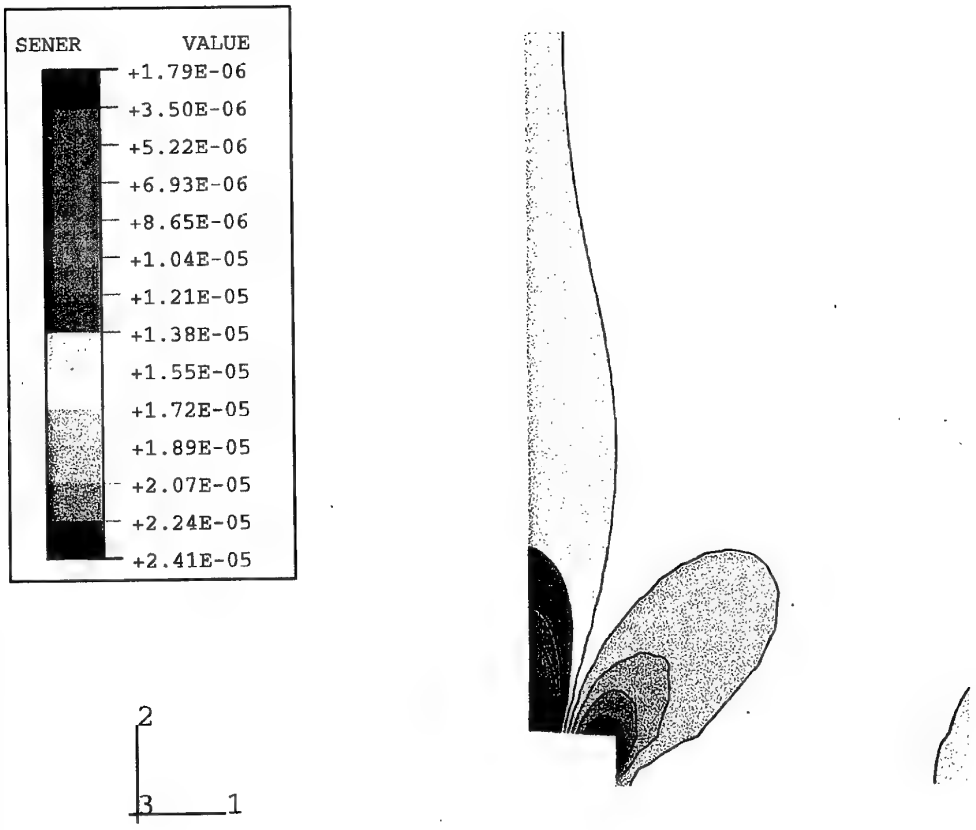

Fig. 157 Strain energy density, dW/dV, contours (in the deformed specimen configuration) for Figure 154. Values in kN.mm/mm^3. Applied displacement u_0=3.3295 mm. Case IV.

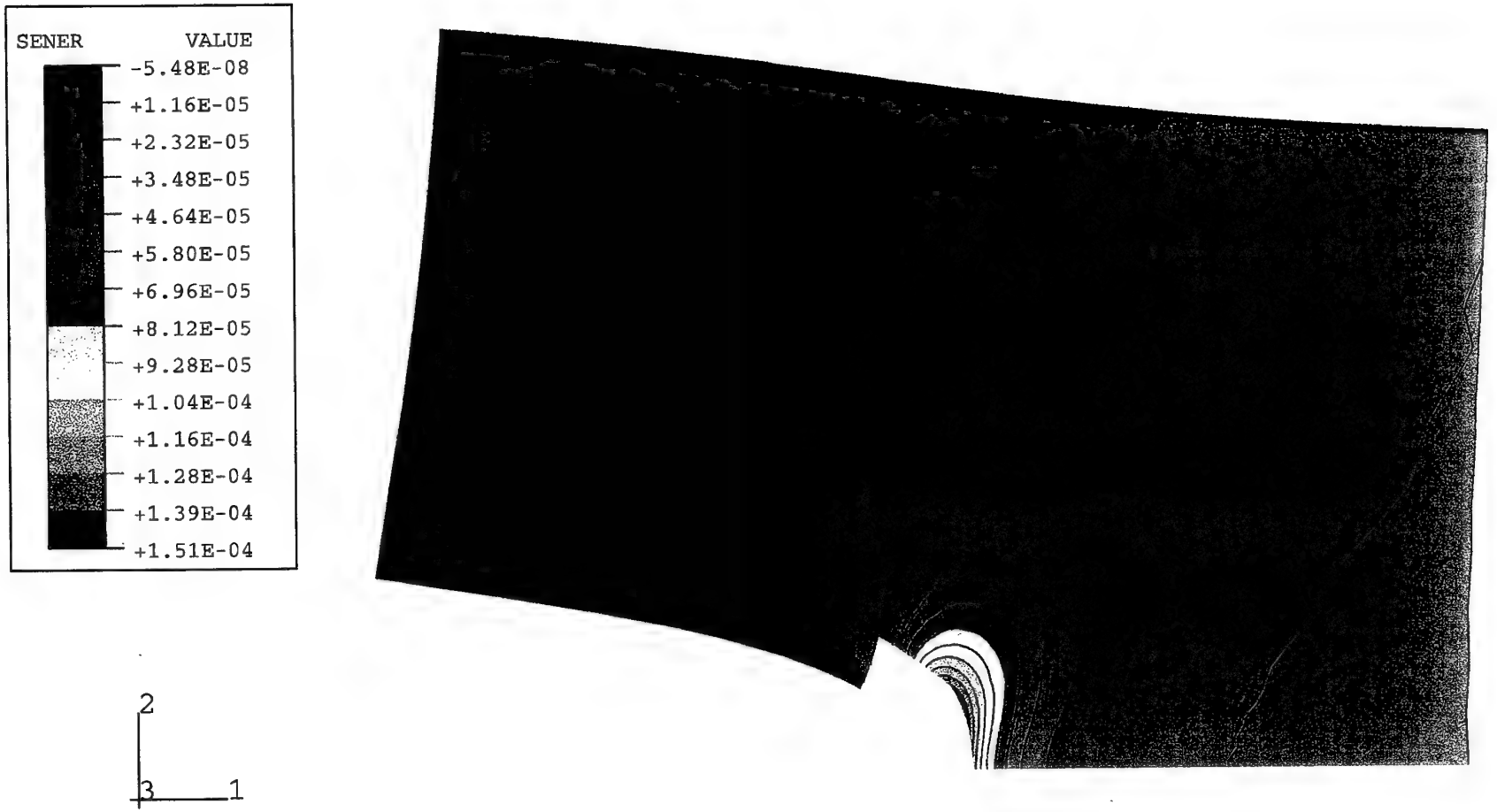

Fig. 158 Strain energy density, dW/dV, contours (in the deformed specimen configuration) for Figure 155. Values in kN.mm/mm^3. Applied displacement u_0=3.3295 mm. Case IV.

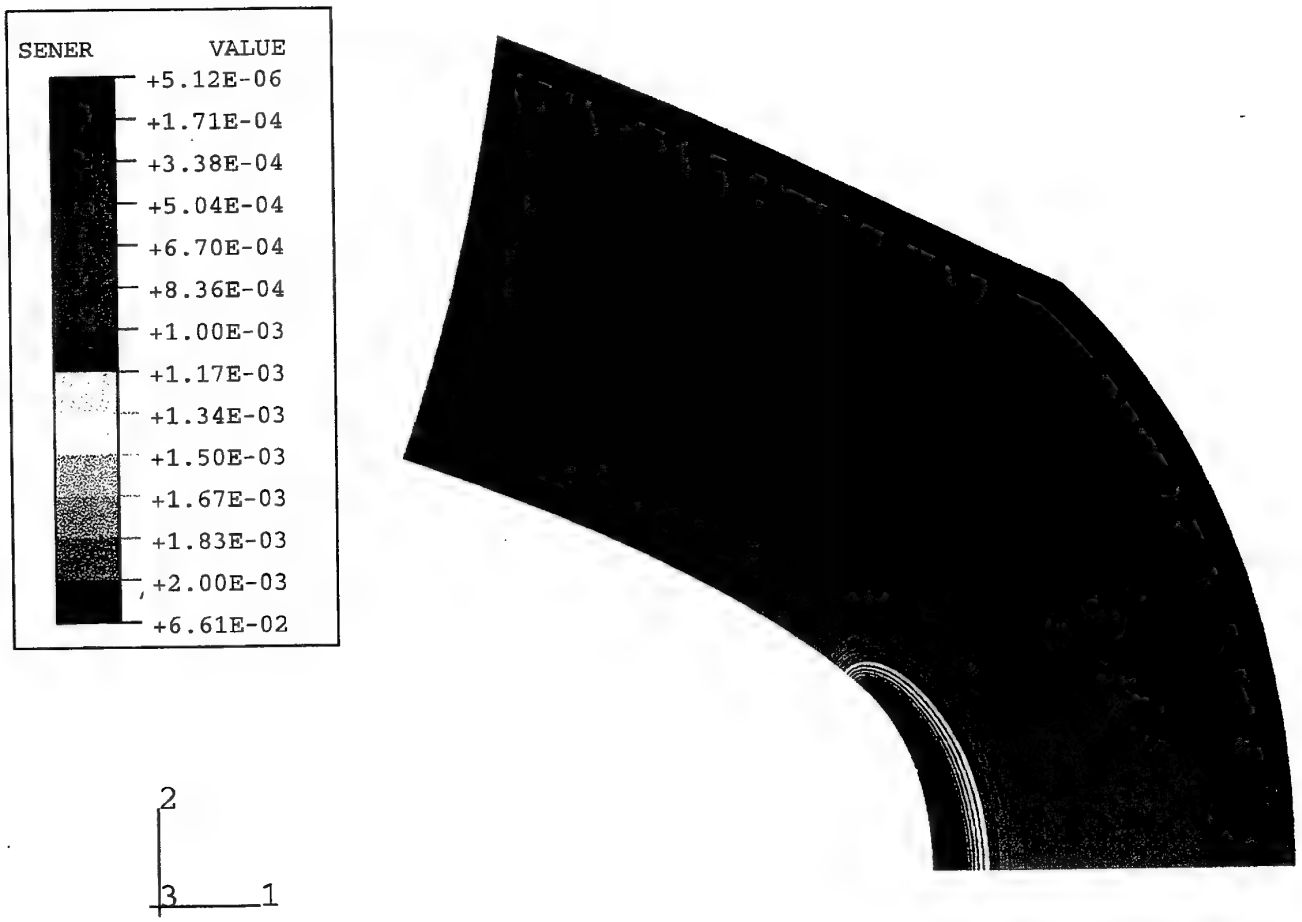

Fig. 159 Strain energy density, dW/dV, contours (in the deformed specimen configuration) for Figure 156. Values in kN.mm/mm^3. Applied displacement u_0=3.3295 mm. Case IV.

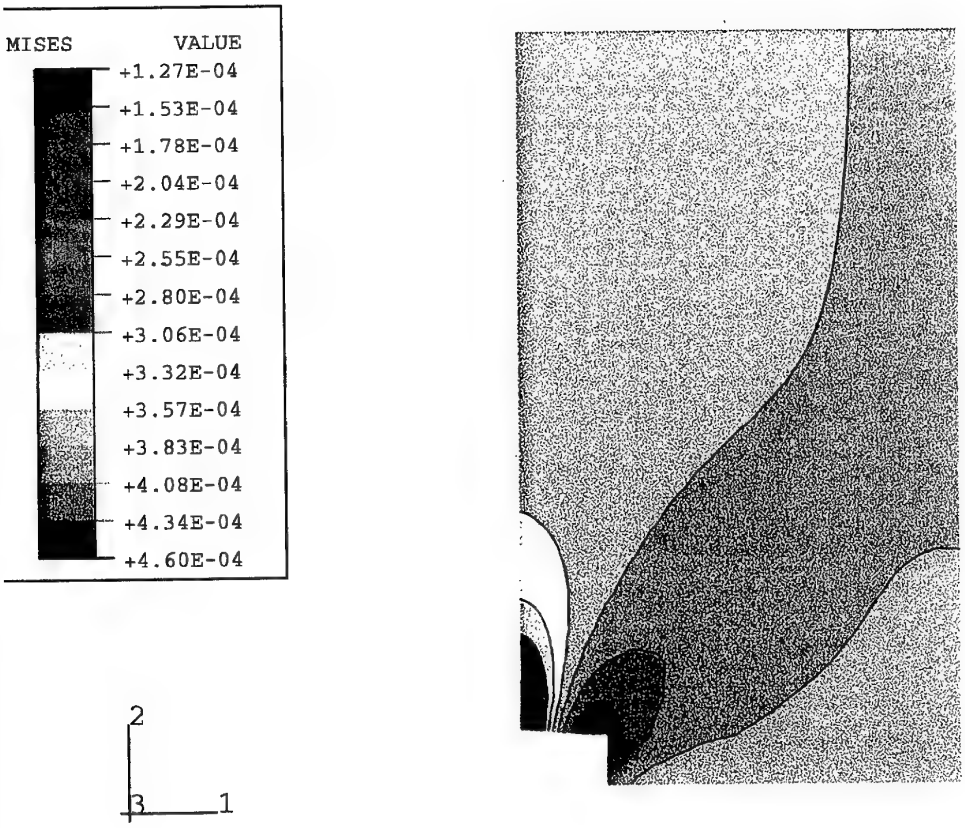

Fig. 160 Mises stress, σ_{eff}, contours (in the deformed specimen configuration) for Figure 154. Values in kN/mm^2. Applied displacement u_0=3.3295 mm. Case IV.

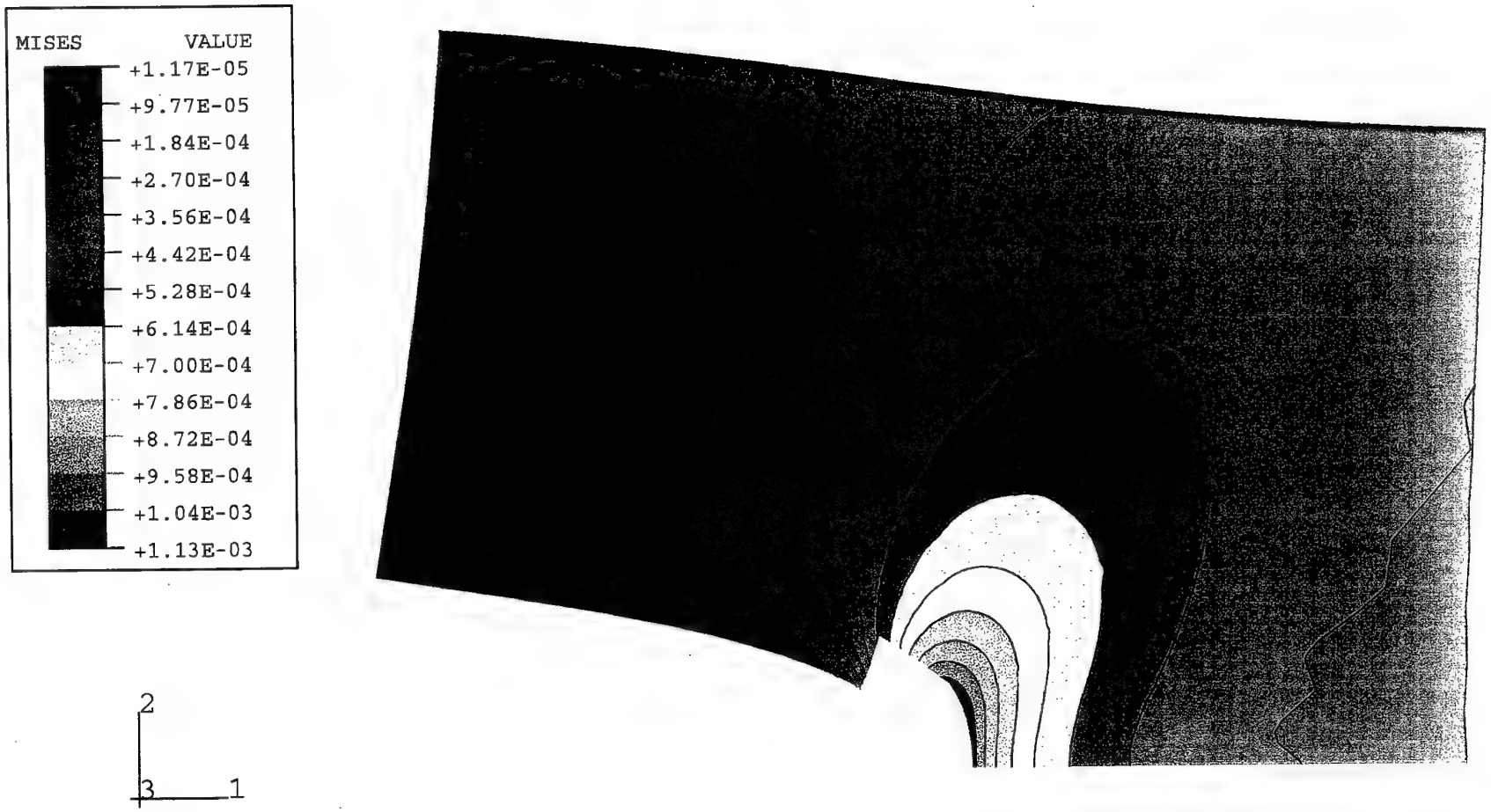

Fig. 161 Mises stress, σ_{eff}, contours (in the deformed specimen configuration) for Figure 155. Values in kN/mm^2. Applied displacement u_0=3.3295 mm. Case IV.

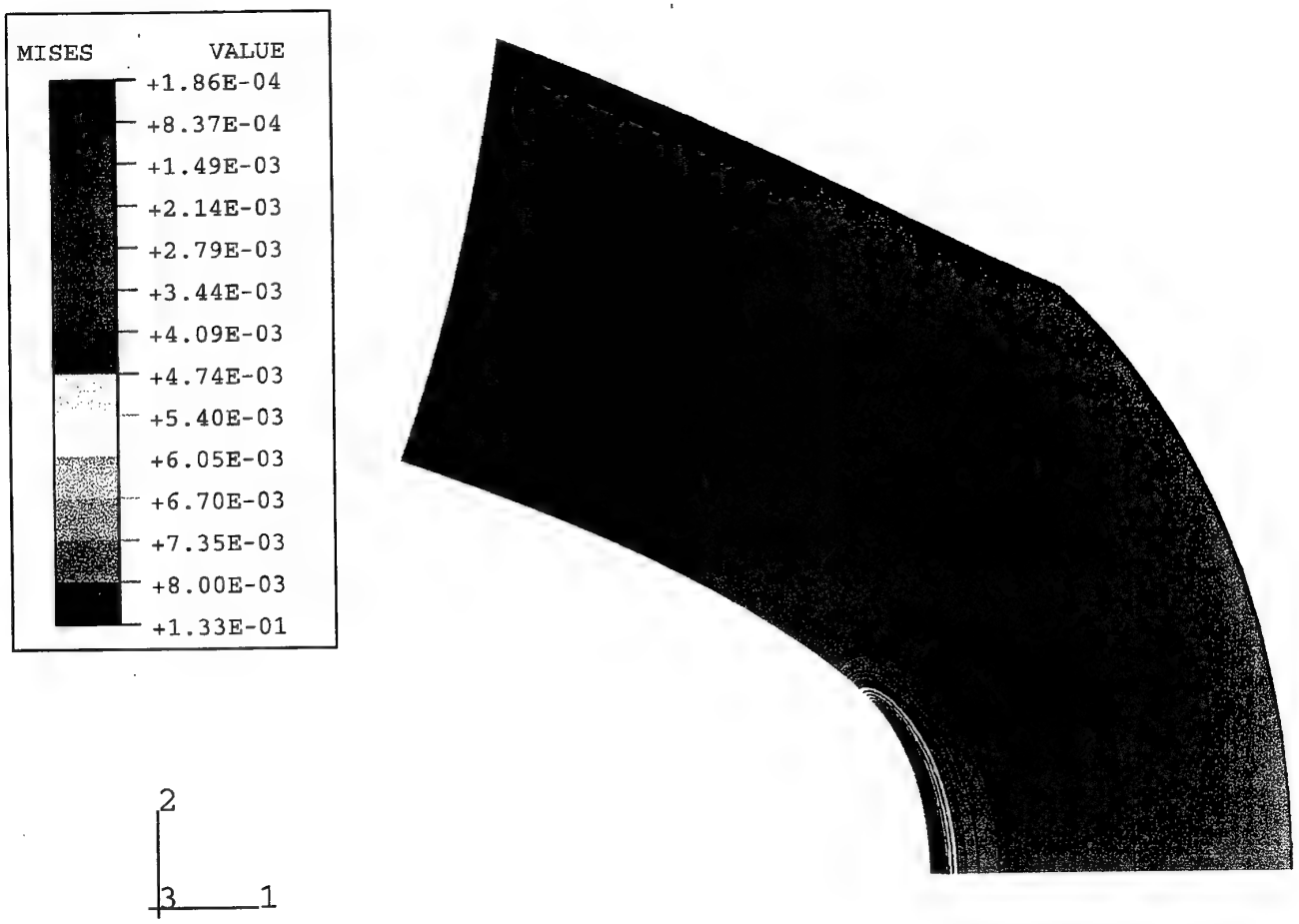

Fig. 162 Mises stress, σ_{eff}, contours (in the deformed specimen configuration) for Figure 156. Values in kN/mm^2. Applied displacement u_0=3.3295 mm. Case IV.

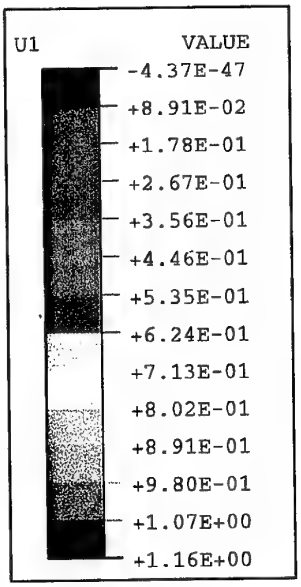

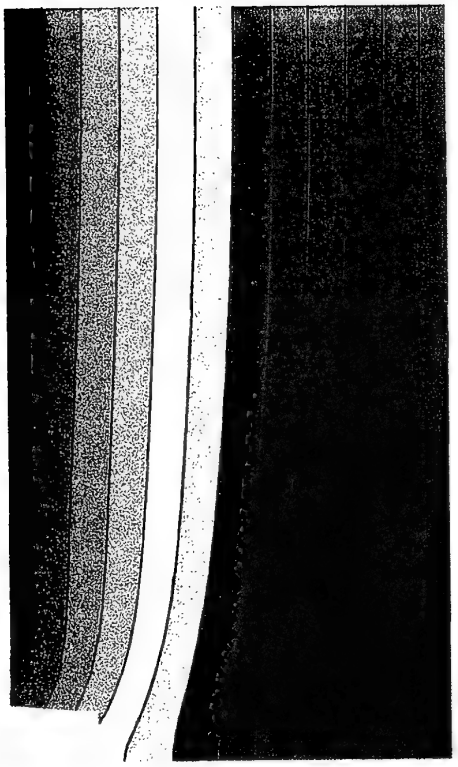

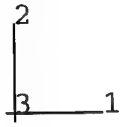

Fig. 163 Displacement along the crack axis direction, u_1, contours (in the deformed specimen configuration) for Figure 154. Values in mm. Applied displacement u_0=3.3295 mm. Case IV.

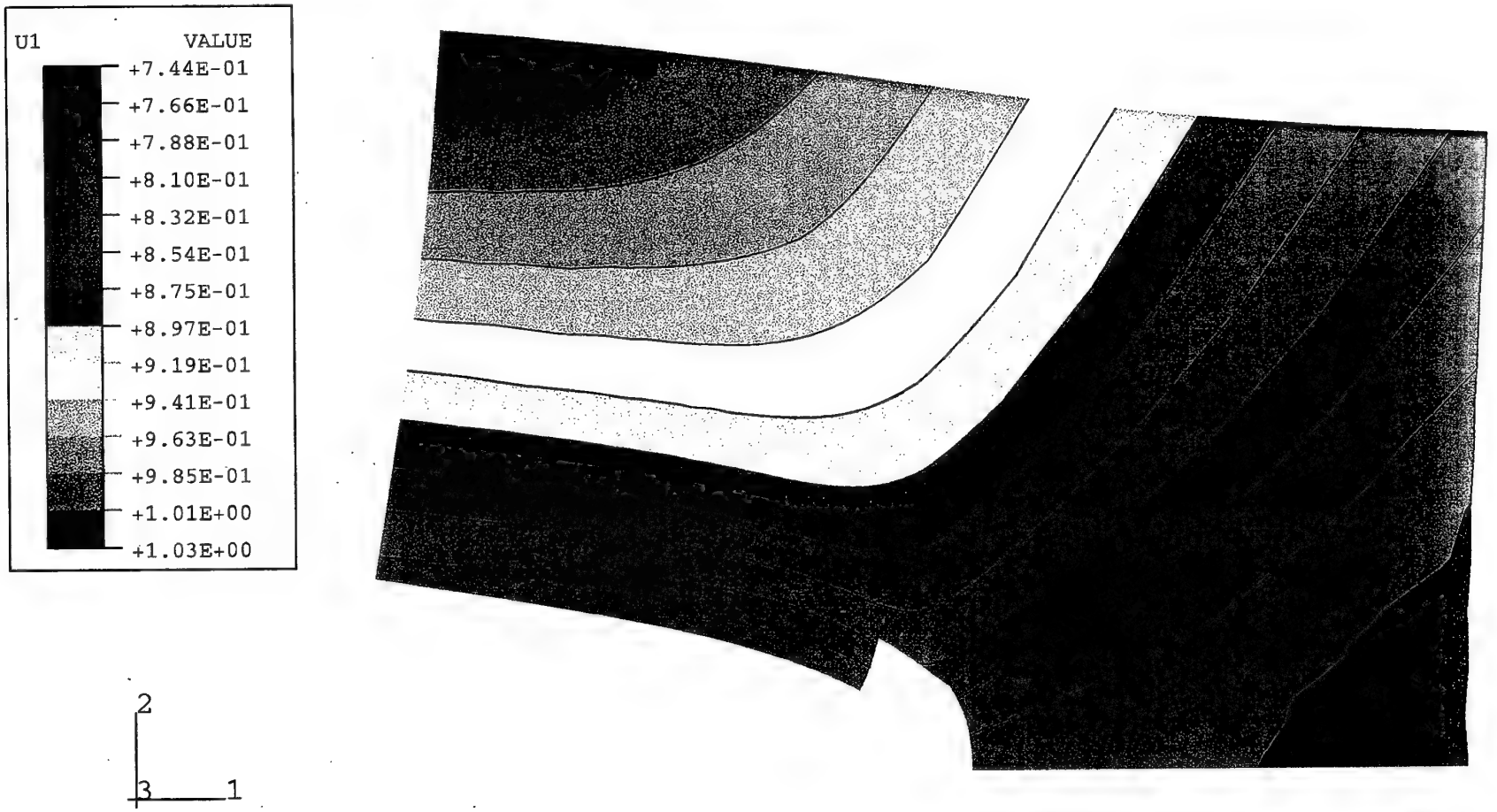

Fig. 164 Displacement along the crack axis direction, u_1, contours (in the deformed specimen configuration) for Figure 155. Values in mm. Applied displacement u_0=3.3295 mm. Case IV.

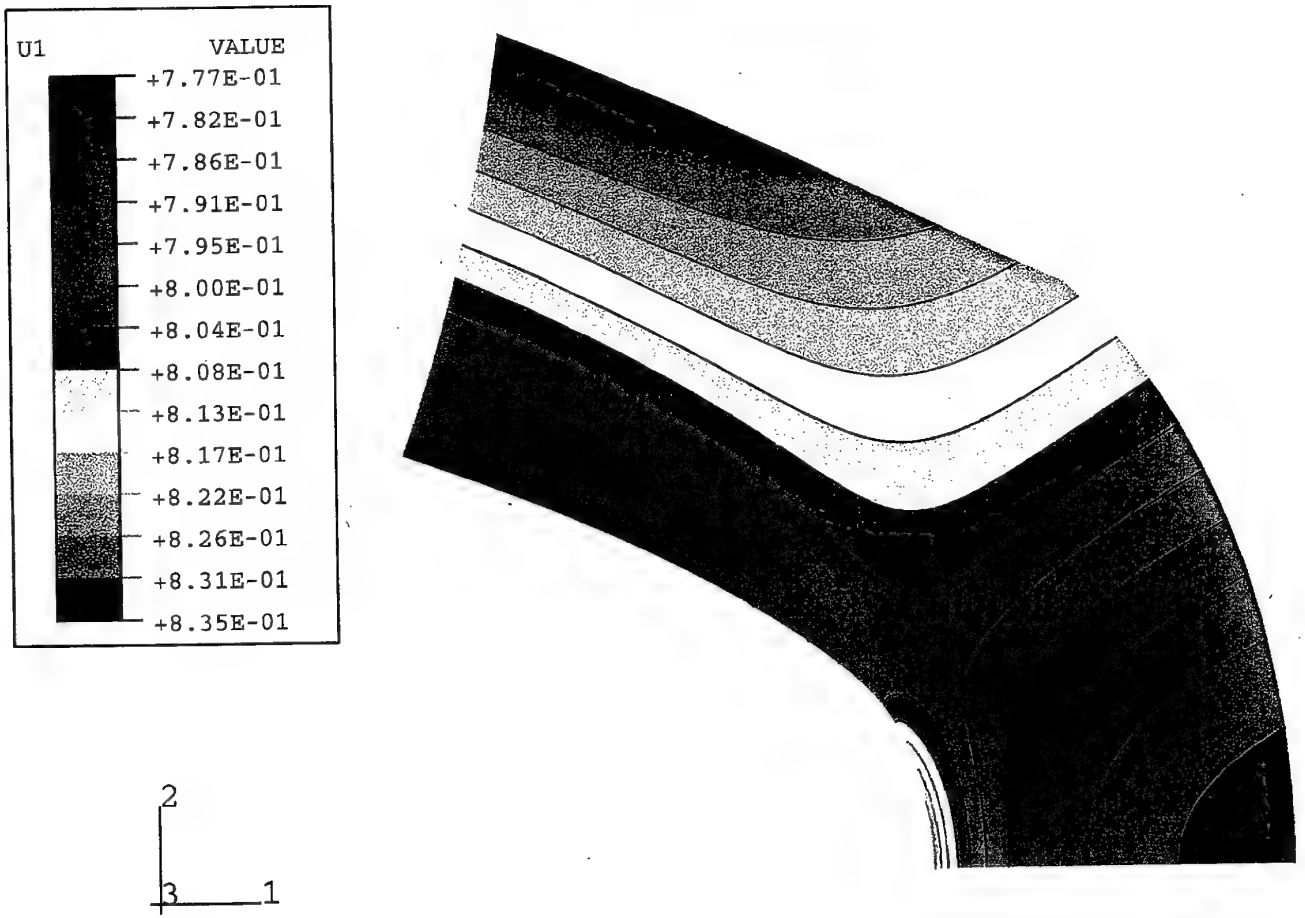

Fig. 165 Displacement along the crack axis direction, u_1, contours (in the deformed specimen configuration) for Figure 156. Values in mm. Applied displacement u_0=3.3295 mm. Case IV.

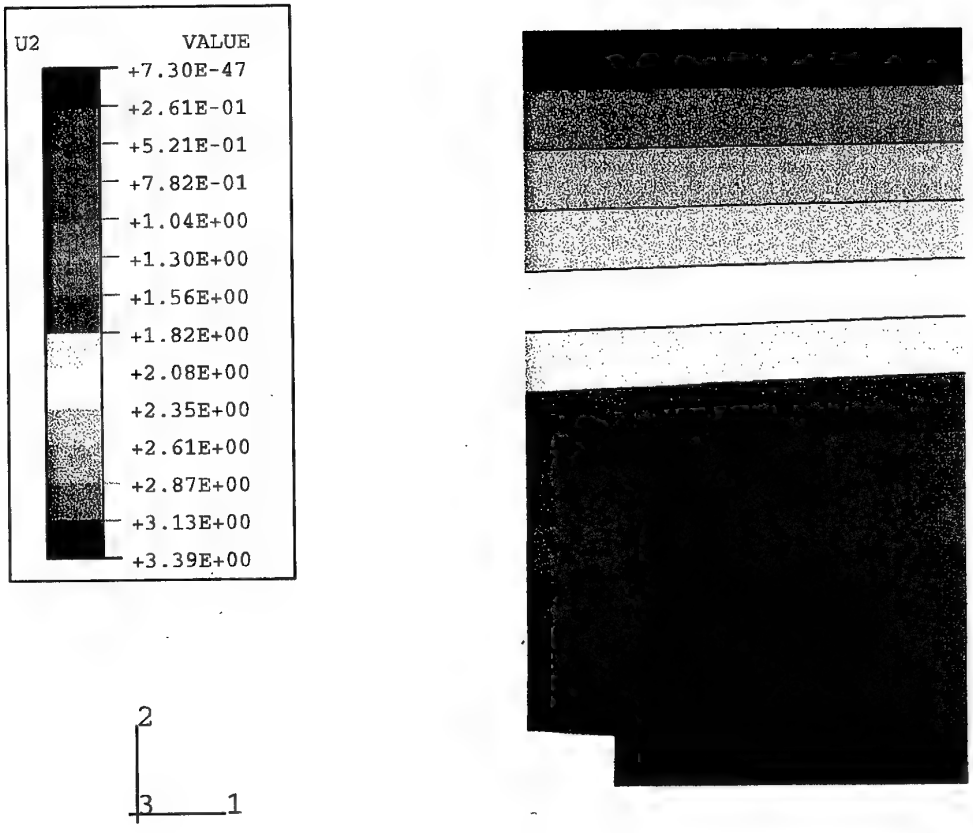

Fig. 166 Displacement along the perpendicular to the crack axis direction, u_2 contours (in the deformed specimen configuration) for Figure 154. Values in mm. Applied displacement u_0=3.3295 mm. Case IV.

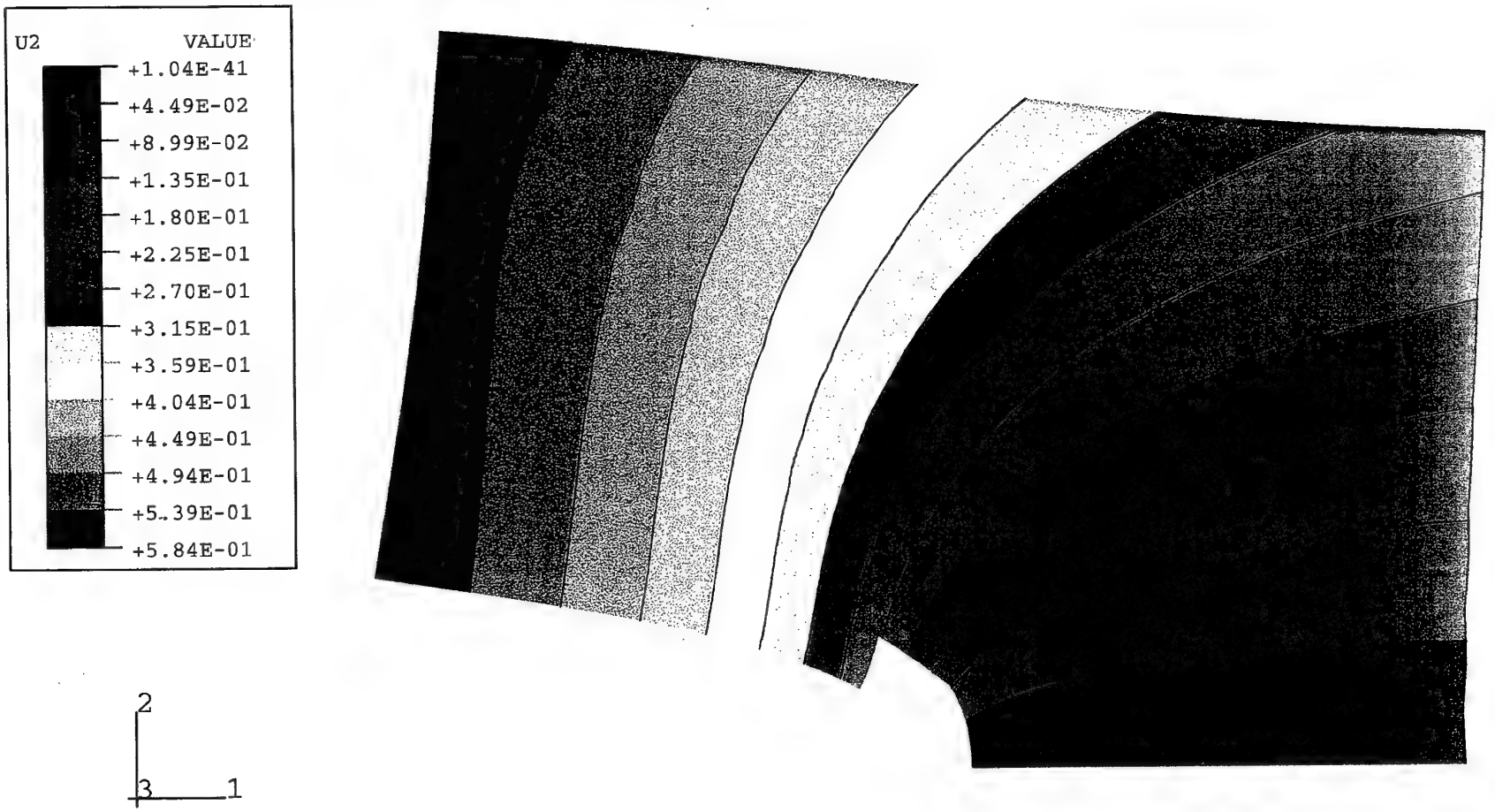

Fig. 167 Displacement along the perpendicular to the crack axis direction, u_2 contours (in the deformed specimen configuration) for Figure 155. Values in mm. Applied displacement u_0=3.3295 mm. Case IV.

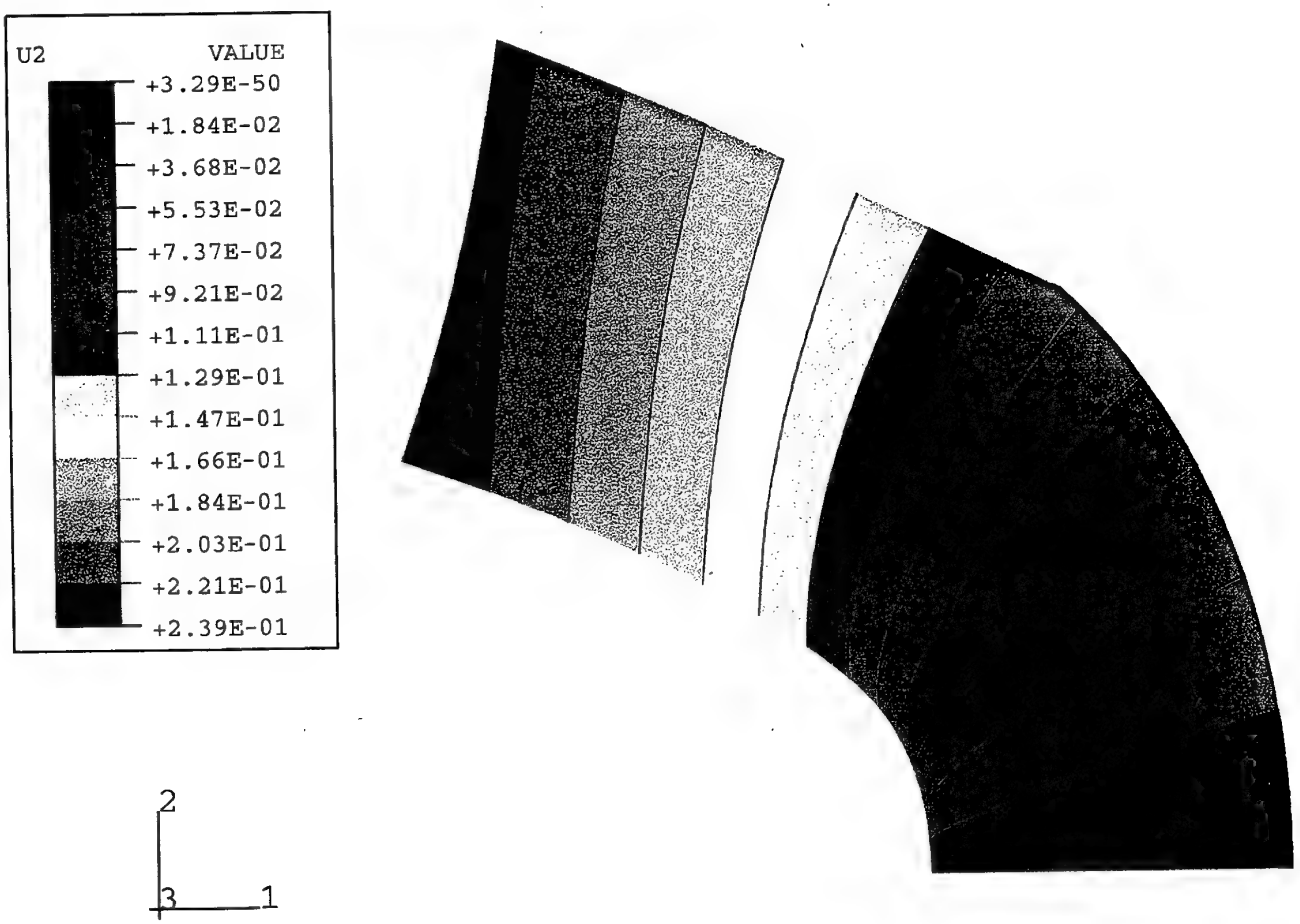

Fig. 168 Displacement along the perpendicular to the crack axis direction, u_2 contours (in the deformed specimen configuration) for Figure 156. Values in mm. Applied displacement u_0=3.3295 mm. Case IV.

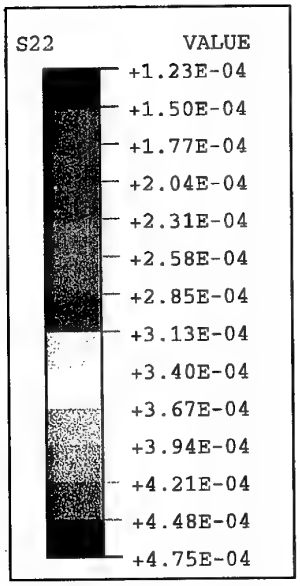

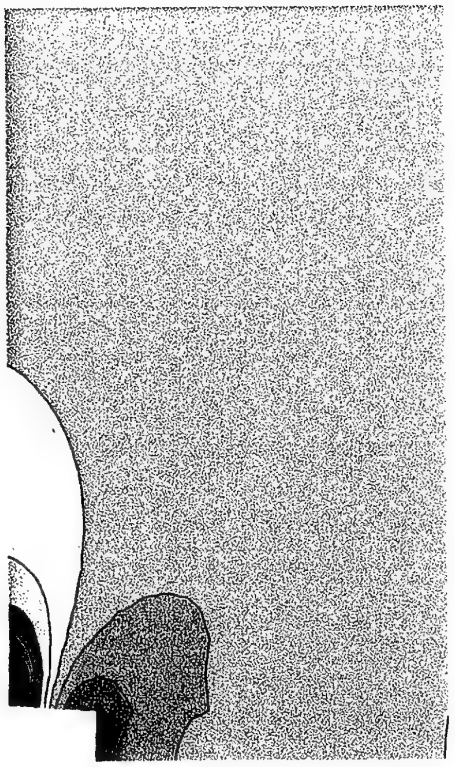

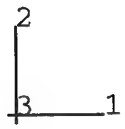

Fig. 169 Normal stress along the perpendicular to the crack axis direction, σ_{22}, contours (in the deformed specimen configuration) for Figure 154. Values in kN/mm^2. Applied displacement u_0=3.3295 mm. Case IV.

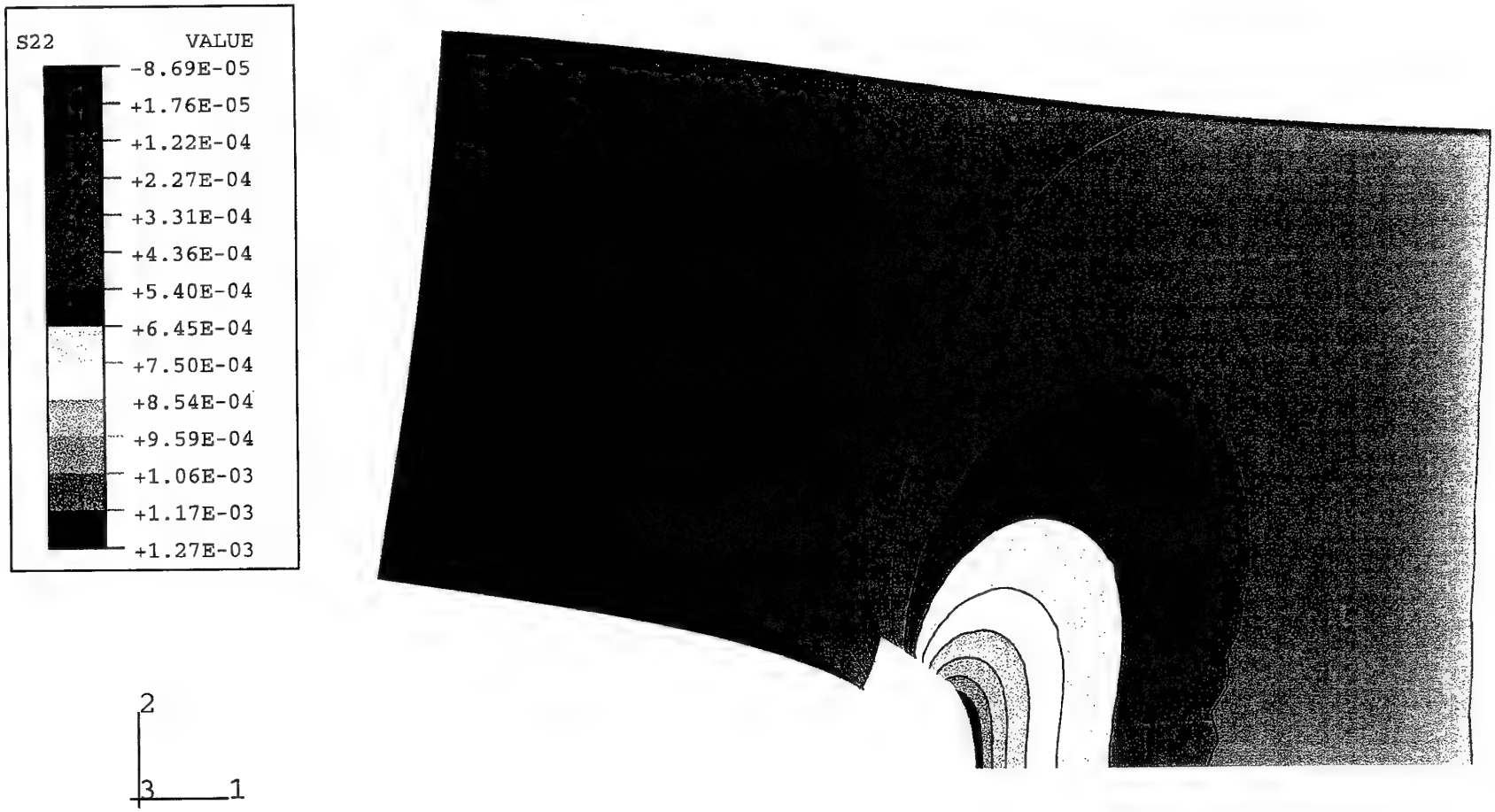

Fig. 170 Normal stress along the perpendicular to the crack axis direction, σ_{22}, contours (in the deformed specimen configuration) for Figure 155. Values in kN/mm^2. Applied displacement u_0=3.3295 mm. Case IV.

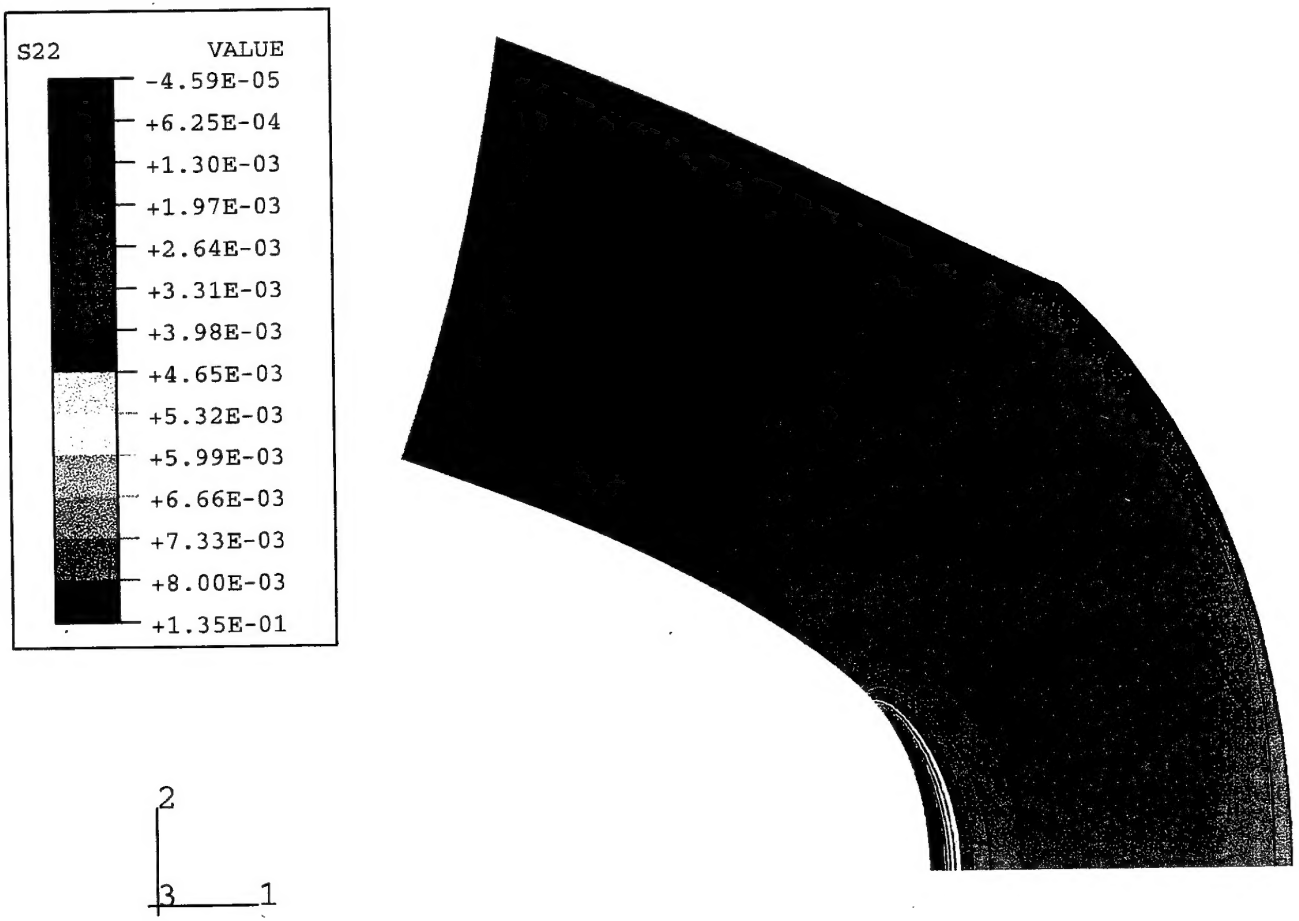

Fig. 171 Normal stress along the perpendicular to the crack axis direction, σ_{22}, contours (in the deformed specimen configuration) for Figure 156. Values in kN/mm^2. Applied displacement u_0=3.3295 mm. Case IV.

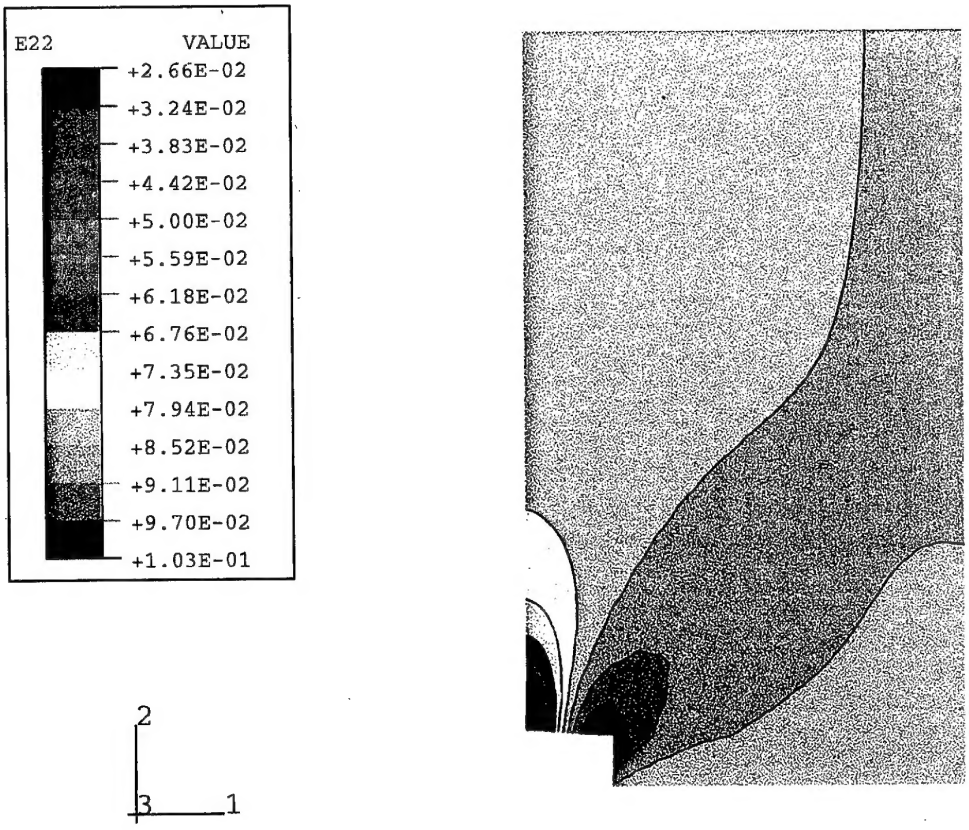

Fig. 172 Normal strain along the perpendicular to the crack axis direction, ε_{22}, contours (in the deformed specimen configuration) for Figure 154. Applied displacement u_0=3.3295 mm. Case IV.

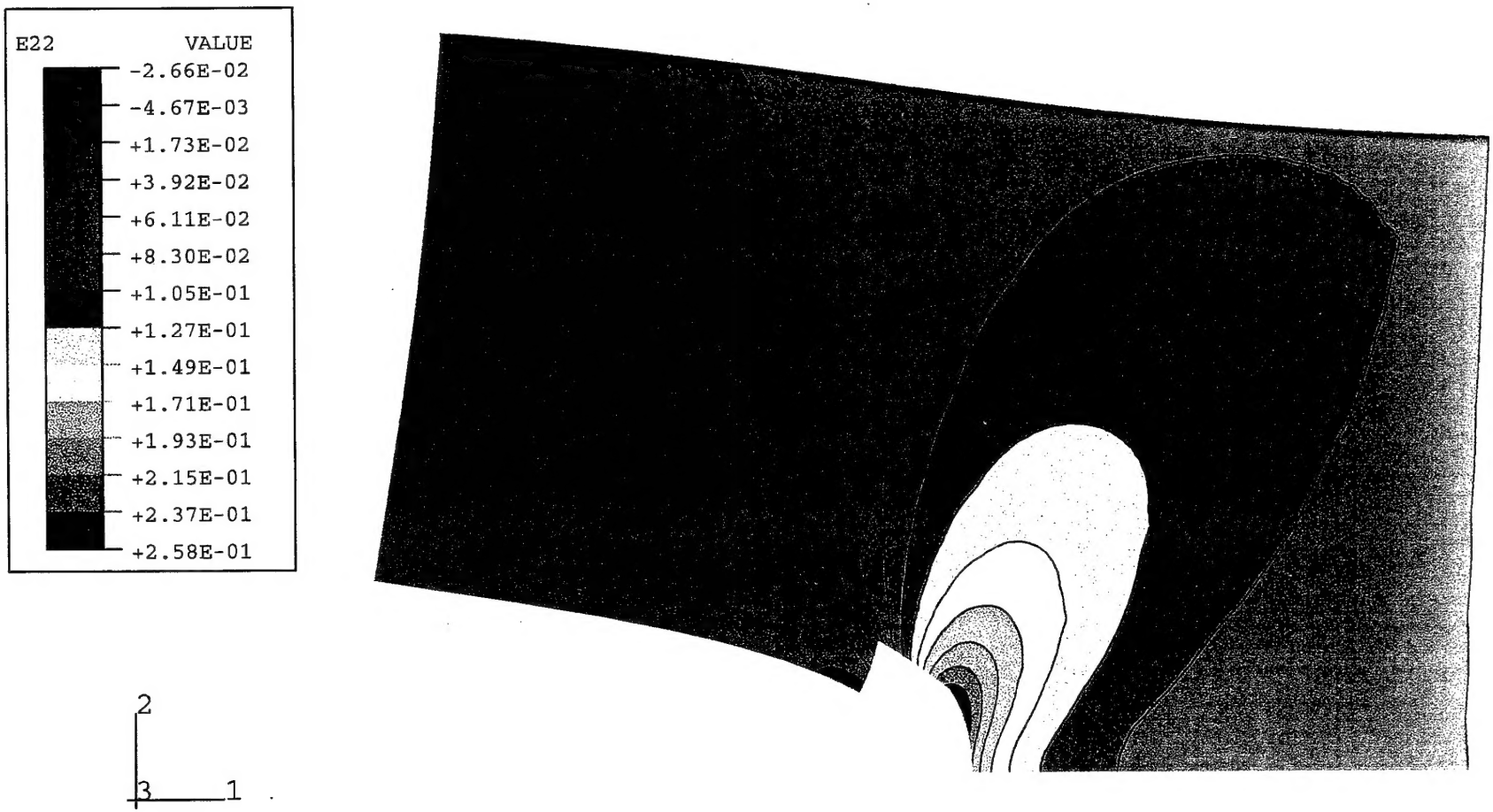

Fig. 173 Normal strain along the perpendicular to the crack axis direction, ε_{22}, contours (in the deformed specimen configuration) for Figure 155. Applied displacement u_0=3.3295 mm. Case IV.

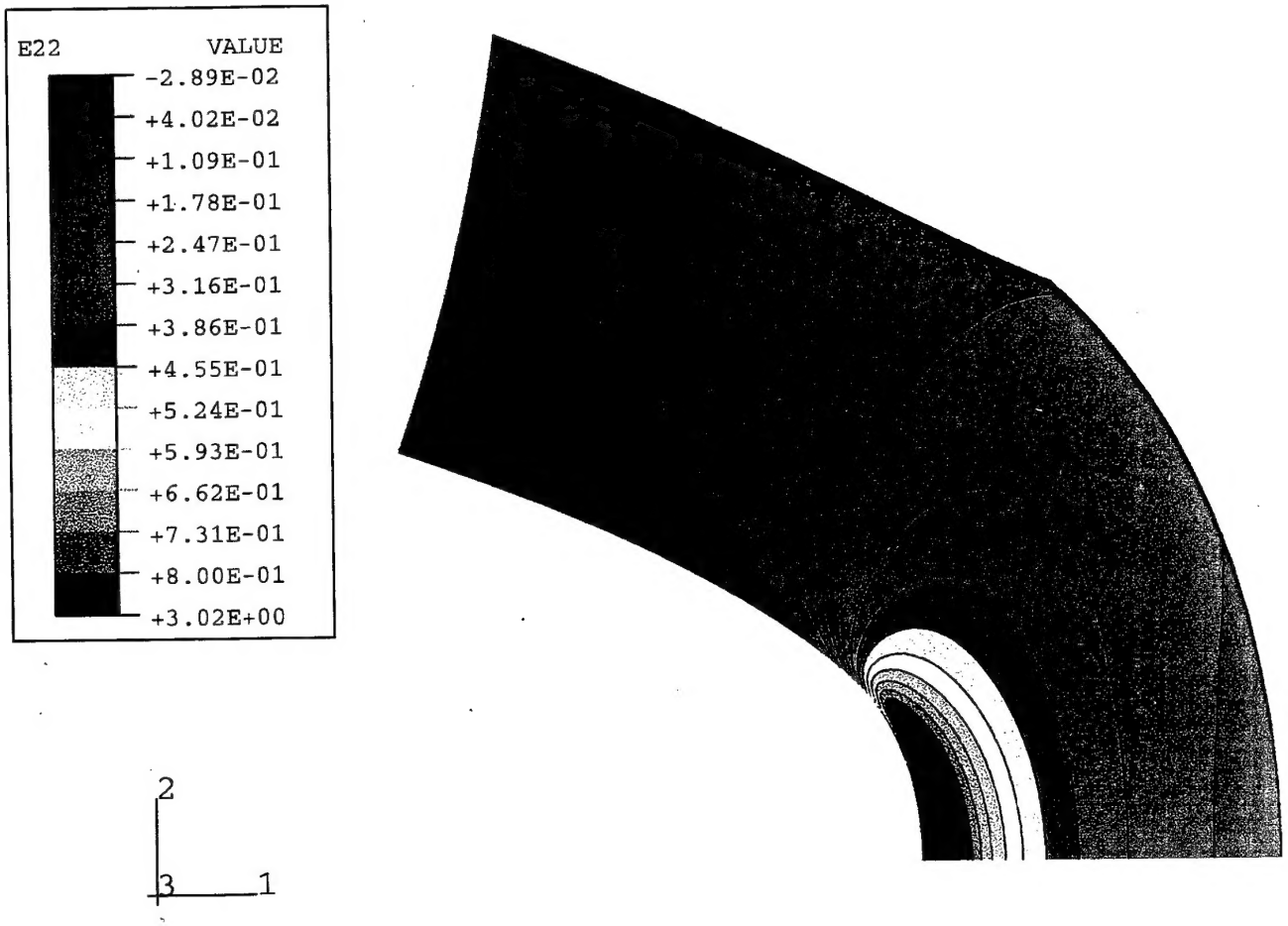

Fig. 174 Normal strain along the perpendicular to the crack axis direction, ε_{22}, contours (in the deformed specimen configuration) for Figure 156. Applied displacement u_0=3.3295 mm. Case IV.